Intelligent Mobility Control of a Hybrid Electric Off-road Vehicle with Individual Wheel Control

by

Andrew Edward Jackson, *BEng*

Submitted in accordance with the
requirements for the degree of
Doctor of Philosophy

The University of Leeds
School of Mechanical Engineering

September 2003

Abstract

This work focuses on the potential benefits that can be gained from the use of Individual Wheel Control on a large off-road vehicle. The vehicle concerned is a theoretical, six-wheel drive, off-road Hybrid-Electric Vehicle based on an existing conventional six-wheel-drive Combat Support Vehicle developed by QinetiQ (formerly DERA). The proposed vehicle utilises Individual Wheel Control through the use of six, in-wheel, Hub Mounted Electric Drives. A novel intelligent mobility control system is developed to fully exploit the capability that this configuration offers.

Initially, simplified vehicle models are developed to design and test the mobility control components. The control systems developed are Traction Control, Anti-lock Braking and Direct Yaw-moment Control. These controllers are developed individually, with the aim of improving vehicle stability and handling behaviour. Once tested, they are combined into a single system on a basic non-linear handling model, where the controller co-ordination scheme is demonstrated. Preliminary testing shows the full controller to reduce driver workload by offering predictable vehicle handling and improved vehicle stability.

An eighteen-degree of freedom vehicle model is then developed, incorporating the vehicle suspension and load transfer characteristics, based on the conventional vehicle. Field test data taken from the existing vehicle trials is used to partially validate the on-road handling behaviour of the vehicle model. On this model, the full mobility controller is tuned to offer optimal performance for a large range of driving conditions and an extension of the controller to limit side-slip at high lateral accelerations is introduced. The controller is then tested on and off-road against a fixed torque distribution system and also the conventional vehicle equipped with various differentials.

By exploiting the high torque capability and controllability of the electric drive, the potential of Individual Wheel Control is demonstrated, along with the benefits offered by the hybrid-electric drivetrain with respect to mobility. Through the simulation work conducted, the major benefits of Individual Wheel Control are shown to be: improved stability and manoeuvrability; more predictable vehicle behaviour leading to reduced driver workload; accurate yaw rate tracking and increased safety at handling limits.

Acknowledgements

I'd like to thank my supervisor, Prof. David Crolla and previous supervisor, Dr Michael Brown for their help and guidance throughout my PhD. I would also like to extend thanks to Michael Parsons, Steven Goldsack, Bob Thompson, Leo Shead, Russell Macpherson and Adrian Woodhouse from QinetiQ, UK for their assistance and interest in the work I have conducted. An acknowledgement must go to the EPSRC and QinetiQ for providing the funding for the work.

Thanks must also go to the various people in room G54b who have offered help and encouragement over the past years, especially Mark Selby.

Outside work, thanks go to my family and friends for both moral and at times, financial support during my time at Leeds.

Publications

Jackson A E., Brown M.D., Crolla D.A., Woodhouse A., Parsons M. "Co-ordinated Mobility Control of a 6x6 Off-road Vehicle with Individual Wheel Control". *Proceedings of EAEC*, 2001

Jackson A.E., Crolla D.A., Woodhouse A., Parsons M. "Co-ordinated Mobility Control of a Multi-wheeled Off-road Vehicle with Individual Wheel Control". *Proceedings of AECV*, 2002.

Jackson A.E., Crolla D.A., Woodhouse A., Parsons M. "Improving Performance of a 6x6 Off-road Vehicle Through Individual Wheel Control". *SAE paper No. 02AC-34*, 2002

Table of Contents

List Of Figures

List of Tables

Notation

α	wheel-slip angle
β	side-slip angle
δ	steer angle
ε_r	adhesion reduction coefficient
ϕ	roll angle
λ_c	castor angle
λ	wheel-slip
μ	road friction coefficient
θ	pitch angle
ρ_{ss}	steady-state path curvature
ω	wheel speed
a	distance from body centre of gravity to front axle
A_d	front of vehicle surface area
A_x	longitudinal vehicle acceleration
A_y	lateral vehicle acceleration
A_z	vertical vehicle acceleration
b	distance from body centre of gravity to central axle
BSF	bump force to suspension force
c	distance from body centre of gravity to rear axle
C_α	tyre cornering stiffness
C_λ	tyre longitudinal stiffness
C_d	aerodynamic drag coefficient
C_s	vertical suspension damping
C_{ss}	damping of compliant steering system
C_t	vertical tyre damping
F_b	bump stop force
F_d	aerodynamic resistance force
F_t	vertical tyre force generated by spring/damper
F_s	vertical suspension force
F_{wx}	longitudinal tyre force
F_{wy}	lateral tyre force
F_z	vertical tyre load
F_{zs}	static vertical tyre load

g	acceleration due to gravity
H_{cgA}	height of centre of gravity of unsprung mass
H_{cgB}	height of centre of gravity of sprung mass (body)
H_{rc}	height of roll centre
H_{pc}	height of pitch centre
I_w	wheel spin inertia
I_{wz}	wheel steer inertia
I_x	body roll inertia
I_y	body pitch inertia
I_z	body yaw inertia
K	stability margin
K_a	traction controller gain
K_b	anti-lock braking controller gain
K_d	direct yaw-moment controller gain
K_s	vertical suspension stiffness
K_{ss}	stiffness of compliant steering system
K_t	vertical tyre stiffness
L	distance between front and rear axle
M_ϕ	moment due to body roll
M_θ	moment due to body pitch
M_b	sprung mass (body)
M_w	unsprung mass (wheels)
M_z	self-aligning moment
Rl_x	longitudinal tyre relaxation length
Rl_y	lateral tyre relaxation length
RR	rolling resistance
r_{ss}	steady state yaw-rate
r_w	tyre rolling radius
s	wheel-slip
S_r	steering ratio
SWF	suspension force to wheel force
SWD	suspension to wheel force displacement
t	half track width at wheels
t_s	half track width at suspension
T	wheel torque

V_x	longitudinal vehicle speed
V_y	lateral vehicle speed
V_z	vertical vehicle speed
X	non-dimensional slip coefficient
X_{trail}	pneumatic trail
x	road input height
Z_b	vertical body displacement
Z_i	vertical displacement at wheel / body section

Additional subscripts

f	front axle
c	central axle
r	rear axle
d	derivative
hw	hand wheel
i	integral
p	proportional
1	front right wheel
2	front left wheel
3	central right wheel
4	central left wheel
5	rear right wheel
6	rear left wheel

Abbreviations

4WD/6WD	Four/Six Wheel Drive
4WS	Four Wheel Steer
ABS	Anti-lock Braking System
ADM	Automatic Driveline Management
AFV	Armoured Fighting Vehicle
ALB	Automatic Load-sensitive Brake-force
ASC	Active Steer Control
ASR	Anti-Slip Regulation
AWD	All Wheel Drive
CSV	Combat Support Vehicle
DYC	Direct/Dynamic Yaw-moment Control
EKBF	Extended Kalman-Bucy Filter
ESS	Energy Storage System
EV	Electric Vehicle
FT	Fixed Trace
GPS	Global Positioning System
HEV	Hybrid Electric Vehicle
HMED	Hub-Mounted Electric Drive
ICE	Internal Combustion Engine
IWC	Individual Wheel Control
LSD	Limited-Slip Differential
MFC	Model Following Control
MMC	Model Matching Control
PID	Proportional Integral Derivative
RLS	Recursive Least Squares
SM	Stability Margin
SMC	Sliding-Mode Control
TCS	Traction Control System
VSC	Vehicle Stability Control

Chapter 1

Introduction and Literature Review

1.1 Introduction

With the growing interest in Hybrid Electric Vehicles (HEV) within the automotive industry, a new impetus has been placed on the development of systems that will make the HEV a viable alternative to the conventional vehicle. With promises of increased range and efficiency as well as reduced emissions, the HEV has the potential to bridge the gap between the conventional Internal Combustion Engine (ICE) powered vehicle and the Electric Vehicle (EV). Although EV's perhaps represent an ideal, offering excellent efficiency and zero emissions, current battery technology hampers the advancement of such vehicles, due to limited range and lengthy charge times. The HEV however, can make use of readily available technology to offer improvements over existing, conventional vehicles. The integration of the electric motor into the conventional powertrain allows for the co-ordinated use of two different power sources as well as the utilisation of the excellent efficiency and torque characteristics associated with the electric motor.

Although hybrid technology has been successfully utilised in the passenger car and public transport sectors of the automotive industry, so far its use in off-road all-wheel drive vehicles seems to have been overlooked. The potential of improved mobility due to the quick torque responses of the electric motor makes the off-road vehicle an ideal application for this emerging technology.

A particular area of interest is that of the Combat Support Vehicle (CSV) and wheeled Armoured Fighting Vehicle (AFV), which require excellent mobility and range, in order to offer logistical support to the front-line. The QinetiQ (formerly DERA) 6x6 CSV (figure 1.1) is an example of such a vehicle. The existing vehicle, which relies on a conventional drivetrain to supply power to the six wheels, has proved itself to have mobility comparable to modern battle tanks. Hybridisation of such a vehicle may improve the capability of the CSV further, leading to increased range and improved mobility over the current vehicle (this theory can also be extended to 4x4 and 8x8 vehicles). In order to ensure this potential is fulfilled, control systems will need to be implemented that optimise the operation of the hybrid drivetrain in terms of both energy and torque production. Control of the hybrid electric

powertrain is beyond the scope of this project although it is of the utmost importance if the benefits of hybridisation are to be realised.

The bulk of this research is focused on the mobility control of the proposed 6x6 hybrid-electric CSV. Utilising six independent in-wheel electric motors in a series-hybrid configuration, advanced mobility control systems will be implemented in computer simulation, using vehicle models, to evaluate the potential benefits of both the hybrid drivetrain and Individual Wheel Control (IWC). Such systems include Traction Control, Anti-lock Braking and Dynamic Yaw-moment Control, all of which aim to improve vehicle mobility and handling. Through the co-ordination and optimisation of these control systems, they are better able to exploit the potential of the hybrid electric drivetrain and therefore IWC is demonstrated.

Fig. 1.1 QinetiQ 6x6 Combat Support Vehicle

1.2 Hybrid Electric Vehicles (HEV's)

The past 2 decades have seen a notable increase in the quantity of research centring on the HEV. With fresh environmental concerns and legislation to ensure that the motor vehicle becomes a more economical and environmental form of transport, industry is looking to the HEV to help alleviate such concerns and meet with the legislation. A number of cars have already entered production with all the major automobile manufacturers looking to do so in the near future. The potential benefits promised by the HEV, at the moment are outweighed by the cost of producing them.

A full review of HEV and EV's is presented by Atkin and Storey (1999), including full details of legislation, battery technology, and current vehicles. Wakefield (1998) offers a brief history of the HEV throughout the 20th century, showing the development of hybrid vehicles and a study of the various hybrid configurations.

Hybrid Configurations

Drivetrain configurations of hybrid electric vehicles vary greatly from model to model but all fall into one of two categories, parallel or series (figure 1.2)

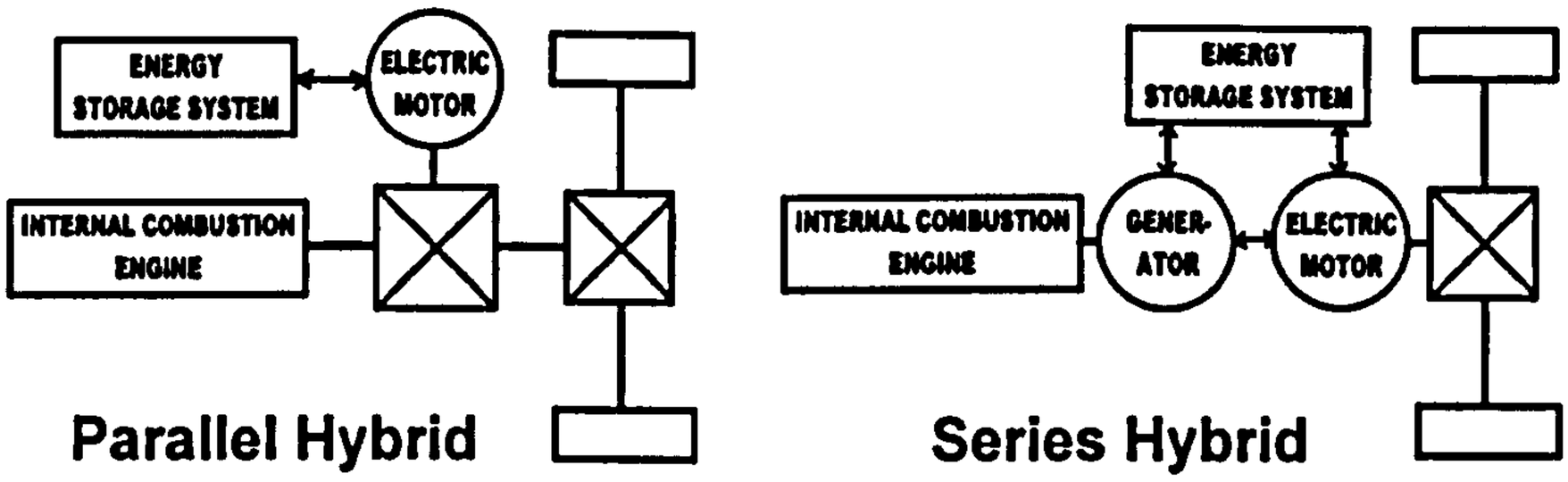

Fig. 1.2 Basic HEV configurations.

In a parallel configuration, both the electric motor and the internal combustion engine are linked to provide torque to the wheels. The motor can also be used for charging the Energy Storage System (ESS) through either regenerative braking or by acting as a generator taking a split of the power produced by the ICE. On the other hand, in the series configuration only the electric motor provides the drive torque, the ICE is linked to a generator that provides power to either the motor or the ESS. No particular configuration has been proved to be superior, although each has specific advantages (Wouk, 1997):

Parallel Advantages:

Generally more powerful than series vehicle for same size of electric motor.

Vehicle can run on either power unit alone (series cannot operate without electric motor running).

Smaller electric motor can be used, reducing mass and cost.

Smaller battery pack and motor are required.

Runs and feels like a conventional car.

Less changes in energy state than series, increasing efficiency (particularly in small vehicles, less so in large multi-wheel vehicles).

Series Advantages:

ICE can be placed anywhere in vehicle, as it is not directly attached to the transmission.

Only a small generator/ICE is required to give a large range.

ICE can run at most efficient point.

Simple transmission required as no mechanical linking exists.

Maximum torque can be produced at all times, even when ICE is off.

It is unlikely that one configuration will emerge as an industry standard. It is more likely that certain configurations will become more suited in specific applications. For instance, due to the acceleration behaviour of city buses and the low top speed, a series configuration drivetrain may prove of more use, given the better efficiency at low speed and the excellent acceleration responses of the electric motor. One study conducted by Wipke (1997) compared the fuel economy of similarly designed series and parallel vehicles using the ADVISOR simulation package (Vehicle Systems Analysis, 2003). It showed that the parallel configuration offered a 4% improvement in fuel economy over a similarly designed series version. This, however cannot be seen as conclusive proof, Senger *et al.* (1997) noted that although ADVISOR is accurate at simulating series HEV's, due to the greater interaction of the ICE in the parallel configuration, simulating a parallel HEV offers slightly less accurate results (the ICE represents the least accurate component simulated in ADVISOR).

1.3 Vehicle Dynamics Modelling

The dynamics of road vehicles is an area of constant interest within automotive research. Accurate modelling of a vehicle's dynamic characteristics allows new components and control systems to be developed and tested before costly vehicle prototypes are considered. The field of vehicle dynamics is often separated into two distinct areas: ride and handling. There is a strong interaction between ride and handling even though each system is primarily concerned with different parameters; ride on vertical movement, rolling and pitching motion, where as handling focuses on longitudinal, lateral and yawing motion. Another reason that the two systems are often dealt with separately is that control systems are usually designed to have a significant affect on either one or the other. Both systems are highly non-linear in their characteristics, however both can be linearised around specific operation points to look at vehicle performance around a trim condition.

The equations of motion governing a vehicle are usually approached in one of two ways, through the use of either Newtonian equations or Lagrangian equations. The former is based around the use of Newton's 2nd law, where as the Lagrange derivation is governed by the conservation of potential and kinetic energy. It is noted by Crolla *et al.* (1996) that the Lagrangian approach is more useful as model complexity increases as the model is separated into a number of basic equations that are easily manageable.

1.3.1 Handling Modelling

In literature, it is usual to find handling models implemented as a linear bicycle model. This is a method of simplifying the model, assuming constant forward speed, looking at only lateral and yawing motions as shown in figure 1.3. Four wheels are simplified into a two wheel model by assuming equal reactions from both left and right wheels and a linear relationship between wheel-slip angle and lateral tyre forces. Small angle theory removes trigonometric values. Crolla *et al* (1996) covers the basics of bicycle handling models giving the derivation of the equations of motion using both the Newtonian and the Lagrange approaches. The bicycle model has sufficient accuracy for use in vehicle dynamics study when dealing with low steer inputs and low to mid lateral accelerations (less than 0.3 or 0.4g). It is often used in literature, especially during development of four-wheel steering control systems and also DYC. It is also useful to determine the fundamental handling characteristics of a vehicle, such as its understeer parameter and its stability. The drawback of such a model is the assumption that forward velocity is constant, which, when the effects of changes in wheel torques are of importance, is not the case. The fundamentals of linear and non-linear handling models are dealt with more thoroughly in Chapter 2.5 and 2.7.

When looking at time based vehicle simulation, there is the question of open or closed-loop simulation (i.e. is there a driver model included). Driver models are considered in Cooke (1996) where a review of various methods is presented. It is noted that most driver models require detailed knowledge of the vehicle in all loading and speeds, which makes development a lengthy process. Open loop testing is sufficient for investigations into vehicle handling and controller development, as it is the purpose of mobility control to greatly reduce the need for the driver to operate in closed-loop mode.

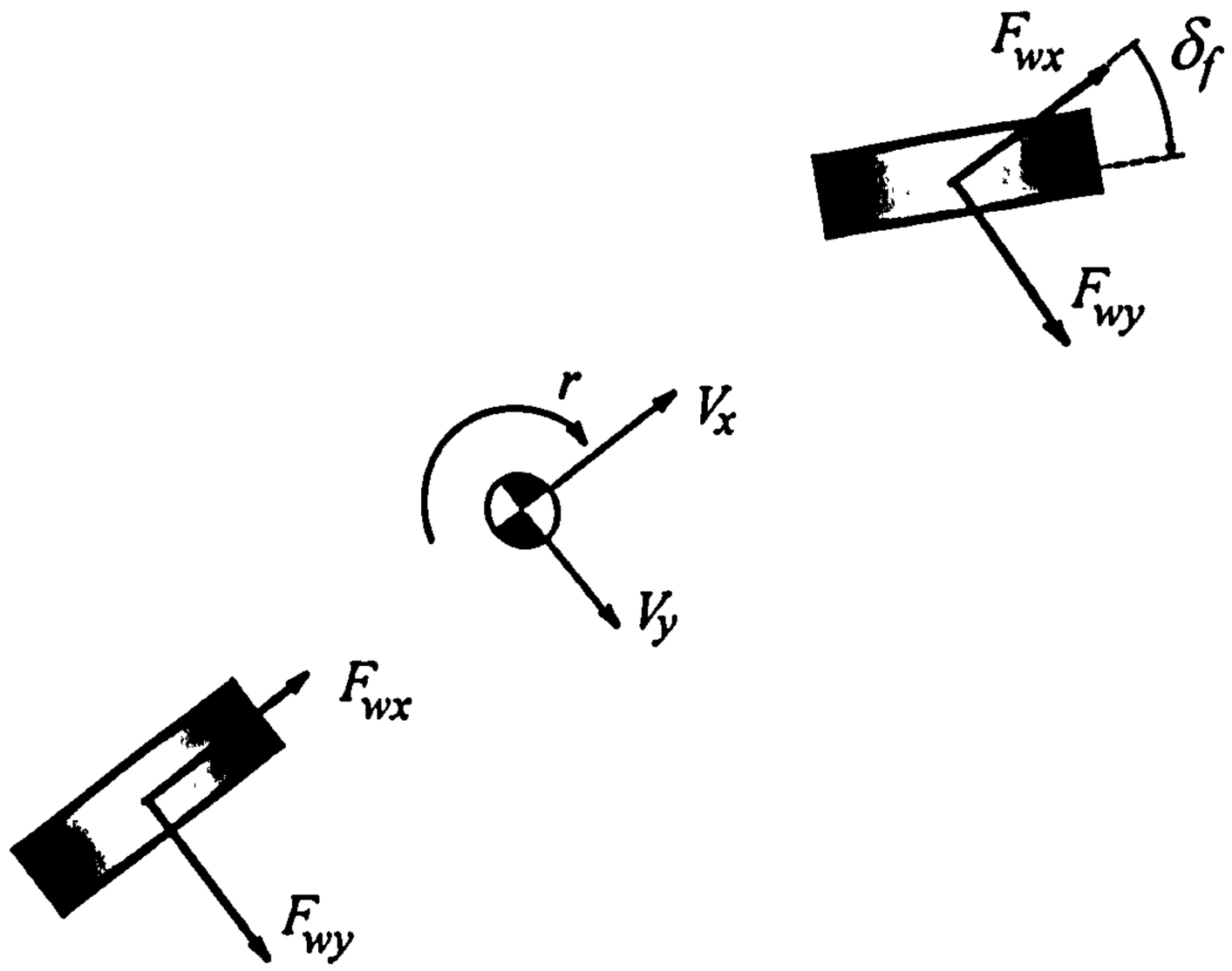

Fig. 1.3 Two wheel bicycle model

1.3.2 Ride Modelling

Ride modelling is often approached assuming a forward constant speed, hence ignoring effects of acceleration on the body. Again, the ride model is often dealt with as a linear model, operating about a specific loading, using a fixed spring coefficient. The complexity of the model can depend on what it intends to show, from a quarter vehicle up to full body. For the majority of ride models found in literature, wheels are dealt with as a point contact with the ground. Tyres are modelled as a spring (sometimes with a damper in parallel) and the suspension as a parallel spring/damper.

Ride is most often approached using a vehicle's frequency response (Crolla *et al.* 1996). The road input is dealt with as a spectral density, representing the road as a number of sine-waves of varying frequency and magnitude. For instance: hills have large amplitude and low frequency and the road surface itself has short amplitudes at high frequencies. By assessing the vehicle's suspension working space, dynamic tyre loading and vertical acceleration in the frequency domain with respect to an input spectral density representing a particular road type, it is possible to assess any frequencies that would be uncomfortable for the driver and also that could do damage to the vehicle.

When looking at basic vehicle handling on a road surface, it is usual for the ride characteristics to be ignored, likewise for investigation into such parameters as suspension working space and driver comfort, the handling is ignored. However, another area of interest,

especially in large vehicles is the phenomenon of vehicle roll-over. This looks at the vehicle roll during cornering, hence the handling and ride models need to be combined. This, however, is still only concerned with steady longitudinal velocity, and hence a full vehicle model is still not required.

1.3.3 Tyre Modelling

Given that all the forces that relate to vehicle handling and ride are transmitted to the ground through the tyre and vice versa, accurate modelling of a tyre's characteristics is an essential part of any vehicle-handling model. Methods of calculating the longitudinal and lateral forces associated with tyre/road contact and how these alter with the wheel-slip ratio, slip-angle and vertical tyre loading are an essential part of vehicle dynamics studies. The fundamentals of tyre behaviour and their impact on vehicle dynamics are dealt with in Pacejka (2002). Other quantities that are of importance include the tyres self-aligning moment and camber angle. The coordinate system adopted by the SAE is shown in (see figure 1.4). Without an accurate representation of the tyre/road interface, then any studies of the vehicle's dynamic performance are destined to be flawed.

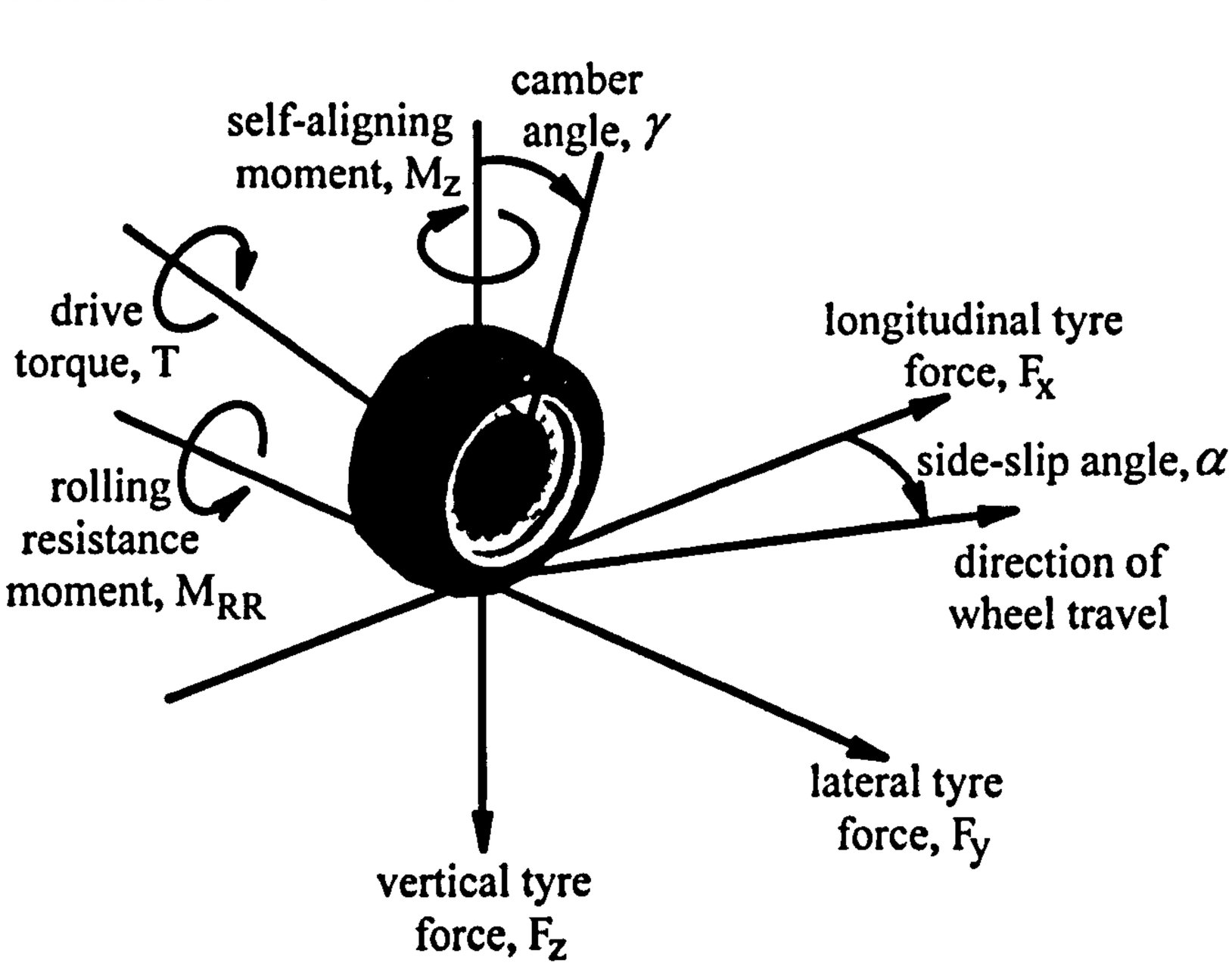

Fig. 1.4 The tyre co-ordinate system adopted by SAE

In Pacejka (1979) the general approach of developing a tyre model is presented. Tyre models can be separated into two forms: - empirical and physical. At the extreme end of physical modelling, where the tyres physical construction is described in great detail, its use becomes less accurate and meaningful for vehicle dynamic simulation. However, when purely

empirical methods are used, the model lacks any description of the mechanics of the tyre. The models presented are developed to match the on-road characteristics of the tyre. The off-road terramechanics are not considered.

Empirical Tyre Models

Empirical models are based on measurements taken from specific tyres. Sets of tyre data can be produced detailing a tyre's operating characteristics under a number of conditions. Unfortunately full sets of tyre data over a desired operating range are difficult to come by as manufacturers tend to only release data over a limited range, if at all. There are various methods by which models can take best advantage of this limited data.

Bakker *et al.* (1989) presents a compact empirical model which first introduced the "magic formula". This formula, depending on the coefficients chosen, has the capability of describing some of the important features of tyre behaviour, such as side force, brake force and self-aligning torque with great accuracy. It is noted that the equations become more complex when combined braking/cornering is undertaken, but results show that the formula are still accurate under such conditions. As it is an empirical model, the accuracy of these characteristics depends largely on the quality of the measured data. Although actual physical processes are not described, all the coefficients are physically meaningful quantities, which means, providing a good set of tyre test data has been collected, it is possible to determine the Pacejka co-efficients. The "magic formula" has become a well-recognised method of tyre modelling and has been expanded on and adapted by a number of researchers. Pacejka *et al.* (1997) later combined it with physical aspects of tyre modelling to provide an improved version of the tyre model. Dynamics of the actual contact patch are included, presenting a more accurate transient response.

Physical Tyre Models

Whereas empirical models rely on measured data and the relationships between characteristics, physical tyre models rely on the physical properties and transformations of the tyre. Various physical models exist, all varying in their complexity.

Dugoff *et al.* (1970) present an important tyre model specifically for use in vehicle handling models. Based on the physical transformation of the tyre as it passes through the contact patch and the forces created therein, it produces the lateral and longitudinal tyre forces from inputted data regarding wheel-slip, slip angles and normal load. Given that it is a physical model, all the coefficients of the model are recognised and easily altered to represent various

different tyres. The Dugoff tyre model has become a popular method of modelling tyres in vehicle dynamic studies due its relative simplicity and ability to accurately give both longitudinal and lateral forces. Although developed in 1970 it has remained popular in a host of literature for the past 30 years with few alterations made, showing the models validity.

A derivation similar to that of Dugoff's is offered by Szostak *et al.* (1988). Here lateral forces are produced using a spring analogy, within the contact patch, with deflection depending on slip angle, where as longitudinal forces are dependent on whether the tyre is in tension (acceleration) or compression (braking). The results are shown to be consistent with known tyre data. This method appears to be more complex that the Dugoff method, but each show equally good results.

Another physical model is the radial spoke method proposed by Sharp (1989) in which the tyre is separated into a number of radial spokes, each of which is able to deform laterally, longitudinally and circumferentially. The main drawback of such a method proved to be the means by which the spoke's stiffness co-efficients were chosen, this involved estimating values and then comparing simulated values for side force and aligning moments with physical data, until accurate values were found. Once correct values were found, the results achieved varied depending on the inputs, but were mainly good, although not entirely true to measured values. If a more effective method of deducing the parameters is found, the fact that the model itself is easily computed means this method has definite advantages.

Both the Pacejka and Dugoff tyre models are presented in more detail in Chapter 2.

1.3.3 Off-road Modelling

The tyre models mentioned above are all concerned with on-road tyre behaviour, where the road surface is considered flat. When a tyre interacts off-road with differing surfaces, road height and road friction co-efficient all vary constantly along with other attributes like the load-sinkage relationship and motion resistance. Variation in road height and size of the road tyre contact patch have an effect on forces generated and currently, no available tyre models can accurately model the full transient properties of an off-road tyre.

The field of vehicle response to various off-road conditions is known as Terramechanics (Wong, 1993). Modelling the terramechanics is a time consuming task and is still not an entirely accurate method of describing a tyre's behaviour on the various surfaces on which it is intended to model. Wong presents the various aspects of the tyre's interaction with an off-

road surface and various empirical and semi-empirical methods of simulation are shown (longitudinal responses only). One of the main attributes with a tyre moving on a soft terrain is the motion resistance associated with compaction of the soil. There are tyre models that simulate tyres interaction with soil, but they model purely in the longitudinal plane and so are of no use to handling models, such as the model presented by Maclaurin (1994). This is a tyre model that models longitudinal tyre force on soil, outputting rolling resistance and tyre force but due to the lack of lateral and combined tyre force, its use is limited.

Literature concerning off-road modelling with respect to handling is severely limited. Cooke (1996) presents handling manoeuvres of a vehicle when subjected to sinusoidal road surfaces of differing frequencies. The work is used to assess the impact of active suspension on both ride and handling. The vehicle's ride frequency response is initially modelled to see the effect on the vehicle's ride characteristics, then the handling response is modelled in the time domain while subjected to a fixed frequency road input. As can be seen, this is a very simplistic off-road model, ignoring the terramechanics, but at present it is perhaps one of the only viable ways of simulating off-road behaviour during handling manoeuvres. At present the only effective way of assessing a vehicle's off-road handling performance is through actual vehicle trials using subjective and objective data.

1.3.4 Simulation Packages

There are a number of simulation packages that are used to model vehicle dynamics. Some of these packages are general and some are developed with specific vehicles in mind. Perhaps the most widely used are ADAMS, VDAS, DADS, ADVISOR^{tm} and Simulink^{tm} although these packages are generally suited for different tasks.

ADAMS (MscSoftware, 2000) is a mechanical system modelling package that utilises user defined rigid bodies and interactions to simulate mechanical systems. ADAMS/car, ADAMS/chassis, ADAMS/driveline and ADAMS/driver are specialist packages that contain specific data libraries that can be used to simulate vehicle dynamics. DADS (Dynamic Analysis and Design Software) operates on the same principles. A vehicle model is developed in DADS by specifying the connectivity of various masses by springs, joints or bushes which are all supplied by DADS (Gunter, 1998). In both packages, equations of motion are automatically generated, so models can offer a great amount of detail without the need for absolute understanding of the dynamics involved.

VDAS is a software package developed at the University of Leeds, especially to model vehicle dynamics. It uses a lumped parameter approach, working with the lagrangian equations that are described by the user to simulate vehicle behaviour, the downside being that models are executed in code, leading to a less intuitive method of vehicle modelling.

ADVISOR[tm] is used to model a hybrid electric powertrain over a duty cycle to assess fuel economy and exhaust emissions. Models of all aspects of the vehicle powertrain are included however it does not include anything other than longitudinal vehicle motion with regards to vehicle dynamics.

One simulation package, not specific to vehicle dynamics modelling is Simulink[tm], that is a toolbox available for MatLAB®. Simulink[tm] allows complex models to be built up from simple building blocks (such as mathematical operators, sources, sinks or functions). Given its modular format, it is ideally suited for modelling and simulating vehicle dynamics. With the addition of control toolboxes, Simulink has became an industry standard for building complex, non-linear dynamic models and controllers.

1.4 Mobility Control

Mobility control deals with the handling and acceleration/braking performance of a vehicle, so that it performs excellently on all types of terrain and conditions. Any form of mobility control must be robust to cope with both external and internal parameter changes. The most common forms of mobility control dealt with in literature are Traction Control, Anti-lock Braking, Direct/Dynamic Yaw-moment Control and Active Steering Control (ASC), although the latter will not be presented due to the nature of the proposed vehicle.

1.4.1 Traction Control System (TCS)

Traction Control, sometimes referred to as wheel-slip control, has been of interest to the automotive industry for many years and is now present on a number of production vehicles. Wheel-slip ratio, λ (herein referred to as wheel-slip) is the relative difference in speed between the wheel and the vehicle, given be the equation 1.1.

$$\lambda = \frac{r_w\omega - V_x}{r_w\omega} \quad (1.1)$$

where r, ω and V_x are the wheel radius, wheel rotating velocity and longitudinal vehicle speed respectively. The available tractive force is a non-linear function of the wheel-slip, depending also on the road friction coefficient μ and also wheel slip-angle and vertical tyre load. (see figure 1.5).

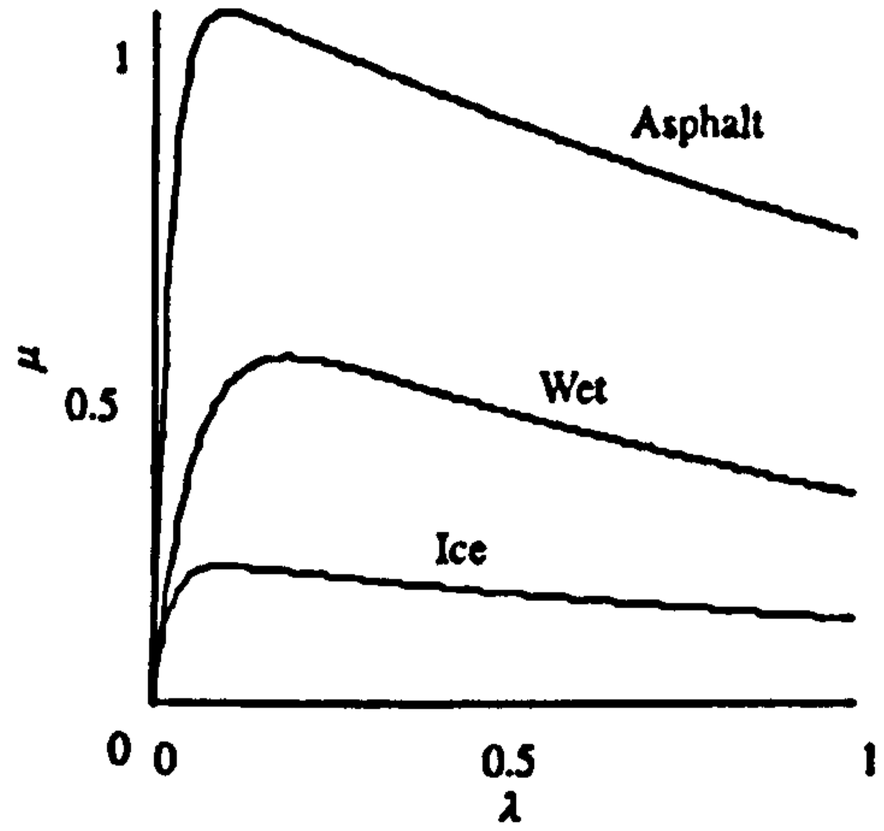

Fig. 1.5 Normalised tyre-road friction plotted against wheel-slip.

The aim of the majority of TCS is to maintain the wheel-slip at a desired value to produce maximum force, inducing adhesion between tyre and road (peak μ values in figure 1.5). The purpose of this is to improve both longitudinal and lateral tyre forces, leading to improved acceleration and lateral stability. This is done by altering the rotational speed of the wheel, which in turn is altered by the drive torque applied to the wheel. Depending on vehicle configuration, this can be done in a number of ways. In a conventional vehicle, the throttle angle, air-fuel ratio and/or spark advance can be adjusted to alter the output engine torque, this can then be distributed to each wheel equally or by the use of limited-slip differentials it can be divided out between the wheels. Also, the braking system is often utilised to reduce the drive torque at individual wheel stations. An EV or series HEV can implement it in much the same way, only the drive torque is altered by varying the current flowing through the electric motor. A series HEV utilising in-wheel motors has the advantage that torque can be altered at each wheel station individually, which is an ideal situation as it means that the controller can adapt left and right wheel torques allowing the vehicle to perform well on split-μ surfaces.

Conventional Vehicles

The various Bosch Anti-slip regulation systems are presented by Sigl and Demel (1990). These systems act in different ways and are optimised to control vehicle dynamics in various driving conditions. One system works to reduce wheel-slip by intervening in the driver throttle demands and to reduce the engine torque. If excessive wheel slip occurs the controller

also intervenes in the ignition system to dramatically reduce the torque (fuel injection is also suspended during this period when ignition is cut out) The Anti-Slip Regulator (ASR) system takes over from the driver to determine maximum allowable drive torque.

A particular method on controlling throttle is presented in Song and Byun (1999). A throttle actuator is controlled to limit the air passing through the throttle. This can be done in two ways, by using a single throttle valve, linked to the accelerator pedal by wire (Drive-By-Wire) such that the driver demands and those of the traction controller can be used to determine the best position for the throttle, the second is to employ two valves, one is mechanically linked to the accelerator pedal and a second is positioned using a DC motor controlled by the TCS. This paper presents the former of these two systems and shows accurate positioning of the throttle valve to control engine torque. A further paper by Song *et al.* (1998) presents the control algorithm for control of the engine throttle. The theory was evaluated on a test vehicle and the traction controller showed good results on a number of road surfaces. The controller also includes online estimation of road conditions where an initial slip controller is used to quickly decrease excess slip and to estimate the road friction coefficient, before the optimised controller comes into play resulting in a robust controller.

Another Bosch system presented in Sigl (1990) is the co-ordination of engine throttle control with brake control. Traction control systems generally work by two different methods, engine control or brake control and an amalgamation of the two. Brake control is used for initial control of drive torque due to the more rapid response where as engine control is slightly slower system but is easier to control.

This method is also approached by Jung *et al.* (2000) They implement a TCS on a conventional vehicle that also incorporates a directional stability system. The traction controller uses a predefined value of optimal slip that promotes good response from all road surfaces. Unfortunately this type of system does not offer optimal traction control as optimal slip varies depending on the road surface. The traction control is implemented by altering the throttle and the brake actuators using a form of sliding-mode control to maintain the desired slip. Brake activation time is kept to a minimum to reduce driveline wear, where as engine control is utilised for longer periods of time with no adverse effects, alleviating the need for lengthy brake activation. Results show effective longitudinal and lateral control in reduction of wheel slip and yaw moment control through activation of individual wheel brakes.

Bauer and Tomizuka (1996) propose two different fuzzy logic traction controllers. Both controllers utilise brake torque to control wheel-slip. The first of which attempts to estimate

the peak wheel slip and maintain the slip at this value during acceleration, and in the positive slope of the $\mu(\lambda)$ curve otherwise. This promotes good stability on all road surfaces. Fuzzy rules are based on the rate of change of μ and λ. λ can be deduced from wheel speed and vehicle speed and μ is estimated by measuring the acceleration of the vehicle. The system proves robust against constant uncertainties, but it does not respond well to time varying uncertainties, like load shifts or engine imbalance. This is due to the method of estimating $d\mu/dt$. If a more accurate method was implemented instead, it will be possible for the controller to adapt to time varying uncertainties, producing a more desirable performance. Also the method of deducing vehicle speed is prone to error.

The second fuzzy logic controller uses a predefined value for peak slip, which will guarantee good responses in all conditions (around 0.15-0.20). This controller is robust against all uncertainties and road conditions, although does not offer optimum performance on all road surfaces. By choosing a value of slip that lies in the positive part of the $\mu(\lambda)$ curve for the majority of road surfaces, stability is maintained and good acceleration responses are achieved. Both fuzzy logic controllers show promising results and due to the non-linear nature of wheel slip, they are ideally suited to the task and very robust.

Park and Kim (1999) present a TCS that focuses on the traction properties during cornering. Instead of focusing on wheel-slip, the slip-angle is of main concern, in order to increase lateral forces, hence improving the vehicles cornering performance. A way of balancing longitudinal and lateral force requirements is presented. Slip-angle is measured and if it is large, slip-ratio is reduced, increasing lateral forces. Although longitudinal forces will be reduced slightly, the increased cornering ability shows a large improvement in vehicle handling over conventional systems. This wheel-slip control is implemented through throttle control of the engine to maintain the desired slip-ratio. Due to its nature it could be classified as a form of dynamic yaw-moment control.

Cheok *et al.* (1996) present an in-depth fuzzy logic controller for traction control of a 4WD vehicle. Individual brake actuators are controlled depending on individual wheel-slips, throttle position and transmission output speed. These brake commands are then used as inputs to control throttle and gear selection. This two tier approach shows good control on split-μ surfaces. The main pitfalls of this controller is the lack of accurate vehicle speed measurements (mainly due to all wheels containing slip, hence speed of non-driven wheel is not available for determining of vehicle reference speed)

The development of an Active Traction Control system (A-TRAC) is the subject in Hosomi (2000). The system developed by Toyota is for an off-road 4WD vehicle which utilises independent wheel braking with an engine torque control system. The system has two operating modes, high and low range. In high range mode (on road and snow covered roads) the controller promotes a limited-slip differential (LSD) effect and stability where as in low range (rocky road, off-road) it has a locked differential effect to promote traction. The results show improvements over vehicle without A-TRAC and in the low range, over vehicles with central and rear diff-locks.

Electric and Hybrid Vehicles

Hori *et al.* (1998) propose two methods for implementing traction control on such a vehicle. One is termed Model Following Control (MFC) and the other is the optimal slip-ratio control. MFC involves a kind of speed control; the controller monitors the wheel speed, and compares it to a simulated model of the vehicle. When the wheel spins, there is a large increase in the actual wheel speed that is not present in the simulated wheel. The difference between the two is then fed back to the current command for the motor, hence decreasing torque, inducing re-adhesion. Although a primitive form of traction control, it works well to prevent wheels from severely skidding, though it cannot be used to maintain a desired slip to improve traction further. A large drawback of such a system and of MFC in general is its lack of robustness. For example, a change in load can dramatically alter the dynamics of the vehicle, hence negating the original model, reducing the effectiveness of the controller.

The second method offered by Hori *et al.* is a popular form of traction control, it involves determining the optimal value that the wheel-slip should take to produce the highest torque (the peak of the $\mu(\lambda)$ graph, see figure 1.5). In order for this to be done effectively both the wheel-slip and the peak tyre/road friction co-efficient must be deduced. The idea presented here requires the vehicle speed to be measured from the velocity of the non-driven wheel to deduce the wheel-slip (another method is required to deduce vehicle speed in an all-wheel drive vehicle). Using a PI controller, the actual slip is controlled so it matches the desired slip deduced by a road condition estimator (see below). Due to the fact that the desired slip is based on the road condition, this controller offers good results in all conditions aided by the quick responses of the in-wheel motors, as is shown in the results offered.

A TCS for an electric vehicle is presented by Yoshimura *et al.* (1997) using fuzzy reasoning. This system again takes into account the yaw rate and attempts to maintain a desired value by altering the torque's transmitted to the left and right tyres. This is a form of DYC (see section

1.5.3) The traction control offered here deals purely with the implementation of the controller itself and shows convincing proof that it helps reduce wheel-slip and offers excellent stability, even on split-μ surfaces. No reference is made as to how wheel-slip or the road-tyre friction co-efficient is measured.

Sakai *et al.* (2000) show a novel skid detection method which does not rely on knowledge of the vehicle chassis speed. It only requires the drive torque and wheel speed to be measured, which makes it ideal for implementation on an electric vehicle. Results show that the wheel slip varies around a predefined value. Although the method is valid for use in EV's it is a far from optimised form of traction control.

The idea that traction control will always result in an increase in vehicle acceleration is perhaps misleading of the nature of wheel-slip control. While in straight running the traction controller may indeed improve the vehicles acceleration, the main focus of traction control is preventing a loss of lateral stability. As the vehicle corners, the presence of the wheel-slip angle alters the position of the peak force with respect to wheel-slip until the peak longitudinal force may be at a wheel-slip close to one. However at this point, despite the increased longitudinal tyre force, the lateral tyre force is greatly reduced. Any controller that aims to maintain wheel-slip at the peak value for longitudinal force will adversely have an effect on the vehicles stability during severe cornering unless this effect is taken into account.

The main problems found with the implementation of wheel-slip control are the methods by which vehicle reference speed and the peak value of μ are found for the particular road surface the vehicle is travelling on. These two areas have become fields of research in their own right and are studied in section 1.5.

1.4.2 Anti-lock braking systems

The theory of ABS is similar to that of traction control. During braking, as in acceleration, it is important that the friction between the tyre and road is maximised, this will cause the vehicle to slow quickly and maintain stability. Locked wheels are a major problem; as the wheel speed verges on zero, the wheel-slip approaches negative one, causing the lateral tyre force to approach zero. This leads to vehicle instability and extended stopping distances. In order for wheel-slip to be maintained at its optimum level, the brake force needs to be regulated by varying the pressure exerted on the brake disc by the brake actuators.

Anti-lock braking systems have actually led to an increase in the number of accidents in equipped road cars (Austin and Morrey, 2000). This is mainly due to an increase in rear collisions where cars unequipped with ABS have a larger stopping distance than a vehicle in front equipped with ABS. Also a lack of knowledge about the nature of ABS has led to an increase in the number of accidents due to over compensation of steering during braking. The main benefits have been shown to occur in a reduction in pedestrian deaths as obstacle avoidance is one of the main benefits of ABS.

The ABS system put forward by Tsiotras and de Wit (2000) uses optimal control theory to realise the "maximum friction" approach. Like optimal wheel-slip control in traction control systems, the goal is to keep the wheel-road friction at a maximum. This is done by maintaining the wheel-slip at the point where $\partial f / \partial \lambda = 0$, where f is frictional force. Unfortunately, due to the transient nature of road conditions, to achieve the peak slip by this method is not entirely effective.

Kachroo *et al.* (1999) use Sliding-Mode Control (SMC) to maintain the wheel-slip at the desired value. Sliding observers and an extended Kalman filter are both used to estimate road conditions. The Kalman filter contains a steady state error, due to its prediction of the road condition. This error is derived from its estimation of vehicle speed. The sliding observer also contains a steady state error, although a much smaller one and the estimated vehicle reference speed is far more accurate. The results of the road condition estimation are comparable to those taken when actual vehicle speed is measured. A drawback of the controller is that it lacks robustness to cope with a large variation in road conditions. Given that the sliding observers are shown to provide accurate estimations of vehicle speed using only wheel speed sensors, this could prove to be a reliable method for vehicle reference speed estimation.

It should be noted that the ABS's mentioned above are not tested when lateral movement or yaw rate are present and so their effectiveness is still subject to further testing.

Kawabe *et al.* (1997) look at SMC of an ABS system applied to a medium sized truck with sluggish braking. A fixed desired value of 0.2 was used for wheel slip, so that good results were obtained on all road surfaces. Combined braking and steering was applied to the controller and the handling responses were much improved over conventional brakes. The problem of chattering of the SMC was also dealt with in order to stabilise the system. Although the optimal slip method was not used, the responses on a number of surfaces showed promising results.

The main problem facing the development of ABS is the estimation of optimal slip, a problem also seen in TCS. Although many solutions are offered, there still remains the downfall that wheel-slip needs to be accurately measured, which in turn requires the vehicle reference speed, a problem reviewed in section 1.5.1. In order for TCS and ABS to work at their full potential, these problems need to be resolved.

1.4.3 Direct Yaw-moment Control (DYC)

Also known as Dynamic Yaw-moment Control, its purpose is to aid stability during both straight line running and during cornering manoeuvres. By varying the torque applied at both left and right wheels (via motor control or brake actuation) yaw-moments can be created as described in figure 1.6. These can either be used to reject disturbances, such as a side wind in straight line running or to aid cornering. There are two particular strategies involved in DYC. The first is to maintain the yaw-rate at a desired value, the second it to improve safety at the limits of a vehicle's handling by placing boundaries on the vehicle's side-slip angle. An ideal control strategy will maintain desired yaw-rates at low and medium lateral accelerations, but limit the side-slip at higher lateral accelerations to maintain lateral stability. This offers an improved handling performance as well as increased vehicle stability and reduced driver compensation.

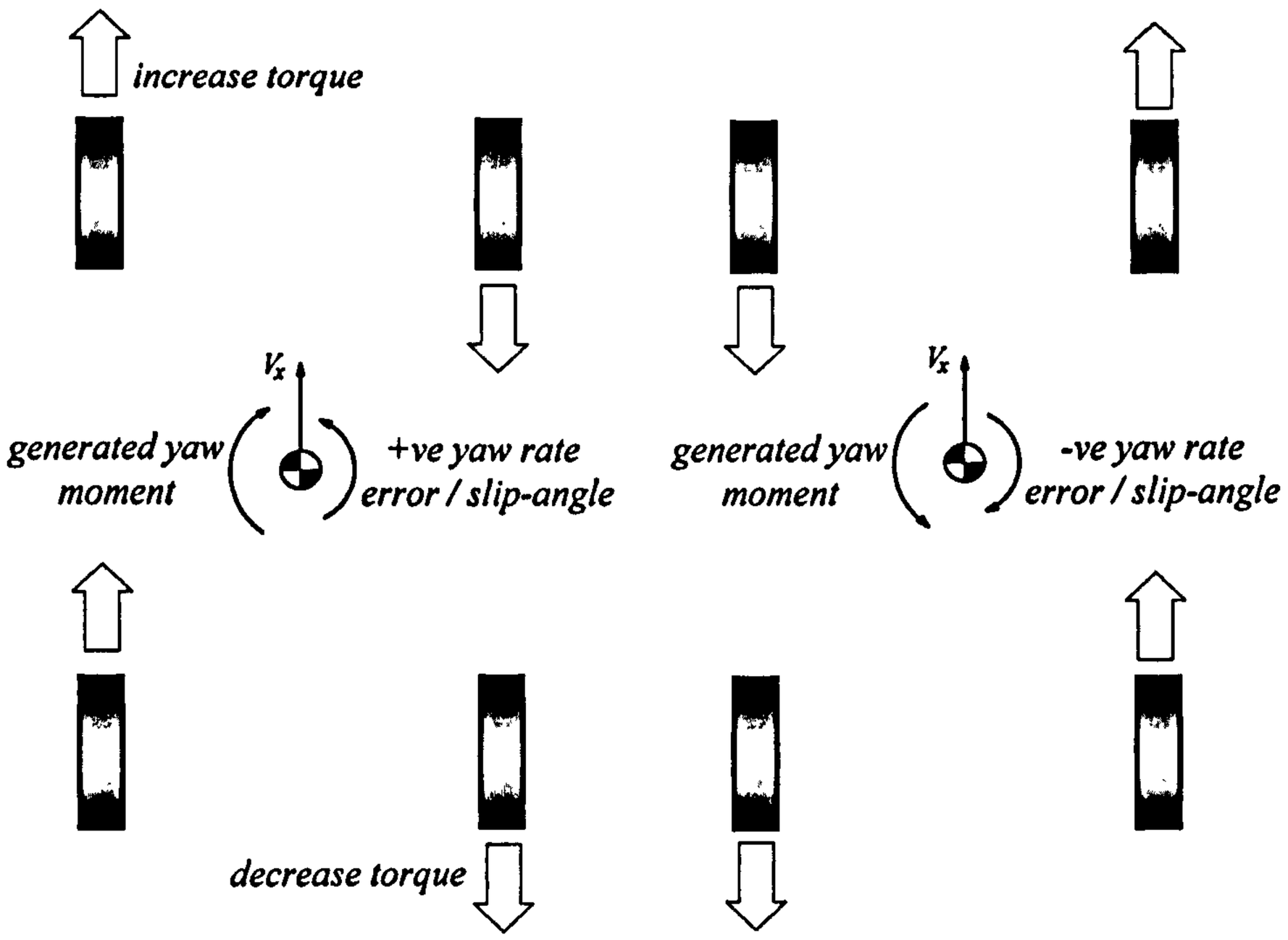

Fig 1.6 Operating principles of DYC

In conventional vehicles, two approaches to DYC have been utilised: the use of Limited Slip Differentials (LSD) or the use of differential braking. Although LSD's offer a passive way of effecting the vehicle yaw response, by utilising controllable LSD's a method of actively altering the vehicles yaw responses can be developed. However such a method is expensive and hence is only used in top of the range cars. The use of differential braking is a more cost effective way of implementing DYC and is apparent throughout the literature. By actively braking certain wheels, yaw-moments can be generated, although these may be at the expense of longitudinal velocity. To get full control of a vehicle yaw-rate, the use of independent electric drives is an ideal approach.

Conventional Vehicles

Nagai *et al.* (1997) use a Model-Matching Controller (MMC) to implement DYC and 4-wheel steer. Actual yaw-rate and slip-angles are compared to those of a desired vehicle model, and the torque applied to the wheels is varied accordingly. Although MMC often suffers from a lack of robustness, the system presented here is robust against all variations in vehicle parameters. When MMC was used for traction control (termed MFC in Sakai *et al,* 1999), changes in vehicle parameters alter the vehicles dynamics, hence altering the speed at which the vehicles wheels should be spinning. This means that the controller will be following a model that is no longer valid for the new parameters resulting in undesirable vehicle responses. For DYC the value that the vehicle is desired to follow, yaw-rate, is less dependent on model parameters, being determined primarily, by the drivers steer input. The DYC is expanded in Shino *et al.* (2000) where optimal control theory is included in the MMC in order to make the slip-angle at the vehicles centre of gravity zero using a feedforward and feedback compensation. The use of both of these methods makes the controller robust against external and internal parameter changes. The resulting controller provides excellent results during steady-state and transient cornering, yet it still remains a relatively simple control system.

Drakunov *et al.* (2000) proposed a yaw control algorithm implemented via SMC. By altering a control variable that represents the braking or driving force of the left and right wheels, the yaw-rate of the vehicle can be controlled so it is maintained at a desired value specified by the steering input, even while accelerating or braking. Because the vehicle's responses to the control input will alter due to road conditions and vehicle load, a robust controller is required. SMC is robust to parameter changes and hence represents a good choice for the control algorithm. Although no results are offered in the paper, it is reported that robustness problems were overcome and that satisfactory responses were achieved. If a less robust controller was

to be used, a method of measuring the road-tyre friction coefficient may be employed to satisfy the problems encountered.

Jung *et al.* (2000) use a simple method to alter the brake pressure on left or right wheels to control yaw-rate. Actual vehicle yaw rate is measured using the method mentioned below. Then the desired yaw-rate and lateral acceleration are calculated from steer angle. Taking the error of yaw rate and lateral acceleration, brake pressures are applied and DYC is achieved. One particular advantage of this system is that yaw-rate alone is not taken into account, as lateral acceleration is also maintained at a desired value, the vehicle will not drift away from its course while maintaining the desired yaw rate. The controller shows excellent responses when vehicle is driven on a split-μ surface and on normal cornering.

Electric and Hybrid Vehicles

A driver assist stability system for an all-wheel-drive electric vehicle is the subject of a paper by Tahami *et al.* (2003). Here, fuzzy logic control is used to implement both yaw-moment control and wheel-slip control, offering a full mobility control. Here the individual wheel demands from the yaw-rate controller are weighted by a value from the slip controllers. A desired yaw-moment is generated by a neural network. Results show good yaw-rate tracking and increased stability shown on breaking on a split-μ surface with accurate wheel-slip control. The controller shows the potential that can be gained from Individual Wheel Control (IWC) on a passenger car although the results are not shown with respect to changes in vehicle loading.

An electric vehicle with 4 independent electric drives is the subject of a paper by Esmailzadeh *et al.* (2003). Here DYC is implemented through optimal control theory to improve directional stability. Two controllers are developed to control the vehicles yaw-rate. One is a semi-optimal controller which is based on yaw-rate feedback and steer angle feedforward, the second is the fully-optimal control which in addition has lateral velocity feedback. The results show the full control to offer slightly better performance than the semi-optimal control, however, both show great improvements over the uncontrolled vehicle. As is the case with many of the papers concerning DYC, a simple bicycle model is utilised to develop the control, meaning the yaw–moment itself is the actual control input to the system. Although, no reference to the actual torque demands are presented, the maximum allowable yaw-moment is investigated with some reference to tyre forces, however the analysis is of very basic tyre-road interaction.

Saeks and Cox (1999) present a form of DYC on a series HEV, utilising a Neural Adaptive Controller to alter the power applied at each of the four wheels depending on input steer angles. The controller's performance is compared to a simple PID controller. The results presented show a great improvement over the PID controller on all road conditions.

Sakai *et al.* (1999) implement DYC on an electric vehicle with in-wheel motors, using a "Robust Model Matching Controller" (R-MMC). Although the controller operated well, comparing actual vehicle response to the desired vehicle response deduced from a vehicle model, the vehicle went unstable on a low friction surface due to the drive torque saturating, increasing wheel slip, causing both longitudinal and lateral tyre forces to reduce producing instability. The simplicity of the R-MMC is an attractive aspect of such a method, but unless its robustness is improved so it can cope with all conditions, its use is rather limited.

Park *et al.* (1996) also implement a form of DYC on an in-wheel electric motor powered vehicle. In this case DYC is combined with traction control in an "intelligent co-ordinated control system". Fuzzy logic is employed to estimate the cornering force from wheel-slip and wheel-slip angles. This is then used in the controller to produce input torques and steer angles. A neural network is used to compensate for modelling uncertainties and disturbances. Results presented show the controller is robust against modeling errors and disturbances such as varying road conditions and side winds.

The DYC controllers presented above, show the definite potential of the system to improve vehicle stability. This is particularly relevant for the vehicles equipped with IWC, which can fully realise the potential of this type of controller.

1.5 State Sensing and Estimation

As is noted above, in order for effective operation of traction, anti-lock braking and yaw-moment controllers, it is necessary that accurate measurements are made of the relevant parameters and where measurements are not directly available, estimates must be made. There are five parameters that are required to allow acceptable operation of the above controllers: wheel speed, vehicle reference speed, road friction co-efficient, yaw-rate and side-slip angle. Wheel speed is easily measured from readily available sensors, standard on any vehicle equipped with ABS. Vehicle reference speed, road friction co-efficient, yaw rate and side-slip angle require extra attention.

1.5.1 Vehicle Reference Speed Measurements

There are a number of solutions offered to this problem, although none are 100% effective. The most common method is to measure the angular velocity of the non-driven wheels, and knowing the effective wheel radius, the forward speed can be deduced. This is a reliable method, although it is less accurate during cornering and it cannot be used in the case of an all wheel drive vehicle. Another method is to use an accelerometer, integrating readings to get the vehicle reference speed (Kimbrough, 1996) or in the case of Automated Highway Systems, magnetic markers by the roadside can be used to measure speed from within the car (Kachroo, 1999).

In Tahami *et al.* (2003) a speed estimator is presented that uses fuzzy logic to determine the reliability of two different estimation methods. One comes from an accelerometer and the other from the estimated wheel slips (using the previous value of vehicle reference speed). No reference is made as to the accuracy of the method.

Bevly *et al.* (2000) proposes a method of determining vehicle speed through the use of the global positioning satellite (GPS) with an accuracy of 5cm/s. Both longitudinal and lateral velocities can be measured which can then be used to deduce wheel slip, yaw rate and wheel slip angles. Although they are subject to noise produced from satellite velocity, GPS velocity measurements (when available) still represent an accurate method of determining vehicle speed. A more accurate method is likely to involve a number of sensors. By utilising on board accelerometers and wheel speed sensors and combining with GPS readings, an algorithm for combining the relevant information can be developed. If done correctly, a more accurate value for vehicle reference speed can be estimated.

1.5.2 Road Condition Estimation

In order for the optimal wheel-slip to be measured for a particular surface it is necessary for the slope of the $\mu(\lambda)$ curve to be estimated. This can then be used to obtain the value of wheel-slip that will give the highest longitudinal tyre force and also give high lateral forces for steering. To do this, the road friction coefficient must be calculated.

One method offered by Ray (1997) uses an extended Kalman-Bucy Filter (EKBF) to estimate the state and tyre forces of an eight degree of freedom vehicle model using simple vehicle mounted sensors, from these resultant force, slip and slip angle estimates are made. These are then compared to several $\mu(\lambda)$ curves produced by an analytical tyre model (this can be taken

from off-line readings or by using a tyre model such as the one presented by Szostak) and the most likely value of μ is inferred. In order for such a system to work effectively, the analytical tyre model must be accurate for the specific tyre. The results achieved showed excellent identification properties under a variety of conditions, although tests were only conducted on asphalt surfaces, so conclusive validation of the system on all road surfaces is not offered.

Gustafsson (1998) uses a different method. Instead of estimating wheel-slips and forces, they are deduced from the velocities of both driven and non-driven wheels. As the $\mu(\lambda)$ curves are linear for low values of slip, if $F_d=\mu(\lambda)F_z$ where F_d represents the drive force of the wheel and F_z is the normal force of the wheel (which can be estimated), then the initial gradient of the $\mu(\lambda)$ curve can be derived (Note that estimating the torque supplied to the wheels from an ICE is a difficult technique). This can then be compared to the gradients of known curves for a variety of road types, and the correct value of μ is estimated. A draw back of the system is that in order for the gradient to be measured, a number of readings need to be taken, hence the driver needs to cause a fair amount of variation in wheel-slip values, which is not desirable in normal driving. Also it is necessary for the slip to remain in the stable part of the $\mu(\lambda)$ curve, which is not always possible.

The method offered by Sado *et al.* (1999) is similar to the one above, although due to its application on an EV, estimating the drive force is made simpler. The wheel-slip and driving force are derived from internal sensors, then the slope of the $\mu(\lambda)$ curve is estimated using a couple of identification algorithms; the Recursive Least Squares (RLS) and Fixed Trace (FT) algorithms. The FT method shows the better results, especially when variations in wheel-slip are small. This is often referred to as the gradient method. By determining the slope of the $\mu(\lambda)$ curve, the TCS can determine which side of the peak the wheel-slip is situated and act accordingly. An improvement on this theory is presented in Hori *et al.* (2000) where a method of locating the optimal slip through the use of fuzzy inference is proposed. This is reported to overcome the drawbacks of using the gradient method which suffers from the substantial decrease in gradient on the right hand side of a $\mu(\lambda)$ curve, hence it can take longer to detect the peak value of slip at higher slip values. The fuzzy method presented uses different strategies on either side of the curve and shows quick results.

Horowitz and de Wit (1999) presents a method for estimating road conditions from wheel angular velocity only. Results shown, demonstrate very good identification characteristics for a range of road conditions providing the wheel-slip is kept away from pure rolling conditions (zero slip).

As mentioned in section 1.4.1, one of the main drawbacks of all of these methods (with the exception of Ray, 1997) is that they assume forward running, when cornering, the presence of the wheel-slip angle alters the position and value of the peak longitudinal force with respect to wheel-slip and hence any method involving comparison to known $\mu(\lambda)$ curves must take this into account.

1.5.3 Yaw-rate and Side-slip Angle Estimation

In order for DYC to be implemented on a vehicle, an accurate method of measuring yaw-rate and side-slip angle is required. Fukada (1999) presents a method of accurately measuring slip-angle for use in Toyota's Vehicle Stability Control (VSC). Side force is determined by use of direct integration from a wheel force sensor and from a tyre force model. These results are then weighted and combined, depending on the non-linear state of the tyre model. Using dynamic equations, both yaw-rate and side-slip angle are then deduced. Slip angles are estimated for an automated highway system by Saraf and Tomizuka (1997) using lateral velocities at the front and rear axles. Lateral acceleration is measured using accelerometers and lateral position is measured using magnetic markers. From these, lateral velocities are estimated at the front and rear axles, and in turn slip angles are estimated.

In a paper by Hac and Simpson (2000) both yaw-rate and side-slip angle are estimated using steering angle, wheel speeds and lateral acceleration as inputs. Yaw-rate values are provided by using the difference in speed at the non-driven wheels and also from a lateral acceleration sensor. Each is given a confidence level depending on the operation of the vehicle, i.e. when the assumptions that allow the estimates are invalid, the confidence level in the relevant estimate is reduced. Finally the actual yaw-rate is produced dependent on an estimate of the road-friction coefficient. The results show good estimation of both parameters and appear robust to parameter variations.

Jung *et al.* (2000) includes a method on determining yaw-rate on their paper on traction control. It is proposed that the difference between the left and right non-driven wheel speeds be used to determine yaw-rate. Longitudinal wheel velocities are measured along with steer angle and assuming the effective tyre rolling radius can be calculated, the yaw rate can be estimated. A more accurate value is available when vehicle load changes are included. Results show the method to be accurate at low speed but highly inaccurate at high speed due to the effects of lateral acceleration. This provides a very simple method of estimating yaw-rate, although it does not have any application in All-Wheel-Drive (AWD) vehicles.

A yaw sensor that has been developed for use in the General motor's StabiliTRAK integrated chassis control system is presented by Madni *et al.* (1997). This sensor consists of a double-ended tuning fork made from crystalline quartz, which vibrates due to gyroscopic forces. The device is reported to be highly robust, cheap and reliable.

1.6 Individual Wheel Control

The area of individual wheel control is one that has received relatively little attention from automotive industry. Although limited-slip differentials offer a form of individual wheel control in conventional vehicles, the full benefits cannot be realised through this method. Limited-Slip Differentials (LSD's) as shown in figure 1.7 can separate the torque provided by the ICE between the two/four wheels, but if a large torque is required at one wheel, the torque available at another must be reduced, i.e. the total torque at the wheels cannot exceed that supplied from the ICE. In Holzwarth and May (1994) analysis of TCS augmented by Limited-Slip Differentials is given. Comparison of engine and brake traction control systems integrated with open differentials, the Torsen torque sensitive Limited-Slip Differential (LSD) and a viscous coupling speed sensitive LSD are shown. The use of torque sensing LSD's means that engine traction control can be as effective as braking traction control with open differentials. The advantage of such a differential is the ability to alter torques at each wheel regardless of wheel speed. Torque is always transferred to the wheel with the better traction so that traction force is not wasted on a wheel that cannot transmit it to the road. This gives more effective drive torque utilisation than an open differential where torque on both wheel is maintained to be almost identical, limited on both wheels to the maximum torque that can be supported by the drive wheel with the least traction. Another method of individual wheel control uses braking at each wheel station to vary the torque available at each wheel although this is not ideal as drive torque can only be reduced. To fully realise IWC, in-wheel electric motors are utilised. This means that it can be implemented in both electric and series hybrid electric vehicles.

A paper presented by Motoyama *et al.* (1993) shows the effect of left right toque split on both axles for a 4WD vehicle. Yaw-moment control is implemented through the identical left/right torque distribution in both axles. Multi-plate clutches are installed at all wheels to control the torque transfer. Results show improved handling behaviour over conventional 4WD systems. The paper also compares the relative effectiveness of both left/right and front/rear torque split, showing that left/right shows the greater potential for improving vehicle turning characteristics. With both simulation and actual test results showing good yaw-rate tracking

and increased turning limit, conclusions as to the effectiveness of such a system are well backed up.

A number of LSD's and torque split devices are presented in table 1.1. Their operating characteristics are shown along with their potential benefits.

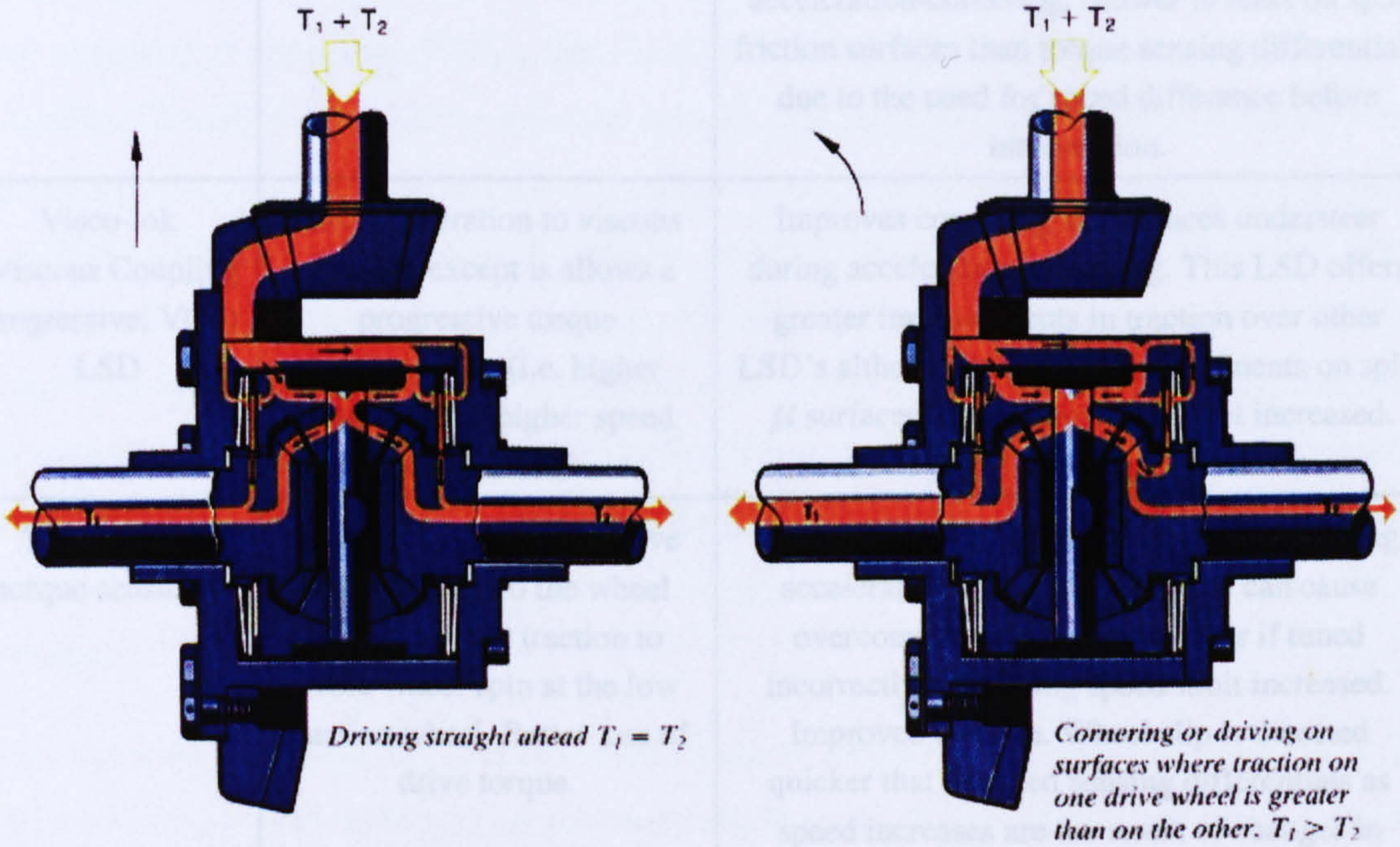

Fig. 1.7 Torque flow in limited-slip differentials (ZF Friedrichshafen, 1999).

The UOT March is an electric vehicle developed by the University Of Tokyo to demonstrate the improved mobility of a passenger car capable of individual wheel control. Sakai *et al.* (1999) implement the DYC on the vehicle and the potential of the system is mentioned in section 1.5.3.

A series HEV with IWC is the subject of ongoing work by Lyshevski *et al.* (2000). At this stage mobility control has not been dealt with, the research focusing mainly on powertrain design and control. It is the authors' belief that the proposed direct-wheel-drive configuration will offer improved mobility, driveability, manoeuvrability, agility and controllability as well as the potential of increased efficiency due to the removal of the transmission.

It is noted that the potential of individual wheel control is dependent on the methods by which it is controlled. In order to weigh up the advantages of IWC, the increased performance due to TCS, ABS and DYC and their integration with IWC needs to be assessed and compared to that of a conventional vehicle (fixed torque distribution).

Torque split device	Operation	Potential improvements in vehicle dynamics and notes.
Viscous coupling (speed sensitive) LSD	LSD works to rectify speed difference between wheels (i.e. torque transferred from faster wheel to slower one.)	Improved traction. Slight understeer effects in cornering due speed difference between inner and outer wheels. Cornering speed limit increased. Reduces understeer during acceleration-cornering. Slower to react on split friction surfaces than torque sensing differentials due to the need for speed difference before intervention.
Visco-lok (Viscous Coupling Progressive, VCP) LSD	Similar operation to viscous coupling except is allows a progressive torque characteristic (i.e. higher torque bias at higher speed differences)	Improves cornering and reduces understeer during acceleration-cornering. This LSD offers greater improvements in traction over other LSD's although increased yaw moments on split μ surfaces. Cornering speed limit increased.
Torsen LSD (torque sensitive)	A larger proportion of drive torque is sent to the wheel with the better traction to avoid wheel spin at the low traction wheel. Better use of drive torque.	Greater reductions in understeer effect during acceleration while cornering but can cause overcompensation and oversteer if tuned incorrectly. Cornering speed limit increased. Improved traction. Wheel slip is detected quicker that in speed sensing differentials as speed increases are the result of changes in torque.
Electro-pneumatic LSD (E-LSD)	Speed sensing differential with the ability to limit the operation of the differential.	Designed for larger vehicles, it's main purpose is to suppress weaving during straight running high speed but also improves handling stability.
BCDiff LSD (torque sensitive)	Operation similar to that of Torsen system except gears are replaced by balls. The system is said to have increased control over torque bias.	BCDiff is said to have improved properties over the Torsen torque sensing differential. If this is the case, the advantages mentioned above will also prove true for this system. It is also more compact than the Torsen system.
Honda ATTS	Acts as a controllable differential. Hydraulic system controls distribution of driving force through wet, multi-plate clutches. Torque split is up to 80:20	Provides improved cornering during acceleration and braking. Improved traction during cornering gives "on-the-rail" feel. Reduction in torque steer in FWD vehicle. Improved vehicle stability.
Haldex traction Limited-slip Coupling (LSC).	Works as speed sensing LSD with fully controllable torque transfer characteristics.	Improved dynamics during acceleration and deceleration. Improved high speed stability and vehicle manoeuvrability. Adaptive to vehicle condition and speed.

Table 1.1 Comparison of a number of limited-slip devices

1.7 Summary

Although the literature reviewed above covers a wide range of subjects, the main focus of the material centres on the vehicle mobility control options. Despite the vast sum of work that has been conducted in the field of hybrid-electric vehicles, there has been little utilisation of the technology in the area of off-road vehicles, work to date centring mainly on passenger cars and commercial transport. Within the field of HEV configurations lies the prospect of Individual Wheel Control. On an off-road vehicle, IWC should greatly improve mobility and handling performance as well as reducing drivetrain complexity. As predicted by Lyshevski *et al.* (2000), IWC has the potential to improve mobility, driveability, manoeuvrability, agility and controllability. Judging by the work that has already been conducted on vehicles with in-wheel electric motors (Hori *et al.*, 2000 Park *et al.*,1999) the potential is there and can offer improvements in handling and vehicle stability. Tahami *et al.* (2003) show that the potential of IWC is there for a 4WD vehicle with electric drives and that co-ordination of wheel-slip control and yaw-moment control can lead to greater vehicle stability in various driving conditions.

From the work reviewed, the field of mobility control focuses on three distinct systems, TCS, ABS and DYC. All of these rely on accurate vehicle speed measurements and the two former systems require accurate prediction of the road/tyre friction co-efficient to determine the optimal wheel-slip. Due to the difficulty in estimating the latter with any accuracy and speed, it is often more beneficial to use a predefined value for optimal wheel-slip that will provide a good response on all surfaces, a method adopted in the papers by Jung *et al.* (2000) and Bauer and Tomizuka (1996). Although optimal traction / braking control will not be achieved, performance should still show an improvement over a vehicle without these mobility controllers and show the validity of the systems. The area of DYC represents another method of improving vehicle performance and safety. Its implementation is best suited for vehicles utilising in-wheel motors. DYC is often implemented in conjunction with traction control systems by incorporating yaw-rate measurements into the traction control system as done by Yoshimura *et al.* (1997), providing an overall directional stability.

In order to implement and test mobility control systems in vehicle simulations, it is vitally important that the vehicle dynamics are accurately modelled. It is essential that an appropriate tyre model be chosen such that accurate longitudinal and lateral forces are simulated, which will be used to model the vehicle performance. The majority of the literature covered has opted for either Pacejka's "Magic Formula" or Dugoff's physical model. Both models are

extremely important in the field of vehicle dynamics and they have received extensive attention from researchers. The most suitable may be decided by the tyre data available or the proposed use of the model. Both show sufficient accuracy to provide the desired precision needed for the modelling of vehicle dynamic, however the Pacejka model is more accurate in limit conditions and also represents the self-aligning moment.

The dynamics of the body and suspension are equally important, although the latter can often be ignored for the analysis of basic handling characteristics. From the literature most systems are implemented on models with fewest possible degrees of freedom that can be used to model the desired vehicle motion. A number of TCS's are implemented on quarter vehicle models, where as bicycle models are often used for handling analysis when implementing DYC.

1.8 Objectives

With the prospect of greatly improving vehicle mobility and performance, this project will be concerned with the development of control systems that can be implemented on a 6x6 HEV with IWC with the view to fully realising the potential such a vehicle presents.

As the case study vehicle utilises IWC, it can, from the point of view of any mobility controller, be viewed as an electric vehicle. Due to this de-coupling of the powertrain and the drivetrain, the vehicle can be separated into two different systems: the electric drivetrain providing torque to the wheels on which mobility control is implemented, and a power generator system that deals with energy supply and storage. This thesis will deal with the former of these two systems. It will be assumed that any power demanded from the powertrain can be delivered either immediately or with a slight delay.

With the aim of proving the potential of IWC, the thesis has the following four objectives:

1. To derive detailed vehicle models, representing the proposed vehicle in sufficient detail, that simulation results will correspond with the limited results obtained from field test data.

2. To develop robust mobility control systems that will improve vehicle handling, braking and traction characteristics and to analyse and propose a method of co-ordinating the mobility control algorithms, with the goal of implementing an overall intelligent mobility control system.

3. To optimise the controller for the vehicle such that the case study vehicle can offer improved handling, acceleration and braking performance over the existing conventional DERA 6x6 CSV.

4. To assess the benefits of Individual Wheel Control with respect to on-road (and to a limited extent off-road) handling and vehicle stability.

The final of these objectives can be split into two sections. Firstly, the benefits that can be gained through control of IWC on the hybrid vehicle itself, as compared to fixed torque distribution, and secondly, the benefits that are gained from the vehicle as opposed to a conventional vehicle with a mechanical transmission such as the QinetiQ CSV.

If all these objectives are met it is possible that the system could be implemented on a research vehicle leading to further validation of both the vehicle dynamics model and the implemented mobility controllers. The use of these controllers should help bring to light further advantages that can be gained from the implementation of the hybrid-electric drivetrain, aside from better fuel economy, range and emission reductions.

Chapter 2

Handling and Single Wheel Modelling

2.1 Introduction

Chapter 1 has presented an overview of the work conducted in both vehicle dynamics and mobility control. This chapter will commence with an introduction to the proposed vehicle and also the various test manoeuvres that are used for assessing vehicle handling performance in the time domain. An investigation into the fundamental handling behaviour of the vehicle through development and analysis of a linear bicycle handling model will then be conducted. This is in order to be familiarised with the handling characteristics that can be expected from a large six-wheeled vehicle.

Next, in order for mobility control strategies to be investigated, there is a necessity for the relevant vehicle dynamics to be described. In this chapter, the initial vehicle models are developed. The nature and complexity of the models will depend entirely on the aspects of vehicle motion that the controller intends to affect. For instance, as Traction Control and Anti-lock Braking Systems are mainly concerned with longitudinal wheel-slip and forward vehicle velocity, a single wheel model is sufficient for development of these controllers. Although acceleration and braking cause other changes in the vehicles motion, such as vehicle pitching and load transfers, they can be ignored at this early development stage, as their effects are of a lower consequence. This model will utilise the Dugoff tyre model (Dugoff *et al.* 1970) which has been shown to be accurate at low and mid lateral accelerations (less than 0.4g)

With regards to developing a yaw-moment controller, it is the vehicle's yawing motion that is of primary concern. In a great deal of papers dealing with yaw-moment control, a simple bicycle model is used and the controller outputs yaw-moments as opposed to the torque demands at each wheel which lead to the development of yaw-moments. In this respect, the lateral and longitudinal tyre forces are important for developing yaw-moments and so are to be included in a basic non-linear handling model which will be developed as shown in figure 2.1. It is on this model that all DYC and co-ordination work will be undertaken as it is of the necessary detail to exhibit the controllers potential performance. This model utilises the single wheel model mentioned above at each wheel station with torque commands for each wheel delivered from the driver and eventually the controller itself.

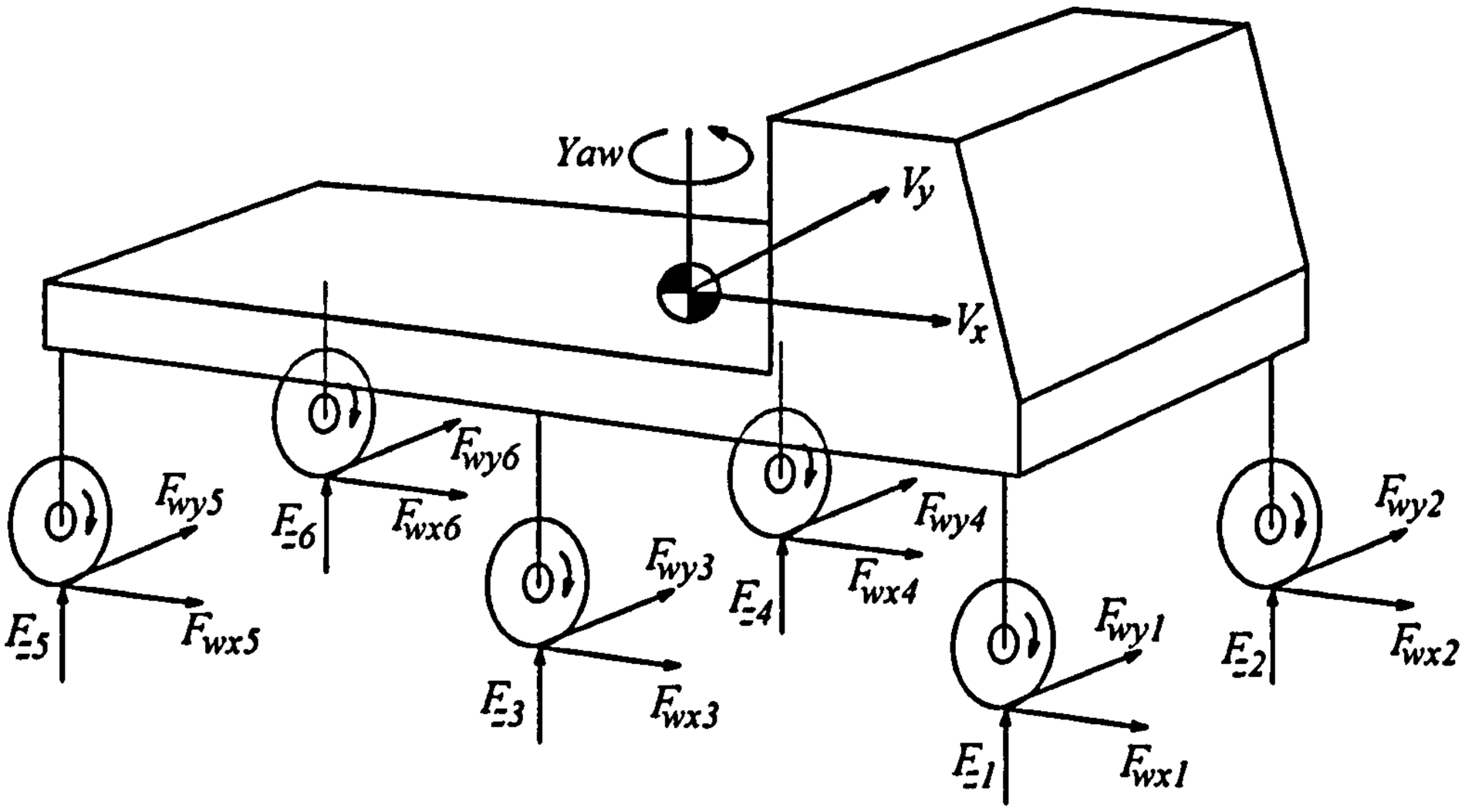

Fig. 2.1 Basic vehicle co-ordinate system

2.2 Vehicle Specifications

The theoretical Hybrid-Electric Vehicle that is the subject of this thesis, is based on an existing Combat Support Vehicle developed by QinetiQ (formally DERA). The proposed vehicle is an eight-tonne, six-wheel-drive, four-wheel-steer hybrid electric vehicle. The four-wheel-steer mechanism is mechanical and hence not a potential area for control. The purpose of basing the vehicle on the existing 6x6 is the ability to validate the model against actual vehicle data collected from the CSV trials conducted by DERA. It also provides a bench mark upon which to compare performance. Although a 6x6 is being used as the initial vehicle platform, the control system will be applicable to any all-wheel-drive vehicles with Individual Wheel Control (IWC) with minimal alterations and parameter tuning

The configuration of the proposed vehicle is a series hybrid with in-wheel motors at each of the six wheel stations. This allows the vehicle to be separated into two distinct systems, a power generation unit and an electric drive-line. If the assumption is made that any power required at the motors is deliverable by the powertrain then for the purposes of controlling the vehicle dynamics, only the electric drive-line need be modelled.

The actual operation of the motors is ignored, and instead a torque-speed curve is used to determine the maximum torque that is available for a particular wheel speed. The Hub-Mounted Electric Drives, developed by QinetiQ and MST have a torque-speed curve as shown in figure 2.2 (Thompson, 1999). There is little need to accurately model the motor's operation as current control of motor torque is reasonably accurate. Instead, the HMED torque-speed curve is used to characterise its operation, imposing a peak power rating of

100kW and a constant power rating of 50kW. By utilising the torque-speed characteristics of the motor, it is possible to determine the maximum torque at any given wheel speed. This is used to limit the driver torque demands and also those made by the proposed mobility controllers. A limit is also placed on the drives preventing the rate of torque from changing too quickly. This rate-limit allows the wheel to reach full torque in one second which was the value specified by QinetiQ.

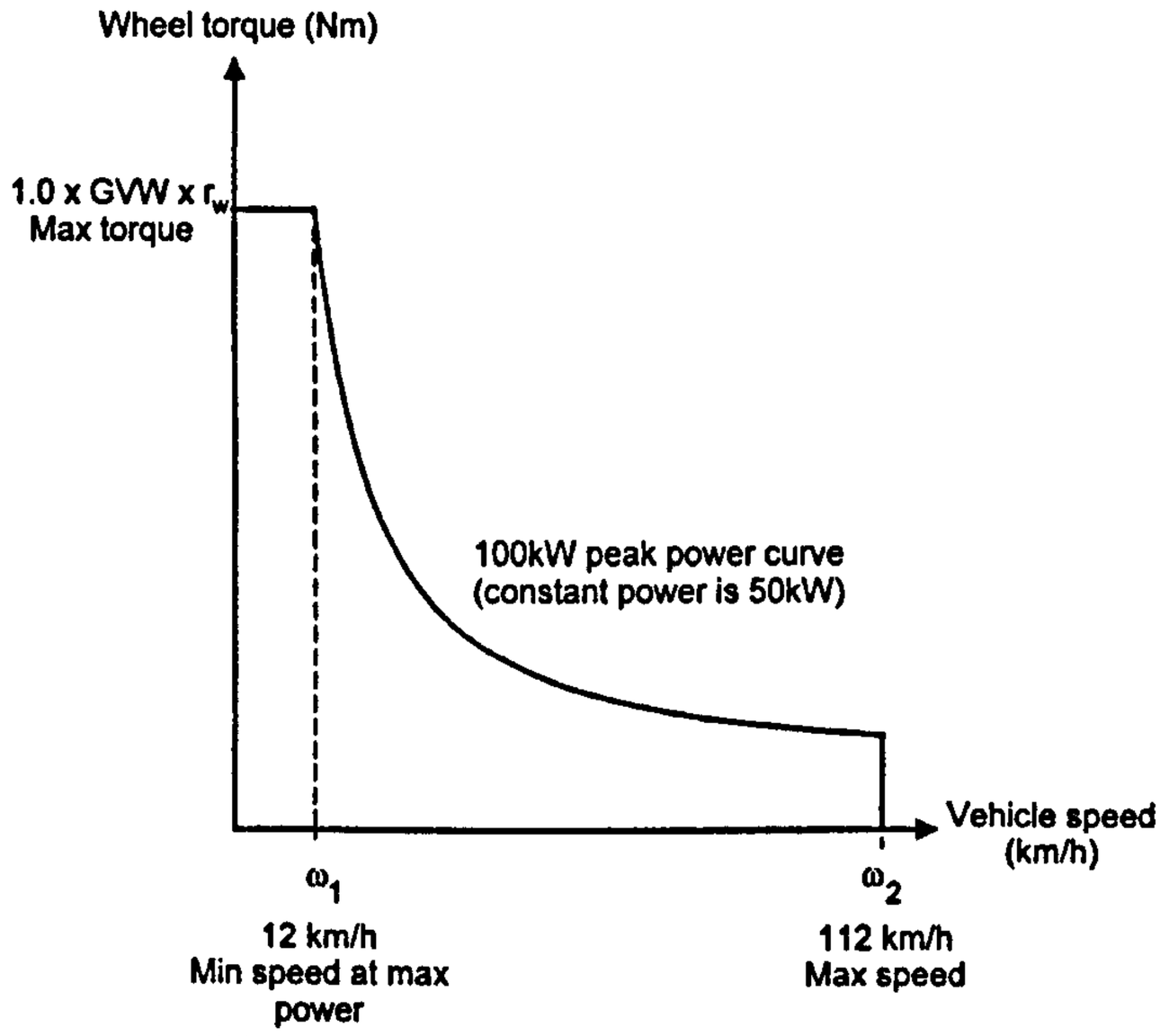

Fig. 2.2 Torque-speed curve for HMED

2.3 Test Manoeuvres

There are a number of test procedures that can be simulated to determine the effectiveness of a particular control system. By assessing the relevance a procedure has to a particular controller, the validity of that controller can be more efficiently evaluated. The following represents time based analysis of the vehicle. Along with these time based test procedures, the frequency response of a vehicle is often of interest, especially with regards to vehicle ride, however its use for assessing handling is limited as the results are difficult to interpret and are of limited use in assessing benefits of controllers. Here are a number of test procedures that can be utilised, used commonly for vehicle testing:

Lane-change

Simulating the response of a vehicle to a lane-change, is a good way of determining the stability of a system at various speeds. It consists of a positive steer angle followed by a negative steer angle to simulate the changing of lanes on a motorway (see figure 2.3). Yaw-

moment control will have the most effect on lane-changing, due to its function being to maintain the yaw-rate selected by the vehicle speed and steer input. A lane-change procedure is specified for passenger cars in ISO-3888 (1994). A double lane-change is often used in literature along with the standard single lane change.

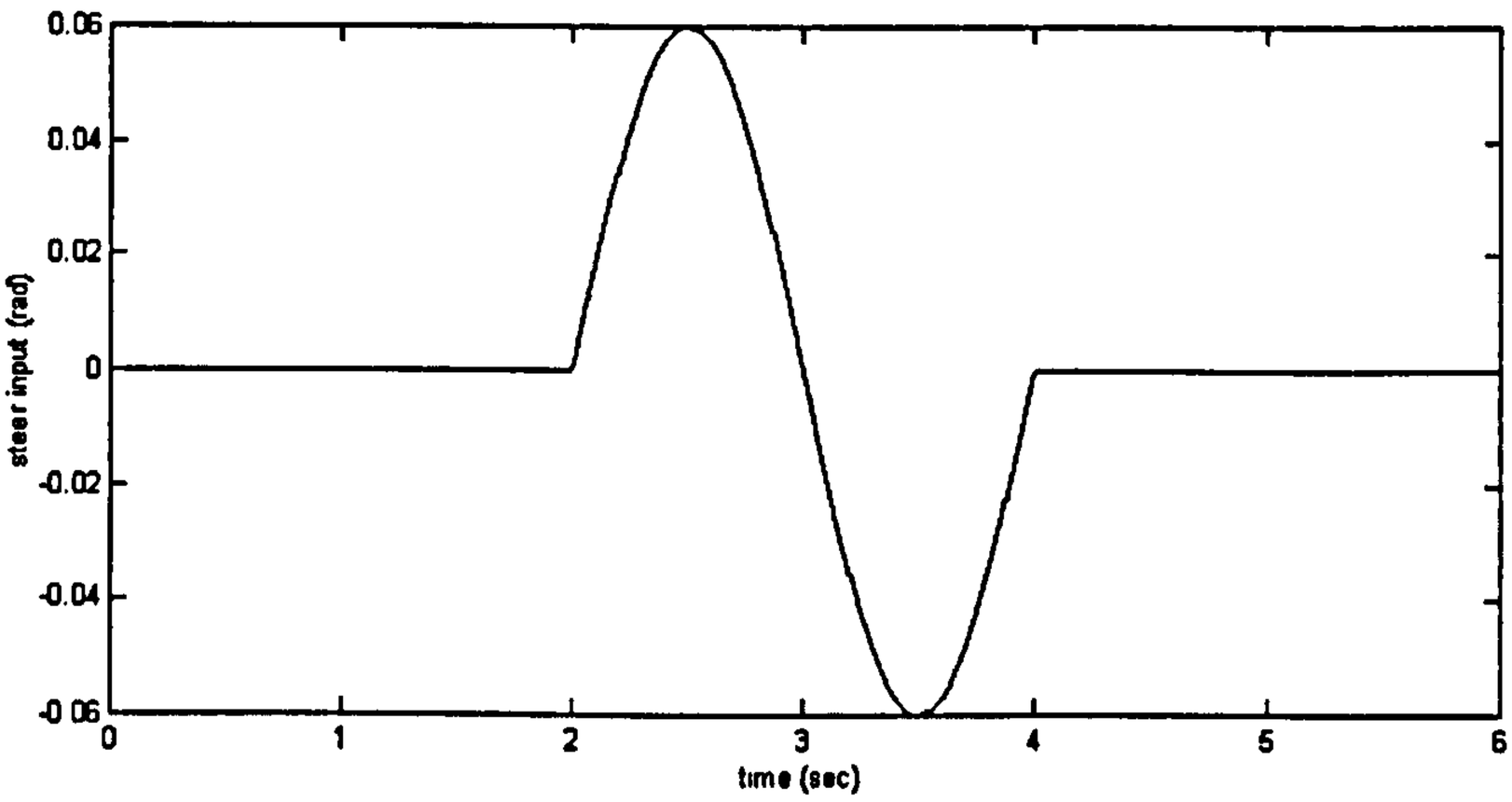

Fig. 2.3 Steer input to lane change manoeuvre.

J-turn

The J-turn is a simple cornering procedure that consists of straight running at a constant forward speed for a set time before commencing a turn that eventually results in a steady-state turn. A test procedure for the steady-state turning of a heavy vehicle is presented in the SAE standard J-2181 (1998). The steering input for a J-turn manoeuvre is shown in figure 2.4.

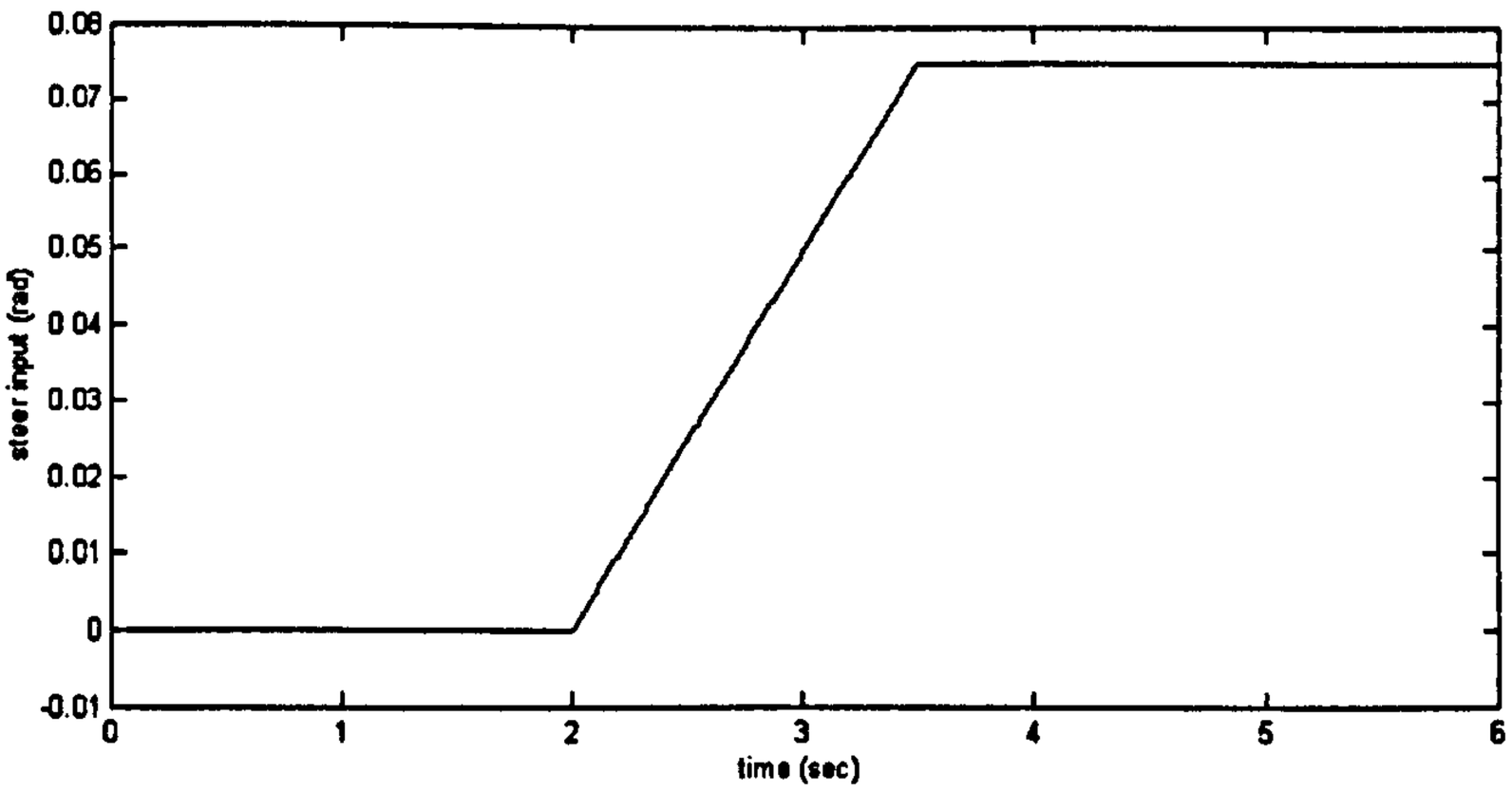

Fig. 2.4 Steer input to J-turn manoeuvre.

Acceleration/Brake Tests

For the purpose of proving the traction controller, acceleration tests can be conducted on a number of simulated road surfaces. Acceleration times on low friction surfaces should be improved through the introduction of traction control. The performance of an ABS controller is assessed by simulating the stopping distances given by each control method.

Split-μ Surfaces

By testing the vehicle reactions to a split-μ surface it is possible to assess the effectiveness of all the mobility systems. When a vehicle traverses a split-μ surface, where the peak drive force and slip are different for left and right wheels, optimum acceleration/brake responses are not achievable without some form of traction control. TCS should alter the speed at which a slipping wheel spins in order to maintain high longitudinal and lateral tyre forces. As is the nature of split-μ roads, the maximum drive torque available at left and right wheels will differ, this can result in a yaw-moment being produced causing the vehicle to yaw undesirably. DYC can be implemented to combat this and maintain forward vehicle motion. The interaction of the DYC and TCS/ABS will need to be considered as both vary the torque applied to each wheel.

Combined Cornering and Acceleration/Braking

Testing the vehicle on a number of these procedures should be sufficient to validate the implemented mobility control algorithms and IWC. By performing J-turn or lane-change manoeuvres while accelerating or braking, the performance of all the mobility systems can be assessed.

Stability Tests

The vehicle travelling at constant forward speed is subjected to a sine-wave input of increasing magnitude. The controller will aim to increase the vehicle's ability to follow this value up to a point where the uncontrolled vehicle becomes unstable at which point the controller should prevent vehicle instability.

Disturbance Rejection

The vehicle is set to run in a straight line at a desired speed, it is then subjected to a side wind that will produce a yaw-moment. Normally it is the job of the driver to respond to this disturbance by altering the steering angle. Through the implementation of DYC, the yaw-rate should be maintained at zero, stabilising vehicle motion with minimal driver intervention.

	Lane Change	J-Turn	Accel tests.	Brake tests	Split-μ surface.	Cornering/ acceleration tests	Cornering/ braking tests	Stability Tests.	Disturbance rejection tests.
TCS	0	0	+ +	0	+	+	0	0	0
ABS	0	0	0	+ +	+	0	++	0	0
DYC	+ +	+ +	0	0	+ +	+ +	+ +	++	+ +

+ + = Extremely relevant + = Of some relevance 0 = Of little relevance

Table 2.1 Relevance of control systems to test procedures.

Due to the nature of some of the test procedures, it is not necessary to test all three mobility controllers on each one. In table 2.1 all the test procedures are presented and their relevance to the three control options is assessed.

If control systems are optimised for one particular test procedure, their performance may suffer on other procedures. As the vehicle will be required in normal operation to perform on all test procedures, the controllers should operate well in all conditions although their operation will be tailored to suit specific applications. i.e. although acceleration responses are the prime concern of the TCS, the controller not should adversely effect the vehicle during lane-change or J-turn manoeuvres. Looking at table 3.1, it is important that all the control systems are optimised for procedures in which they have relevance.

Off Road Test

Given the nature and use of the proposed vehicle it is essential that the controller is valid, even when the vehicle is off-road. However, it is not possible to accurately model a vehicle's handling responses in off-road conditions. The only real way of effectively testing off-road behaviour is by use of an actual vehicle using subjective and objective data. As this vehicle is primarily an off-road vehicle, off-road simulation cannot be ignored entirely. A simulated terrain consisting of varying μ values and ground heights should be sufficient to make an initial assessment of the vehicles off-road behaviour. It must, however, be noted that any conclusions drawn from such simulations are of limited use and cannot be taken as proof that the vehicle will perform in such a manner on a real off-road surface. The actual terramechanics are ignored for the sake of simplicity, but due to the off-road nature of the vehicle, it is paramount that performance on this type of surface is stable.

2.4 Tyre Modelling

As mentioned in section 1.2, the most important aspect of vehicle dynamics modelling is accurate representation of the tyre properties. The tyre/road interface is where the vehicle's longitudinal, lateral and yawing motions are developed. Forces are also transmitted vertically through the tyre. From literature, two tyre models have received the majority of the attention when used in vehicle dynamics simulation: the Dugoff and the Pacejka "magic formula" models. Here, both models are presented.

2.4.1 Dugoff Tyre Model

The Dugoff tyre model is a steady-state, physically based tyre model that can evaluate combined lateral and longitudinal tyre forces. Values representing the cornering and longitudinal stiffness' at a specific tyre loading are used, hence the tyre behaviour is not fully transient, only representing operation around a static loading point. The tyre model formulas are based on those provided by Huh *et al.* (2000) which have been derived from Dugoff's formulas presented in Dugoff *et al.* (1970). It should be noted that in the work presented by Huh, equations modelling wheel-slip show the following conditions:

$$s_i = \begin{cases} \dfrac{r_w\omega_i - V_x}{r_w\omega_i} & \text{if } r_w\omega_i \le V_x \quad \text{(in acceleration)} \\ \dfrac{V_x - r_w\omega_i}{V_x} & \text{if } r_w\omega_i > V_x \quad \text{(in braking)} \end{cases} \tag{2.1}$$

The inequalities shown appear to be incorrect. The nature of wheel-slip in acceleration is such that wheel speed, $r_w\omega_i$ is greater than or equal to vehicle speed, V_x, not vice versa as presented. In the literature, a number of different definitions of wheel-slip are presented. Although all are presumed to offer desired results required by the model into which they are implemented, the use of a number of these in the Dugoff model gave inaccurate responses. To avoid confusion, the following are utilised in the model to calculate wheel slip, which are the definitions proposed in the Dugoff paper and hence behave correctly in the Dugoff model:

$$s_i = \begin{cases} 1 - \dfrac{V_x}{r_w\omega_i} & \text{if } r_w\omega_i \ge V_x \quad \text{(in acceleration)} \\ 1 - \dfrac{r_w\omega_i}{V_x} & \text{if } r_w\omega_i < V_x \quad \text{(in braking)} \end{cases} \tag{2.2}$$

The Dugoff model uses the following equations:

$$F_{wx} = \frac{C_\lambda \cdot \lambda}{1-\lambda} \cdot X(2-X) \tag{2.3}$$

$$F_{wy} = \frac{C_\alpha \cdot \tan\alpha}{1-\lambda} \cdot X(2-X) \tag{2.4}$$

Where:

$$X = \frac{\mu F_z (1-\lambda)(1-\varepsilon_r) V_i \sqrt{\lambda^2 + \tan^2\alpha)}}{2\sqrt{C_\lambda{}^2\lambda^2 + C_\alpha{}^2 \tan^2\alpha}} \tag{2.5}$$

$$X = \begin{cases} X & \text{if } X \le 1 \\ 1 & \text{if } X > 1 \end{cases} \tag{2.6}$$

The force/slip curves for several different slip angles are shown in figure 2.5 and figure 2.6. These are generated using the Dugoff tyre model, executed in the Simulink environment and show that the tyre model accurately models tyre forces, when curves are compared to actual experimental sets of curves presented in Dugoff (1970). The main drawback of the Dugoff model is the fact that it is inaccurate at high lateral forces. In Manning *et al.* (2002), it is noted that the Pacejka model is accurate at these higher values and hence when studying the vehicle at the limit, the use of Pacejka model is more desirable.

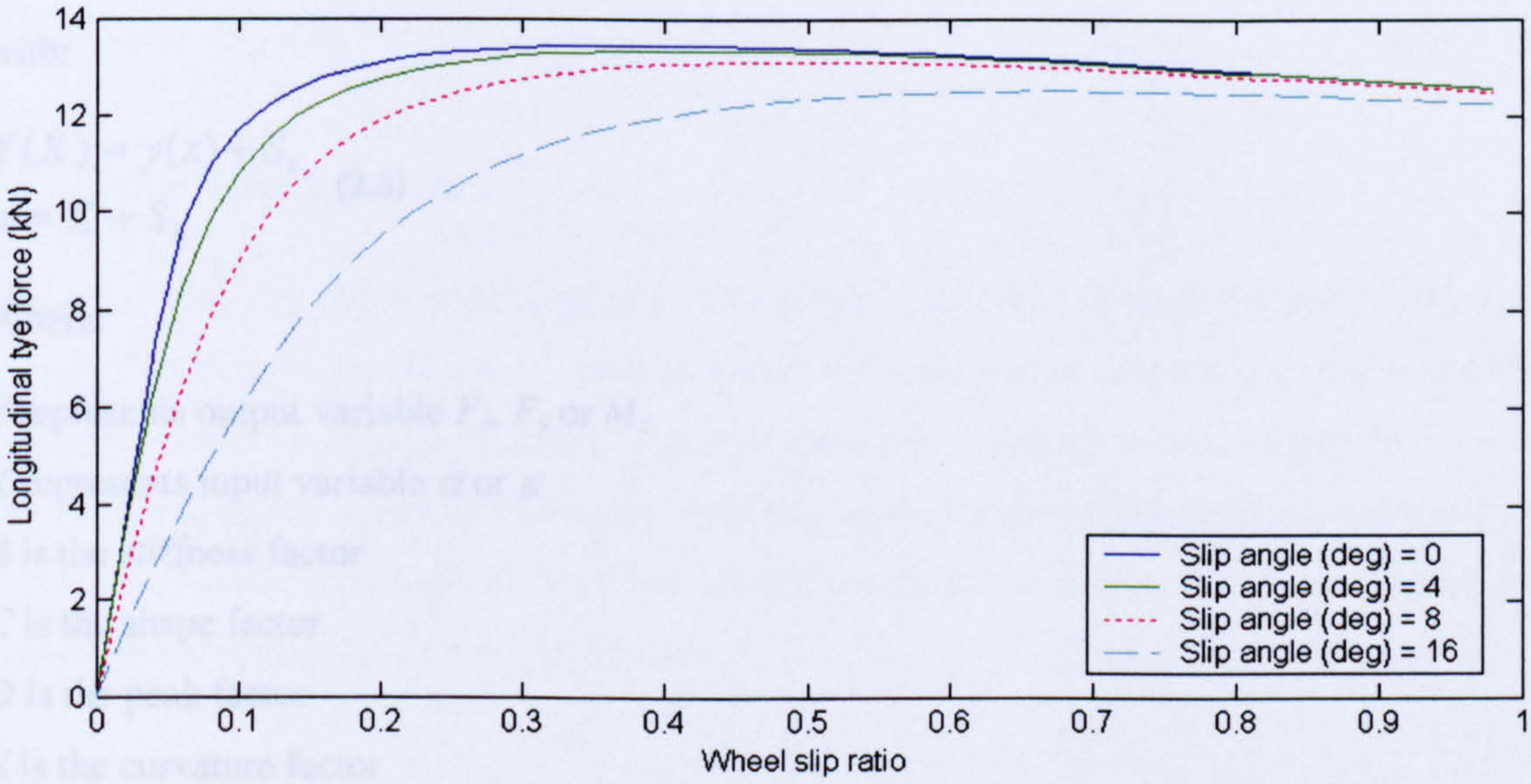

Fig. 2.5 Longitudinal tyre force plotted against wheel slip for various angles.

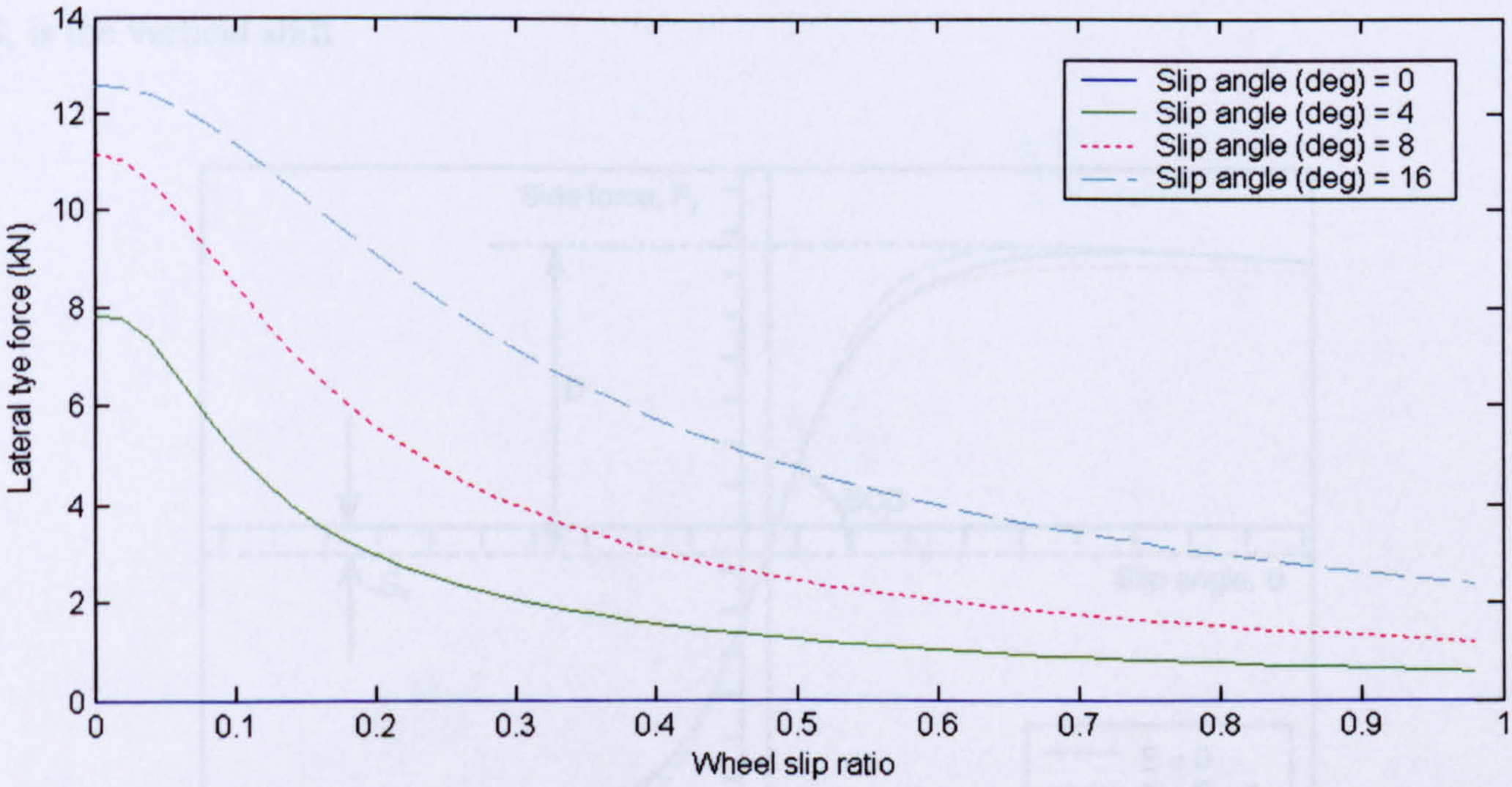

Fig. 2.6 Lateral tyre force plotted against wheel slip for various slip angles

2.4.2 Pacejka Tyre Model

The Pacejka tyre model makes use of the "magic formula". This formula can be altered to describe lateral or longitudinal forces as well as self-aligning moments of the tyre by varying the inputs to the model and the parameters used. Equations for pure longitudinal and lateral forces can also be used to describe combined acceleration/cornering of the tyre with the introduction of extra co-efficients. The Formula is shown in equation 2.7.

$$y = D\sin[C\arctan\{Bx - E(Bx - \arctan Bx)\}] \quad (2.7)$$

with:

$$\begin{aligned} Y(X) &= y(x) + S_v \\ x &= X + S_h \end{aligned} \quad (2.8)$$

Where:

Y represents output variable F_x, F_y or M_z

X represents input variable α or κ

B is the stiffness factor

C is the shape factor

D is the peak factor

E is the curvature factor

S_h is the horizontal shift

S_v is the vertical shift

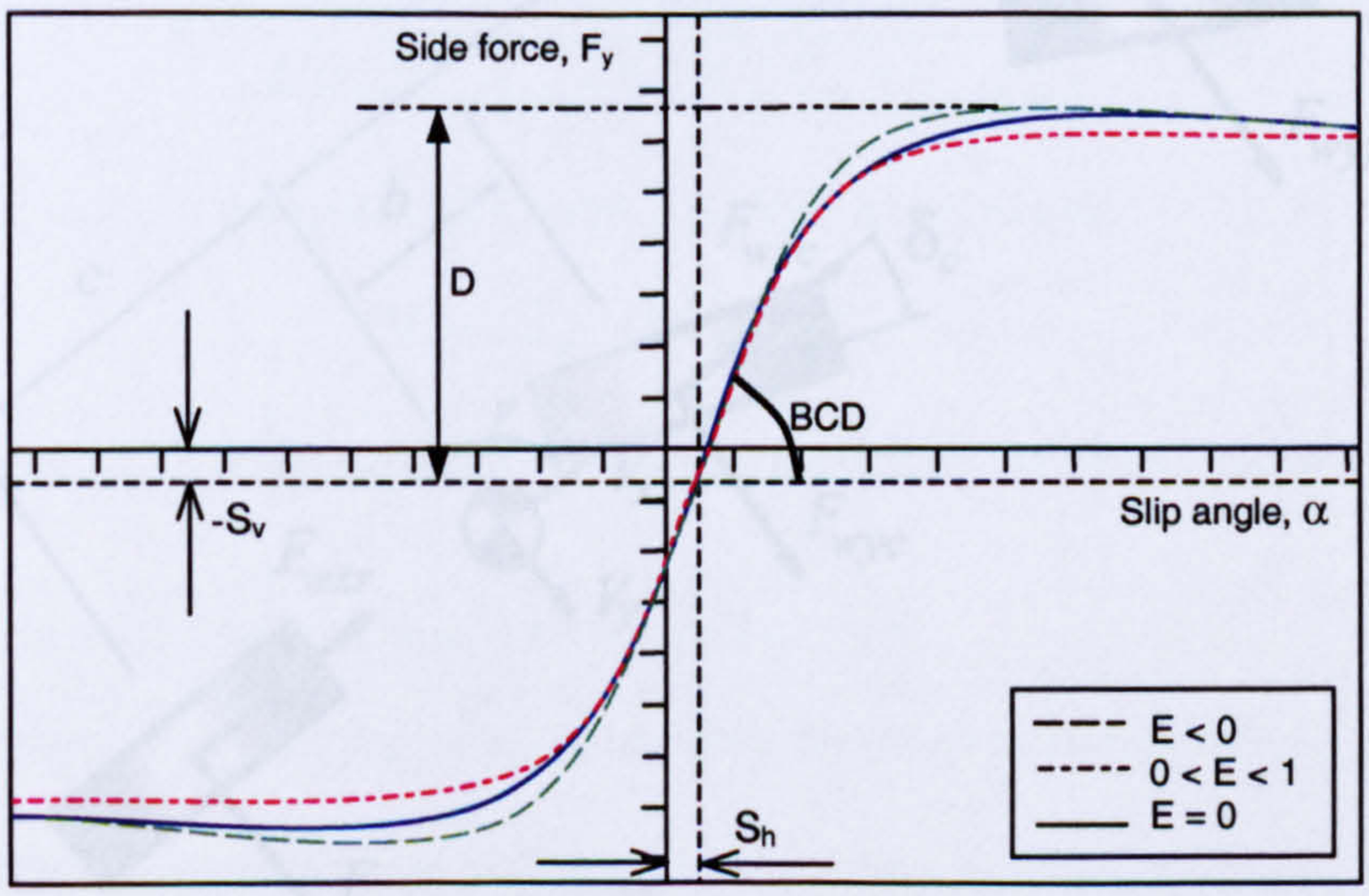

Fig. 2.7 Pacejka tyre co-efficients when describing lateral tyre force

All the coefficients are made up from further coefficients, dependent on what Y is representing. The coefficients are derived from the shape of the tyre force curves as shown in figure 2.7, although determining accurate coefficients from curves can be computationally intensive, but there are packages available that can determine coefficients directly from tyre force curves such as Tyregene[tm]. Because the Pacejka tyre model is tuned directly from actual tyre data if offers an accurate method of modelling the on-road behaviour of a tyre, however it all depends on the quality and quantity of the data on which the model is based, which is always limited due to tyre companies' reluctance to disclose accurate tyre data to their competitors.

2.5 Linear Handling Model

The basic handling characteristics of any vehicle can be assessed through the use of a bicycle model. The bicycle model can be used to assess the steady-state response, stability and the frequency response of the vehicle and although these don't give an accurate representation of the vehicle at higher lateral accelerations, they can be used to assess the fundamental handling characteristics of the vehicle in the three driving conditions to which they refer. Figure 2.8 shows the bicycle model of a 6WD vehicle.

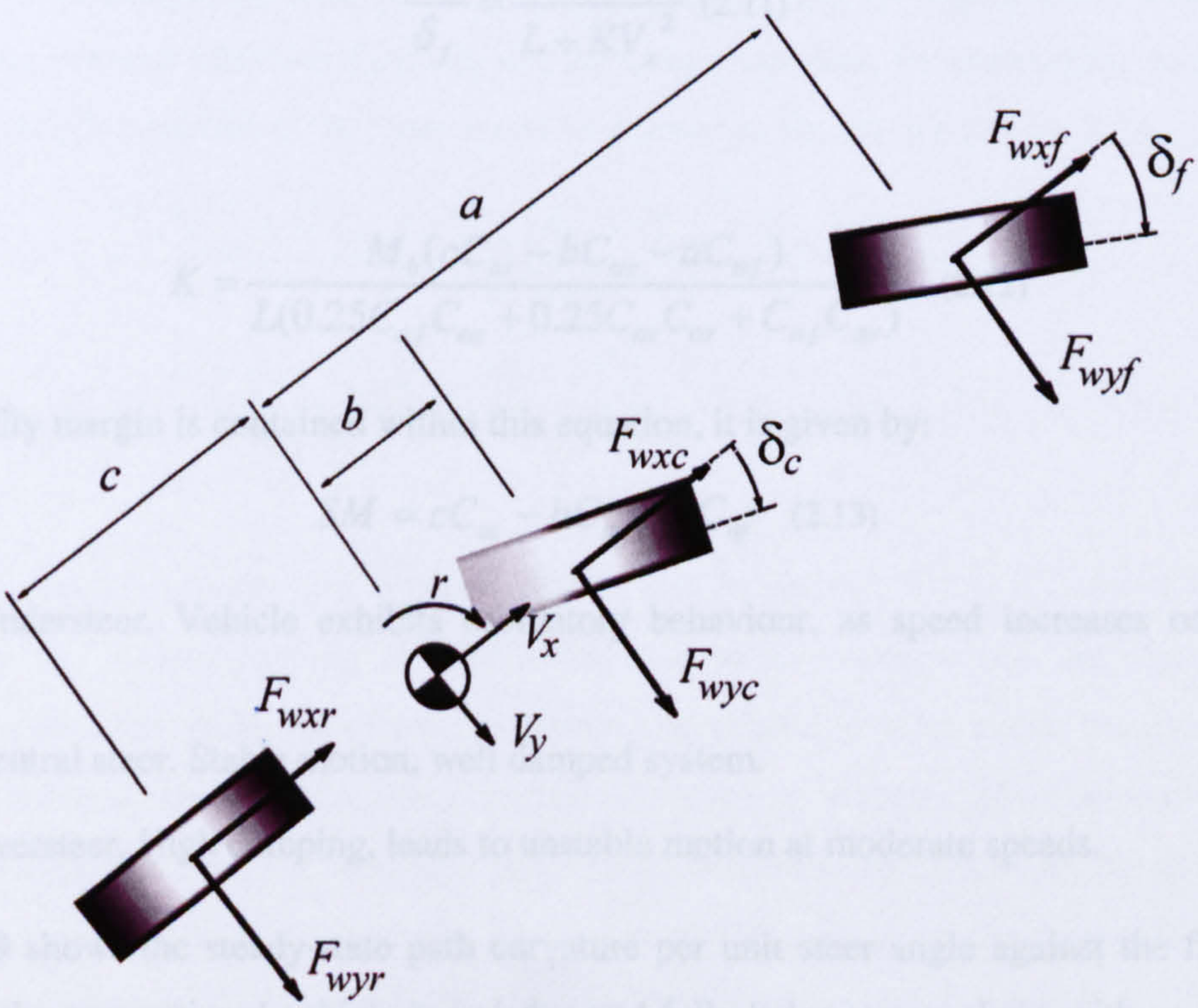

Fig.2.8 Three wheel bicycle model

2.5.1 Steady State Response

The steady state response looks at the vehicle in a constant radius turn at constant speed. The equation of motion regarding a six wheeled vehicle with 4WS travelling at constant forward speed is given in equation 2.9:

$$\begin{bmatrix} M_b & 0 \\ 0 & I_z \end{bmatrix}\begin{bmatrix} \dot{V}_y \\ \dot{r} \end{bmatrix}+\begin{bmatrix} \frac{C_{\alpha f}+C_{\alpha c}+C_{\alpha r}}{V_x} & M_bV_x+\frac{aC_{\alpha f}+bC_{\alpha c}-cC_{\alpha r}}{V_x} \\ \frac{aC_{\alpha f}+bC_{\alpha c}-cC_{\alpha r}}{V_x} & \frac{a^2C_{\alpha f}+b^2C_{\alpha c}+c^2C_{\alpha r}}{V_x} \end{bmatrix}\begin{bmatrix} V_y \\ r \end{bmatrix} \quad (2.9)$$
$$=\begin{bmatrix} C_{\alpha f}+S_rC_{\alpha c} \\ aC_{\alpha f}+bS_rC_{\alpha c} \end{bmatrix}\begin{bmatrix} \delta_f \end{bmatrix}$$

Equation 2.9 can be used to determine the steady state characteristics of the vehicle by setting the dynamic terms dV_y/dt and dr/dt to zero and using Cramer's rule to define the relationship between r_{ss} and δ_f:

$$\frac{r_{ss}}{\delta_f}=\frac{V_xL(0.25C_{\alpha f}C_{\alpha c}+0.25C_{\alpha c}C_{\alpha r}+C_{\alpha f}C_{\alpha r})}{L^2(0.25C_{\alpha f}C_{\alpha c}+0.25C_{\alpha c}C_{\alpha c}+C_{\alpha f}C_{\alpha r})+M_bV_x^{\,2}(cC_{\alpha r}-bC_{\alpha c}-aC_{\alpha f})} \quad (2.10)$$

This can be rewritten in terms of steady-state path curvature per unit steer angle, ρ_{ss} as:

$$\frac{\rho_{ss}}{\delta_f}=\frac{1}{L+KV_x^{\,2}} \quad (2.11)$$

Where:

$$K=\frac{M_b(cC_{\alpha r}-bC_{\alpha c}-aC_{\alpha f})}{L(0.25C_{\alpha f}C_{\alpha c}+0.25C_{\alpha c}C_{\alpha r}+C_{\alpha f}C_{\alpha r})} \quad (2.12)$$

The stability margin is contained within this equation, it is given by:

$$SM=cC_{\alpha r}-bC_{\alpha c}-aC_{\alpha f} \quad (2.13)$$

SM>0, Understeer. Vehicle exhibits oscillatory behaviour, as speed increases oscillations increase.

SM=0, Neutral steer. Stable motion, well damped system.

SM<0, Oversteer. High damping, leads to unstable motion at moderate speeds.

Figure 2.9 shows the steady-state path curvature per unit steer angle against the front steer angle for the conventional vehicle in unladen and fully laden states, along with an estimated half-laden set-up to give neutral steer. It can be seen that within the speed range of the

vehicle, it remains stable as the critical speed is far beyond the capability of both the conventional and hybrid drivetrain.

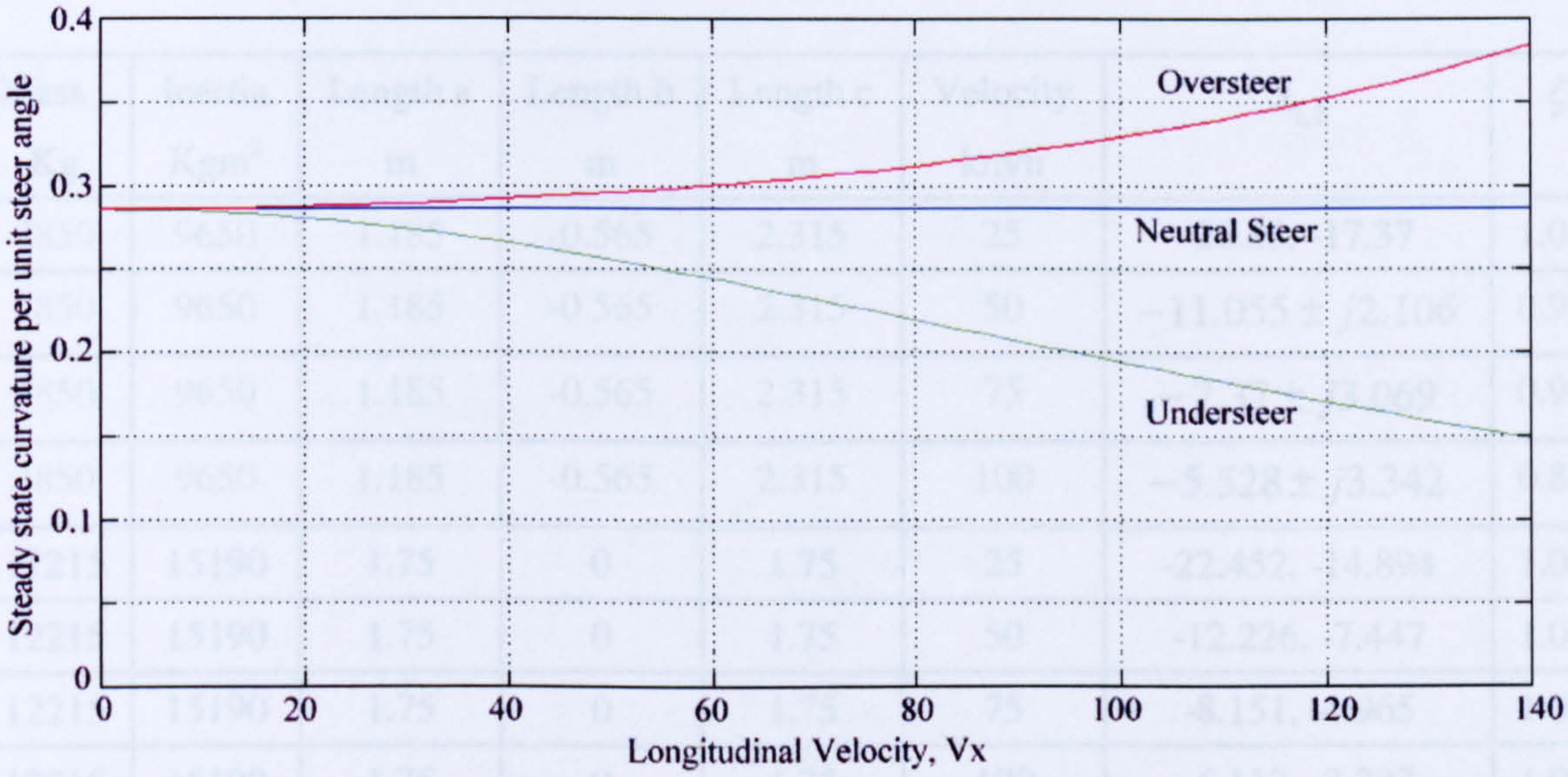

Fig. 2.9 Steady-state path curvature against speed (km/h) for Unladen (Green), Semi-laden (Blue) and Laden vehicle (Red).

2.5.2 Stability

In order to further assess the stability of the system, the vehicle's transient response to disturbances in straight running can be deduced and the vehicles eigen-values calculated to evaluate the vehicles effective damping and stiffness properties. By rearranging equation 2.9 the characteristic equation of the system can be derived as shown in equation 2.14.

$$\lambda^2 + \left\{ \frac{(a^2 C_{\alpha f} + b^2 C_{\alpha c} + c^2 C_{\alpha r}) M_b + (C_{\alpha f} + C_{\alpha c} + C_{\alpha r}) I_z}{M_b V_x I_z} \right\} \lambda + \left\{ \frac{(a-b)^2 C_{\alpha f} C_{\alpha c} + (a+c)^2 C_{\alpha f} C_{\alpha r} + (b+c)^2 C_{\alpha c} C_{\alpha r}}{M_b I_z V_x^{\,2}} + \frac{c C_{\alpha r} - b C_{\alpha c} - a C_{\alpha f}}{I_z} \right\} = 0 \quad (2.14)$$

From this, root placements and system damping can be derived. Table 2.2 shows the eigen-values for the various loading configurations and vehicle speeds and the corresponding damping ratios. As can be seen from the results, the vehicle remains stable in all conditions, which is backed up by the steady-state characteristics shown in figure 2.9. The under-steering unladen vehicle has complex roots and hence displays oscillatory behaviour, the neutral steer vehicle has real roots, that remain in the stable region, where as the over-steering laden vehicle has real roots, that approach the unstable region as speed increases. In the fully laden case, the vehicle is said to be conditionally stable, as speed increases it approaches the

unstable side on the complex plane, however only at speeds higher than the vehicle can obtain.

Mass Kg	Inertia Kgm^2	Length a m	Length b m	Length c m	Velocity km/h	$\lambda_{1,2}$	ζ
7850	9650	1.185	-0.565	2.315	25	-26.85, -17.37	1.023
7850	9650	1.185	-0.565	2.315	50	$-11.055 \pm j2.106$	0.982
7850	9650	1.185	-0.565	2.315	75	$-7.37 \pm j3.069$	0.923
7850	9650	1.185	-0.565	2.315	100	$-5.528 \pm j3.342$	0.856
12215	15190	1.75	0	1.75	25	-22.452, -14.894	1.031
12215	15190	1.75	0	1.75	50	-12.226, -7.447	1.031
12215	15190	1.75	0	1.75	75	-8.151, -4.965	1.031
12215	15190	1.75	0	1.75	100	-6.113, -3.723	1.031
16580	20730	1.89	0.14	1.61	25	-22.273, -13.547	1.031
16580	20730	1.89	0.14	1.61	50	-11.528, -6.38191	1.044
16580	20730	1.89	0.14	1.61	75	-8.048, -3.891	1.067
16580	20730	1.89	0.14	1.61	100	-6.353, -2.602	1.101

Table 2.2 Determining stability of vehicle in various conditions.

2.5.3 Frequency Response

The frequency response shows the dynamic response of the vehicle to sinusoidal steer input of increasing frequency. This will give an indication of the vehicles response to the entire frequency range, although as noted by Crolla *et al.* (1996) relating the results to actual vehicle motion is rather difficult. It should be noted that the gains at zero frequency correspond to the steady state gains shown in figure 2.9. Frequency response is deduced from equation 2.9 by utilising the following equation for the input:

$$\delta_f = \Delta_f e^{i\omega t} \quad (2.15)$$

And the following outputs:

$$\dot{V}_y = i\omega X_v \quad (2.16)$$

$$\dot{r} = i\omega X_r \quad (2.17)$$

$$v = X_v e^{i\omega t} \quad (2.18)$$

$$r = X_r e^{i\omega t} \quad (2.19)$$

and then cancelling $e^{i\omega t}$ throughout gives:

$$\begin{bmatrix} i\omega M_b + \dfrac{C_{\alpha f} + C_{\alpha c} + C_{\alpha r}}{V_x} & M_b V_x + \dfrac{aC_{\alpha f} + bC_{\alpha c} - cC_{\alpha r}}{V_x} \\ \dfrac{aC_{\alpha f} + bC_{\alpha c} - cC_{\alpha r}}{V_x} & i\omega I_b + \dfrac{a^2 C_{\alpha f} + b^2 C_{\alpha c} + c^2 C_{\alpha r}}{V_x} \end{bmatrix} \begin{bmatrix} X_v \\ X_r \end{bmatrix} = \begin{bmatrix} C_{\alpha f} + S_r C_{\alpha c} \\ aC_{\alpha f} + bS_r C_{\alpha c} \end{bmatrix} \begin{bmatrix} \Delta_f \end{bmatrix}$$

(2.20)

This can then be rewritten using Cramers rule as:

$$X_v / \Delta f = \frac{V_r + iV_i}{D_r + iD_i} \quad (2.21)$$

$$X_r / \Delta f = \frac{R_r + iR_i}{D_r + iD_i} \quad (2.22)$$

Where:

$$D_r = -\omega^2 M_b I_b + \frac{0.5L^2 C_{\alpha f} C_{\alpha c} + L^2 C_{\alpha f} C_{\alpha r} + 0.5L^2 C_{\alpha c} C_{\alpha r}}{V_x^2} + M_b (cC_{\alpha r} - bC_{\alpha c} - aC_{\alpha f}) \quad (2.23)$$

$$D_i = \frac{\omega(I_b (C_{\alpha f} + C_{\alpha c} + C_{\alpha r}) + M_b (a^2 C_{\alpha f} + b^2 C_{\alpha c} + c^2 C_{\alpha r}))}{V_x} \quad (2.24)$$

$$V_r = \frac{(S_r a^2 + b^2 - ab - abS_r) C_{\alpha f} C_{\alpha c} + (c^2 + ac) C_{\alpha f} C_{\alpha r} + (bcS_r + c^2 S_r) C_{\alpha c} C_{\alpha r}}{V_x} - MV_x (aC_{\alpha f} + bS_r C_{\alpha c})$$

(2.25)

$$V_i = \omega I_b (C_{\alpha f} + S_r C_{\alpha c}) \quad (2.26)$$

$$R_r = \frac{(a + S_r b - b - S_r a) C_{\alpha f} C_{\alpha c} + lC_{\alpha f} C_{\alpha r} + (S_r b + S_r c) C_{\alpha c} C_{\alpha r}}{V_x} \quad (2.27)$$

$$R_i = \omega M_b (aC_{\alpha f} + S_r bC_{\alpha c}) \quad (2.28)$$

When equations 2.23 to 2.28 are placed in equation 2.21 and equation 2.22, they can be used to find the magnitude and phase of the vehicles yaw-rate gain. Once they have been evaluated they can then be used to find the lateral acceleration from the equation $i\omega X_v + V_x X_r$. Bode diagrams for both the yaw rate and the lateral acceleration gain and phase are shown in figure 2.10 to figure 2.13 for the vehicle in laden and unladen states at speeds of 10m/s and 20m/s. These show both the under-steering unladen vehicle and the over-steering laden vehicle.

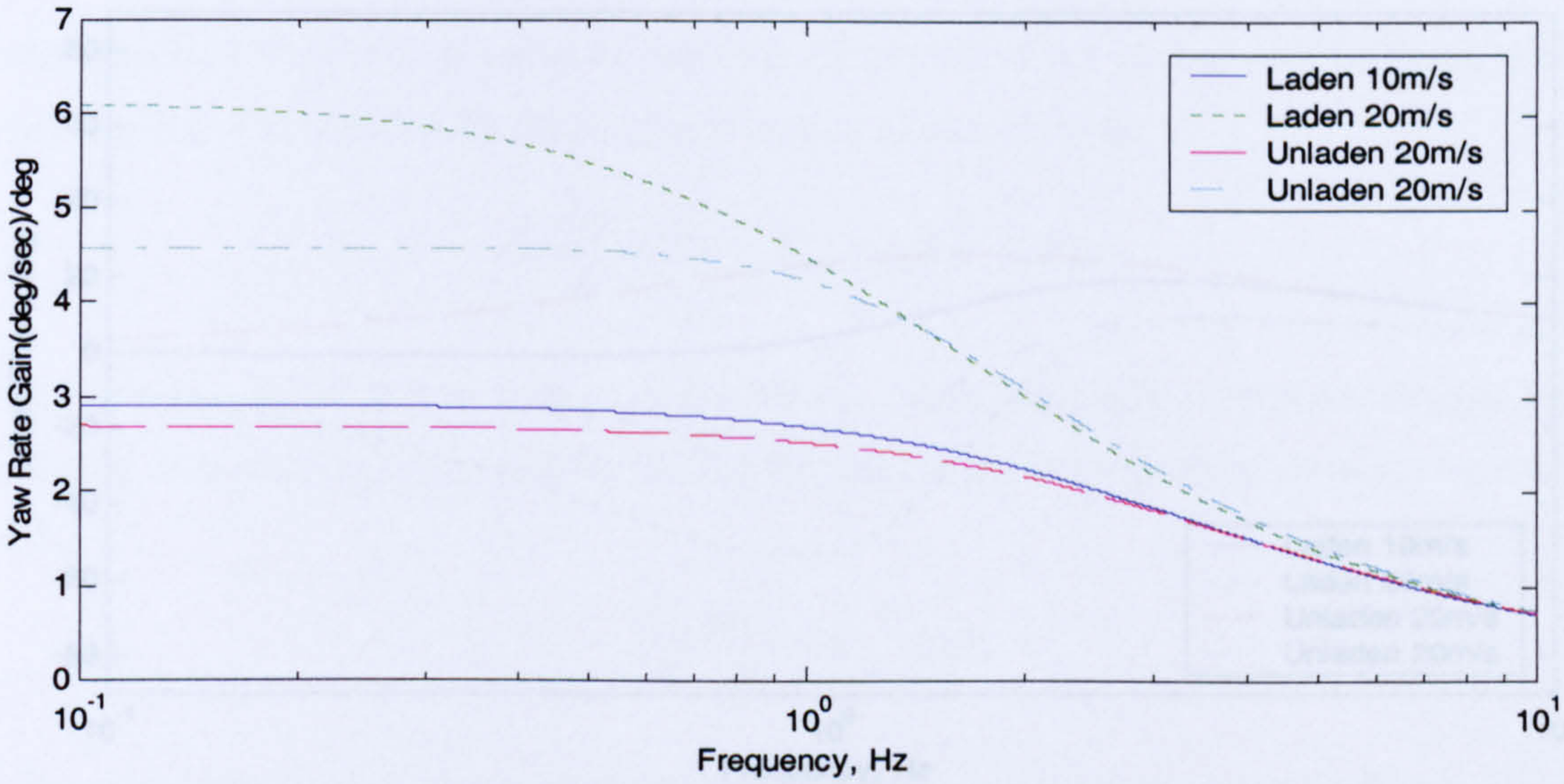

Fig. 2.10 Yaw rate gain frequency response

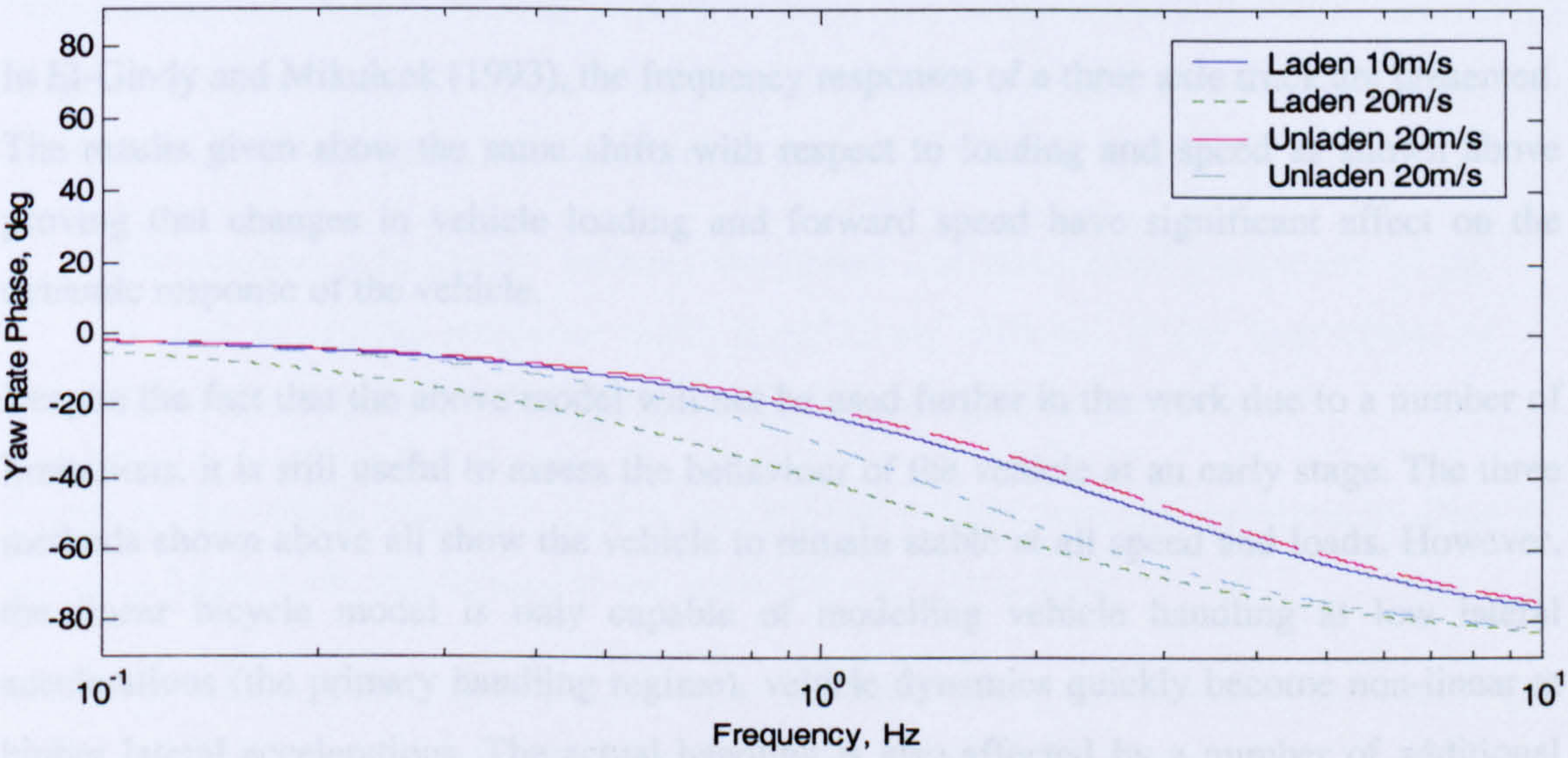

Fig. 2.11 Yaw rate phase frequency response.

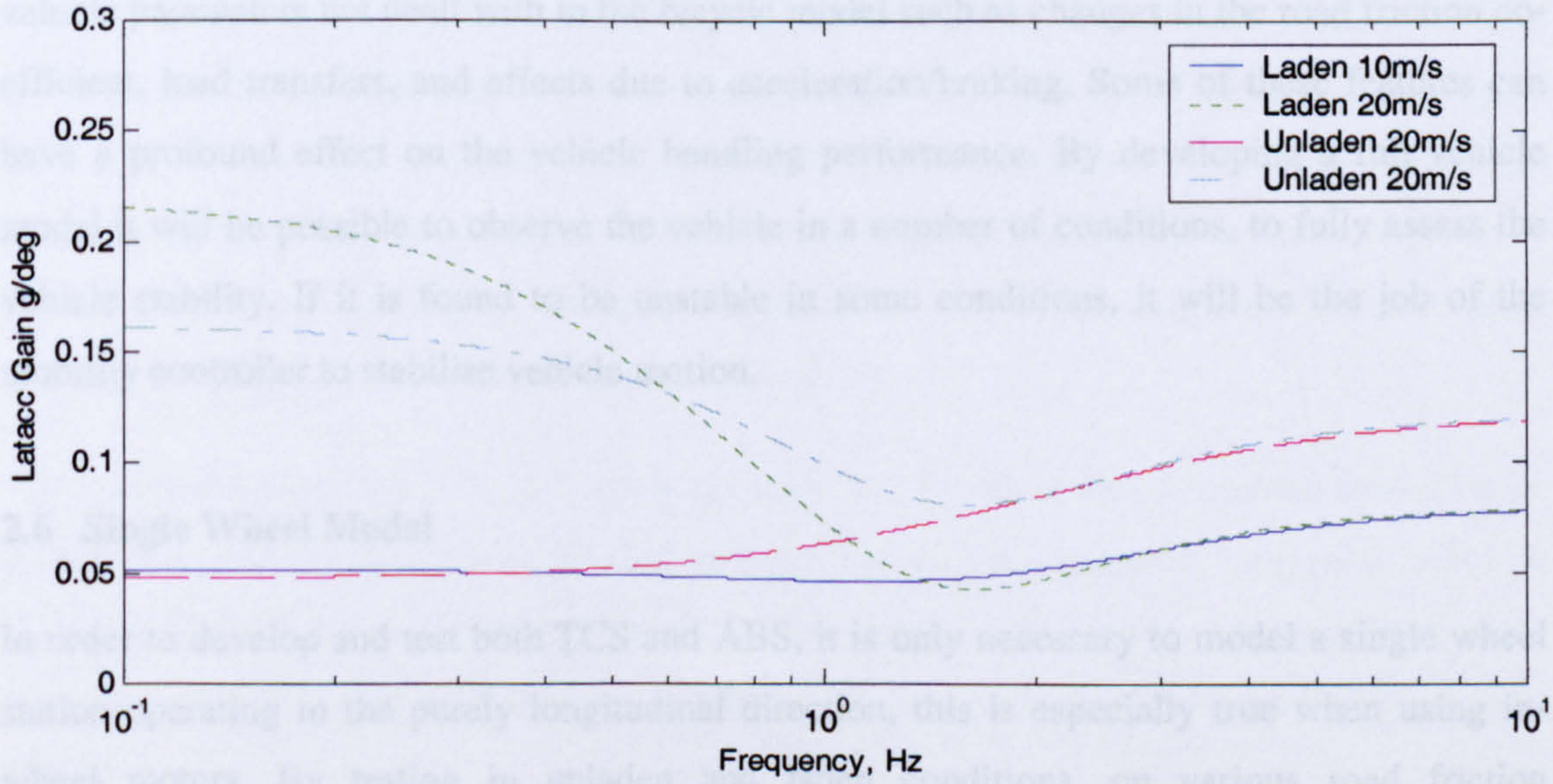

Fig. 2.12 Lateral acceleration gain frequency response.

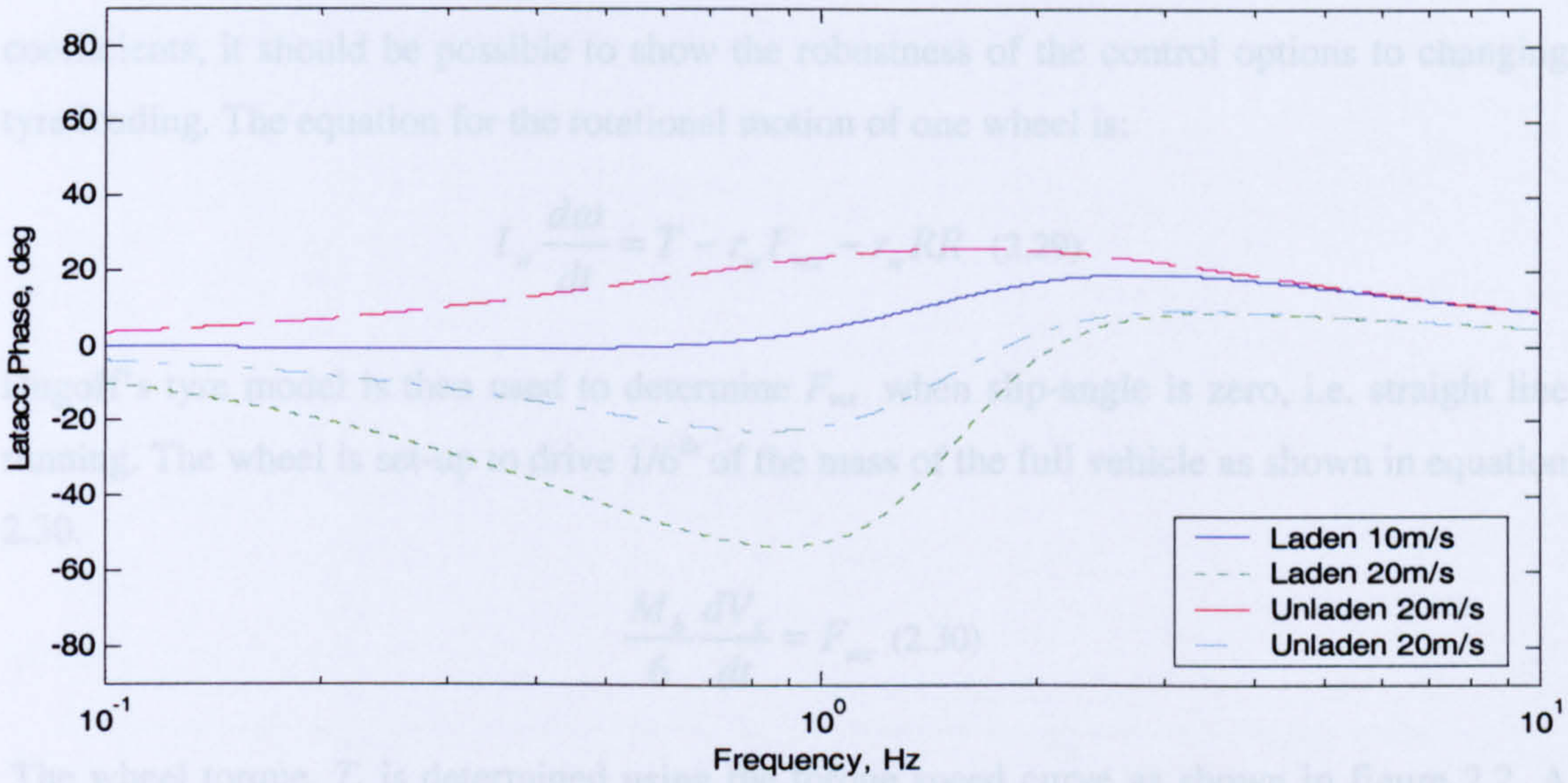

Fig. 2.13 Lateral acceleration phase frequency response.

In El-Gindy and Mikulcek (1993), the frequency responses of a three axle truck are presented. The results given show the same shifts with respect to loading and speed as shown above proving that changes in vehicle loading and forward speed have significant effect on the dynamic response of the vehicle.

Despite the fact that the above model will not be used further in the work due to a number of limitations, it is still useful to assess the behaviour of the vehicle at an early stage. The three methods shown above all show the vehicle to remain stable at all speed and loads. However, the linear bicycle model is only capable of modelling vehicle handling at low lateral accelerations (the primary handling regime), vehicle dynamics quickly become non-linear at higher lateral accelerations. The actual handling is also affected by a number of additional vehicle parameters not dealt with in the bicycle model such as changes in the road friction coefficient, load transfers, and effects due to acceleration/braking. Some of these features can have a profound effect on the vehicle handling performance. By developing a full vehicle model it will be possible to observe the vehicle in a number of conditions, to fully assess the vehicle stability. If it is found to be unstable in some conditions, it will be the job of the mobility controller to stabilise vehicle motion.

2.6 Single Wheel Model

In order to develop and test both TCS and ABS, it is only necessary to model a single wheel station operating in the purely longitudinal direction, this is especially true when using in-wheel motors. By testing in unladen and laden conditions, on various road friction

coefficients, it should be possible to show the robustness of the control options to changing tyre loading. The equation for the rotational motion of one wheel is:

$$I_w \frac{d\omega}{dt} = T - r_w F_{wx} - r_w RR \quad (2.29)$$

Dugoff's tyre model is then used to determine F_{wx} when slip-angle is zero, i.e. straight line running. The wheel is set-up to drive $1/6^{th}$ of the mass of the full vehicle as shown in equation 2.30.

$$\frac{M_b}{6}\frac{dV_x}{dt} = F_{wx} \quad (2.30)$$

The wheel torque, T, is determined using the torque speed curve as shown in figure 2.2. A Proportional Derivative controller is used to reach and maintain desired speed. The rolling resistance, RR, is dependent on a number of factors including vehicle speed, vertical tyre load, road surface and the braking/tractive effort on the tyre. It is noted in Wouk (1993) that:

> "The complex relationship between the design and operational parameters of the tyre and its rolling resistance make it extremely difficult, if not impossible, to develop an analytical method for predicting the rolling resistance of tyres"

A data set for rolling resistance against longitudinal wheel speed was provided by QinetiQ, shown in figure 2.14, will be used in the model for each static load.

Results of vehicle speed, wheel torque, wheel slip and wheel force are shown for a step input in desired vehicle speed from 5km/h to full speed. The results are shown in figure 2.15 to figure 2.18 for each quantity respectively. Each simulation was run on 3 different road surfaces: μ=0.8 (dry asphalt) μ=0.5 (wet asphalt) and μ=0.2 (ice). From figure 2.15 and figure 2.17, it can be seen that on the dry road surface, the vehicle accelerates quickly and wheel-slip remains low as would be expected. When the test is performed on the icy road, wheel-slip greatly increases resulting in reduced longitudinal tyre force and the vehicle's slow acceleration. This is all as is expected from the model.

The implementation of a TCS on this wheel should aim to reduce this wheel-slip dramatically, giving improved acceleration on all road surfaces and as a consequence, increase lateral tyre forces leading to improved vehicle stability. This single wheel model can now be used to develop both a TCS and ABS. It can also be integrated into a larger basic non-linear handling model.

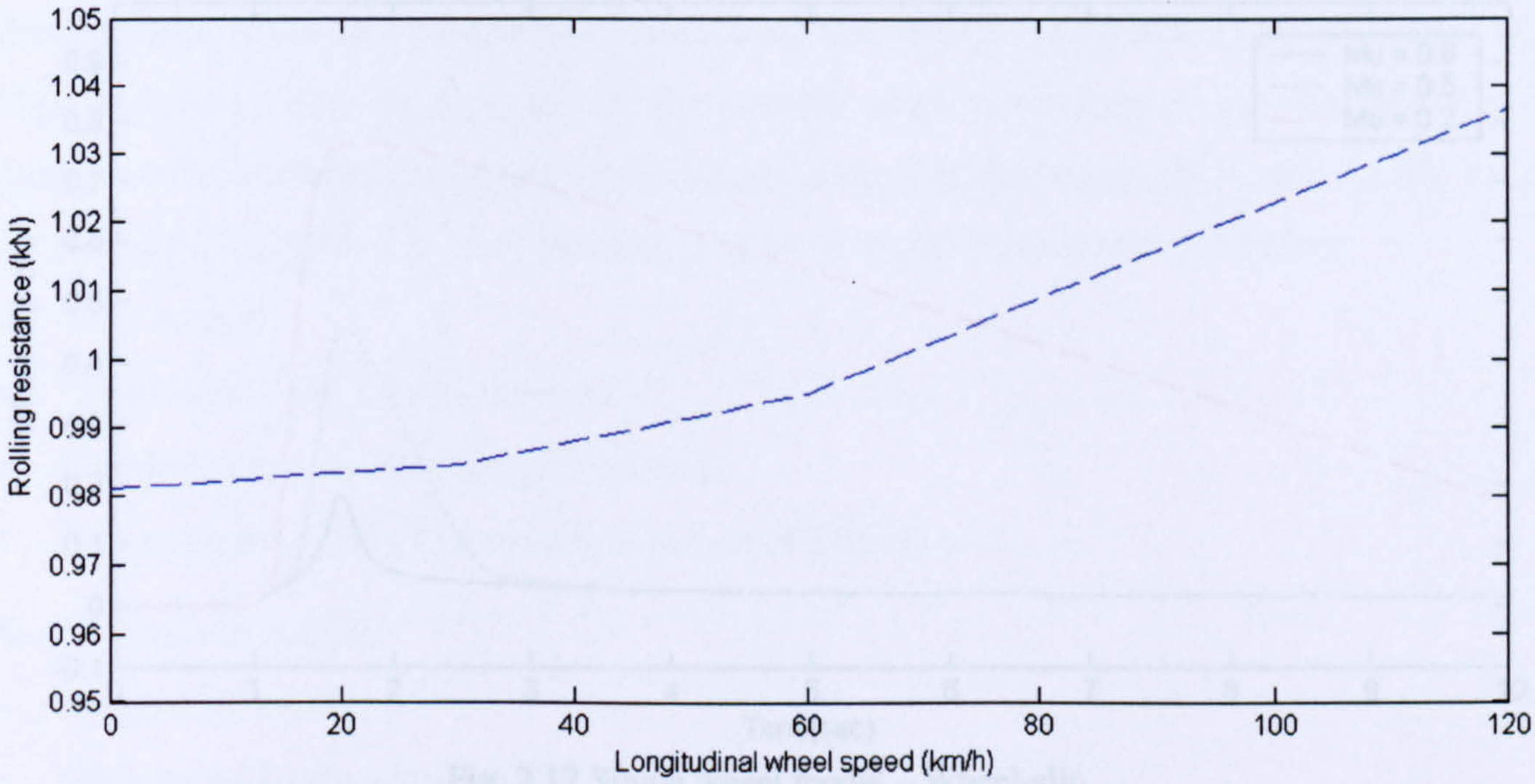

Fig. 2.14 Varying rolling resistance with respect to vehicle speed

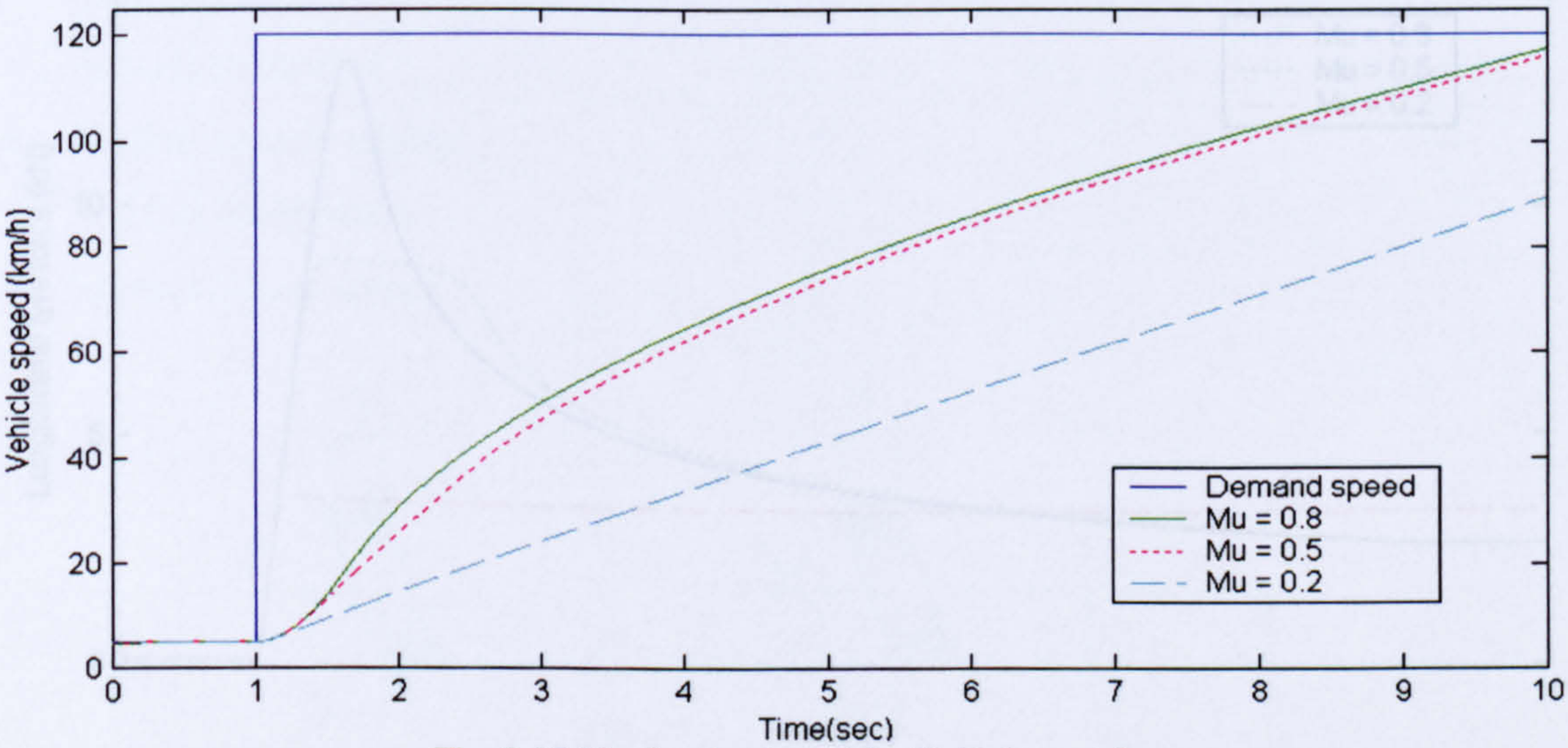

Fig. 2.15 Single wheel model – Vehicle speed

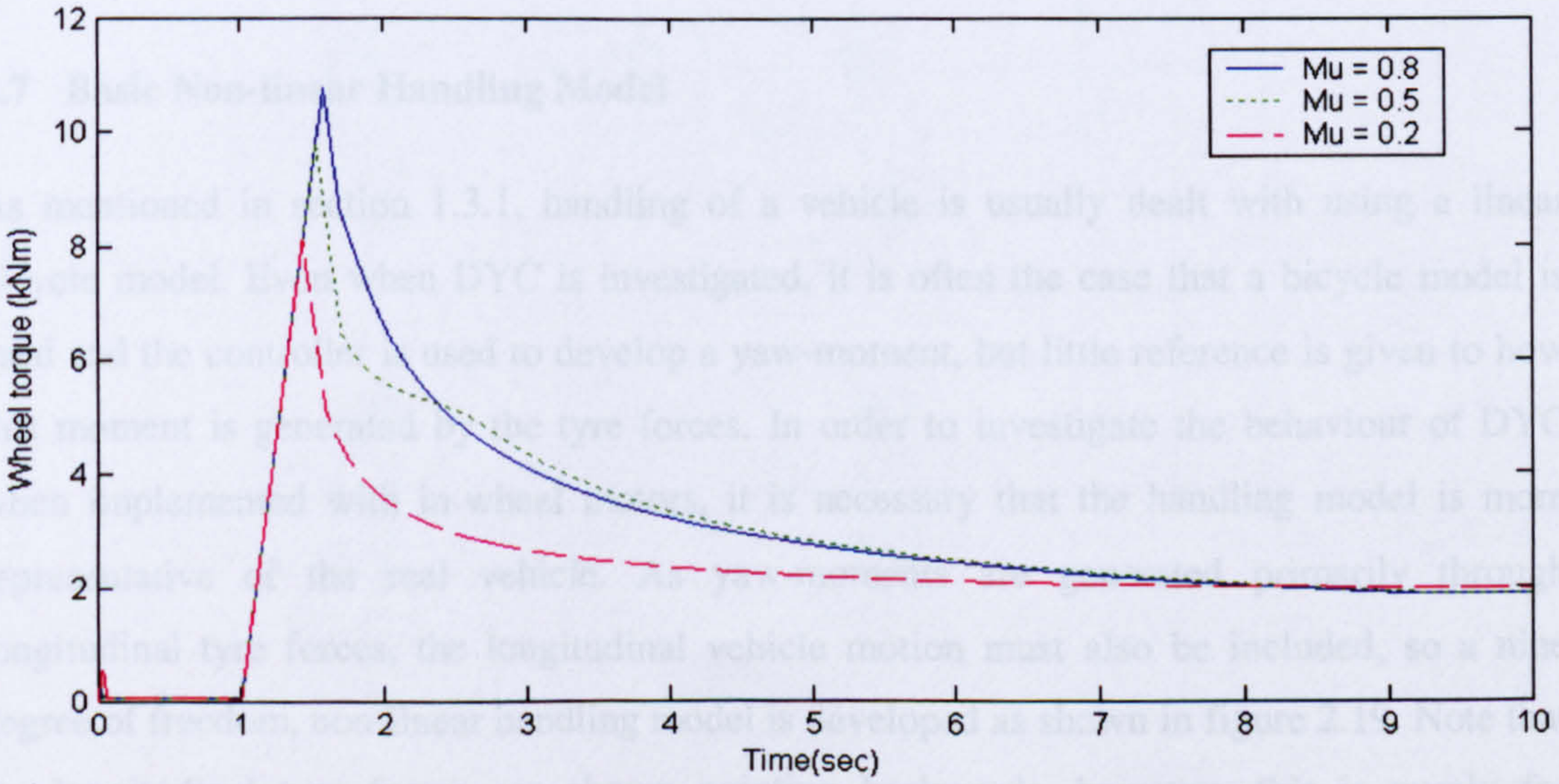

Fig. 2.16 Single wheel model – Drive torque

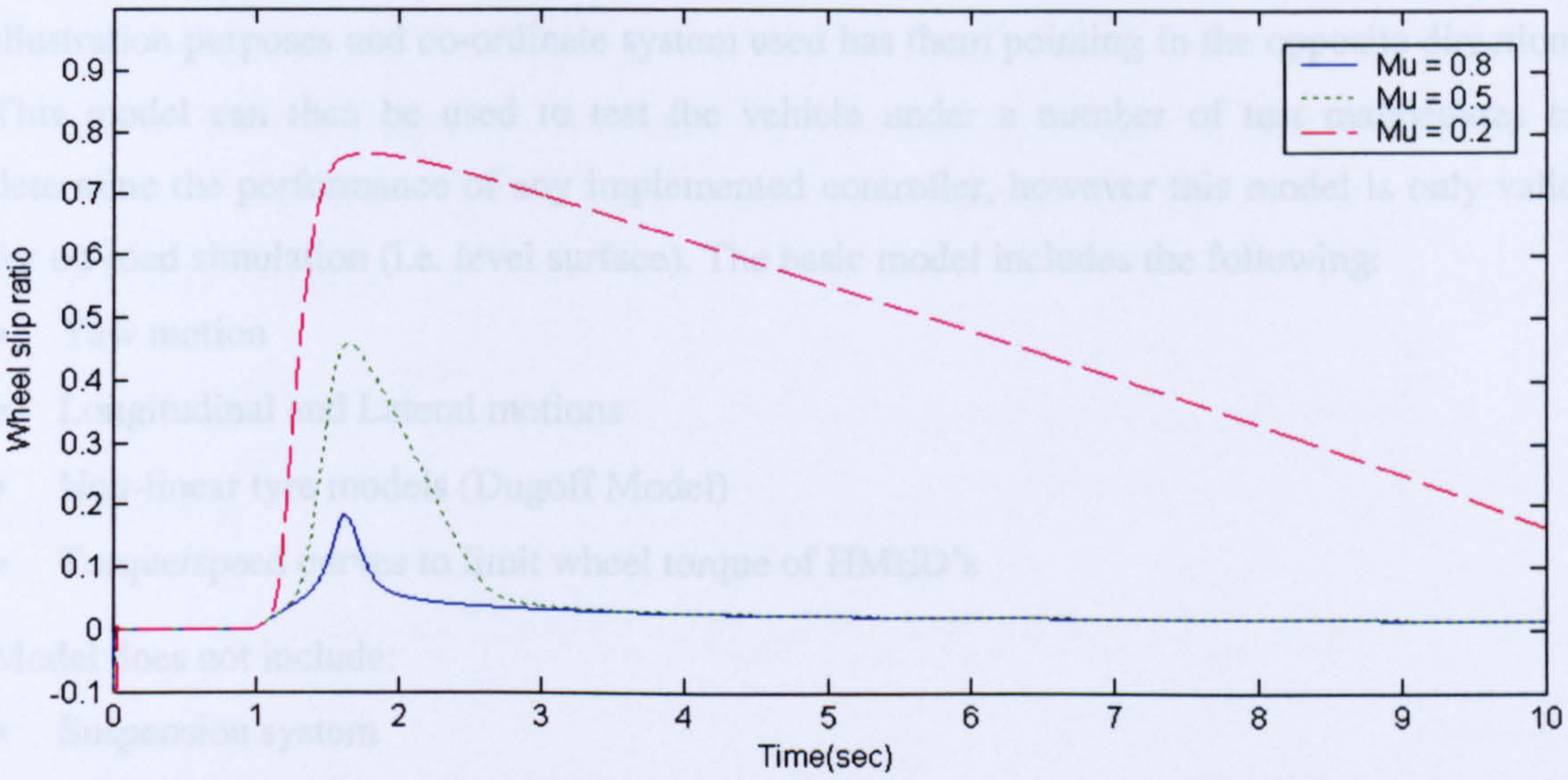

Fig. 2.17 Single wheel model – Wheel-slip

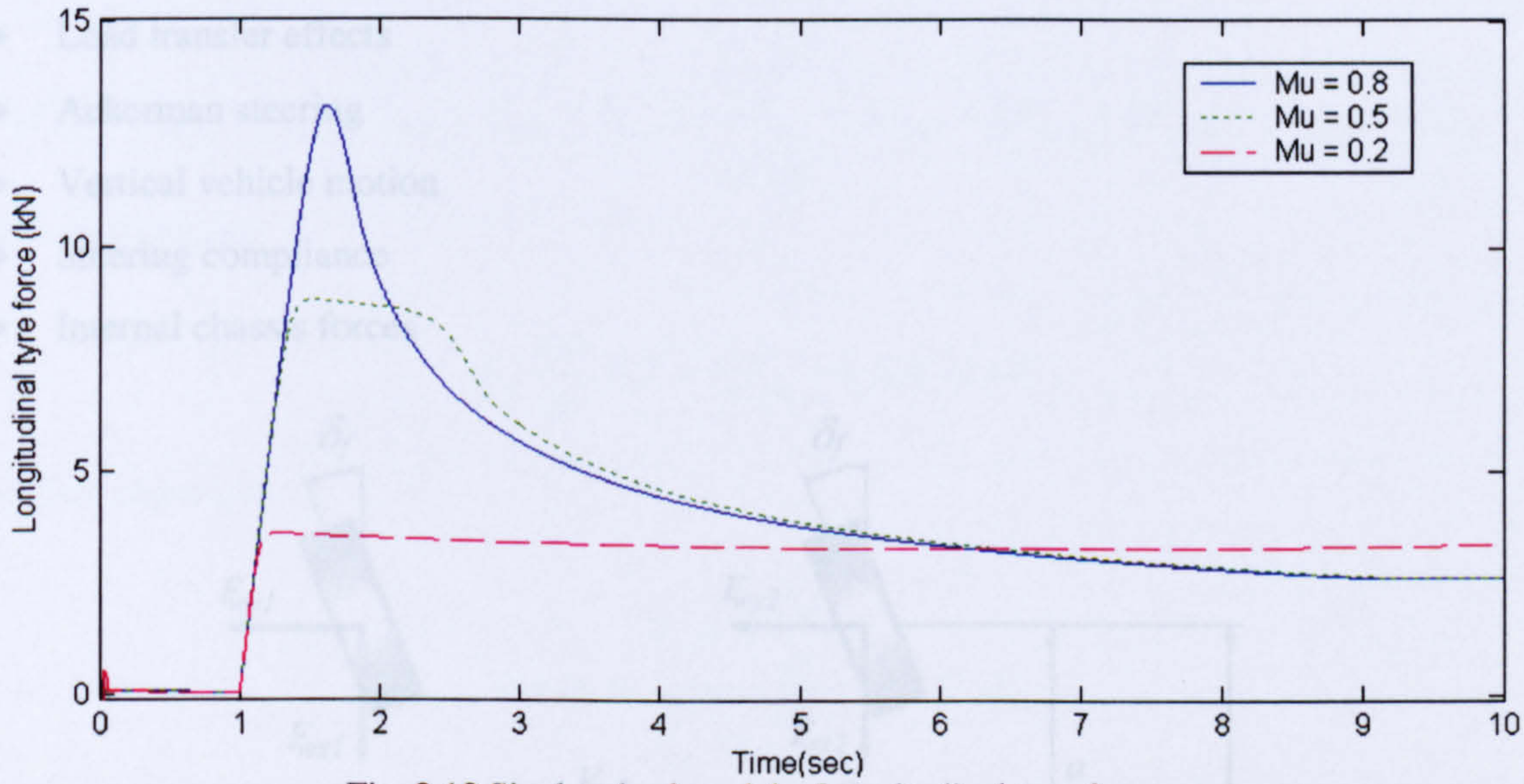

Fig. 2.18 Single wheel model – Longitudinal tyre force

2.7 Basic Non-linear Handling Model

As mentioned in section 1.3.1, handling of a vehicle is usually dealt with using a linear bicycle model. Even when DYC is investigated, it is often the case that a bicycle model is used and the controller is used to develop a yaw-moment, but little reference is given to how this moment is generated by the tyre forces. In order to investigate the behaviour of DYC when implemented with in-wheel motors, it is necessary that the handling model is more representative of the real vehicle. As yaw-moments are generated primarily through longitudinal tyre forces, the longitudinal vehicle motion must also be included, so a nine degree of freedom, non-linear handling model is developed as shown in figure 2.19. Note that the longitudinal tyre forces are shown pointing backwards, however, this is purely for

illustration purposes and co-ordinate system used has them pointing in the opposite direction. This model can then be used to test the vehicle under a number of test manoeuvres to determine the performance of any implemented controller, however this model is only valid for on-road simulation (i.e. level surface). The basic model includes the following:

- Yaw motion
- Longitudinal and Lateral motions
- Non-linear tyre models (Dugoff Model)
- Torque/speed curves to limit wheel torque of HMED's

Model does not include:

- Suspension system
- Pitching and rolling motion
- Load transfer effects
- Ackerman steering
- Vertical vehicle motion
- Steering compliance
- Internal chassis forces

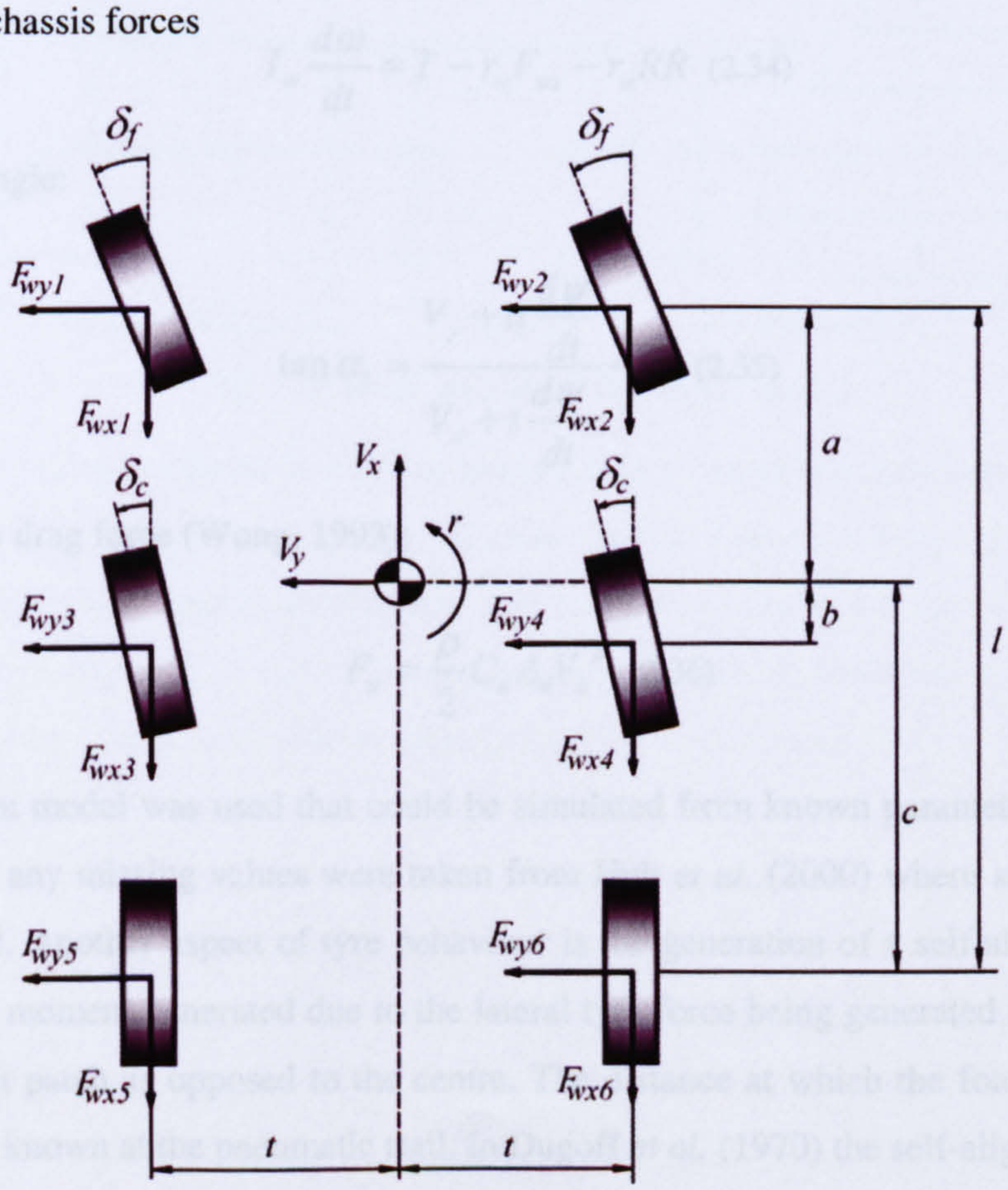

Fig. 2.19 Nine degree of freedom handling model

Using the Newtonian approach, the following equations of motion are used to describe the dynamics of the vehicle body (full set of equations in Appendix A.1.3):

Longitudinal motion:

$$M_b(\frac{dV_x}{dt} - V_y\frac{d\psi}{dt}) = F_{wx1} + F_{wx2} + F_{wx3} + F_{wx4} + F_{wx5} + F_{wx6} - F_d \quad (2.31)$$

Lateral motion:

$$M_b(\frac{dV_y}{dt} + V_x\frac{d\psi}{dt}) = F_{wy1} + F_{wy2} + F_{wy3} + F_{wy4} + F_{wy5} + F_{wy6} \quad (2.32)$$

Yawing motion:

$$I_z.\frac{d^2\psi}{dt^2} =$$

$$t(F_{wx1} - F_{wx2} + F_{wx3} - F_{wx4} + F_{wx5} - F_{wx6}) + aF_{wy1} + aF_{wy2} + bF_{wy3} + bF_{wy4} - cF_{wy5} - cF_{wy6} + M_z \quad (2.33)$$

Wheel Rotation:

$$I_w\frac{d\omega}{dt} = T - r_wF_{wx} - r_wRR \quad (2.34)$$

Wheel-slip angle:

$$\tan\alpha_i = \frac{V_y + a\frac{d\psi}{dt}}{V_x + t\frac{d\psi}{dt}} - \delta_i \quad (2.35)$$

Aerodynamic drag force (Wong, 1993):

$$F_d = \frac{\rho}{2}C_dA_dV_x^2 \quad (2.36)$$

A Dugoff tyre model was used that could be simulated from known parameters for the tyres included and any missing values were taken from Huh *et al.* (2000) where similar size tyres are simulated. Another aspect of tyre behaviour is the generation of a self-aligning moment, M_Z. This is a moment generated due to the lateral tyre force being generated towards the rear of the contact patch as opposed to the centre. The distance at which the force acts from the tyre centre is known at the pneumatic trail. In Dugoff *et al.* (1970) the self-aligning moment is modelled as a linear relationship as expressed in equation 2.37, where the pneumatic trail is a constant, although the pneumatic trail is known to vary with tyre load and slip-angle it will be

expressed as a constant at this stage. This equation will be used in the vehicle model. Moments generated at each tyre are summed to form the self-aligning moment, M_z which then contributes to the yawing motion of the vehicle as shown in equation 2.33.

$$M_{zi} = -X_{trail} F_{wyi} \quad (2.37)$$

A full set of equations used in this model are presented in Appendix A.1.3. These equations were then implemented in Simulink. The simulation is split into five blocks: inputs; control and torque production; tyre models; 6WD 4WS vehicle model and outputs. The main inputs to the system are desired and initial vehicle speed, steer input and road friction coefficient. Any number of outputs can be observed, but the ones of primary concern are yaw-rate, longitudinal and lateral speeds and accelerations, side-slip angle and individual wheel-slips. A simple PID controller is used to model a driver's response to a speed demand using speed error as an input and desired torque as an output. This model can be simulated undertaking a number of manoeuvres on various road surfaces to develop the control strategy that will later be implemented on the full vehicle model.

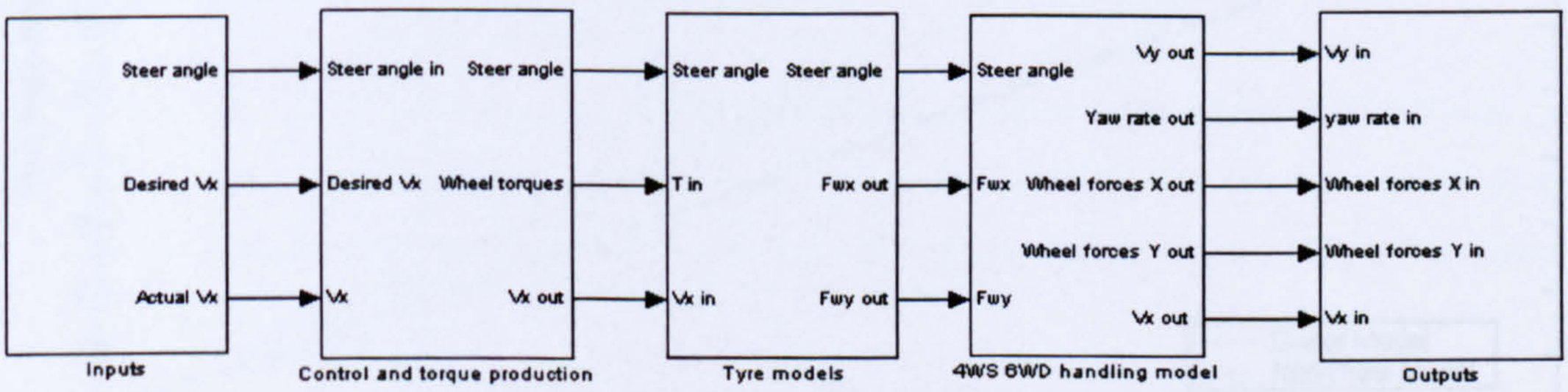

Fig. 2.20 Block diagram of Simulink[tm] model

The model should still operate in a linear manner at low lateral accelerations, however as the lateral acceleration increases, the model will enter the non-linear handling regime. By plotting the steer angle against lateral acceleration it is possible to determine the limit of the linear handling regime. Figure 2.21 shows the response for the unladen vehicle along side the results from the same test utilising the linear bicycle model. It can be seen that the initial part of the graph is linear up until approximately 0.4g after which vehicle handling becomes non-linear and deviates from the linear model. This initial region is called the primary handling (Dixon, 1991) where handling is predominantly linear and is adequately modeled using the linear bicycle model presented above. The non-linear region up until the limits of handling is termed the secondary handling regime where the vehicle behaves in a non-linear fashion although the vehicle has yet to reach the limits of handling. In the region at the limits of handling, where the vehicle is said to be in the final handling regime, the vehicle behaves in a highly non-linear fashion. The basic non-linear handling model is intended to describe all three regions,

although greater accuracy will be available from the full model to be developed in Chapter 4. The limit of handling occurs in two different ways: final understeer and final oversteer. The former results in maintained vehicle stability, however the vehicle ceases to react to steer inputs. Final oversteer results in vehicle instability, however the vehicle still react to steer input and a reverse steering angle will often result in the vehicle regaining stability (a method used by rally drivers during cornering).

It is expected, as the full vehicle model is developed and the suspension and load transfer effects are incorporated, the non-linear regime will begin at lower values of lateral acceleration. Figure 2.21 shows that the bicycle model is slightly different to the non-linear model. This is due to the introduction of the self-aligning moment generated by the pneumatic trail, which isn't taken into account in the linear model.

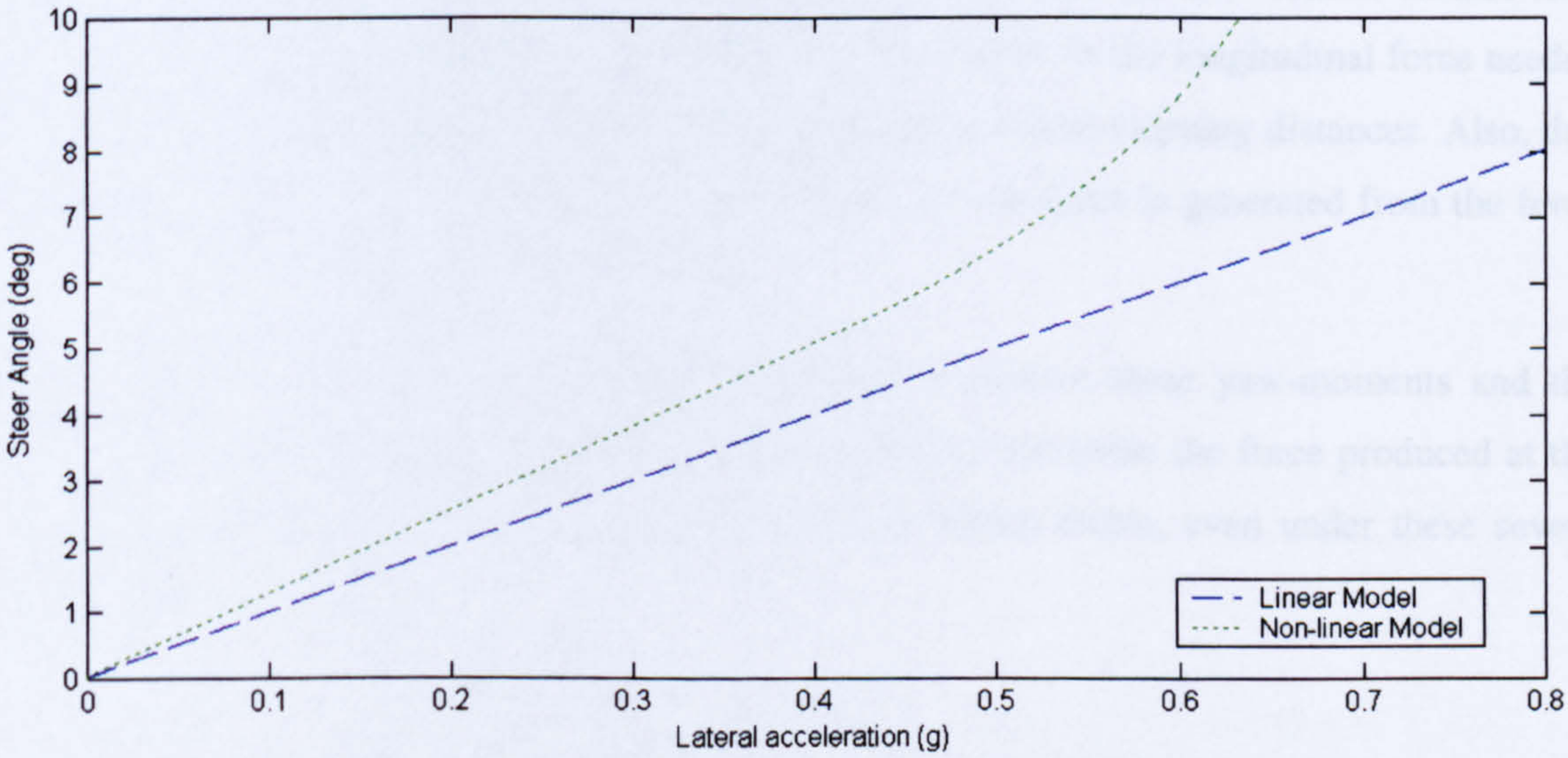

Fig. 2.21 Lateral acceleration response to steer input for linear and non-linear models

The model is simulated undertaking a number of manoeuvres. Figure 2.22 shows the yaw-rate response for both the unladen and laden vehicle undertaking a lane-change on a dry and a wet asphalt surface at 40km/h. It can be seen that the unladen vehicle exhibits the understeering behaviour that was predicted by the bicycle model in section 2.5. Again, as predicted the laden vehicle has oversteering behaviour although on the lower friction coefficient peak yaw-rates are not achievable as lateral tyre forces saturate. It will be the role of the controller to ensure the yaw-rate of the vehicle follows the desired yaw–rate, whatever the vehicle loading or road surface and ensuring that stability is maintained.

Figure 2.23 and figure 2.24 show yaw-rate and longitudinal velocity responses for the vehicle accelerating on a split-μ surface from 5km/h to 80km/h and figure 2.25 and figure 2.26 show

the same results for heavy braking on a split-μ surface taking speed from 80km/h to 0. The left three tyres are assumed to be travelling on a dry asphalt surface ($\mu = 0.8$) and the right tyres on wet asphalt ($\mu = 0.5$).

In the case of acceleration, as the peak μ is lower on the right set of tyres, the max available force on the right tyres is less than that available on the left. This causes the wheels on the lower friction co-efficient surface to spin easier, resulting in the wheel-slip going above the peak value, causing the available tractive force to be reduced further, along with reduced lateral tyre forces. This imbalance in force results in a yaw-moment being generated, removing the vehicle from its desired path and also the increase in wheel-slip adversely effects the vehicle's acceleration performance.

For the braking case, as the brakes are applied, the wheels on the low friction surface lock followed by those on the higher friction surface. This results in the longitudinal force needed to stop the vehicle being reduced, potentially causing increased stopping distances. Also, due to the differing friction coefficients, an undesirable yaw-moment is generated from the force imbalance between the left and right tyres.

It will be the duty of the yaw-moment controller to remove these yaw-moments and the responsibility of the traction/anti-lock braking control to maximise the force produced at the tyre/road interface. By doing so the vehicle should remain stable, even under these severe circumstances.

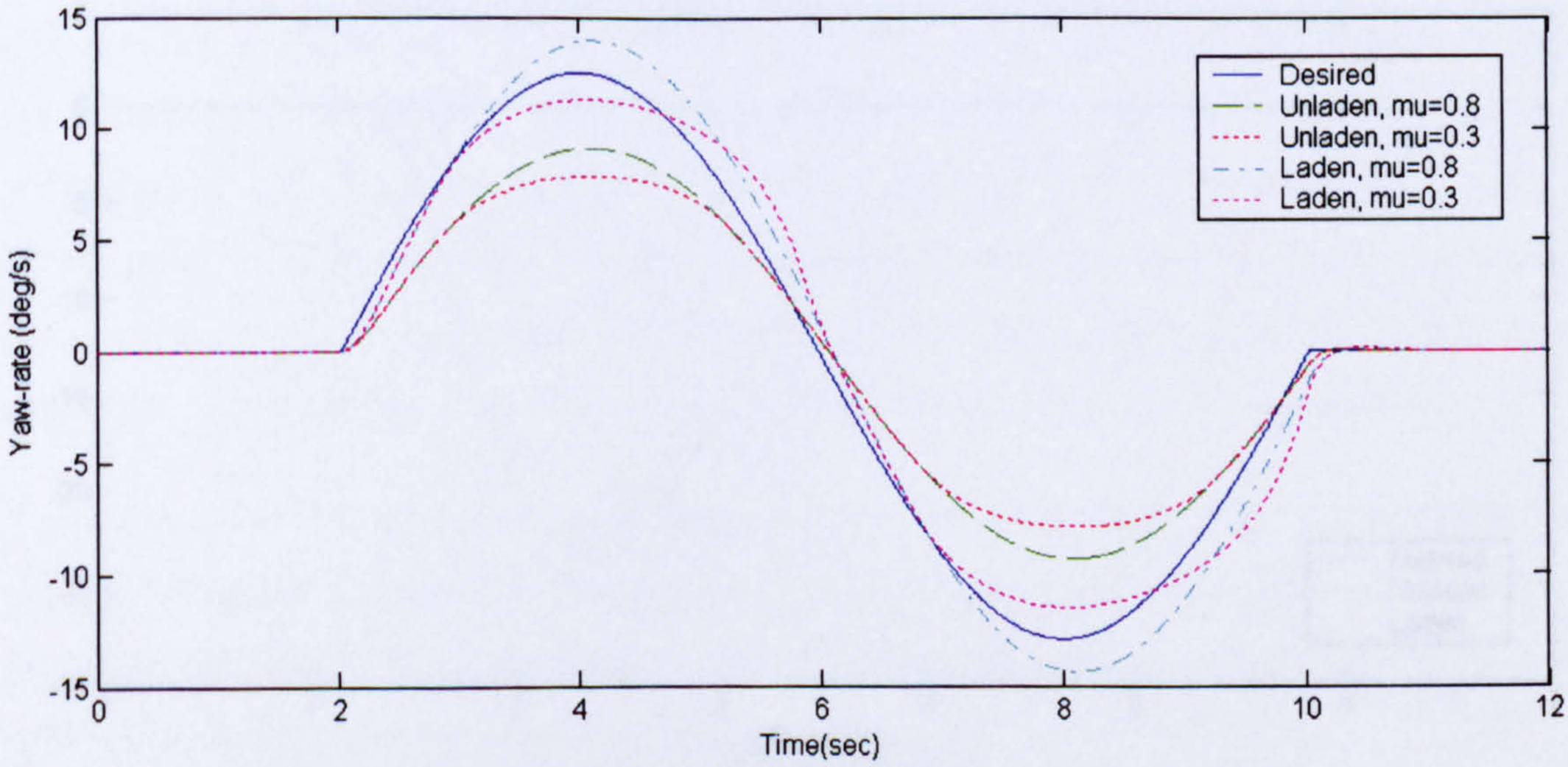

Fig. 2.22 Yaw-rate response to lane-change steer input at 60km/h

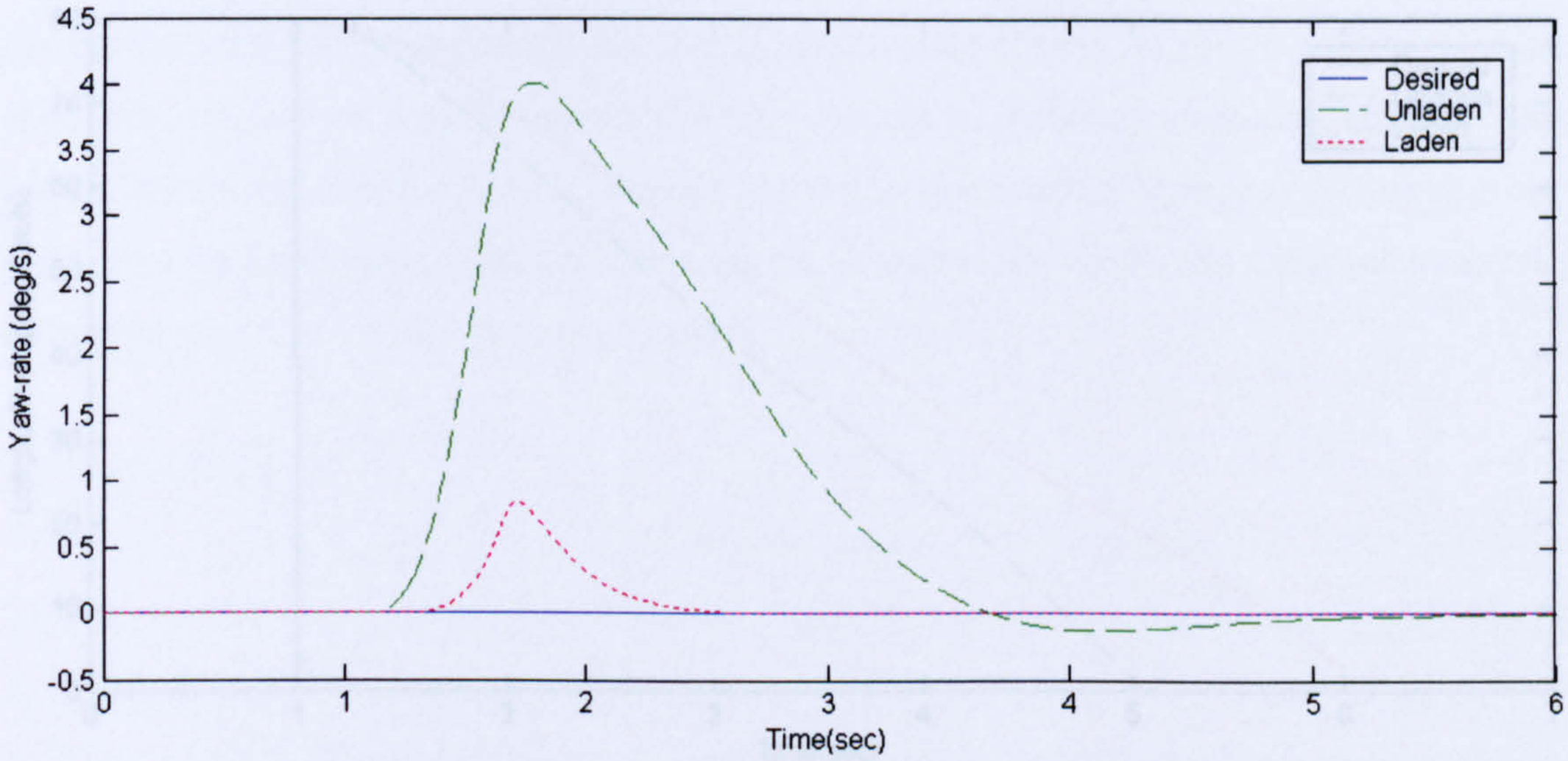

Fig. 2.23 Yaw-rate response to acceleration on a split-μ surface

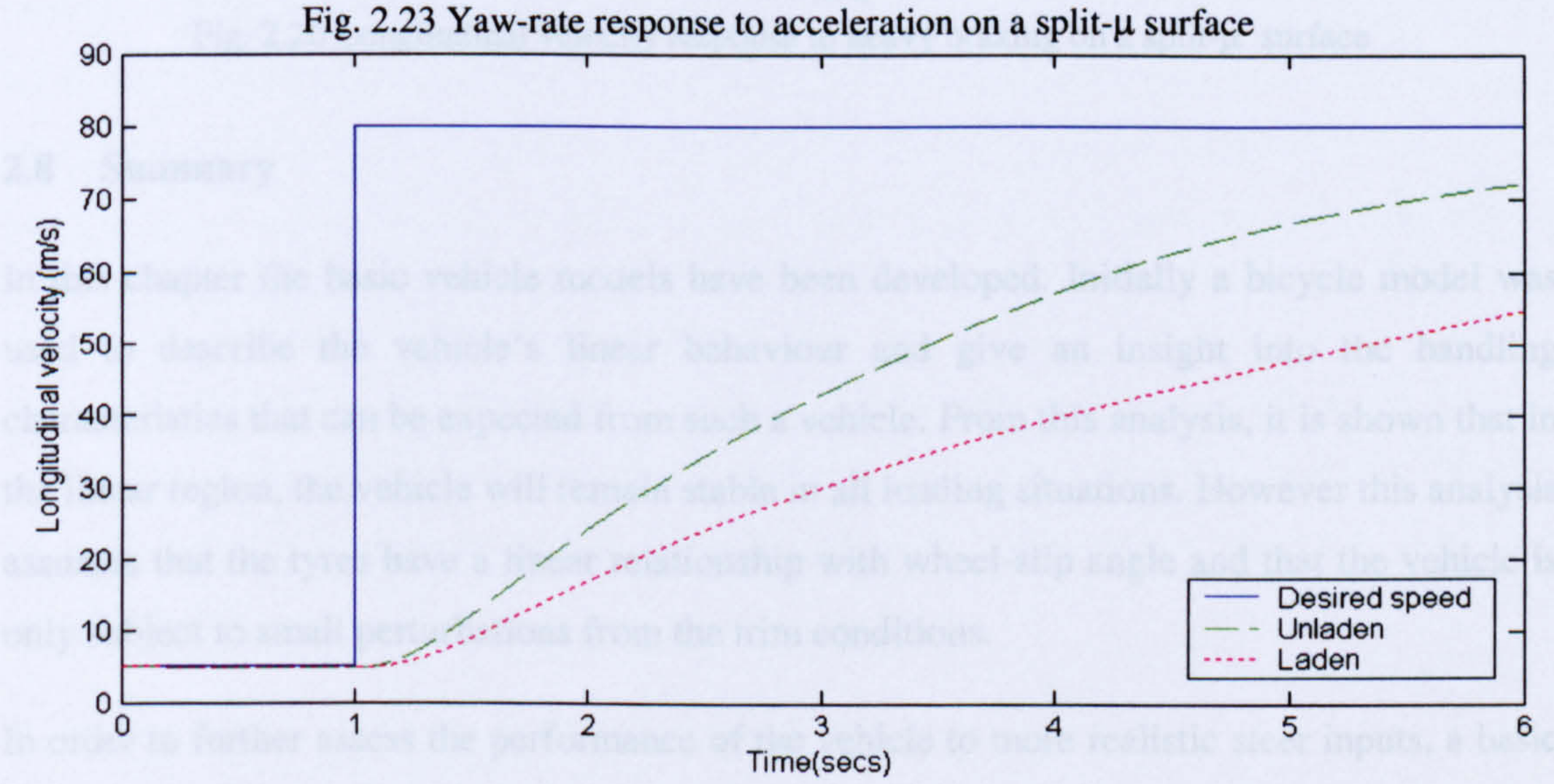

Fig. 2.24 Longitudinal velocity response to acceleration on a split-μ surface

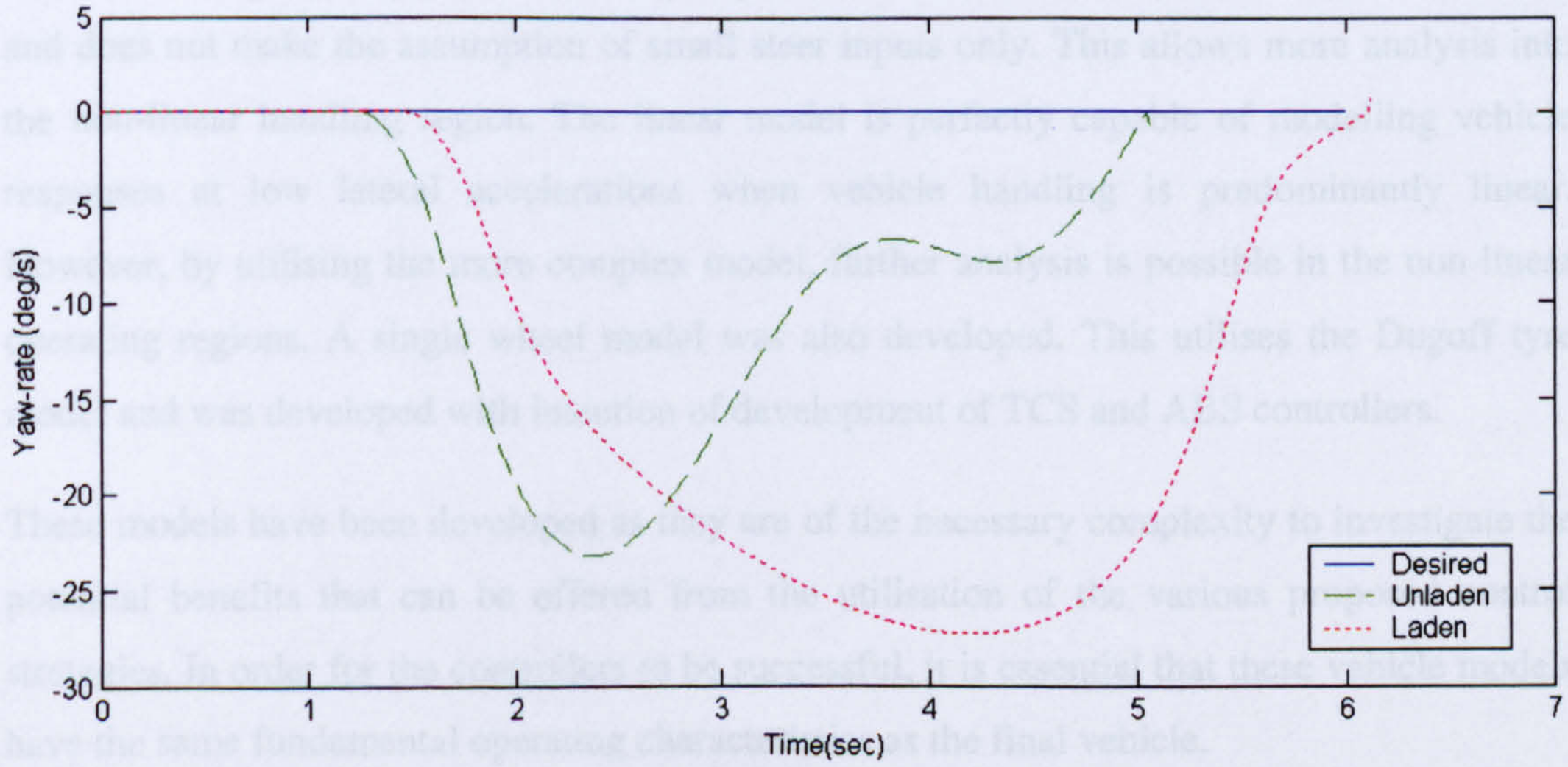

Fig. 2.25 Yaw-rate response to heavy braking on a split-μ surface

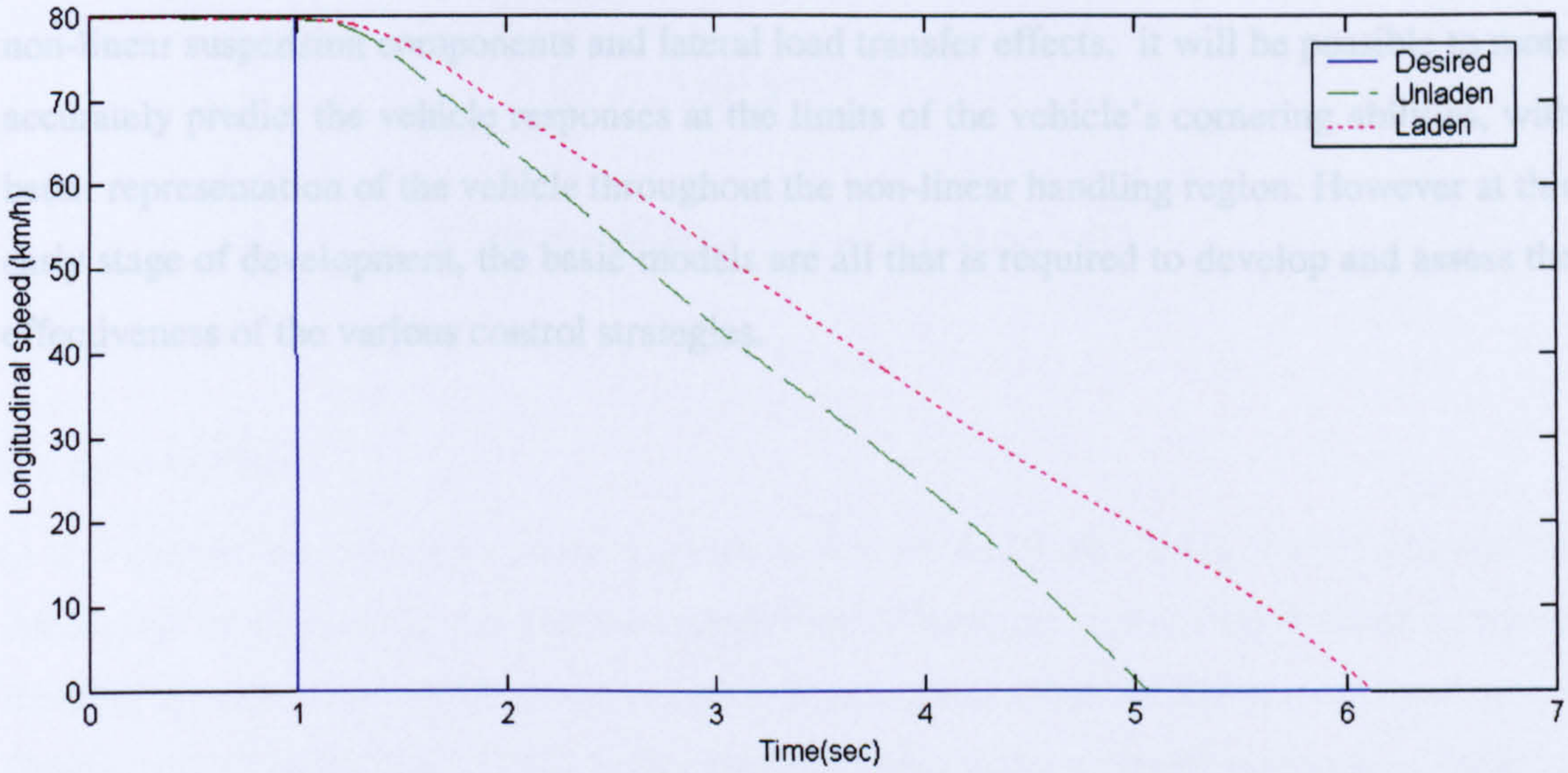

Fig. 2.26 Longitudinal velocity response to heavy braking on a split-μ surface

2.8 Summary

In this chapter the basic vehicle models have been developed. Initially a bicycle model was used to describe the vehicle's linear behaviour and give an insight into the handling characteristics that can be expected from such a vehicle. From this analysis, it is shown that in the linear region, the vehicle will remain stable in all loading situations. However this analysis assumes that the tyres have a linear relationship with wheel-slip angle and that the vehicle is only subject to small perturbations from the trim conditions.

In order to further assess the performance of the vehicle to more realistic steer inputs, a basic non-linear handling model was developed. This model includes the non-linear tyre models and does not make the assumption of small steer inputs only. This allows more analysis into the non-linear handling region. The linear model is perfectly capable of modelling vehicle responses at low lateral accelerations when vehicle handling is predominantly linear. However, by utilising the more complex model, further analysis is possible in the non-linear operating regions. A single wheel model was also developed. This utilises the Dugoff tyre model and was developed with intention of development of TCS and ABS controllers.

These models have been developed as they are of the necessary complexity to investigate the potential benefits that can be offered from the utilisation of the various proposed control strategies. In order for the controllers to be successful, it is essential that these vehicle models have the same fundamental operating characteristics as the final vehicle.

The models developed in this chapter will form the basis of the final vehicle model onto which the integrated control strategy will be implemented and tuned. With the addition of

non-linear suspension components and lateral load transfer effects, it will be possible to more accurately predict the vehicle responses at the limits of the vehicle's cornering abilities, with better representation of the vehicle throughout the non-linear handling region. However at this early stage of development, the basic models are all that is required to develop and assess the effectiveness of the various control strategies.

Chapter 3

Controller Development

3.1 Introduction

In this chapter the mobility control algorithms will be developed using the vehicle models introduced in Chapter 2. As mentioned previously, literature centres on 3 main forms of mobility control: Traction Control, Anti-lock Braking and Direct or Dynamic Yaw-moment Control (TCS, ABS and DYC respectively). These initial control algorithms will be developed on the relevant vehicle model and will then form the basis of a more complex integrated vehicle control system that will aim to improve vehicle handling and mobility. Results from these initial control exercises will give an insight into the full potential of Individual Wheel Control.

TCS and ABS will be developed using the single wheel model, then DYC will be implemented on the basic non-linear handling model. Once developed and tested individually, they are integrated into a combined mobility controller and tested on the basic non-linear handling model.

3.2 Controller Design Specifications

Before the controller is developed, the requirement of its performance must be proposed. This specification is designed so that the greatest potential can be derived from the use of Individual Wheel Control. The operation of the controller is based on the potential that has been shown in literature regarding mobility control. The requirements of the controller are:

1. To robustly, accurately and rapidly track a desired yaw-rate during low to mid-lateral accelerations (i.e. under primary and secondary handling conditions) regardless of loading and road surface.
2. To stabilise vehicle handling on split-μ surfaces.
3. To limit wheel-slip during acceleration to improve tractive performance and maintain lateral stability.
4. To prevent wheels from locking during deceleration to improve stopping distances and maintain lateral stability.

5. To reduce driver workload, limiting the time it can be said the driver operates in a closed-loop manner.
6. To limit side-slip angle at high lateral acceleration or in the final handling region.

The controllers will now be developed to demonstrate these specifications although point 6 will not be dealt with until Chapter 5.

3.3 Control Methods

The following subsections give a brief introduction to some of the control algorithms that can be used to implement the mobility control systems mentioned in Chapter 1 and their suitability to the proposed tasks. There are, of course, other control systems that are of use, but the following are the most prominent in the literature reviewed.

3.3.1 Linear Control

Proportional/Integral/Derivative control (PID)

As PID control is simple to implement in software it is a useful tool to the control engineer hence it is commonly used in industry. They are robust and applicable for both simple control problems and also more complex non-linear systems. Given that they are linear controllers, they are best suited to linear plants, their performance degrading when used in more complex, non-linear systems (Dorf and Bishop, 1998).

The linear behaviour of the DC motor makes PID control useful for torque/speed control. Park and Kim (1999) used a PI controller to implement a simple TCS on a conventional vehicle, varying the throttle angle. It is used in conjunction with a more complex system to derive and control the wheel-slip, giving good results.

Pole-placement control

Another linear control method is pole-placement (Franklin *et el.* 1998). Any linear system will have certain pole positions that give a desired closed-loop response. If the systems transfer function is known, a controller can be designed that will move the systems poles to the desired closed-loop pole positions. This is a simple control method, although its use becomes more complex as the order of the system increases. It is possible for complex non-linear systems to be linearised about a normal operating point and pole placement to be implemented, although the performance of the controller will be reduced.

Pole-placement can be robust. Although changes in system parameters will result in the closed-loop poles moving from the desired locations and hence altering the response, there is the possibility of determining poles that will offer good responses for various plant conditions. Pole-placement, like most other linear control methods can be implemented in both transfer function and state-space form, in either discrete or continuous time (Plummer, 1999)

Optimal Controllers

Optimal controllers (Plummer, 1999) are similar in structure to pole-placement, but the controller is designed to minimise certain quantities expressed as a cost function. Minimum Variance Control (MVC) places poles to minimise the average error and Linear Quadratic Control (LQG) attempts to minimise the error while at the same time minimising the control signal. This is especially useful where power considerations are important. MVC is used by Tsiotras and de Wit (2000) to implement ABS using the peak frictional force and shows excellent results.

Another optimal controller is the H_∞ method, which minimises the maximum signal in the frequency domain. H_∞ is also a robust controller as it minimises responses to modelling errors at certain frequencies.

3.3.2 Non-linear control

Adaptive Control

The obvious advantage of adaptive control (Plummer and Brown, 1999 and Dorf and Bishop, 1998) is the ability to design and alter the controller on-line as plant dynamics change, implementing any changes immediately. This leads to a highly desirable controller. There are various types of adaptive control methods, such as indirect, direct and gain scheduling. Indirect adaptive control utilises separate plant parameter estimation and controller design stages. In direct adaptive control, plant parameter and controller design stages are combined to give a desired method of deducing the controller coefficients directly. Both of these methods use a Recursive Least Squares (RLS) to estimate the parameters of the plant, which subsequently adapts the control signal. These methods, however, are difficult to implement and add increased complexity to the system, which is why simpler adaptive controllers are often favoured.

Gain scheduling, although of limited use is the most common adaptive controller in industry. It employs a number of fixed-coefficient control algorithms, each one designed to deal with the system when it is in a specific state. This is only of use when the system operates in a limited number of known modes. With regards to IWC, gain scheduling could be used in the supervisory control, where the control algorithm of the DYC is altered depending on the operation of the traction or anti-lock braking controllers.

Intelligent Knowledge-Based Systems (IKBS)

The use of IKBS is particularly useful for supervisory control and fault detection. Expert systems, using proposition or predicate logic, are capable of decision-making based on a number 'if', 'then' rules, mimicking a human expert. This is ideal for overall control of the HEV systems when outputs are pre-defined constants, for example, if the vehicle reference speed can no longer be measured then the output from the expert controller may be to shut down the traction control system. Fuzzy logic is another form of IKBS, which deals with uncertainties in both input and output.

Fuzzy Logic Control

Fuzzy logic control is a non-linear control method, that is particularly useful when the system itself is highly non-linear. It is noted in Plummer (1995) that

> "As the complexity of the process representation and its uncertainty increases, we realise that these traditional mathematical tools are rather inadequate and the task becomes increasingly difficult"

The advantages of fuzzy logic control are that it is robust and requires little knowledge about the mathematics of the system. Logic can be derived using basic knowledge about the systems operation.

De Koker *et al.* (1996) implemented a fuzzy logic Traction Control System. De Koker noted that fuzzy control provided a robust method of predicting wheel-slip although a substantial amount of tuning of the membership functions was required before adequate results were obtained. Another potential downside is that if the controller is quite complex (i.e. it contains a large number of membership functions) the speed of the system maybe incapable of efficiently implementing the control. This condition can be remedied by increasing processor speed or reducing complexity of the fuzzy logic.

Yoshimura *et al.* (1997) also noted excellent response for the fuzzy traction control when it came to preventing slip. Bauer *et al.* (1996) employed two separate fuzzy controllers in their Traction Control System, one was used to estimate the peak slip, the other used to regulate the slip at the desired level. Both offer robust control against changing road conditions although the former was less effective with the introduction of time-varying uncertainties.

Neural Network Control

The use of neural networks as controllers allows for robust control of highly complex non-linear systems. A major advantage of neural networks is their ability to be trained, automatically learning how to control a machine. This makes neural networks extremely robust; there is no need for a mathematical model of the system and they are tolerant to uncertainties and faults (Plummer and Brown, 1999b). Potential drawbacks include a lack of system representation and there is no accurate way of determining the optimum neural structure for specific tasks. Although they have received only limited attention for implementation of TCS, ABS or DYC, they have been adopted in the powertrain control of HEV's (Baumann *et al.*, 1998) with promising results.

Sliding-Mode Control

A more mathematical system than the two above, Sliding-Mode Control has received particular attention as a means of implementing TCS (Kawabe *et al*, 1997), ABS (Drakunov *et al*, 1995) and yaw control (Drakunov *et al*, 2000)

A switching surface is set up that separates the systems state space into areas with fixed control laws. The control system has the ability to switch from one law to another. The control laws are trajectories (various types exist) that point towards the switching surface. When they reach the control surface they switch trajectory, to again point towards the switching surface. By using various trajectories it is possible for the system to move in a stable manner down the switching line to the origin (Banks, 1986). SMC is relatively independent of the system parameters and so is robust. If the frequency of the switching is too high, "chattering" (Friedland, 1996) can occur where the control device can not operate as quick as the control laws change and so it never reaches the switching surface.

Results from using SMC show its potential, reporting good responses for TCS, ABS and DYC and an excellent ability to overcome uncertainty.

3.3.3 Control Discussion

As separate systems for TCS, ABS, DYC are initially to be developed, it would be impractical to attempt each of the above control methods. Given that it is intended that the full vehicle model is to be developed, resulting in a highly complex model, fuzzy-logic is ideally suited for implementation of all the above systems The co-ordination of the individual mobility controllers is ideally suited for IKBS or fuzzy logic as its operation is intuitive and requires a logical approach. In addition to fuzzy logic, PID control will be also assessed, due to its robust operation and simplicity. It is thought, however, that as the vehicle model becomes increasing non-linear, PID controller ability will diminish.

If the system were to be simplified to a simple linear mathematical model, the number of viable control options would increase, however the ability of that model to accurately represent the system is reduced. A vehicles handling behaviour is linear during low to mid lateral accelerations, however as the lateral acceleration increases, the non-linearity increases, hence the need for robust non-linear control.

3.4 Traction Control Implemented on Single Wheel Model

Utilising the single wheel model developed in section 2.6, a single wheel TCS can be developed. The nature of wheel-slip means that the TCS is only active at certain times. Its job is to prevent the wheel from excessively slipping, i.e. when the wheel-slip is above a desired value. When it is below this value, it is up to the driver to control the wheel torque to obtain the maximum longitudinal force. Therefore any traction controller is only required to activate when wheel-slip goes above a user defined value (or in the case of a optimum wheel-slip system, the wheel-slip corresponding to maximum tyre force).

If a torque is demanded by the driver, the controller must first determine the maximum torque available at the particular wheel speed. This puts a cap on the torque before the traction controller subtracts the control torque from it, ensuring that the controller has an effect. This is the torque demand (driver demand torque minus control torque demand) which is then sent to the motor model. (see figure 3.1)

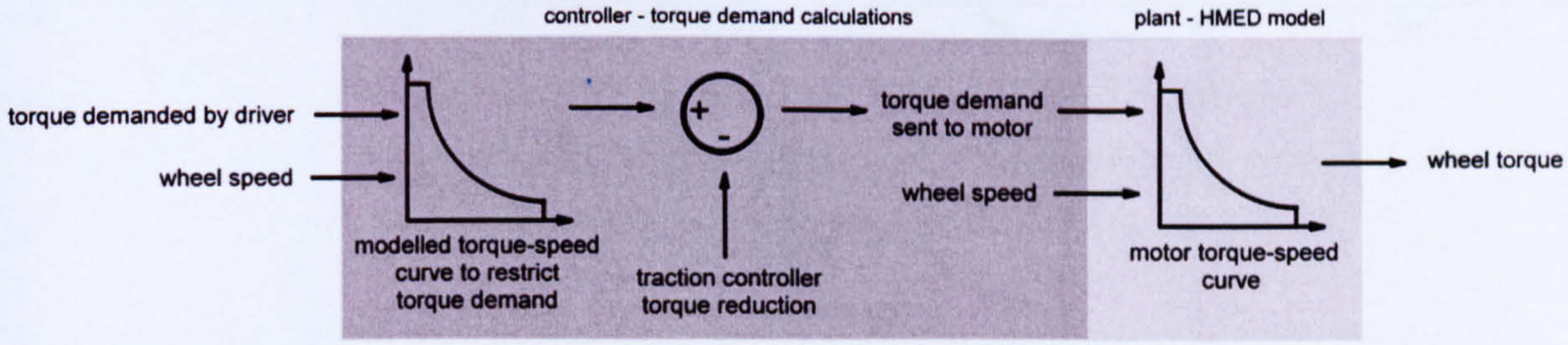

Fig. 3.1 Wheel torque calculations.

The following sections present two popular control methods that will be utilised to control the wheel-slip on the single wheel model.

3.4.1 PD Control

When a vehicle is accelerated on a low μ surface, wheel-slip increases. When it goes over the optimum wheel-slip, the longitudinal tyre force available decreases. It is the job of the controller to keep the wheel-slip at or below the optimal or desired wheel-slip. When wheel-slip goes above this value it is the traction controllers job to reduce slip back below this value. Wheel-slip is not desired to settle at a particular value, it is only required to stay at or below the optimal value. This infers that there is no steady-state value, hence no steady-state error which removes the need for integral control. Only proportional and derivative control are utilised for the individual TCS's. The controller is designed to turn on when wheel-slip goes above the optimal or pre-defined slip. For the purpose of controller design, a desired wheel-slip value of 0.2 is used which promotes good responses on all road surfaces. This means the controller works as shown in Equation 3.1 where e = desired wheel-slip – actual wheel slip.

$$U = \begin{cases} O & if\ \lambda < 0.2 \\ K_{tp}e + K_{td}\dfrac{de}{dt} & if\ \lambda \geq 0.2 \end{cases} \quad (3.1)$$

3.4.2 Fuzzy Logic Control

The next controller to be developed for the TCS is a fuzzy logic controller. The controller is designed in the Fuzzy Logic Toolbox provided by Mathworks for MatLAB. In order for good responses to be achieved it was decided that two input variables would be used, wheel-slip error and rate of change of wheel-slip error. When a vehicle is accelerated and wheel-slip occurs, when it passes 0.2, the slip error is small but the rate of change of error is large, so by using this extra input it is possible to have a bigger initial effect, than using slip error alone. The membership functions are shown in figure 3.2. The following rules were decided on and presented in table 3.1 (the output is the torque reduction).

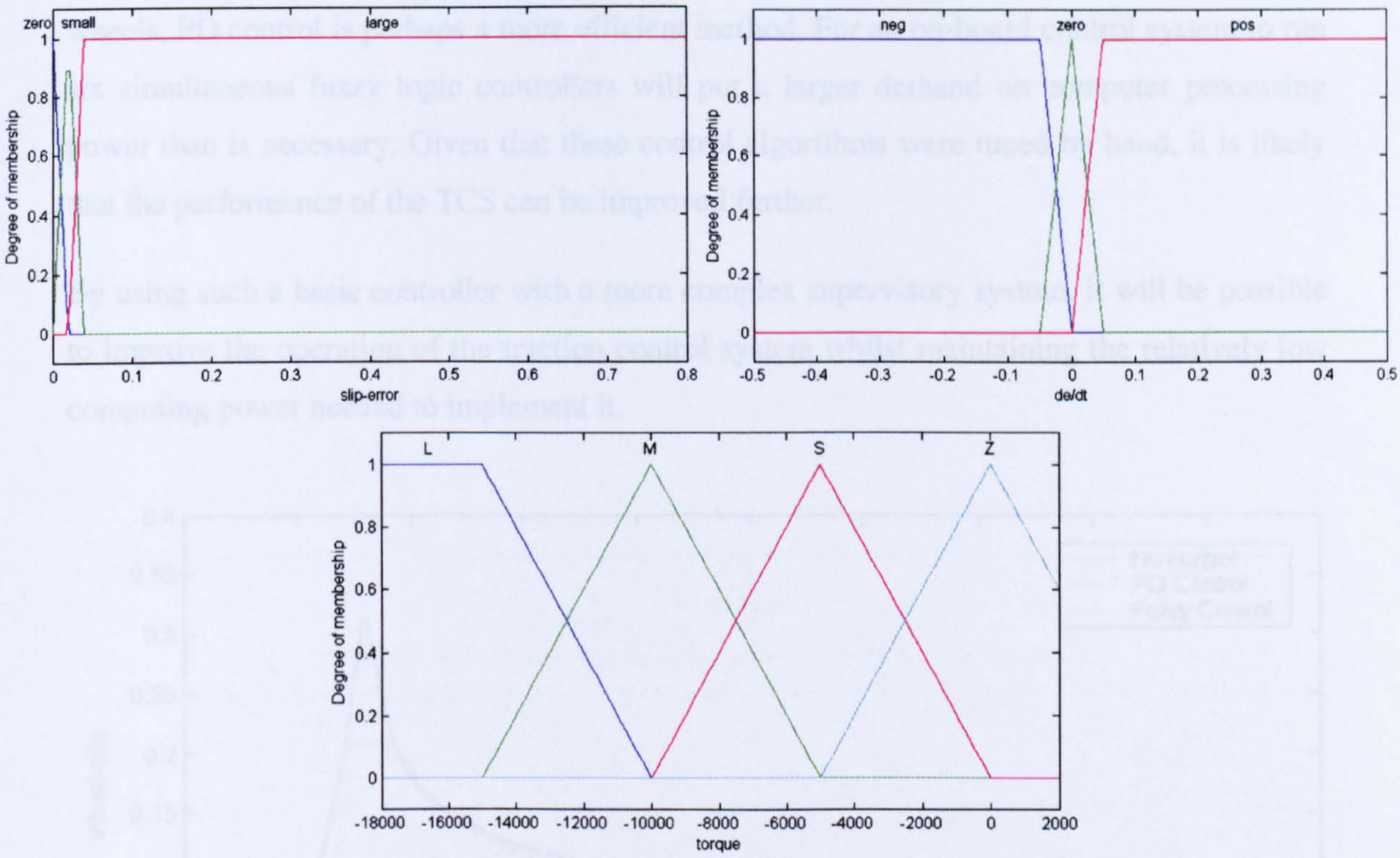

Fig. 3.2 Fuzzy logic membership functions for Input variable for slip error, input variable for rate of change of slip error (de/dt) and output variable for torque.

		Rate of change of wheel-slip error		
		negative	zero	positive
Wheel-slip error	zero	zero	zero	large
	small	small	medium	large
	large	large	large	large

Table 3.1 Fuzzy logic rules for traction controller

3.4.3 Traction Controller Results

The vehicle is simulated accelerating from 5km/h to 80km/h in unladen and laden states on a two different road surfaces. The wheel-slip responses are shown from figure 3.3 to figure 3.6. The tuners were both tuned by hand and although perhaps not representing the optimal control, the results show that both controllers show an excellent capability to limit wheel-slip to a value of 0.2. It is also shown that both controllers are robust to changes in vehicle loading and road surface. As the vehicle model becomes increasingly complex, the tyre loading and road friction will also become increasingly transient, this robustness is essential. The fuzzy logic control shows a slightly quicker response to the wheel-slip increasing above the desired value. Despite this, there is relatively little difference between the performance of the two controllers. Due to the simplicity of the controller and the need for TCS's for each of the six

wheels, PD control is perhaps a more efficient method. For an on-board control system to run six simultaneous fuzzy logic controllers will put a larger demand on computer processing power than is necessary. Given that these control algorithms were tuned by hand, it is likely that the performance of the TCS can be improved further.

By using such a basic controller with a more complex supervisory system, it will be possible to improve the operation of the traction control system whilst maintaining the relatively low computing power needed to implement it.

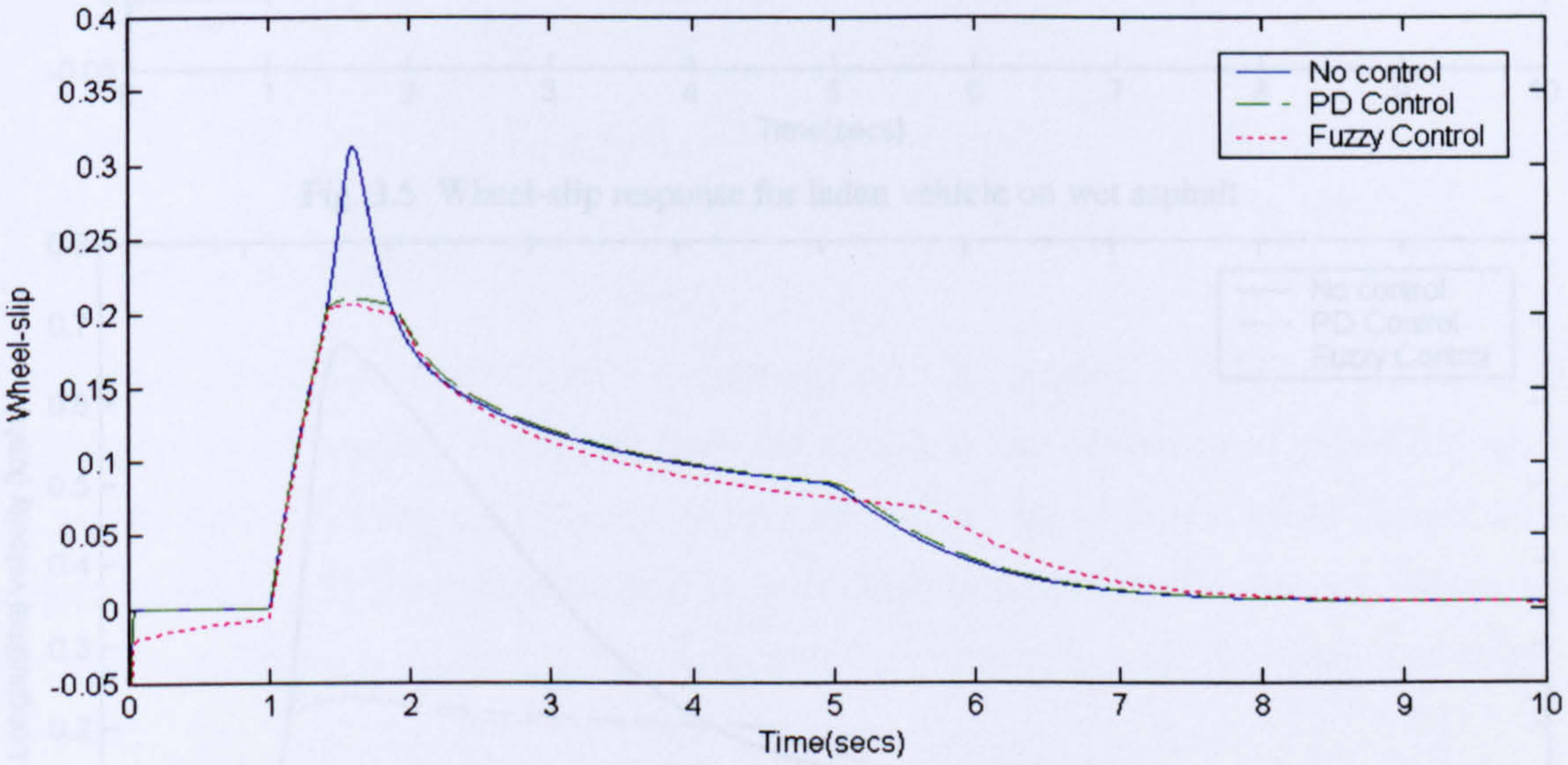

Fig. 3.3 Wheel-slip response for unladen vehicle on wet asphalt

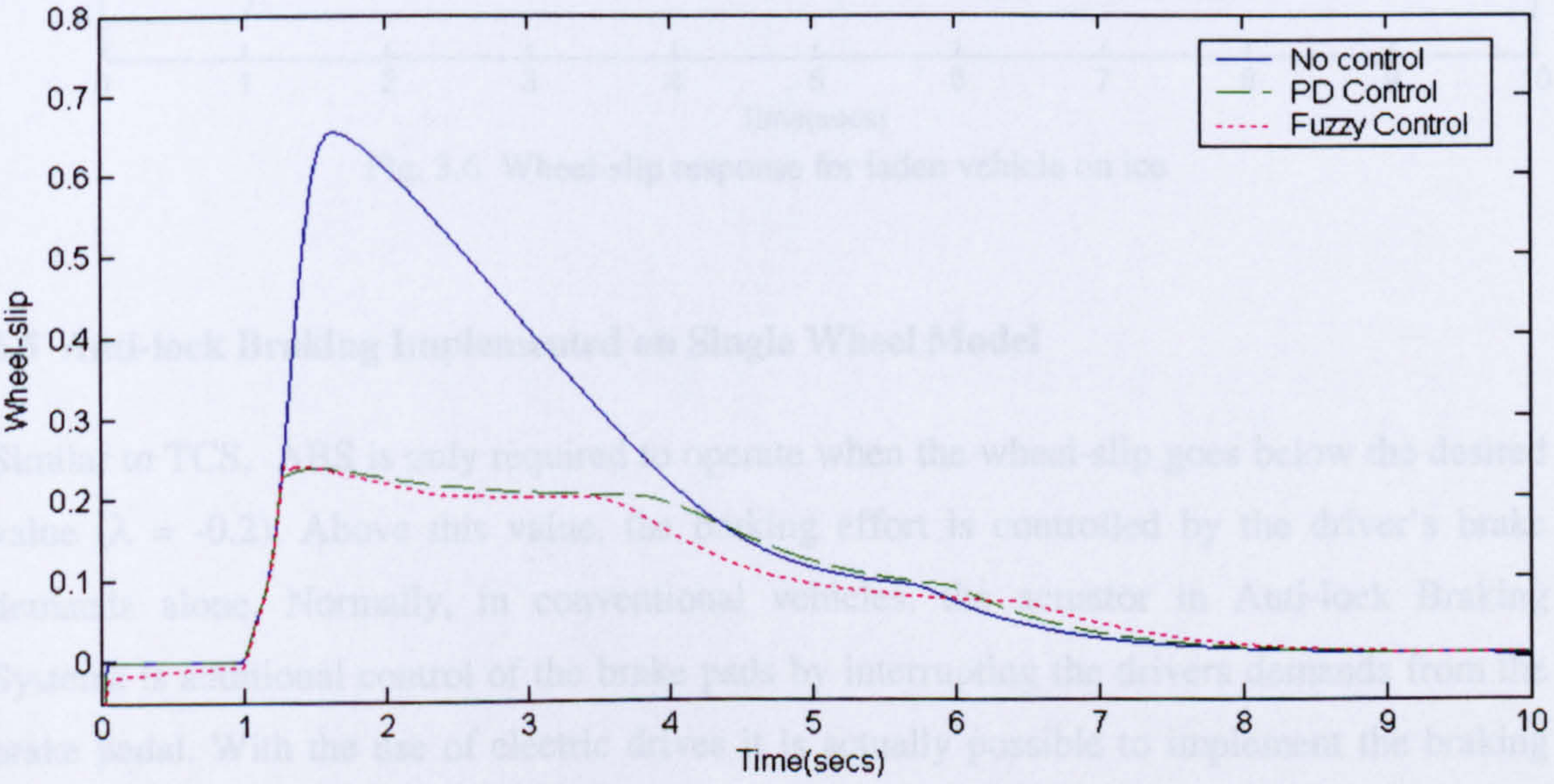

Fig. 3.4 Wheel-slip response for unladen vehicle on ice

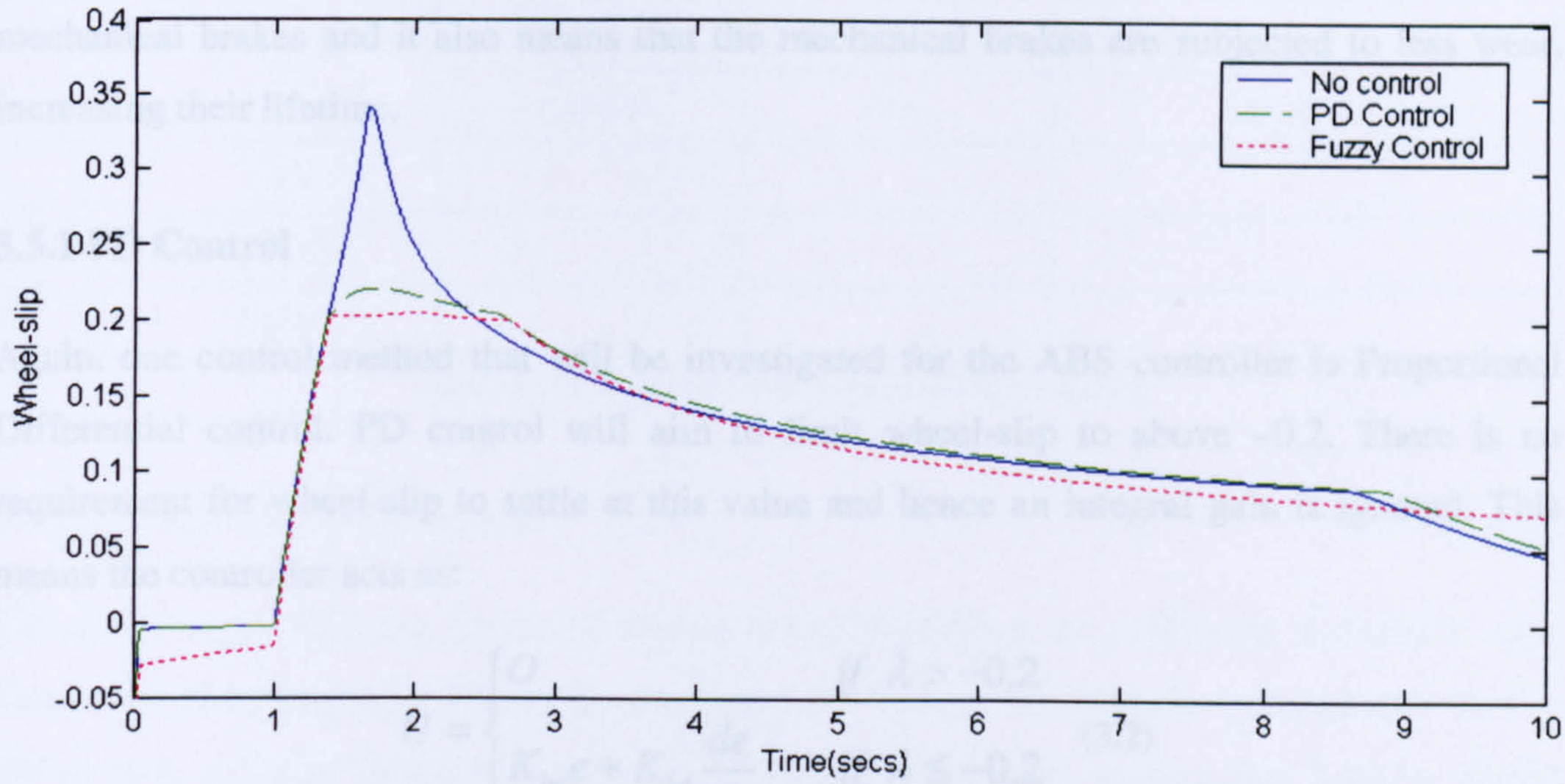

Fig. 3.5 Wheel-slip response for laden vehicle on wet asphalt

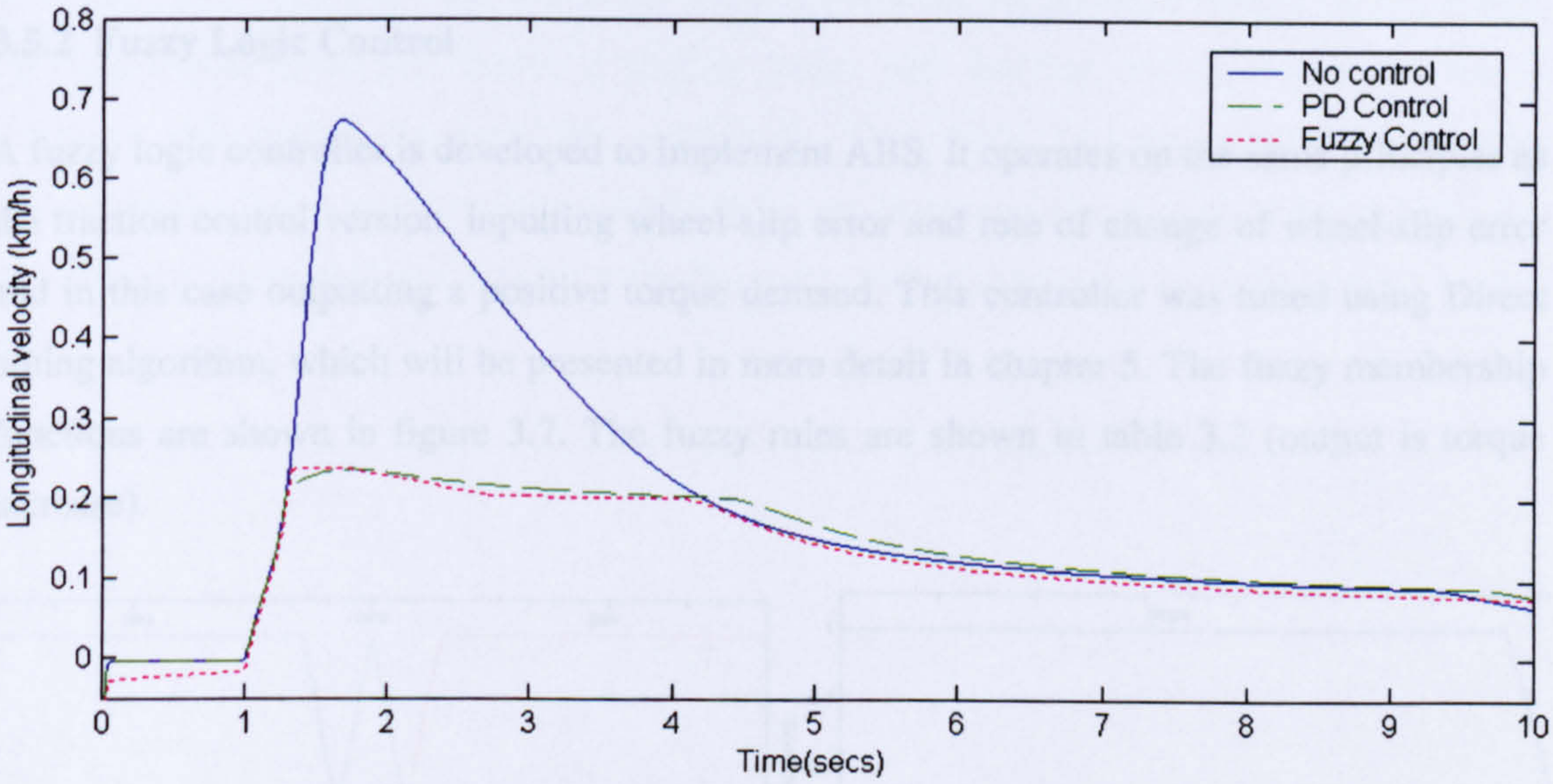

Fig. 3.6 Wheel-slip response for laden vehicle on ice

3.5 Anti-lock Braking Implemented on Single Wheel Model

Similar to TCS, ABS is only required to operate when the wheel-slip goes below the desired value (λ = -0.2). Above this value, the braking effort is controlled by the driver's brake demands alone. Normally, in conventional vehicles, the actuator in Anti-lock Braking Systems is additional control of the brake pads by interrupting the drivers demands from the brake pedal. With the use of electric drives it is actually possible to implement the braking electronically, resulting in regenerative braking, although a strategy may be developed at a later date to combine both the mechanical and electrical braking. The advantage of the electrical braking is that the braking torque is much easier to control than force applied by

mechanical brakes and it also means that the mechanical brakes are subjected to less wear, increasing their lifetime.

3.5.1 PD Control

Again, one control method that will be investigated for the ABS controller is Proportional Differential control. PD control will aim to limit wheel-slip to above –0.2. There is no requirement for wheel-slip to settle at this value and hence an integral gain is ignored. This means the controller acts as:

$$U = \begin{cases} O & if\ \lambda > -0.2 \\ K_{bp}e + K_{bd}\dfrac{de}{dt} & if\ \lambda \le -0.2 \end{cases} \quad (3.2)$$

3.5.2 Fuzzy Logic Control

A fuzzy logic controller is developed to implement ABS. It operates on the same principles as the traction control version, inputting wheel-slip error and rate of change of wheel-slip error and in this case outputting a positive torque demand. This controller was tuned using Direct tuning algorithm, which will be presented in more detail in chapter 5. The fuzzy membership functions are shown in figure 3.7. The fuzzy rules are shown in table 3.2 (output is torque increase).

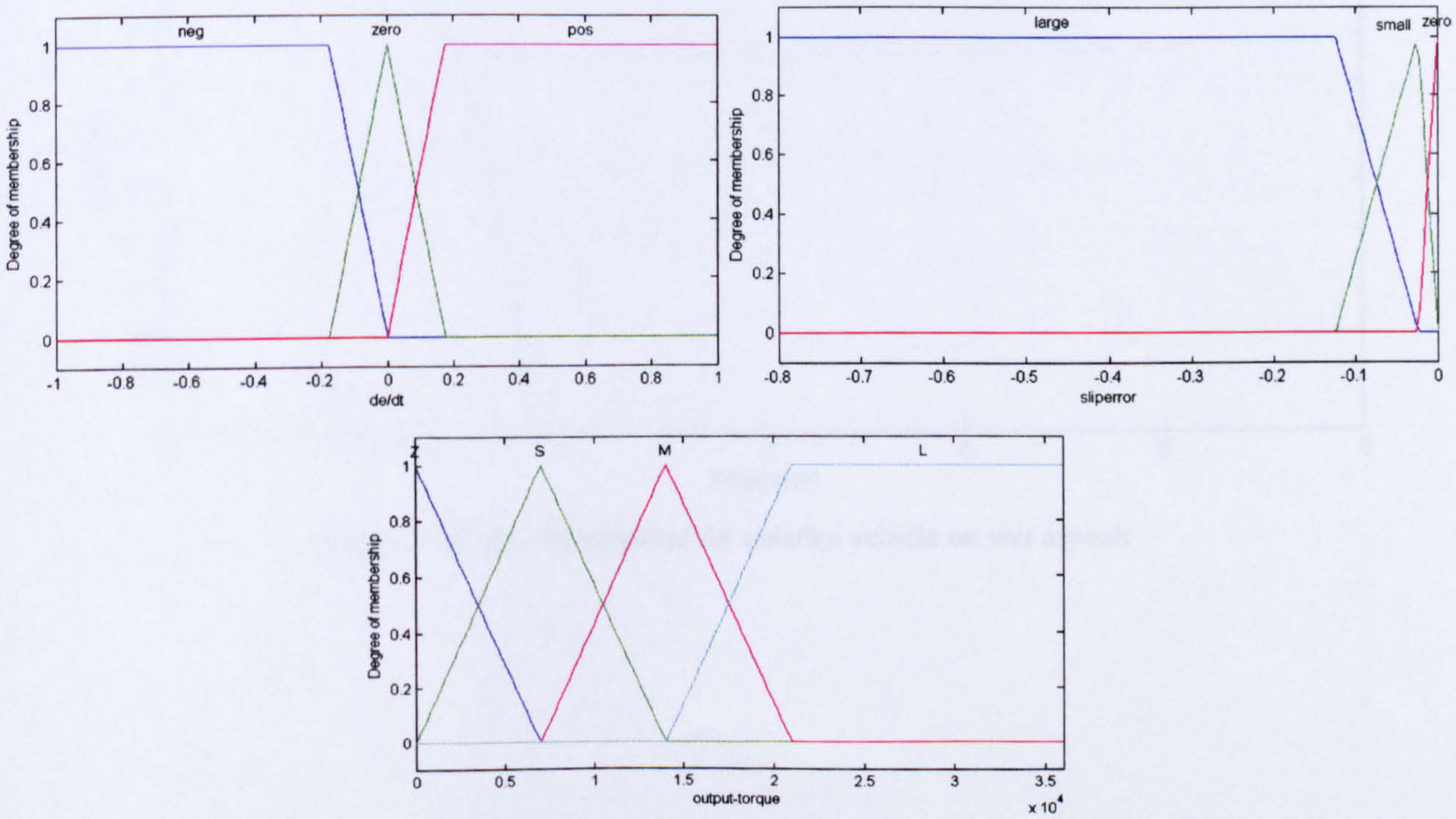

Fig. 3.7 Fuzzy logic membership functions for Input variable for slip error, input variable for rate of change of slip error (de/dt) and output variable for torque.

		Rate of change of wheel-slip error		
		negative	zero	positive
Wheel-slip error	zero	large	zero	zero
	small	large	medium	zero
	large	large	large	large

Table 3.2 Fuzzy logic rules for anti-lock braking

3.5.3 Anti-lock Braking Results

The above controllers are simulated during heavy braking on two different surfaces in both laden and unladen states. Figure 3.8 to figure 3.11 show the wheel-slip responses for the simulations utilising PD and fuzzy-logic control along with the uncontrolled vehicle. Figure 3.12 and figure 3.13 show the wheel and vehicle speed for the unladen vehicle on ice. Again, the fuzzy-logic controller shows a slightly better slip limiting ability, but again this is marginal (PD control has not been optimised). This slight increase in performance that appears in the fuzzy-logic case is outweighed by the increased complexity of the control. It is the PD controllers that will be utilised in the integrated controller to be developed in section 3.7.

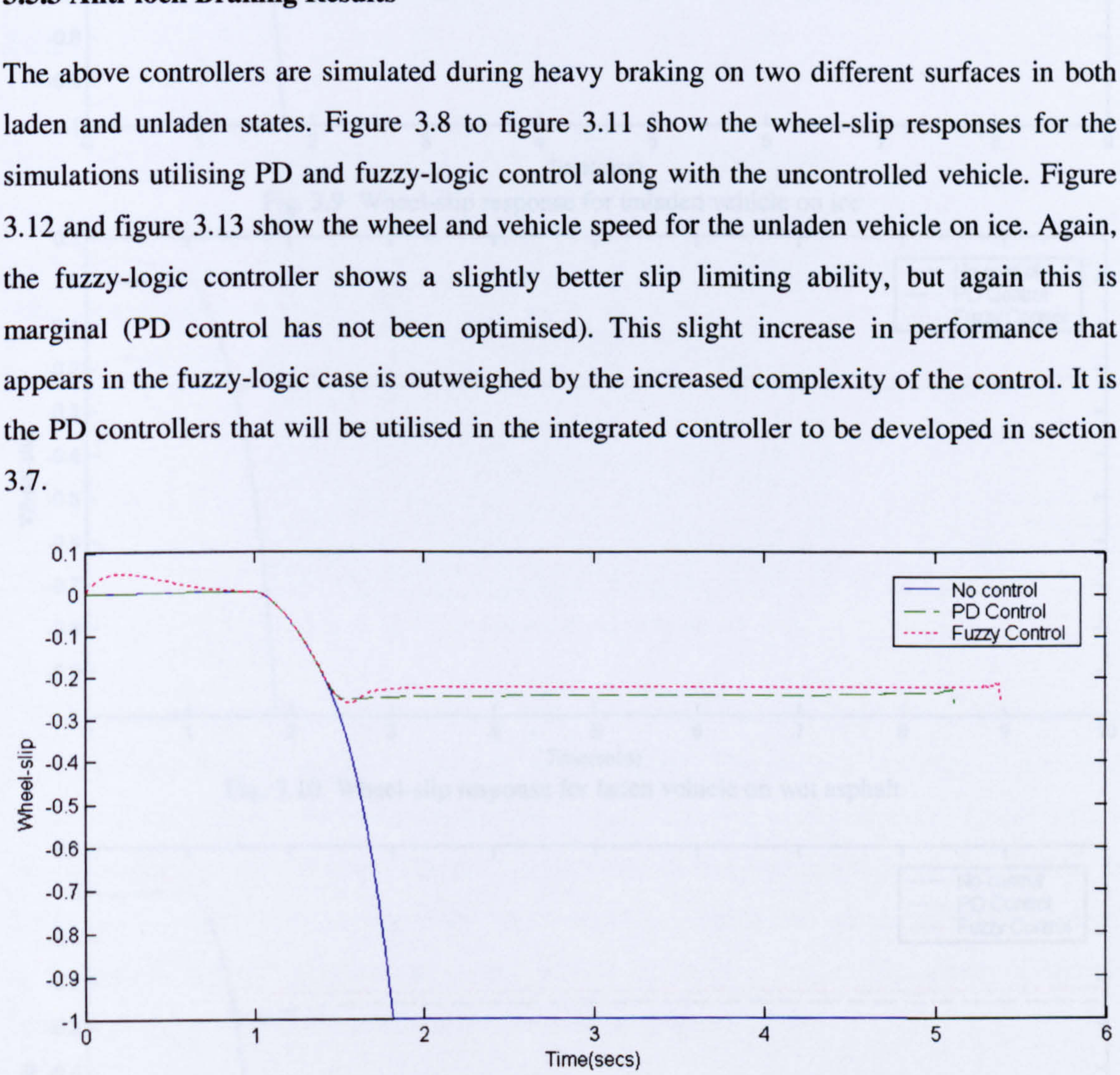

Fig. 3.8 Wheel-slip response for unladen vehicle on wet asphalt

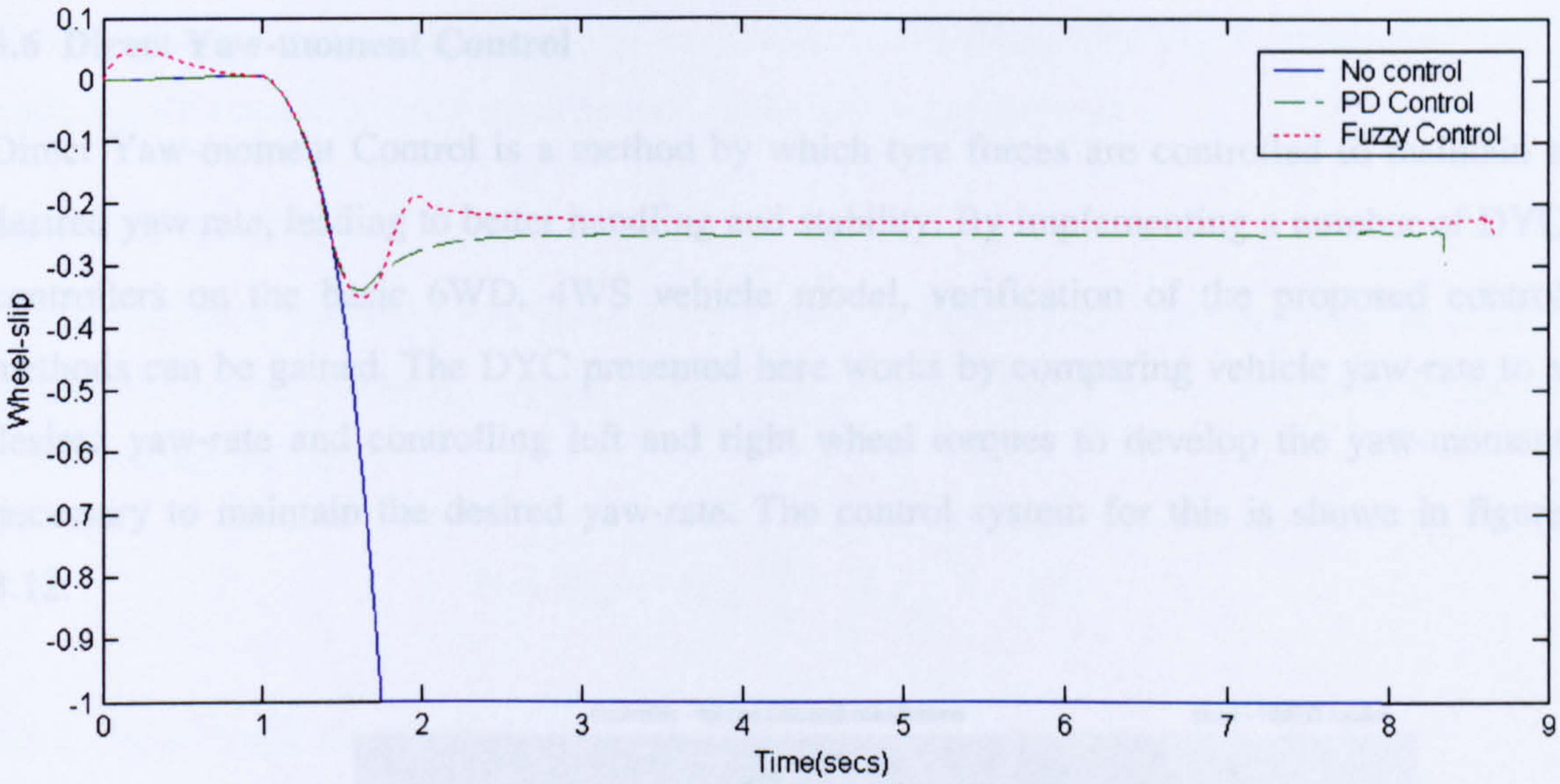

Fig. 3.9 Wheel-slip response for unladen vehicle on ice

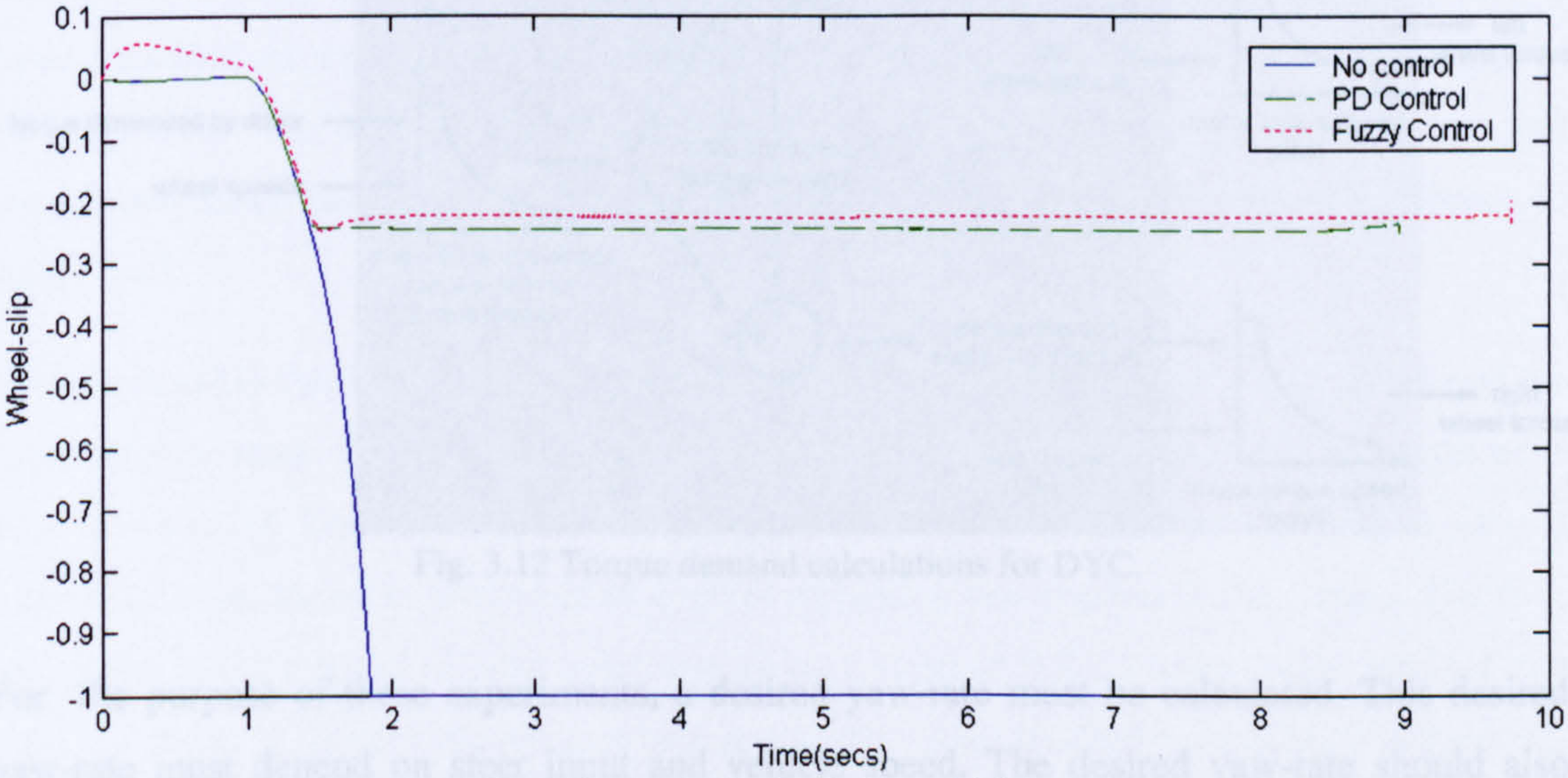

Fig. 3.10 Wheel-slip response for laden vehicle on wet asphalt

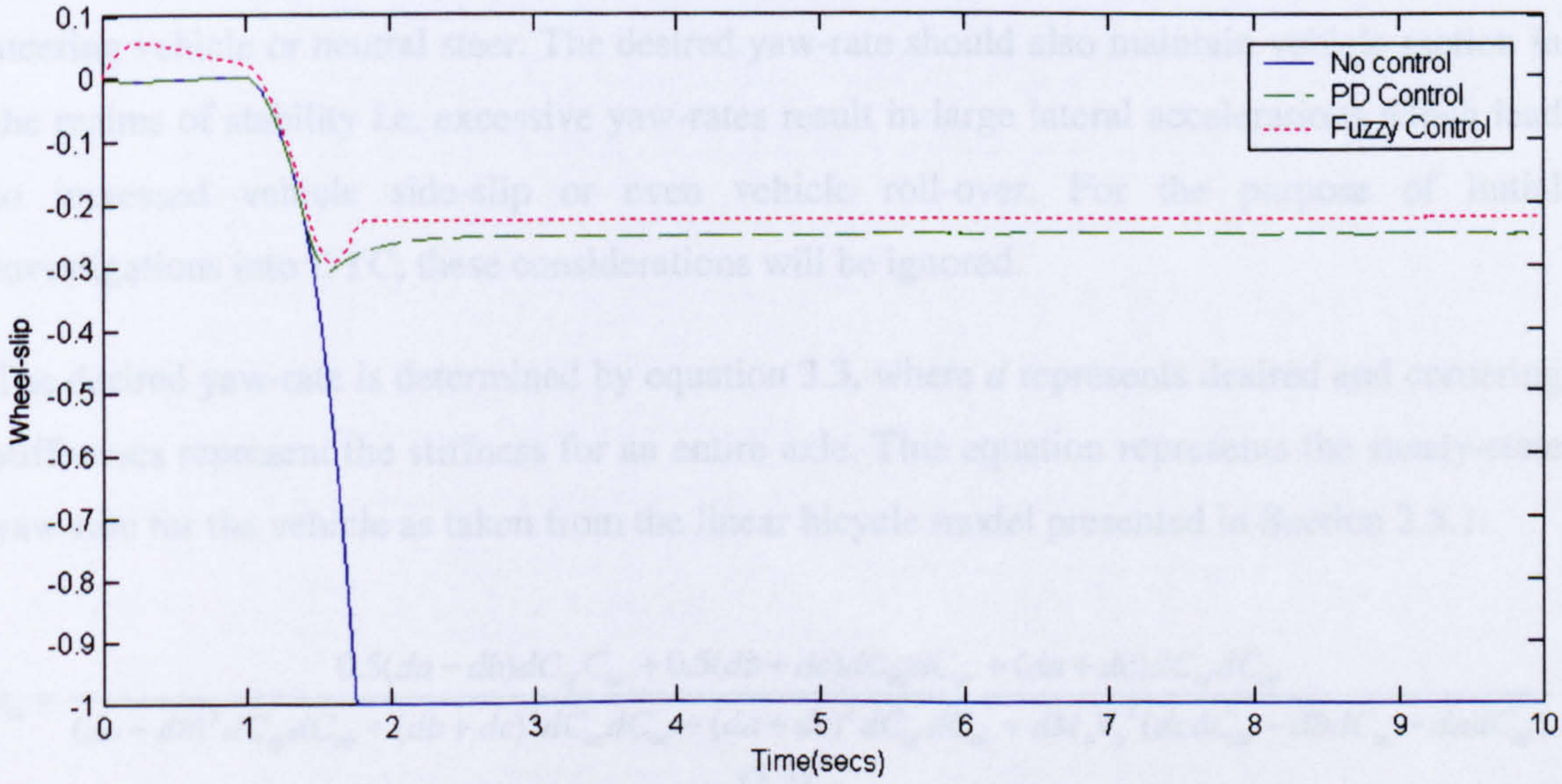

Fig. 3.11 Wheel-slip response for laden vehicle on ice

3.6 Direct Yaw-moment Control

Direct Yaw-moment Control is a method by which tyre forces are controlled to maintain a desired yaw rate, leading to better handling and stability. By implementing a number of DYC controllers on the basic 6WD, 4WS vehicle model, verification of the proposed control methods can be gained. The DYC presented here works by comparing vehicle yaw-rate to a desired yaw-rate and controlling left and right wheel torques to develop the yaw-moment necessary to maintain the desired yaw-rate. The control system for this is shown in figure 3.12.

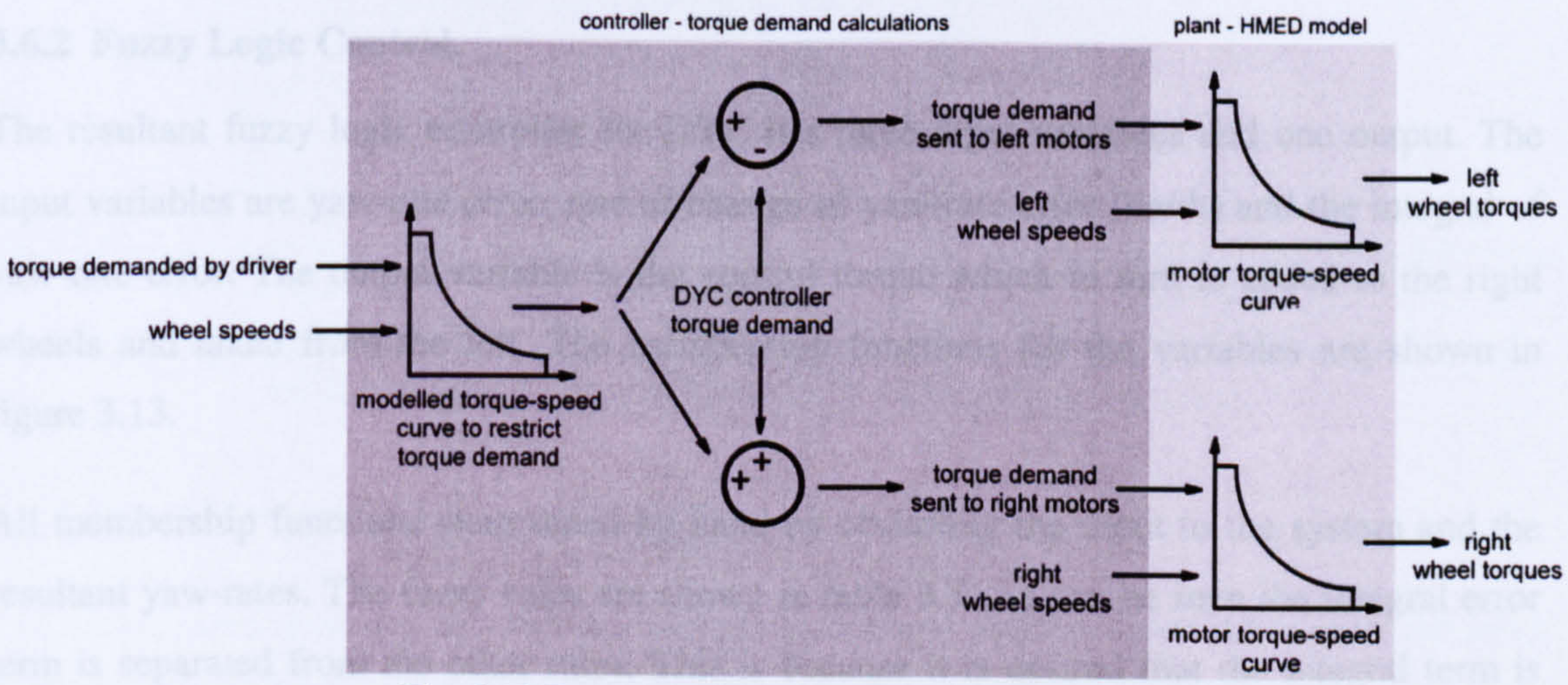

Fig. 3.12 Torque demand calculations for DYC.

For the purpose of these experiments, a desired yaw-rate must be calculated. This desired yaw-rate must depend on steer input and vehicle speed. The desired yaw-rate should also depend on the drivers preferred handling, for instance a driver may prefer an slightly under-steering vehicle or neutral steer. The desired yaw-rate should also maintain vehicle motion in the realms of stability i.e. excessive yaw-rates result in large lateral accelerations which lead to increased vehicle side-slip or even vehicle roll-over. For the purpose of initial investigations into DYC, these considerations will be ignored.

The desired yaw-rate is determined by equation 3.3, where *d* represents desired and cornering stiffnesses represent the stiffness for an entire axle. This equation represents the steady-state yaw-rate for the vehicle as taken from the linear bicycle model presented in Section 2.5.1:

$$r_{ss} = \frac{0.5(da-db)dC_{of}C_{or} + 0.5(db+dc)dC_{or}dC_{or} + (da+dc)dC_{of}dC_{or}}{(da-db)^2 dC_{of}dC_{or} + (db+dc)^2 dC_{or}dC_{or} + (da+dc)^2 dC_{of}dC_{or} + dM_b V_x^{\,2}(dcdC_{or} - dbdC_{or} - dadC_{of})} \cdot \delta_f \tag{3.3}$$

The parameters chosen, lead to a desired yaw-rate exhibiting very slight understeer. Fuzzy logic and PID controllers are implemented in the following sections.

3.6.1 PID Control.

A PID controller was implemented to control the vehicle yaw-rate. The output of the control is added to one set of wheels and subtracted from the other. Equation 3.4 shows the operation of the PID controller.

$$U = K_{dp}e + K_{dd}\frac{de}{dt} + K_{di}\int_0^\infty e \quad (3.4)$$

3.6.2 Fuzzy Logic Control.

The resultant fuzzy logic controller for DYC has three input variables and one output. The input variables are yaw-rate error, rate of change of yaw-rate error (de/dt) and the integral of yaw-rate error. The output variable is the control torque which in turn is added to the right wheels and taken from the left. The membership functions for the variables are shown in figure 3.13.

All membership functions were tuned by hand by observing the input to the system and the resultant yaw-rates. The fuzzy rules are shown in table 3.3. As can be seen the integral error term is separated from the other rules. This is because it is desired that the integral term is more subtle that the other terms and so a lower weighting was applied to these rules. The final weighting of the integral of error rules was given a value of 0.35, a lower value resulted in a slow reduction of steady state errors where as a higher value resulted in oscillatory behaviour.

		rate of change of absolute yaw-rate error		
		negative	zero	positive
yaw-rate error	-ve large	decrease	greatly decrease	greatly decrease
	-ve small	decrease	decrease	greatly decrease
	zero	maintain	maintain	maintain
	+ve small	increase	increase	greatly increase
	+ve large	increase	greatly increase	greatly increase

Integrated yaw-rate error	-ve large	0.35 * greatly decrease
	-ve small	0.35 * decrease
	+ve small	0.35 * increase
	+ve large	0.35 * greatly increase

Table 3.3. Fuzzy logic rules for yaw-moment control.

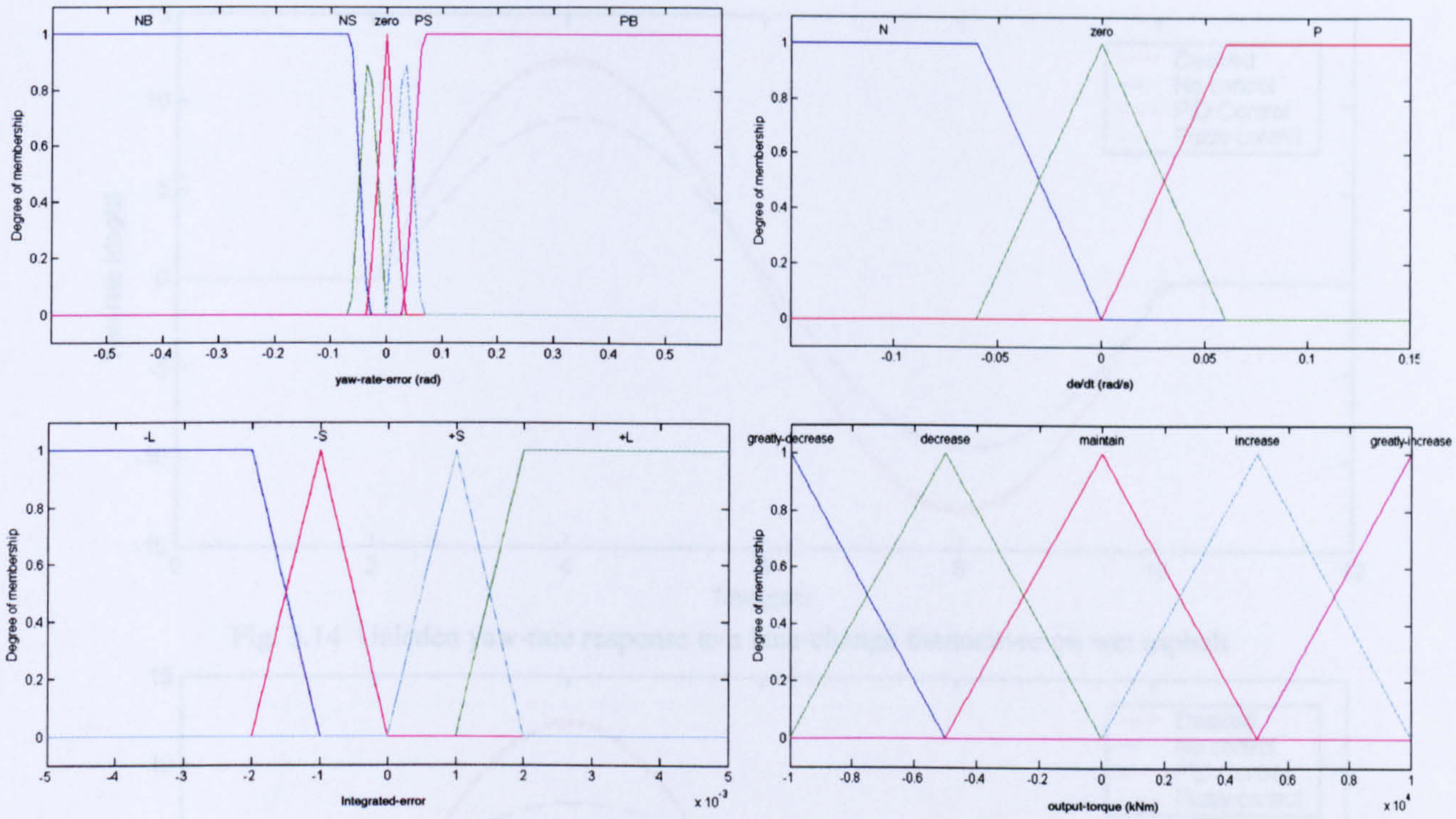

Fig. 3.13 Fuzzy logic membership functions for Input variable for yaw-rate error, input variable for rate of change of yaw-rate error (de/dt) and output variable for torque.

3.6.3 Direct Yaw-moment Control Results

The above controllers are simulated undertaking a lane-change manoeuvre on two different surfaces in both laden and unladen states at 60km/h. Figure 3.14 to figure 3.17 show the yaw-rate responses for the simulations utilising PID and fuzzy-logic control along with the uncontrolled vehicle. The desired yaw-rate is also shown. Figure 3.14 and figure 3.15 show the understeering, unladen vehicle on wet asphalt and snow respectively. As can be seen in both cases, the controller accurately tracks the desired yaw-rate on both surfaces. Figure 3.16 and figure 3.17 show the same for the oversteering, laden vehicle. It can be seen that the controllers both counteract the oversteering nature of the vehicle. Both the PID and fuzzy-logic controllers exhibit an almost identical ability to accurately track the desired yaw-rate.

Figure 3.18 and figure 3.19 show the input steer angle (at wheels) against the output yaw-rate for the lane-change manoeuvres on the snow covered road in unladen and laden conditions respectively at 60km/h. From both figures, it can be seen that there is negligible hysterisis present in the responses for both controllers as opposed to the non-controlled vehicle. This means there is less delay between the driver demanding a yaw-rate through the steer angle and that desired yaw-rate being produced. Through this, the vehicle reacts quicker to driver inputs which promotes better responses in emergency manoeuvres such as obstacle avoidance. Again it is seen that there is little difference between the PID and fuzzy logic controllers.

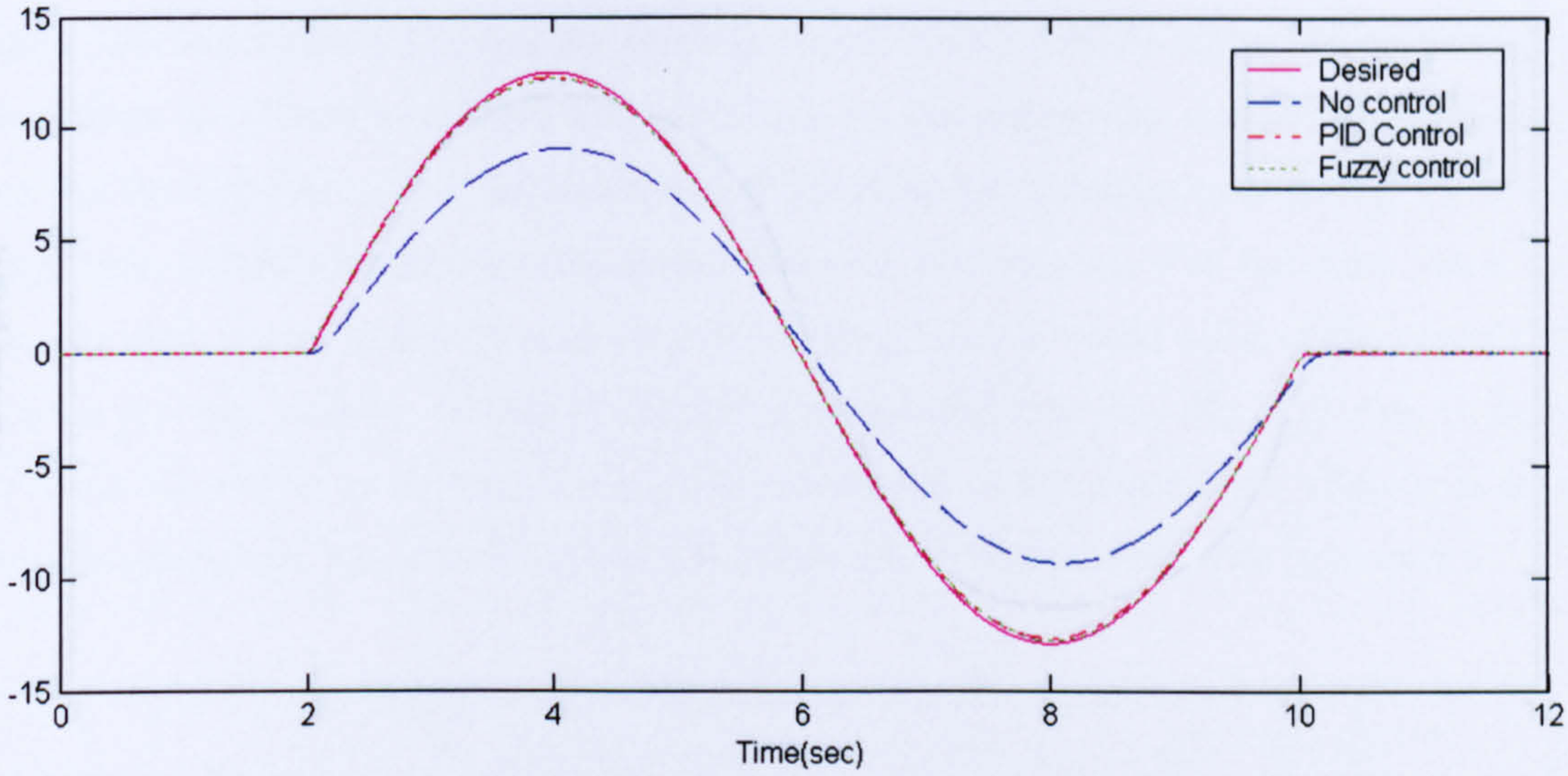

Fig. 3.14 Unladen yaw-rate response to a lane-change manoeuvre on wet asphalt

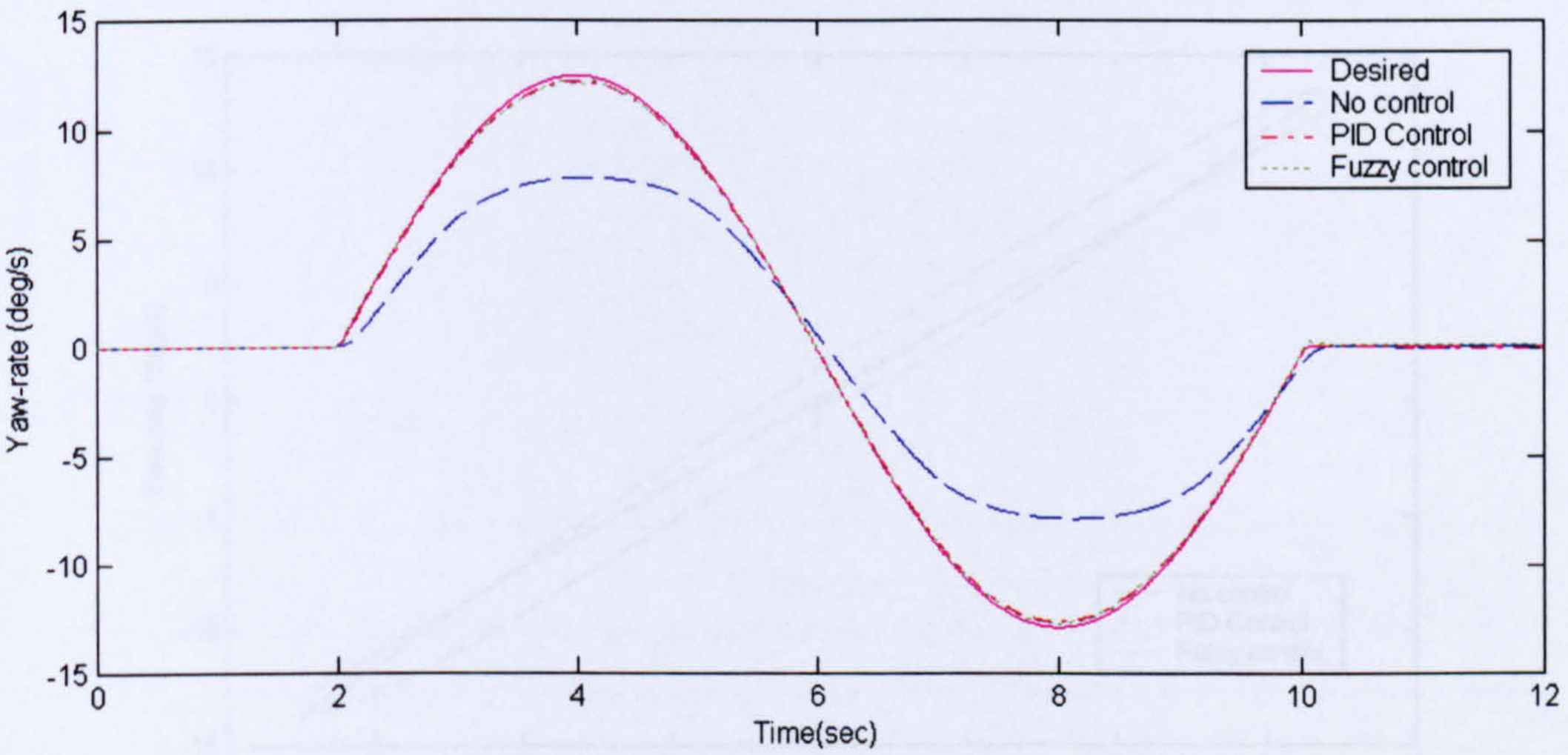

Fig. 3.15 Unladen yaw-rate response to a lane-change manoeuvre on a snow covered road

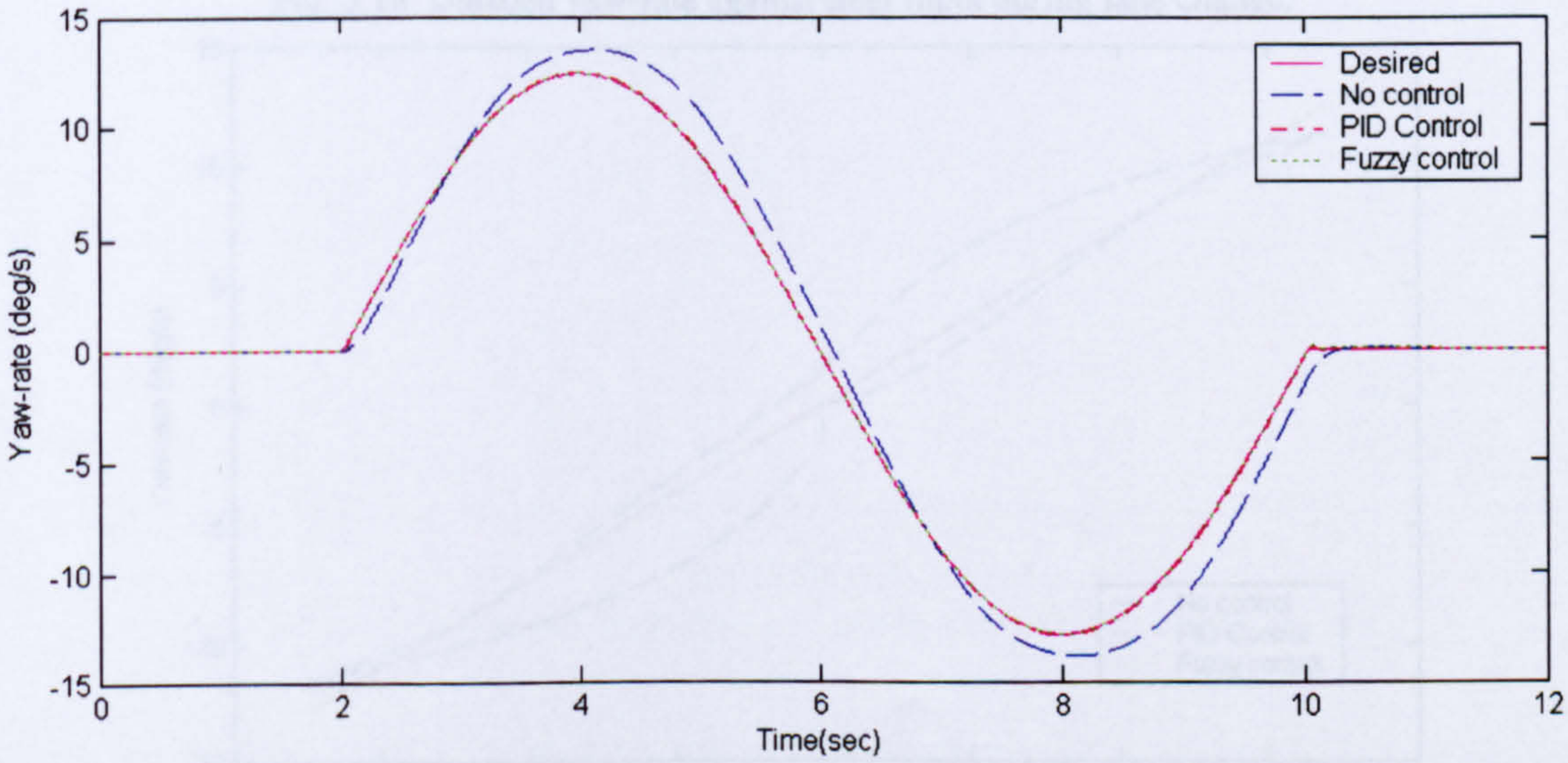

Fig. 3.16 Laden yaw-rate response to a lane-change manoeuvre on wet asphalt

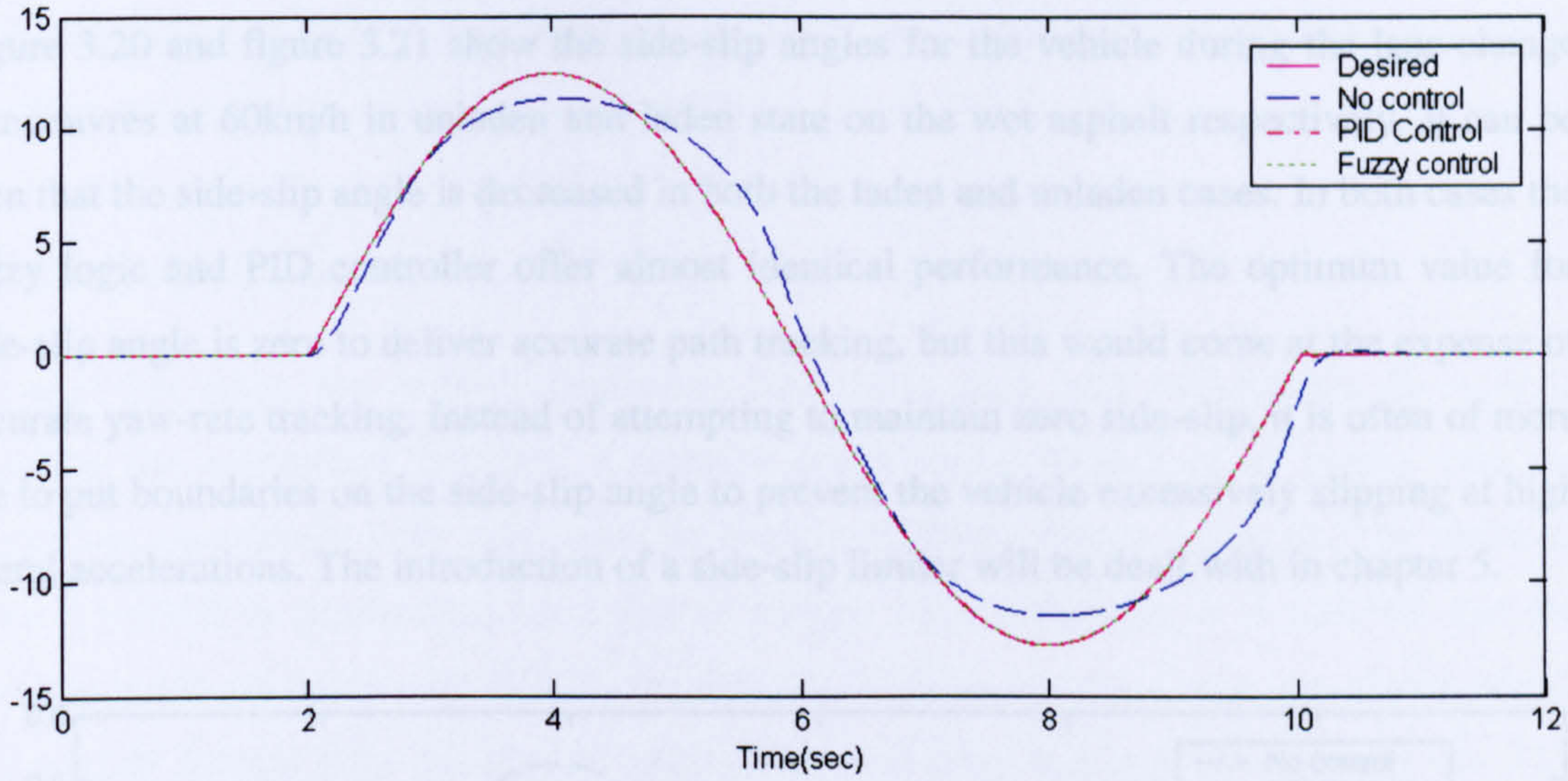

Fig. 3.17 Laden yaw-rate response to a lane-change manoeuvre on a snow covered road

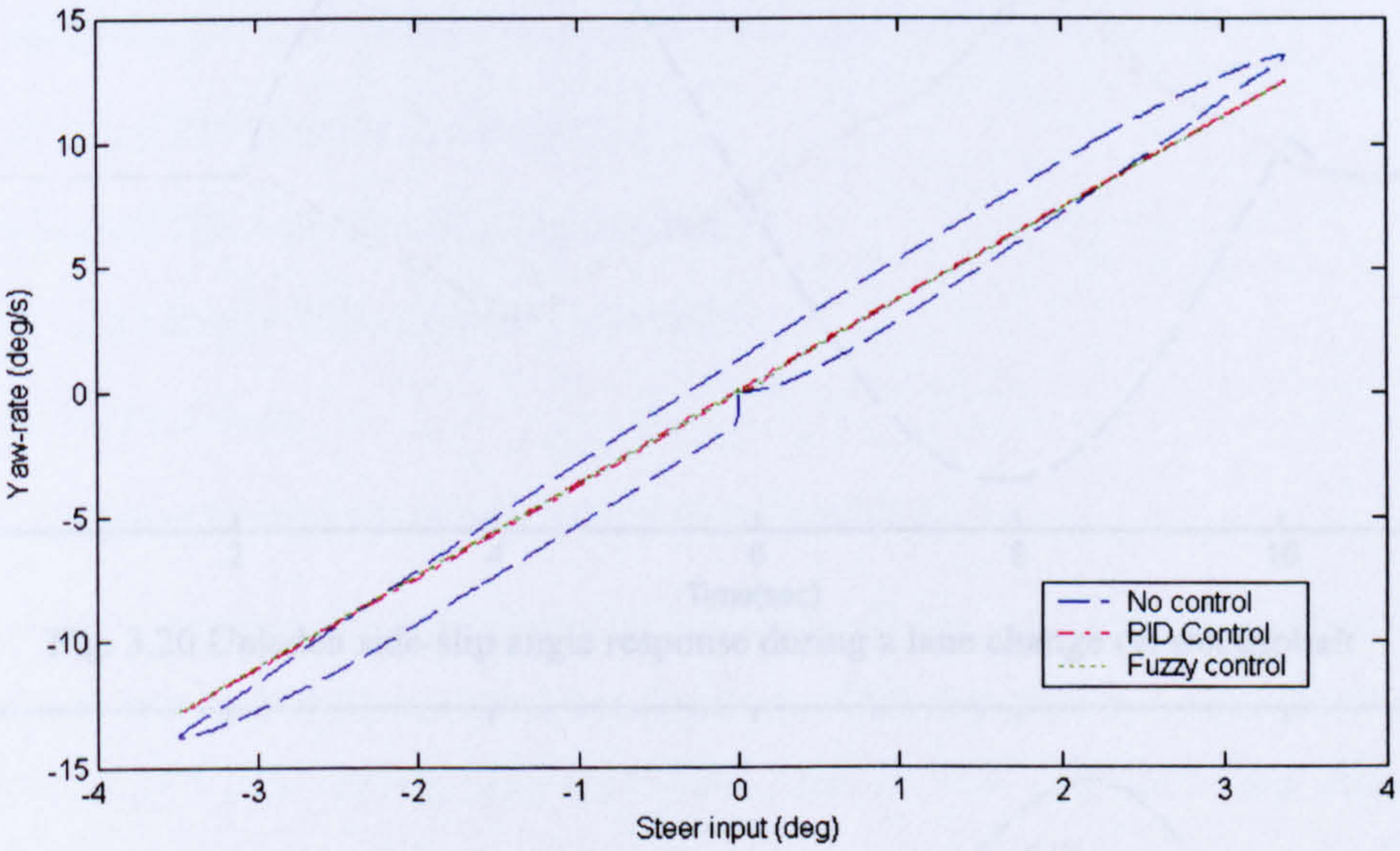

Fig. 3.18 Unladen yaw-rate against steer input during lane change.

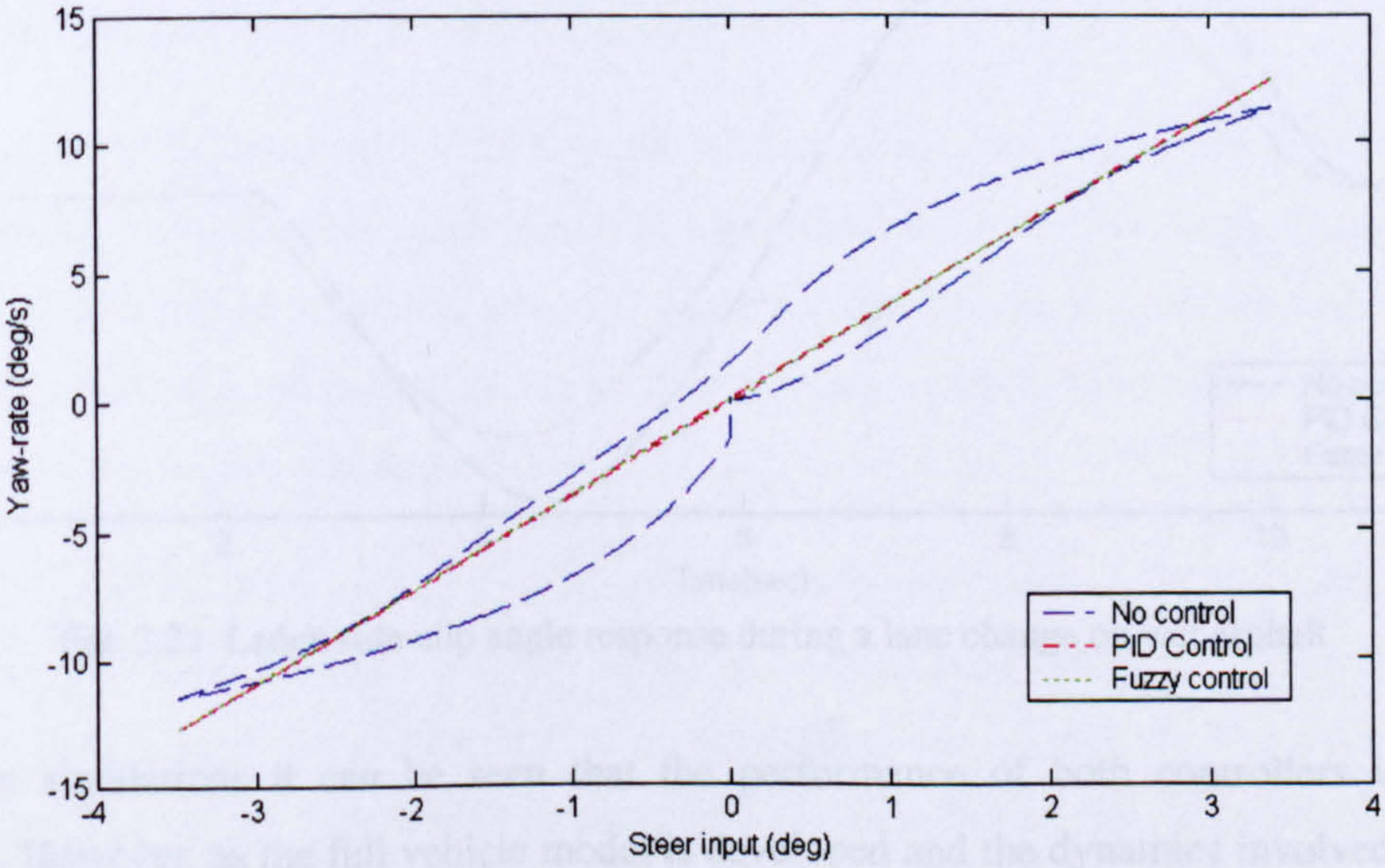

Fig. 3.19 Laden yaw-rate against steer input during lane change.

Figure 3.20 and figure 3.21 show the side-slip angles for the vehicle during the lane-change manoeuvres at 60km/h in unladen and laden state on the wet asphalt respectively. It can be seen that the side-slip angle is decreased in both the laden and unladen cases. In both cases the fuzzy logic and PID controller offer almost identical performance. The optimum value for side-slip angle is zero to deliver accurate path tracking, but this would come at the expense of accurate yaw-rate tracking. Instead of attempting to maintain zero side-slip, it is often of more use to put boundaries on the side-slip angle to prevent the vehicle excessively slipping at high lateral accelerations. The introduction of a side-slip limiter will be dealt with in chapter 5.

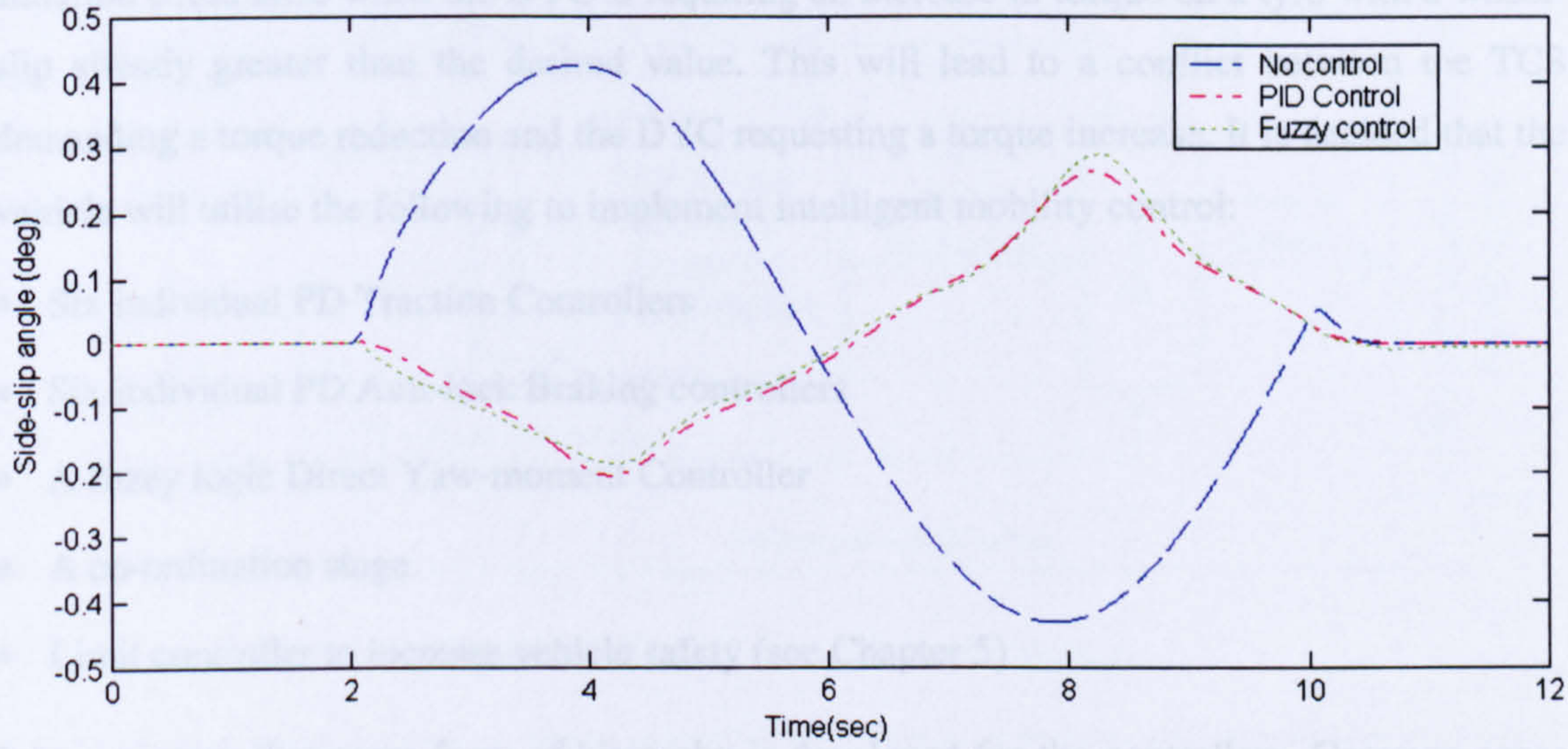

Fig. 3.20 Unladen side-slip angle response during a lane change on wet asphalt

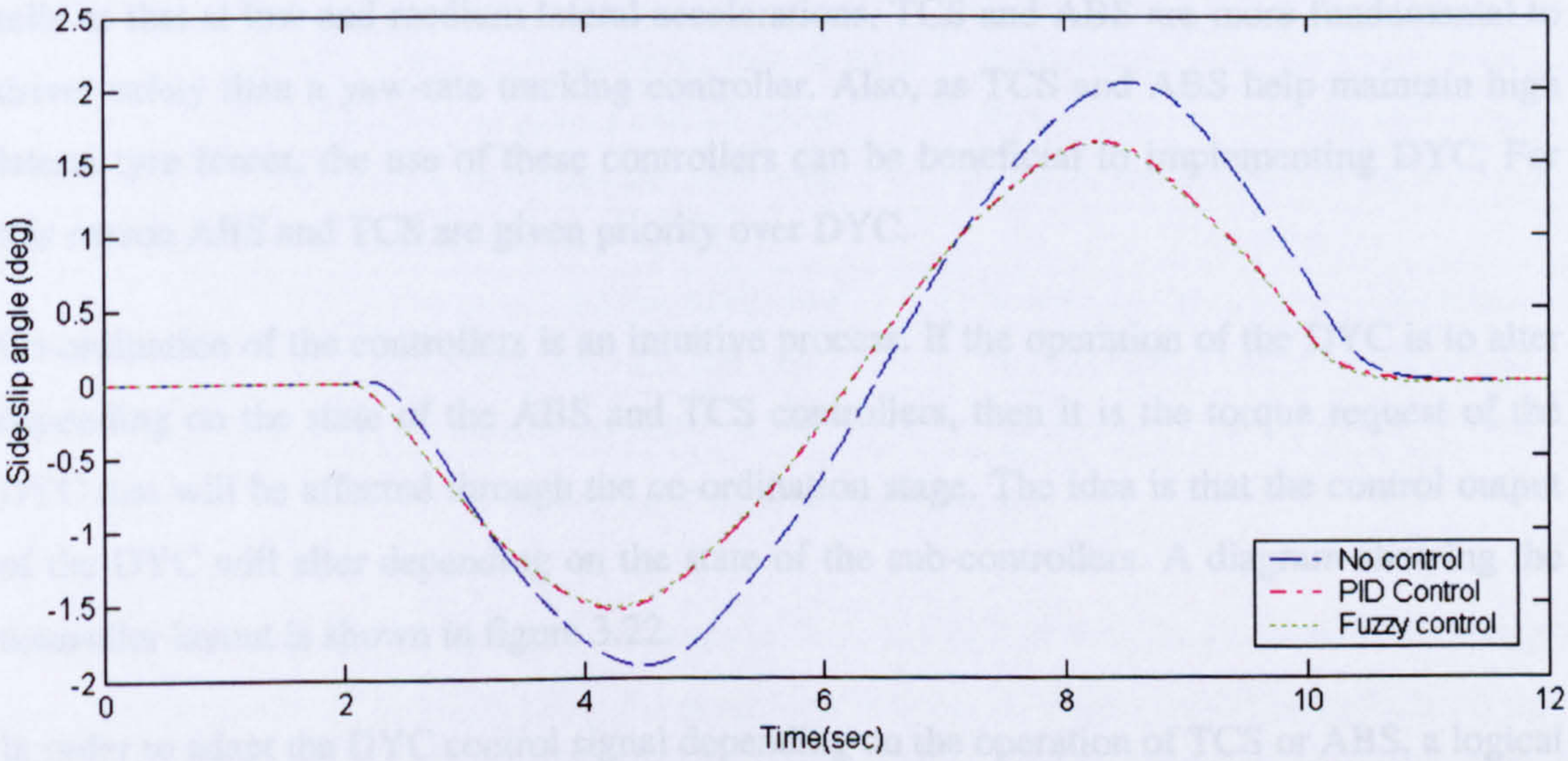

Fig. 3.21 Laden side-slip angle response during a lane change on wet asphalt

From the simulations it can be seen that the performance of both controllers is almost identical. However, as the full vehicle model is developed and the dynamics involved become

more non-linear, the fuzzy logic controller is ideally suited due to its robust nature and hence it will be utilised in the overall control system.

3.7 Controller Co-ordination

Up until this point, the mobility controllers have been dealt with individually. In order to integrate the controllers together, a strategy needs to be developed to ensure that the controllers co-ordinate with each other to avoid conflicting torque demands. For instance, when a vehicle is accelerating on a split-μ surface while cornering, it is possible that the situation could arise when the DYC is requiring an increase in torque on a tyre with a wheel-slip already greater than the desired value. This will lead to a conflict between the TCS demanding a torque reduction and the DYC requesting a torque increase. It is decided that the vehicle will utilise the following to implement intelligent mobility control:

- Six individual PD Traction Controllers
- Six individual PD Anti-lock Braking controllers
- A fuzzy logic Direct Yaw-moment Controller
- A co-ordination stage
- Limit controller to increase vehicle safety (see Chapter 5)

It is necessary that some form of hierarchy is developed for the controllers. Common sense tells us that at low and medium lateral accelerations, TCS and ABS are more fundamental to driver safety than a yaw-rate tracking controller. Also, as TCS and ABS help maintain high lateral tyre forces, the use of these controllers can be beneficial to implementing DYC. For this reason ABS and TCS are given priority over DYC.

Co-ordination of the controllers is an intuitive process. If the operation of the DYC is to alter depending on the state of the ABS and TCS controllers, then it is the torque request of the DYC that will be affected through the co-ordination stage. The idea is that the control output of the DYC will alter depending on the state of the sub-controllers. A diagram showing the controller layout is shown in figure 3.22.

In order to adapt the DYC control signal depending on the operation of TCS or ABS, a logical operation takes place where by a signal named wheel-slip state demands a restriction to the DYC output. This signal takes the form of an integer between –3 and +3. The positive refers to the operation of the Traction Controllers and the negative to the Anti-lock Braking as

shown in table 3.4. From these values, the control outputs of the DYC are saturated depending on the desired effect and summed with the sub-controller torque demands and those made by the driver, giving a final torque demands for the HMED's.

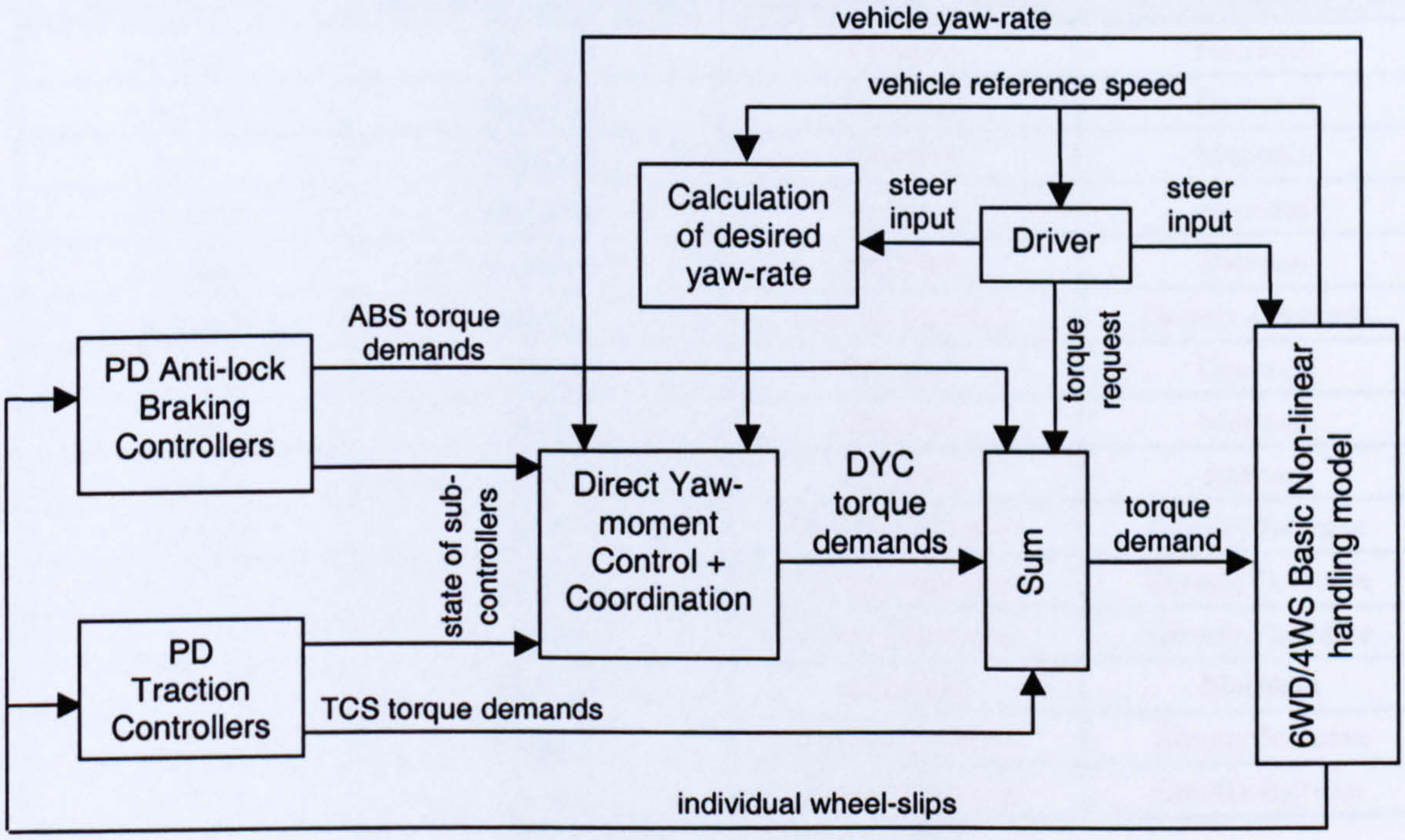

Fig 3.22 TCS, ABS and DYC control system

Wheel-slip state	Meaning	Effect on DYC
-3	ABS active on at least one wheel on both sides	No reduction in torque on any wheel
-2	ABS active on at least one left wheel	No reduction in torque on left wheels
-1	ABS active on at least one right wheel	No reduction in torque on right wheels
0	Neither ABS or TCS active	No effect
1	TCS active on at least one right wheel	No increase in torque on right wheels
2	TCS active on at least one left wheel	No increase in torque on left wheels
3	TCS active on at least one wheel on both sides	No increase in torque on any wheels

Table 3.4 Control integration logic

This logic is implemented in the co-ordination control block of the Simulink model. Through the work on the DYC in Section 3.4, the need for the integral of the error to be included in the controller was deemed unnecessary as no steady state error was found, hence it has been removed. The rule base for the fuzzy logic DYC is presented in table 3.5. The fuzzy logic membership functions are the presented in figure 3.23. The controller was tuned in an *ad hoc*

manner. Once the full vehicle model is developed, the membership functions will be tuned to optimise the controller operation in all conditions.

Inputs		Outputs	
Yaw-rate error	Rate of change of |error|	Right command torque	Left command torque
-ve large	Negative	Increase	Decrease
-ve small	Negative	Increase	Decrease
zero	Negative	Maintain	Maintain
+ve small	Negative	Decrease	Increase
+ve large	Negative	Decrease	Increase
-ve large	Zero	Greatly Increase	Greatly Decrease
-ve small	Zero	Increase	Decrease
zero	Zero	Maintain	Maintain
+ve small	Zero	Decrease	Increase
+ve large	Zero	Greatly Decrease	Greatly Increase
-ve large	Positive	Greatly Increase	Greatly Decrease
-ve small	Positive	Greatly Increase	Greatly Decrease
zero	Positive	Maintain	Maintain
+ve small	Positive	Greatly Decrease	Greatly Increase
+ve large	Positive	Greatly Decrease	Greatly Increase

Table 3.5 Fuzzy logic rules for DYC

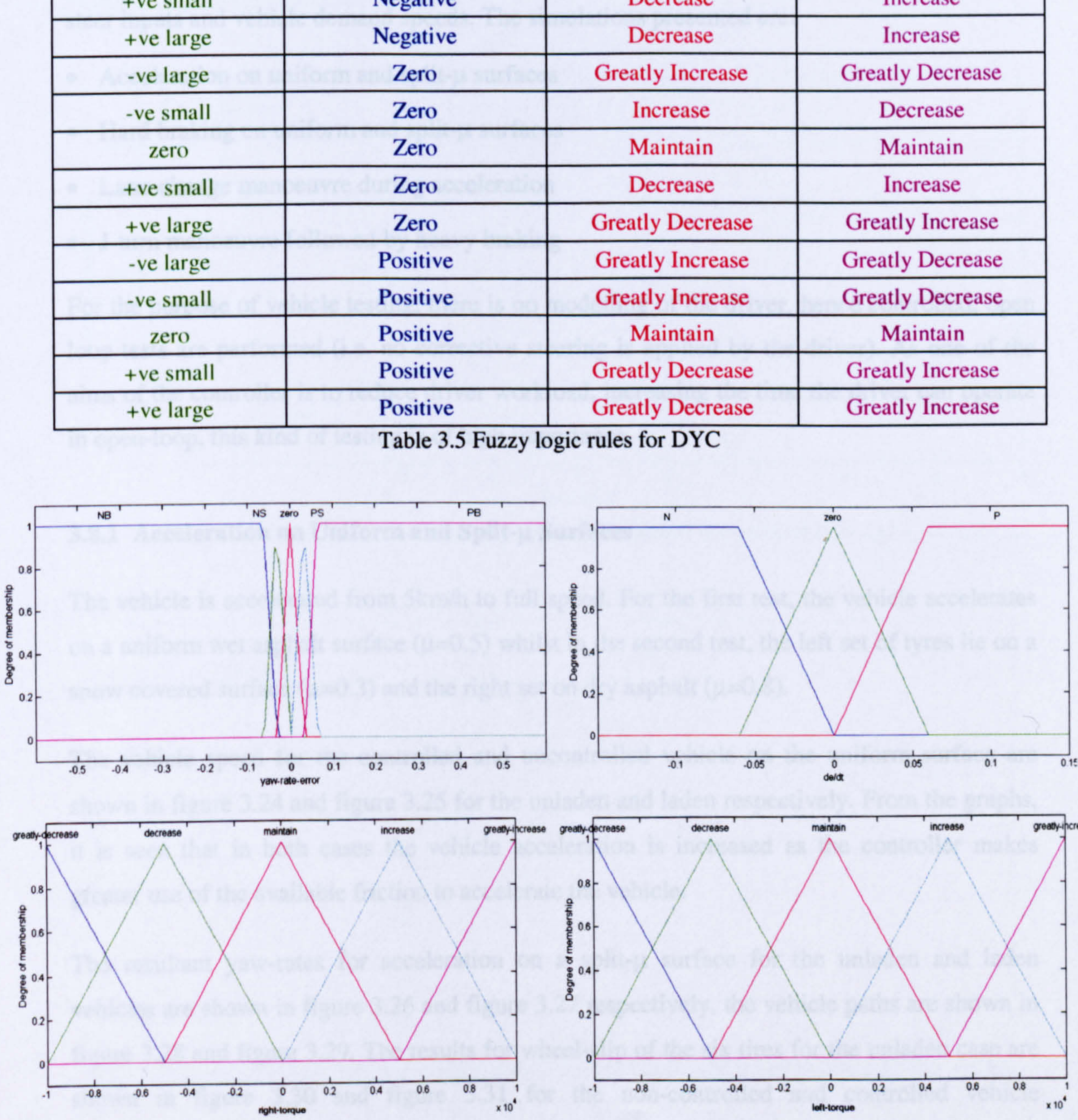

Fig. 3.23 Fuzzy logic membership functions for Input variable for yaw-rate error, input variable for rate of change of yaw-rate error (de/dt) and output variables for left and right torques.

3.8 Preliminary Testing

Now that a control strategy has been developed, it must be tested to assess the validity of the coordination method chosen. The aim of this preliminary testing is to gauge the controllers ability to address the specifications set out in Section 3.2. Through simulation under a number of conditions, with an emphasis on combined controller operation, this can be achieved.

The model, with and without the controller, is simulated on various different road surfaces under a number of vehicle manoeuvres. These manoeuvres are simulated by inputting various steer inputs and vehicle demand speeds. The simulations presented are:

- Acceleration on uniform and split-μ surfaces
- Hard braking on uniform and split-μ surfaces
- Lane-change manoeuvre during acceleration
- J-turn manoeuvre followed by heavy braking

For the purpose of vehicle testing, there is no modelling of the driver, hence controlled, open loop tests are performed (i.e. no corrective steering is applied by the driver). As one of the aims of the controller is to reduce driver workload, increasing the time the driver can operate in open-loop, this kind of testing is of high importance.

3.8.1 Acceleration on Uniform and Split-μ Surfaces

The vehicle is accelerated from 5km/h to full speed. For the first test, the vehicle accelerates on a uniform wet asphalt surface (μ=0.5) whilst in the second test, the left set of tyres lie on a snow covered surface (μ=0.3) and the right set on dry asphalt (μ=0.8).

The vehicle speed for the controlled and uncontrolled vehicle on the uniform surface are shown in figure 3.24 and figure 3.25 for the unladen and laden respectively. From the graphs, it is seen that in both cases the vehicle acceleration is increased as the controller makes greater use of the available friction to accelerate the vehicle.

The resultant yaw-rates for acceleration on a split-μ surface for the unladen and laden vehicles are shown in figure 3.26 and figure 3.27 respectively, the vehicle paths are shown in figure 3.28 and figure 3.29. The results for wheel-slip of the six tires for the unladen case are shown in figure 3.30 and figure 3.31 for the non-controlled and controlled vehicle respectively. From figure 3.26 and figure 3.27 it can be seen that the implemented controller greatly reduces the instability produced from the split-μ surface and the removes the majority

of the yaw-rate error. This is obvious from looking at figure 3.28 and figure 3.29. In practice, the developed control algorithm reduces the need for driver intervention to maintain the desired course. From the graphs it can be seen that in the laden case, due to the large vertical tyre loads, the generated yaw-moment is small. This kind of control is much more essential for the vehicle when unladen, where its operation greatly reduces unwanted yaw-moments. The wheel-slip responses shown in figure 3.30 and figure 3.31 show that the controller manages to maintain wheel-slip close to the desired value, while the non-controlled vehicle's wheel-slip goes up to around 70%.

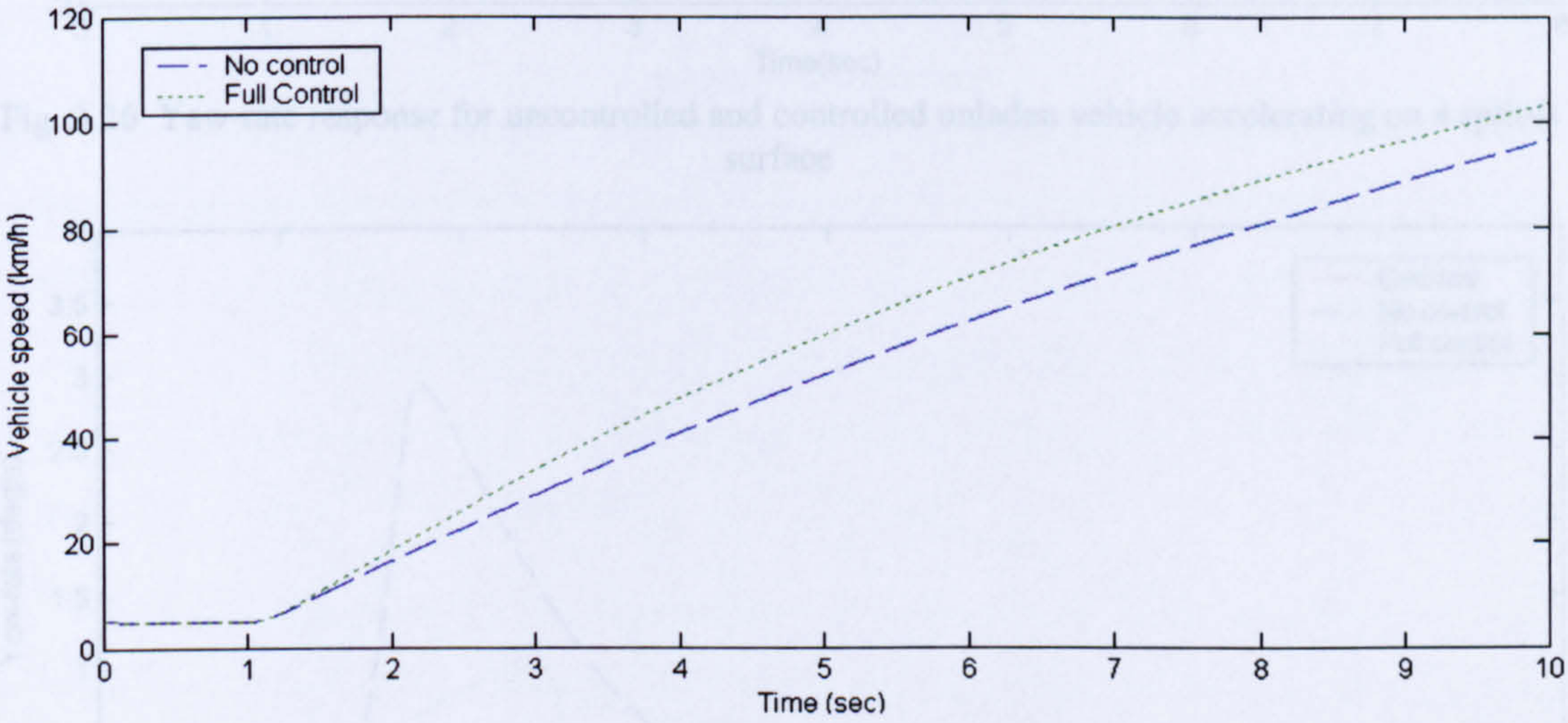

Fig. 3.24 Speed response for uncontrolled and controlled unladen vehicle accelerating on wet asphalt.

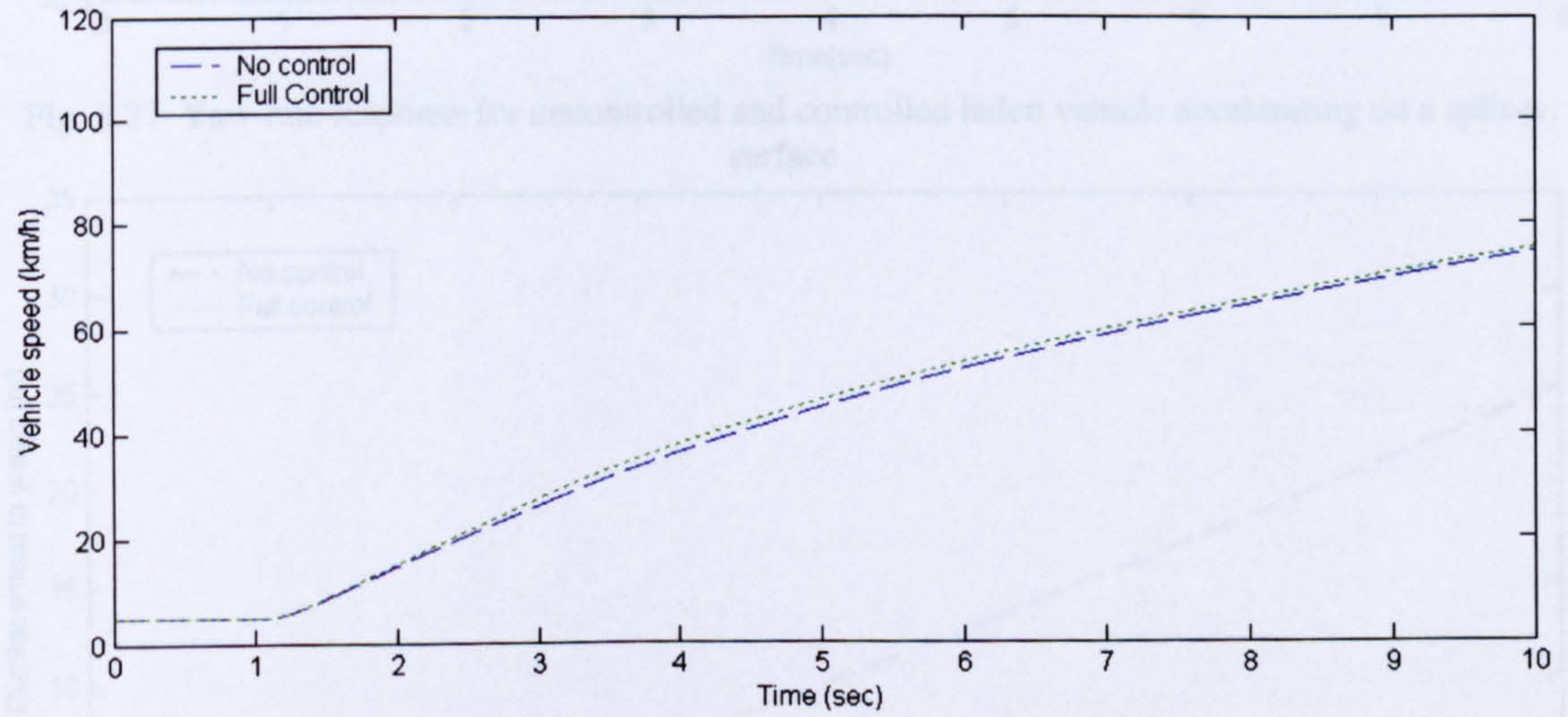

Fig. 3.25 Speed response for uncontrolled and controlled laden vehicle accelerating on wet asphalt.

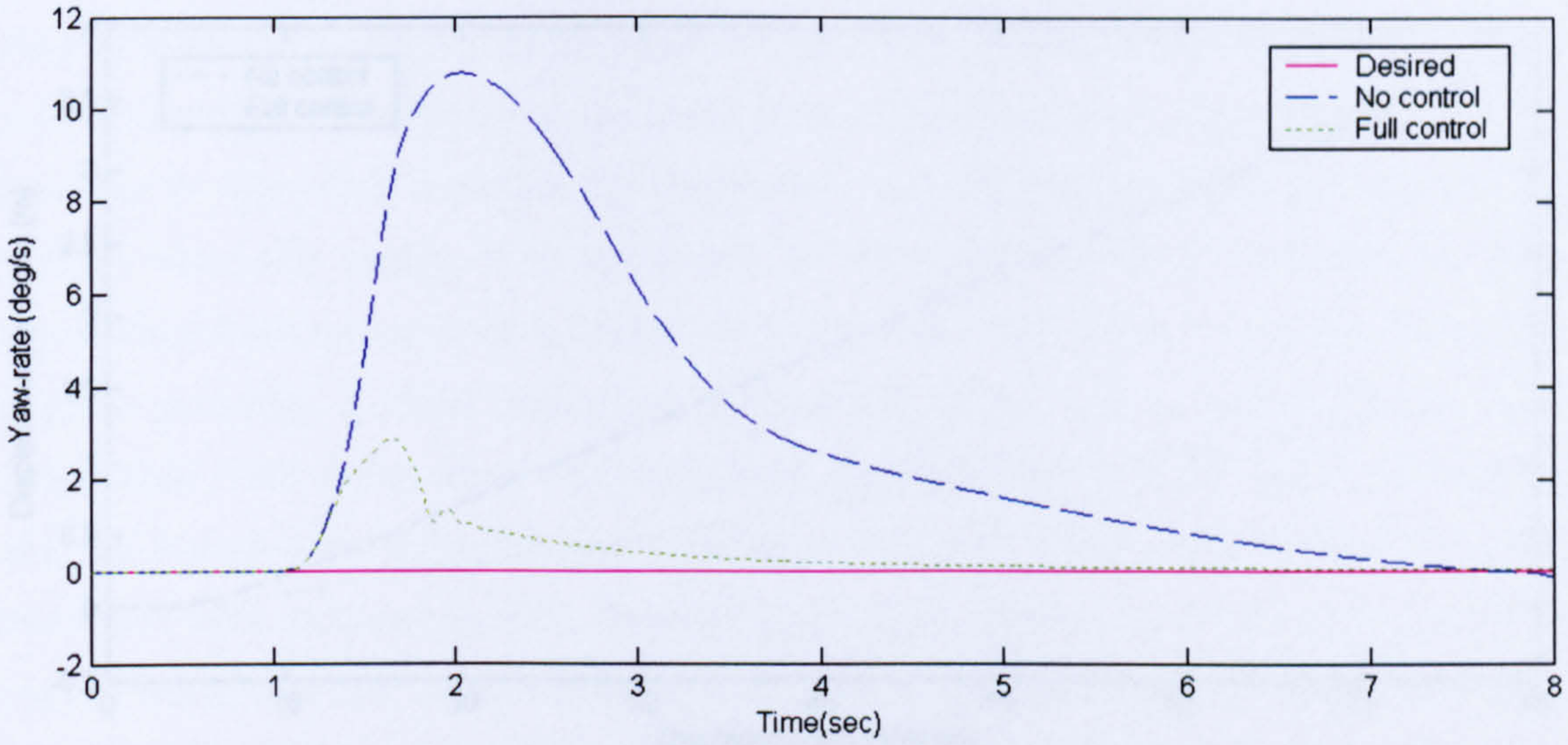

Fig. 3.26 Yaw-rate response for uncontrolled and controlled unladen vehicle accelerating on a split-μ surface

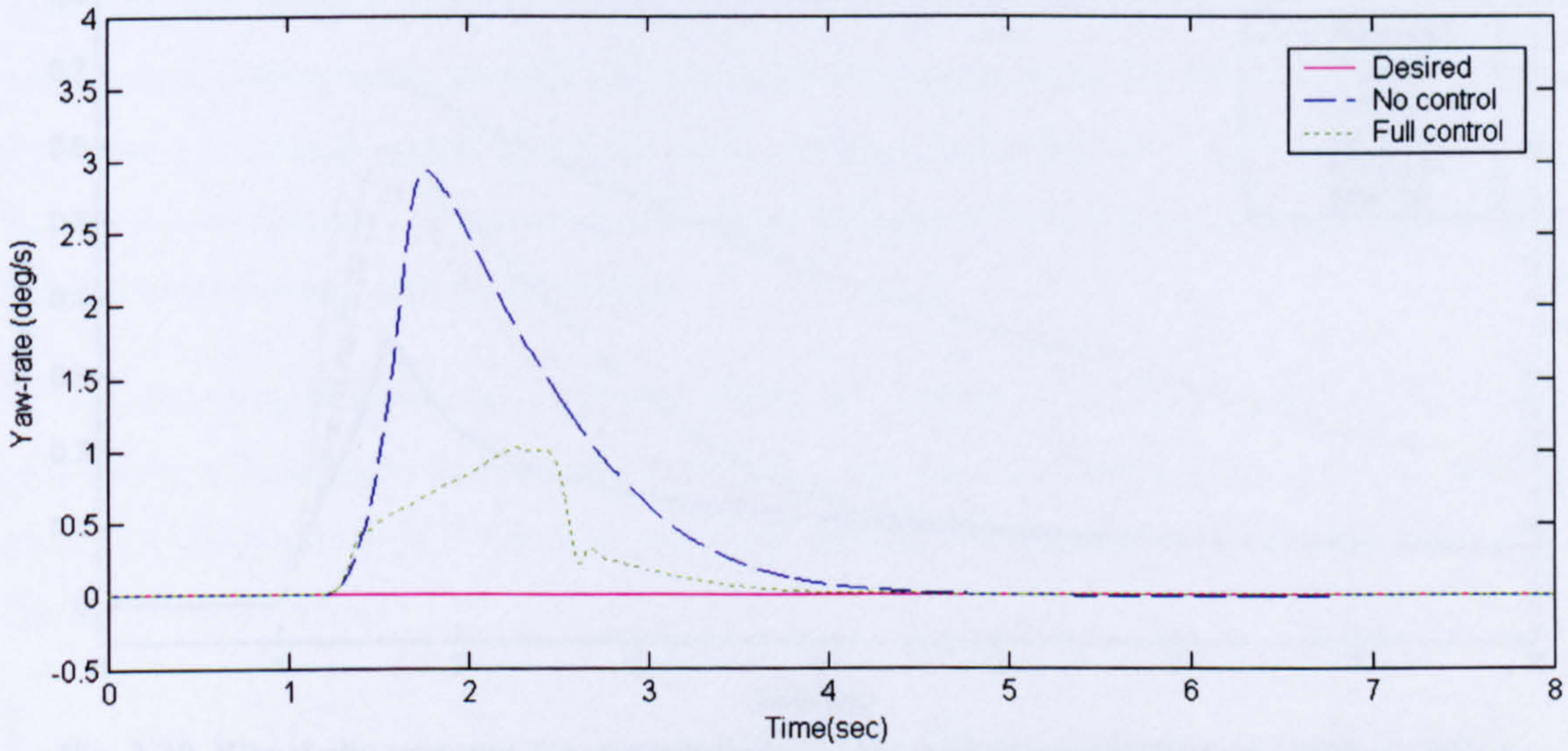

Fig. 3.27 Yaw-rate response for uncontrolled and controlled laden vehicle accelerating on a split-μ surface

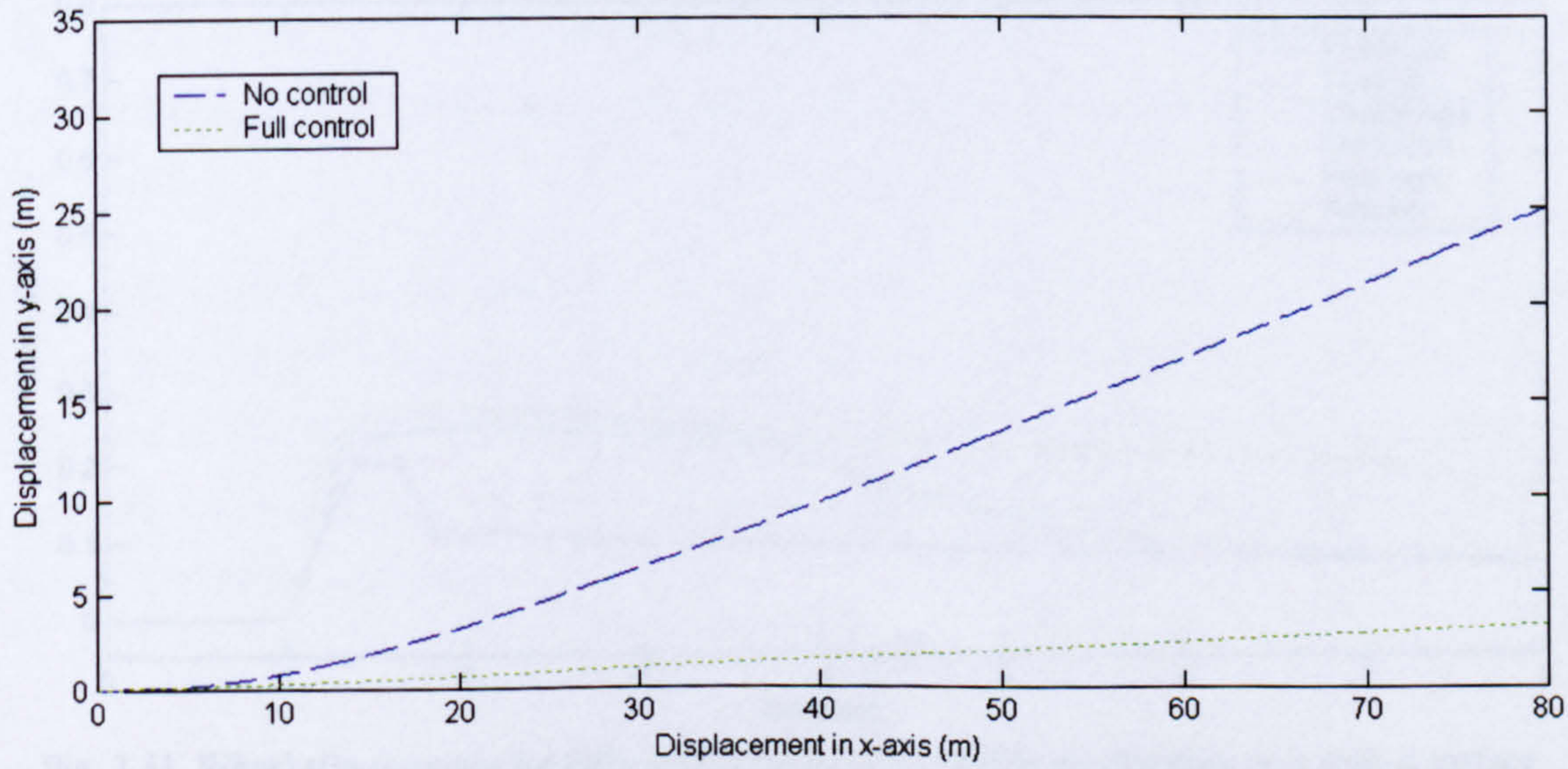

Fig. 3.28 Vehicle path for uncontrolled and controlled unladen vehicle accelerating on a split-μ surface

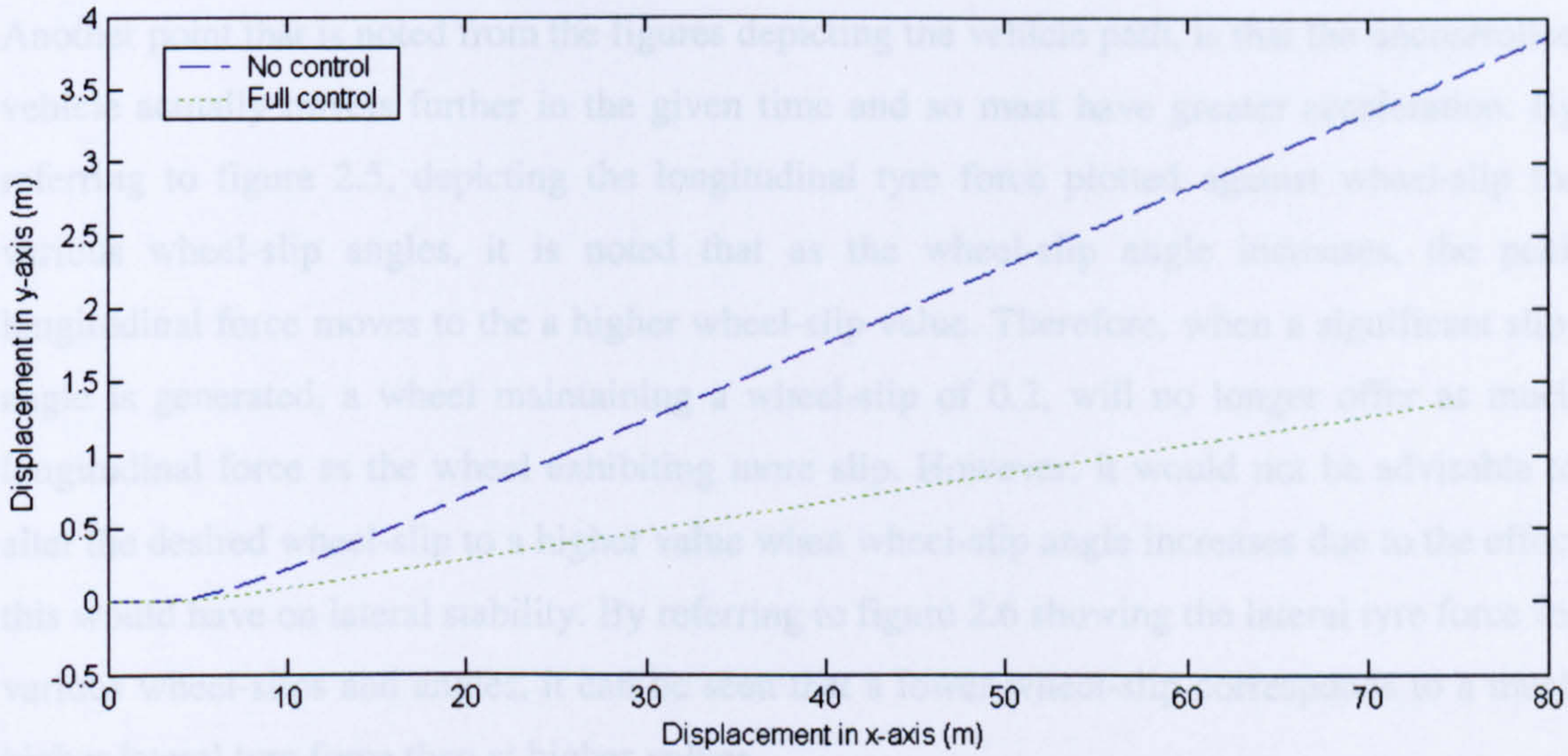

Fig. 3.29 Vehicle path for uncontrolled and controlled laden vehicle accelerating on a split-μ surface

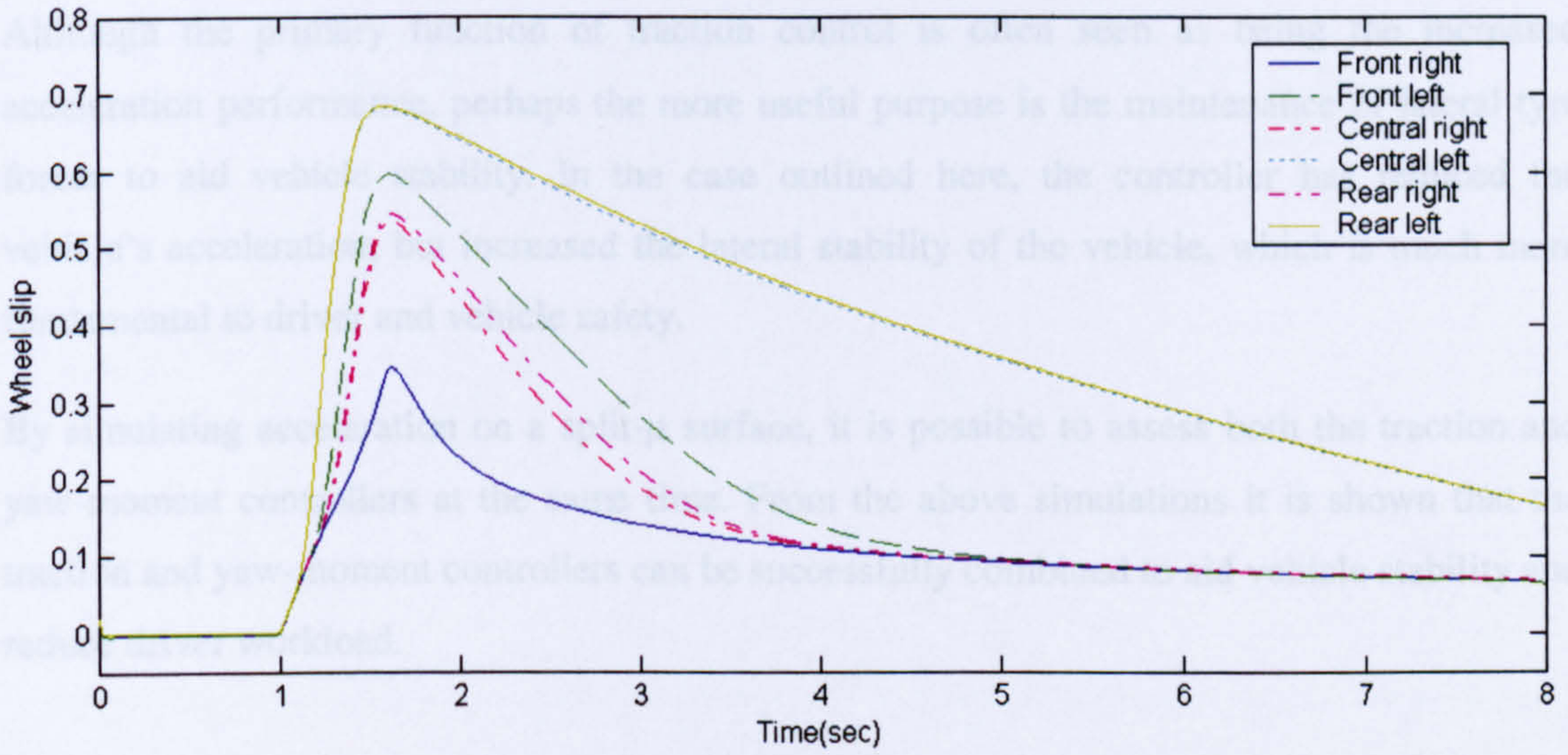

Fig. 3.30 Wheel-slip response for uncontrolled unladen vehicle accelerating on a split-μ surface

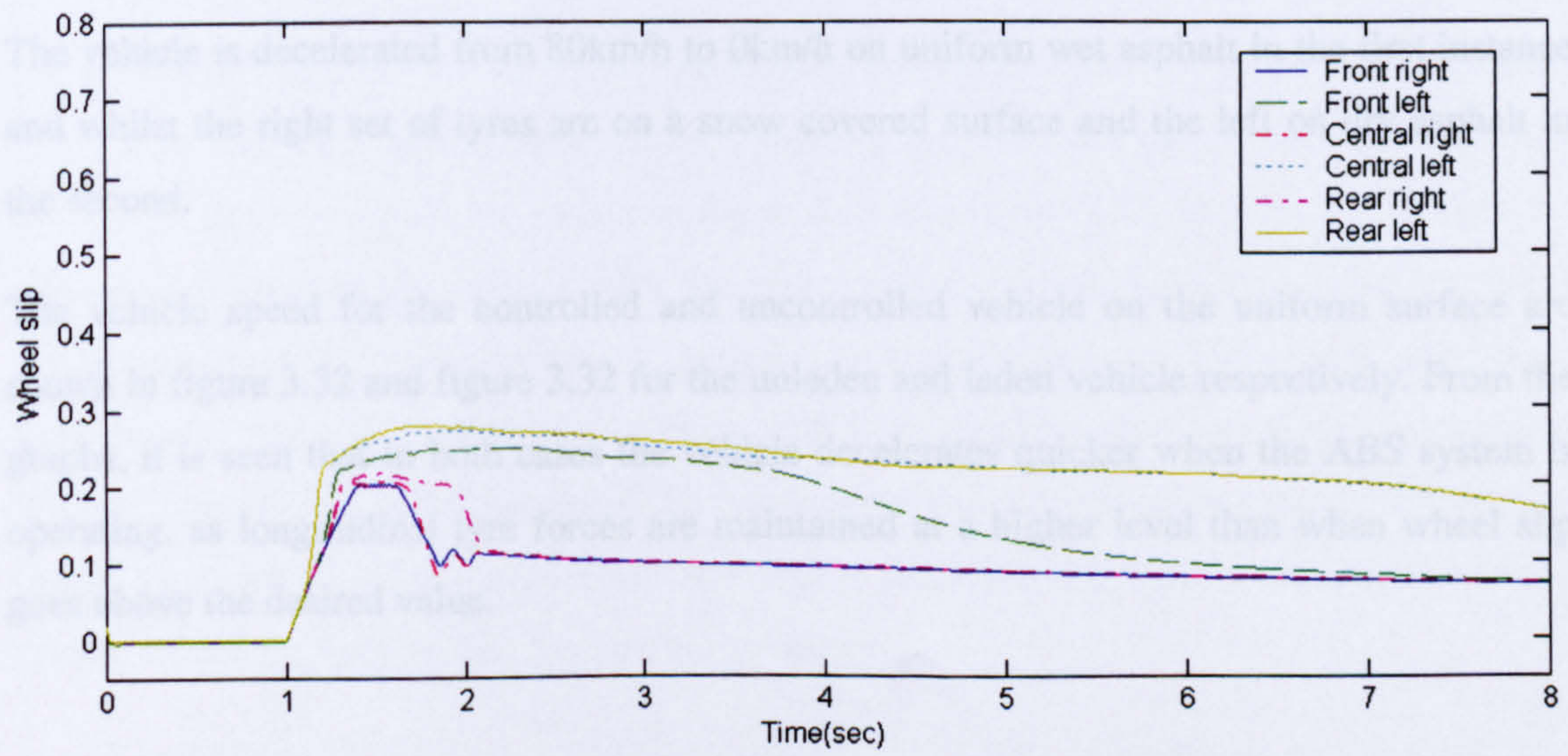

Fig. 3.31 Wheel slip-response for fully controlled unladen vehicle accelerating on a split-μ surface

Another point that is noted from the figures depicting the vehicle path, is that the uncontrolled vehicle actually travels further in the given time and so must have greater acceleration. By referring to figure 2.5, depicting the longitudinal tyre force plotted against wheel-slip for various wheel-slip angles, it is noted that as the wheel-slip angle increases, the peak longitudinal force moves to the a higher wheel-slip value. Therefore, when a significant slip-angle is generated, a wheel maintaining a wheel-slip of 0.2, will no longer offer as much longitudinal force as the wheel exhibiting more slip. However, it would not be advisable to alter the desired wheel-slip to a higher value when wheel-slip angle increases due to the effect this would have on lateral stability. By referring to figure 2.6 showing the lateral tyre force for various wheel-slips and angles, it can be seen that a lower wheel-slip corresponds to a much higher lateral tyre force than at higher values.

Although the primary function of traction control is often seen as being the increased acceleration performance, perhaps the more useful purpose is the maintenance of lateral tyre forces to aid vehicle stability. In the case outlined here, the controller has reduced the vehicle's acceleration, but increased the lateral stability of the vehicle, which is much more fundamental to driver and vehicle safety.

By simulating acceleration on a split-μ surface, it is possible to assess both the traction and yaw-moment controllers at the same time. From the above simulations it is shown that the traction and yaw-moment controllers can be successfully combined to aid vehicle stability and reduce driver workload.

3.8.2 Heavy Braking on Uniform and Split-μ Surfaces

The vehicle is decelerated from 80km/h to 0km/h on uniform wet asphalt in the first instance and whilst the right set of tyres are on a snow covered surface and the left on dry asphalt in the second.

The vehicle speed for the controlled and uncontrolled vehicle on the uniform surface are shown in figure 3.32 and figure 3.32 for the unladen and laden vehicle respectively. From the graphs, it is seen that in both cases the vehicle decelerates quicker when the ABS system is operating, as longitudinal tyre forces are maintained at a higher level than when wheel slip goes above the desired value.

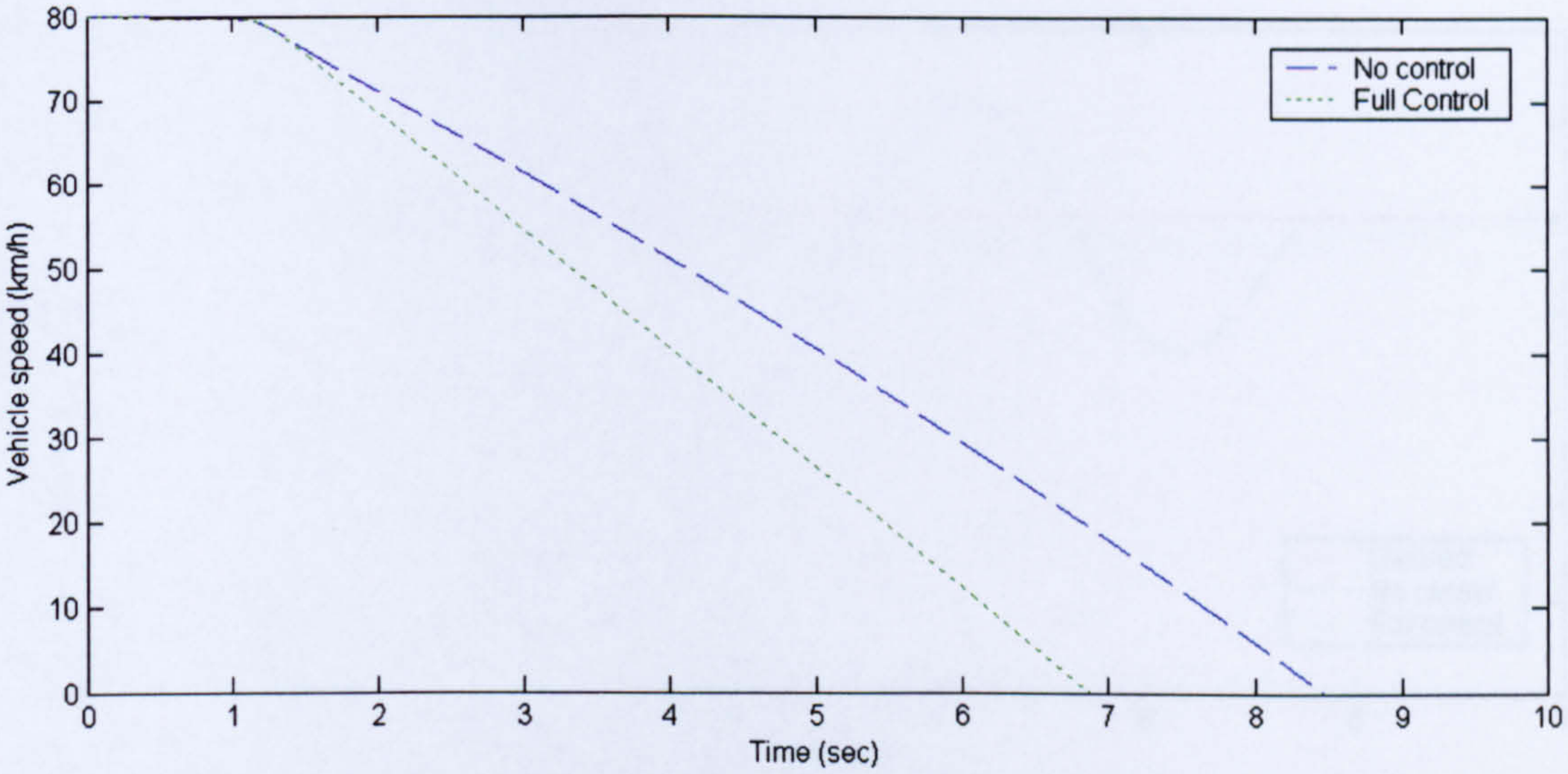

Fig. 3.32 Vehicle speed response for uncontrolled and controlled laden vehicle braking on wet asphalt.

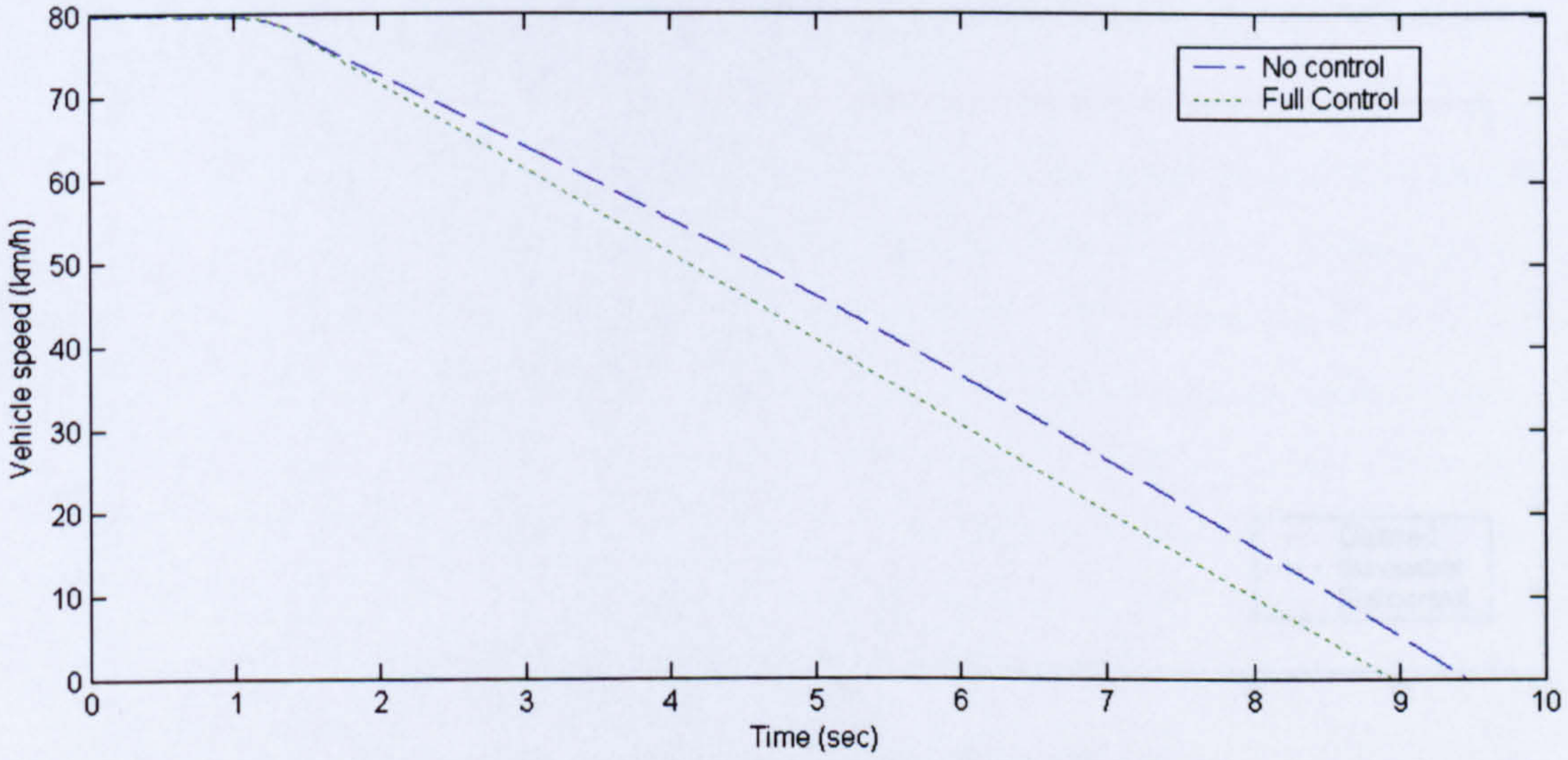

Fig. 3.32 Vehicle speed response for uncontrolled and controlled laden vehicle braking on wet asphalt.

The yaw-rates responses are shown for the unladen and laden vehicle in figure 3.34 and figure 3.35 for braking on a split-μ surface. The wheel-slip responses for the uncontrolled and fully controlled unladen vehicle are shown in figure 3.36 and figure 3.37 respectively. In both the unladen and laden cases, the controller maintains vehicle stability. Heavy braking is a more severe manoeuvre than heavy acceleration and in an uncontrolled case, the wheels lock almost immediately, this greatly reduces the lateral tyre force available and hence the uncontrolled vehicle becomes unstable and spins. By preventing the wheels from locking, lateral and longitudinal tyre forces are maintained at a higher value and the vehicle can come to a stop quickly with little intervention through the steering wheel.

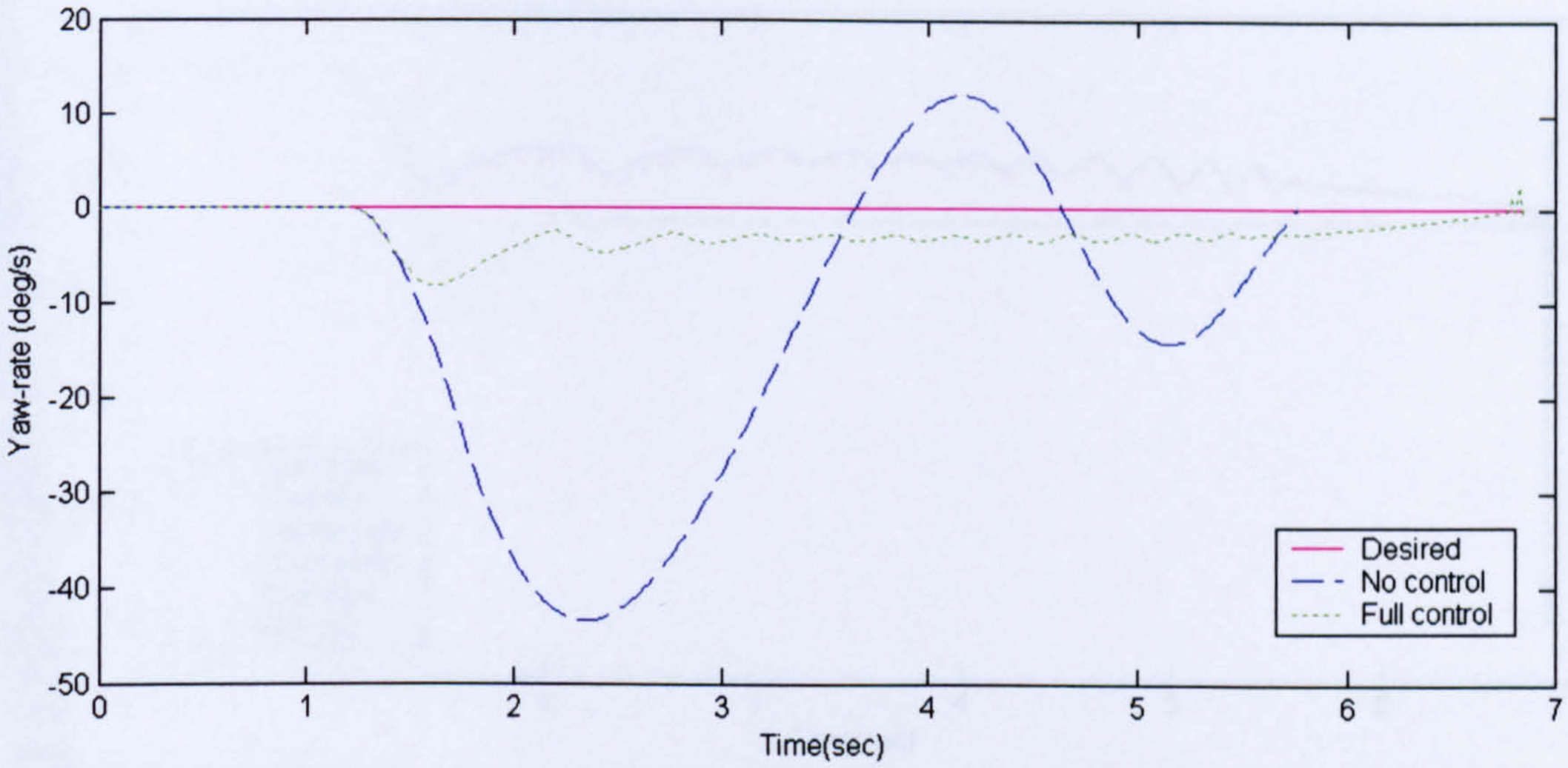

Fig. 3.34 Yaw rate response for uncontrolled and controlled unladen vehicle braking on a split-μ surface

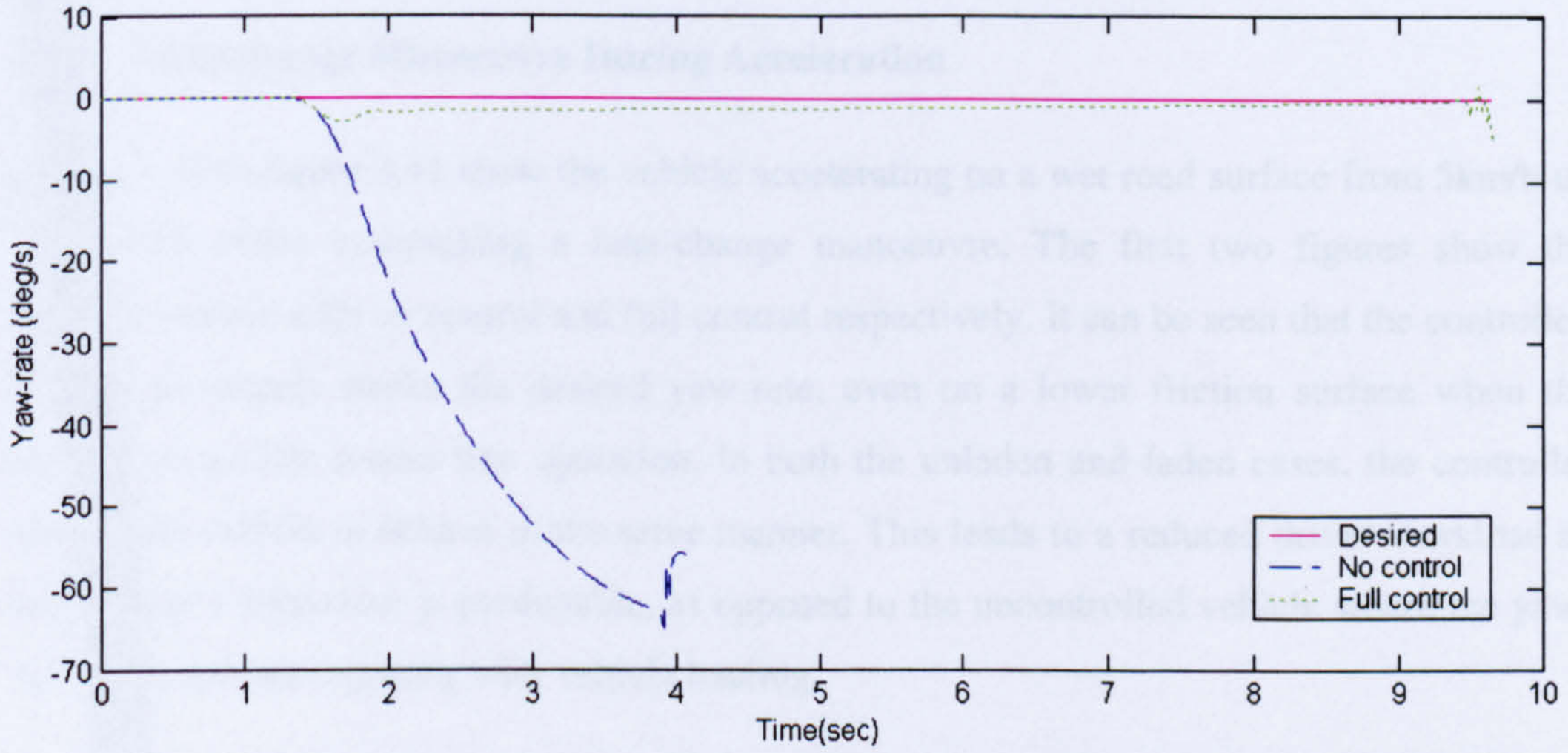

Fig. 3.35 Yaw rate response for uncontrolled and controlled laden vehicle braking on a split-μ surface

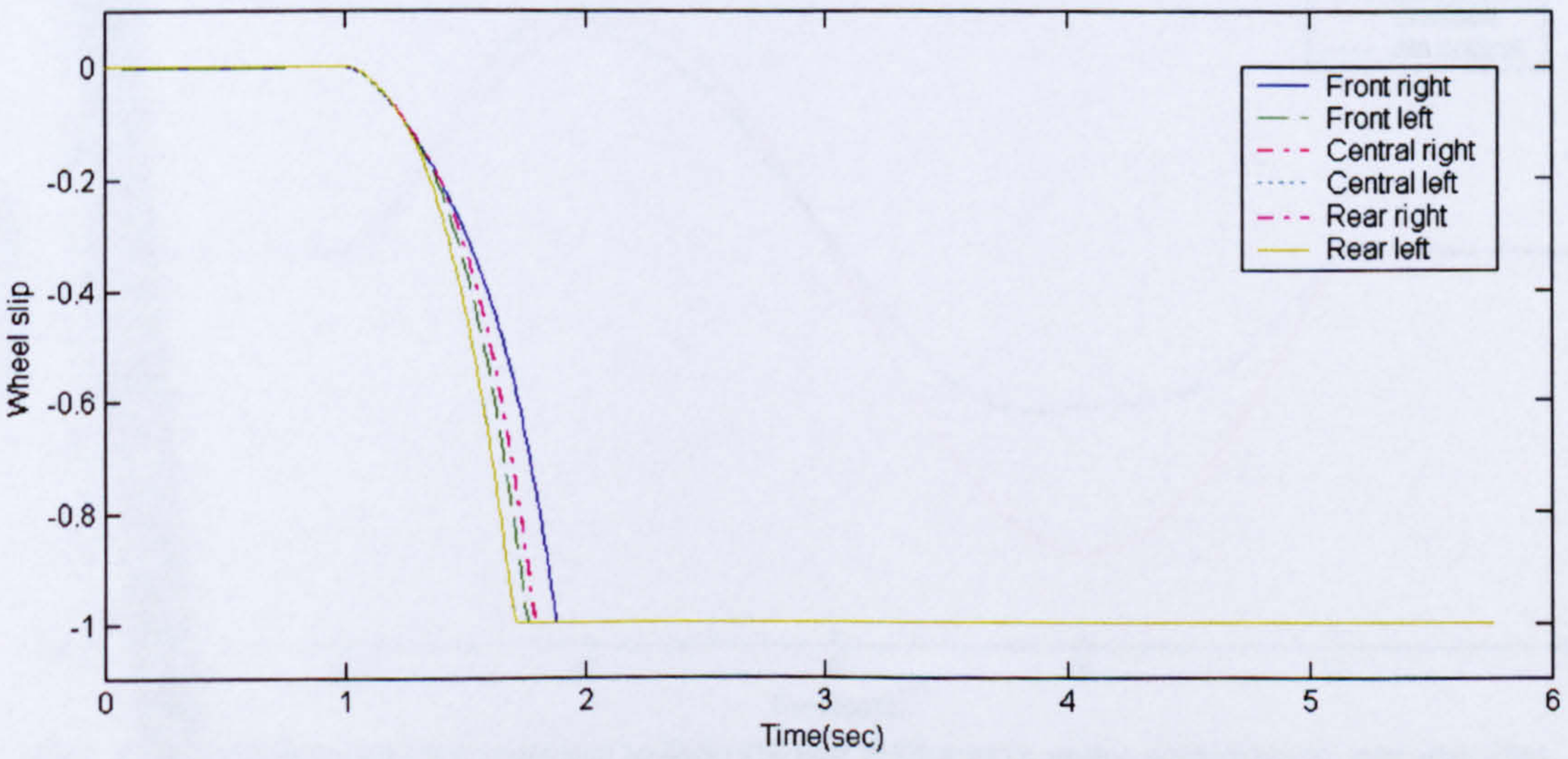

Fig. 3.36 Wheel-slip response for uncontrolled unladen vehicle braking on a split-μ surface

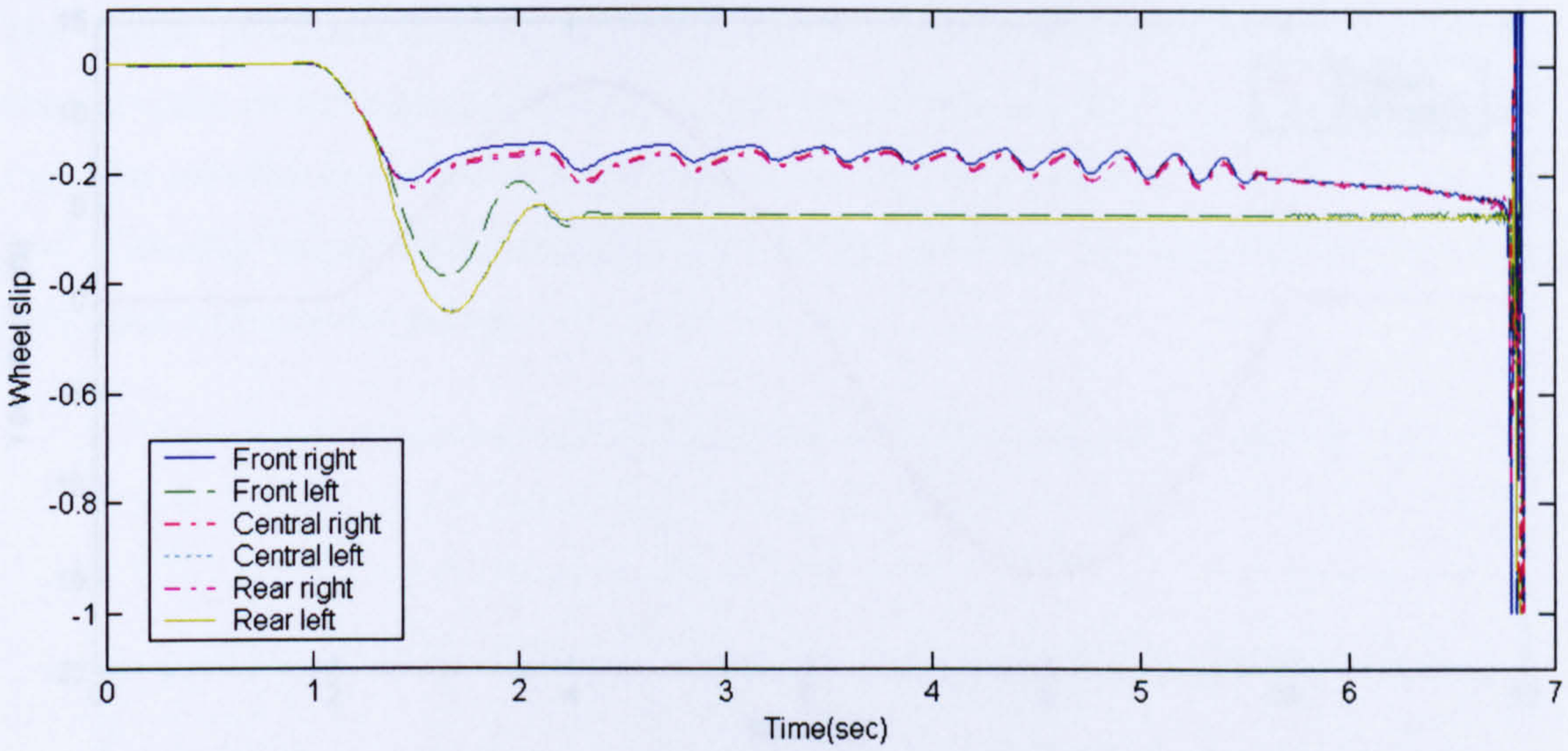

Fig. 3.37 Wheel-slip response for controlled unladen vehicle braking on a split-μ surface

3.8.3 Lane-change Manoeuvre During Acceleration

Figure 3.38 to figure 3.41 show the vehicle accelerating on a wet road surface from 5km/h up to 80km/h while undertaking a lane-change manoeuvre. The first two figures show the unladen vehicle with no control and full control respectively. It can be seen that the controlled vehicle accurately tracks the desired yaw-rate, even on a lower friction surface when the traction controller comes into operation. In both the unladen and laden cases, the controller causes the vehicle to behave in the same manner. This leads to a reduced driver workload as the vehicle's behaviour is predictable, as opposed to the uncontrolled vehicle where the yaw-rate response alters greatly with vehicle loading.

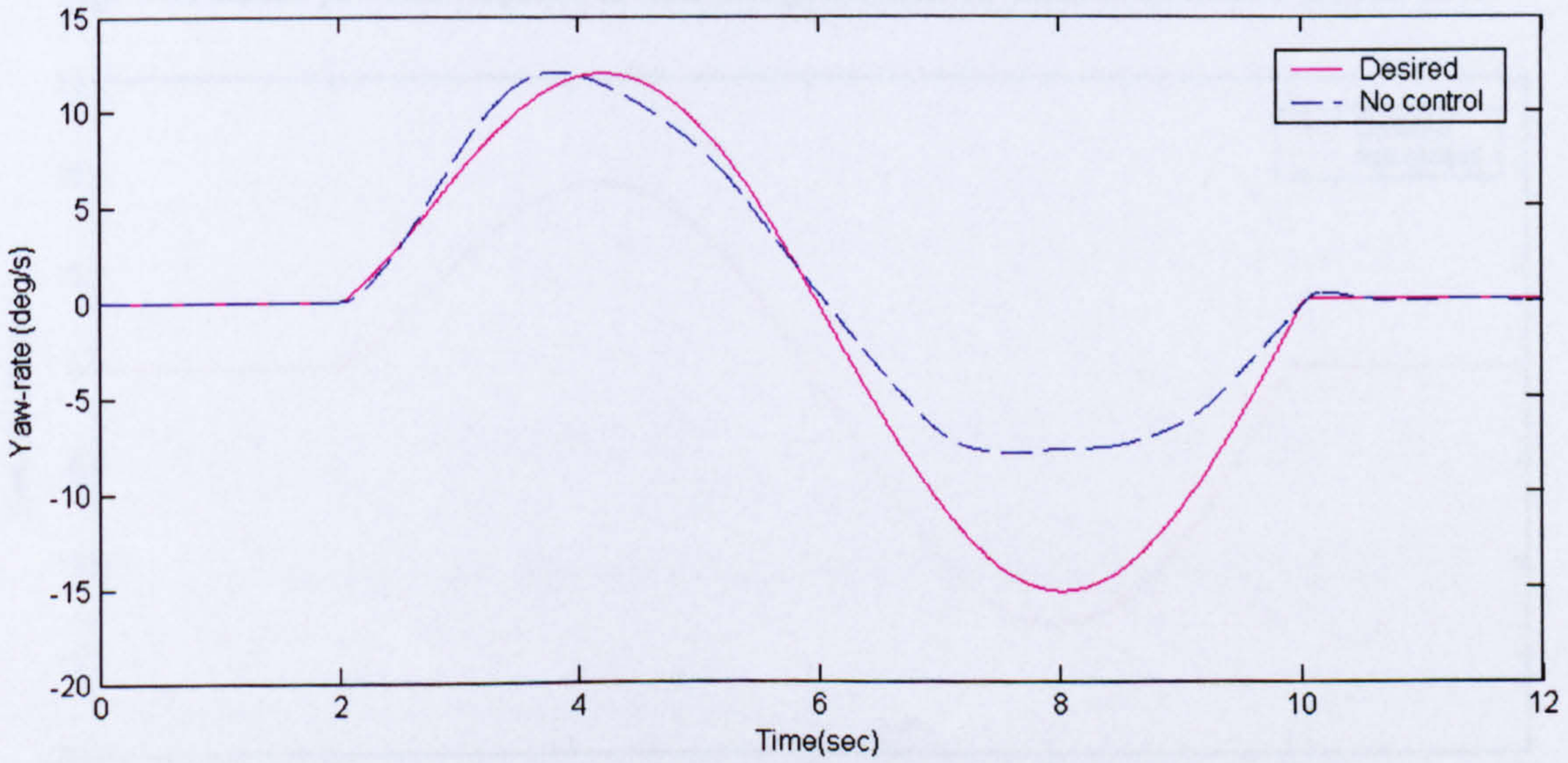

Fig. 3.38 Unladen yaw-rate response to lane-change manoeuvre under acceleration, uncontrolled.

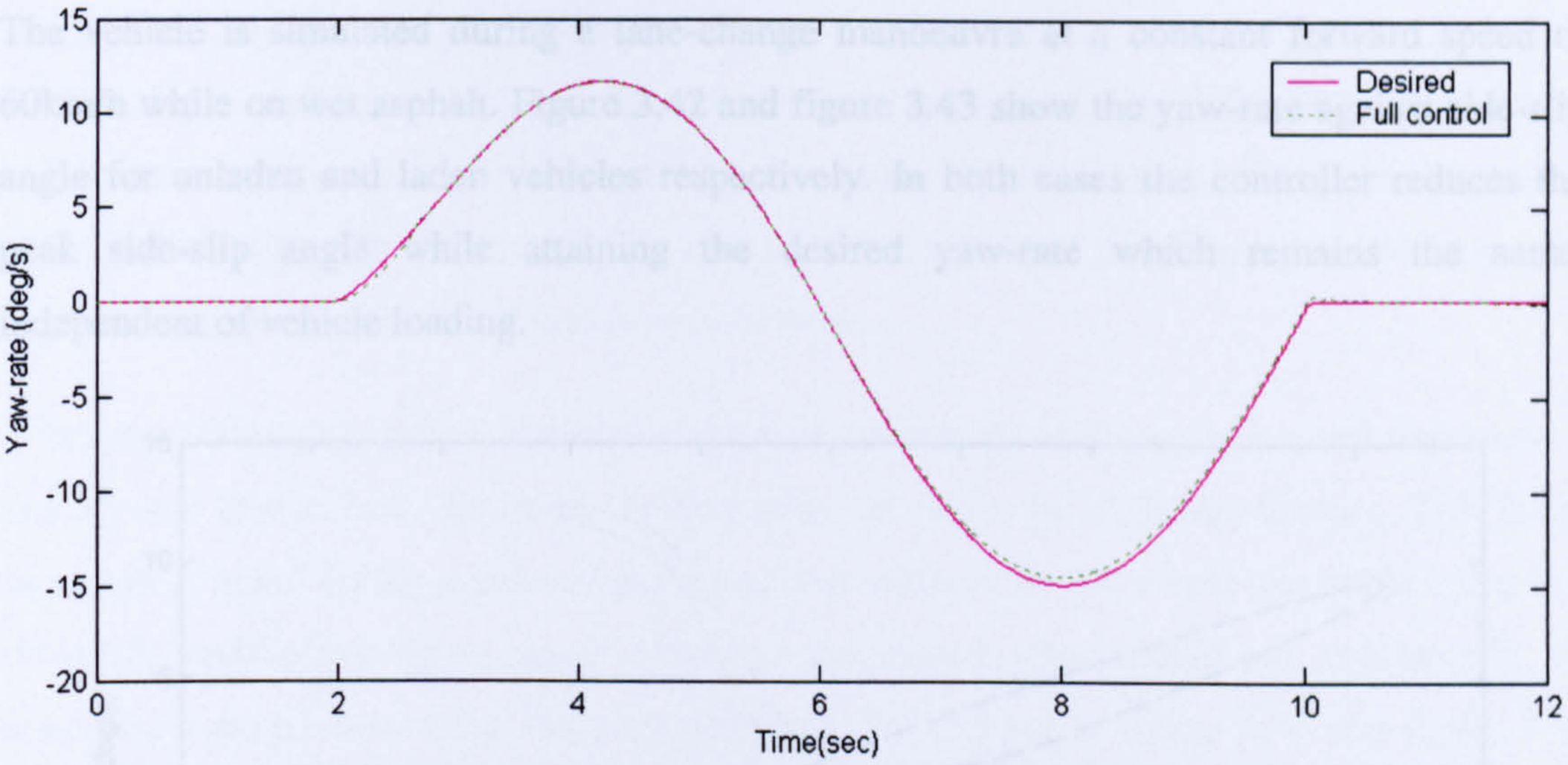

Fig. 3.39 Unladen yaw-rate response to lane-change manoeuvre under acceleration, controlled.

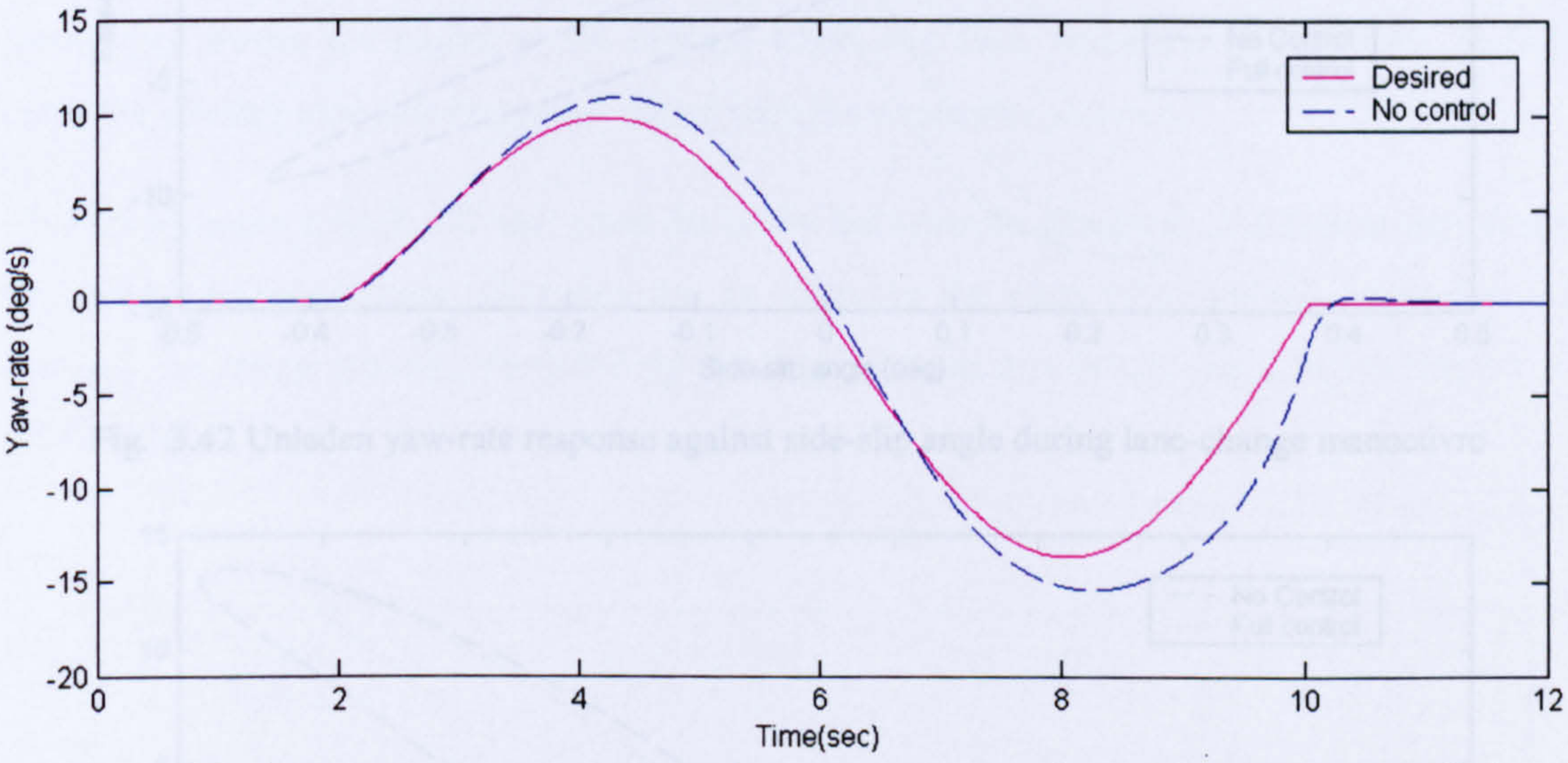

Fig. 3.40 Laden yaw-rate response to lane-change manoeuvre under acceleration, uncontrolled.

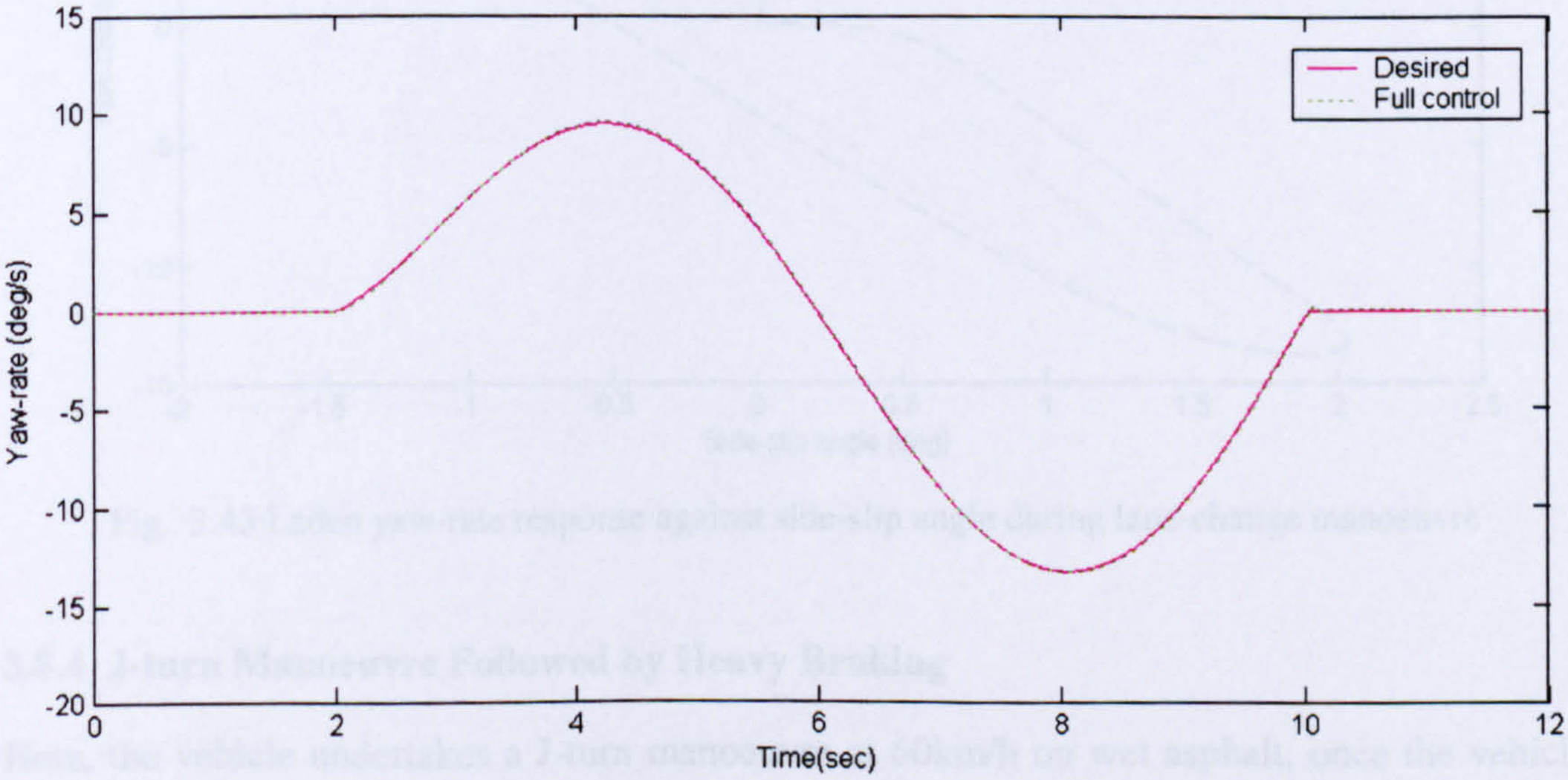

Fig. 3.41 Laden yaw-rate response to lane-change manoeuvre under acceleration, controlled.

The vehicle is simulated during a lane-change manoeuvre at a constant forward speed of 60km/h while on wet asphalt. Figure 3.42 and figure 3.43 show the yaw-rate against side-slip angle for unladen and laden vehicles respectively. In both cases the controller reduces the peak side-slip angle while attaining the desired yaw-rate which remains the same, independent of vehicle loading.

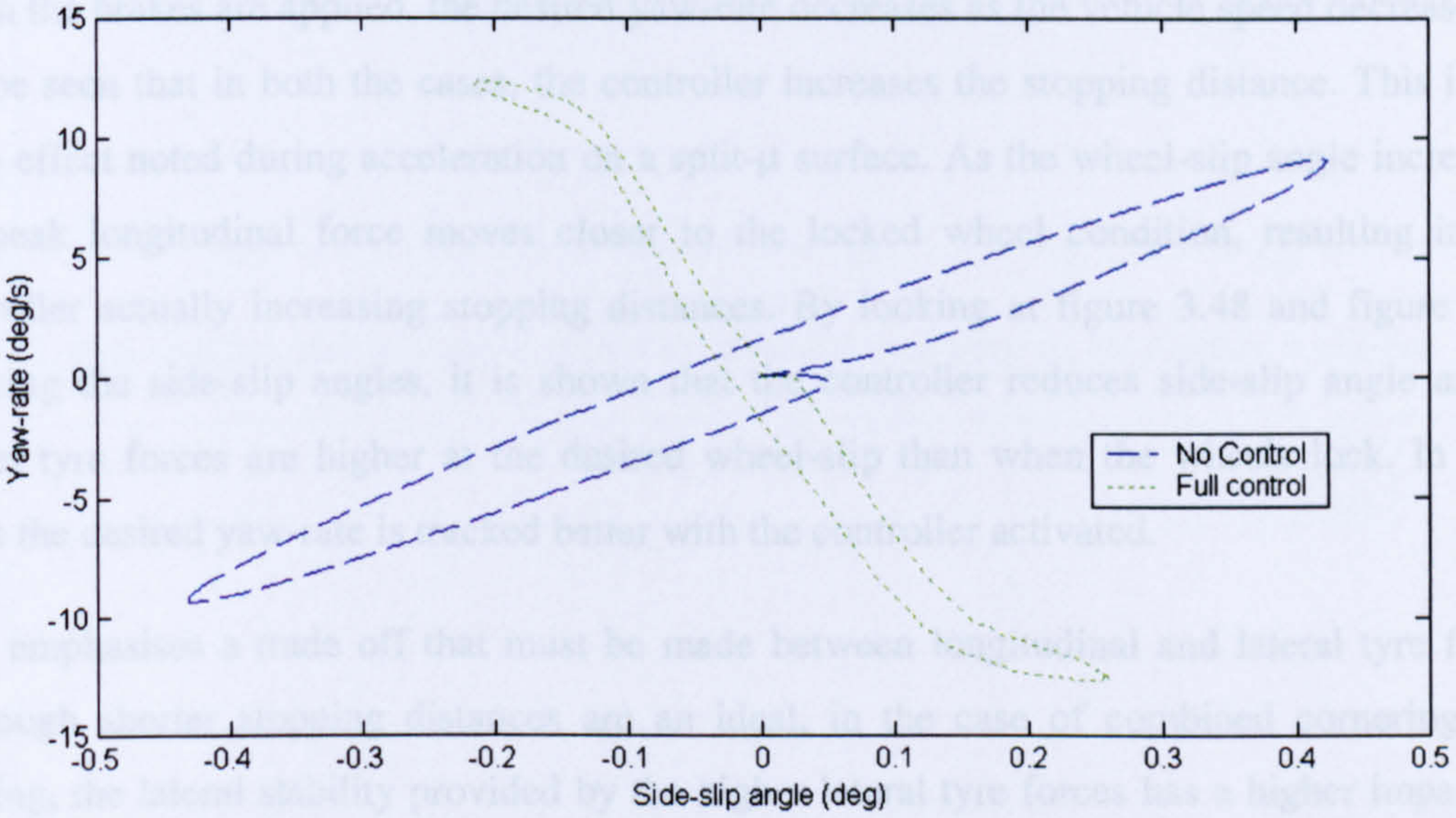

Fig. 3.42 Unladen yaw-rate response against side-slip angle during lane-change manoeuvre

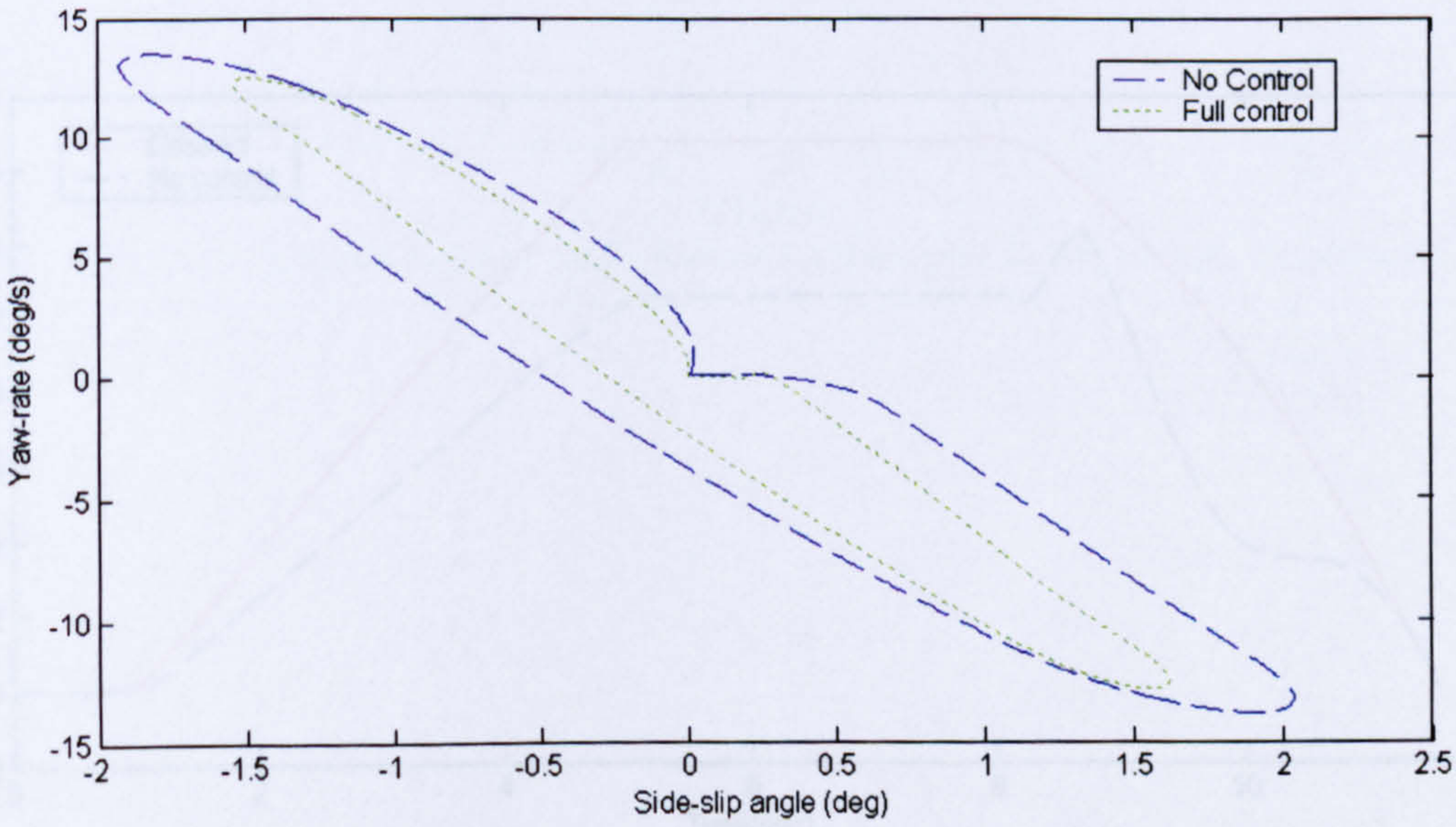

Fig. 3.43 Laden yaw-rate response against side-slip angle during lane-change manoeuvre

3.8.4 J-turn Manoeuvre Followed by Heavy Braking

Here, the vehicle undertakes a J-turn manoeuvre at 60km/h on wet asphalt, once the vehicle enters steady-state cornering the brakes are applied to bring the vehicle to a stop. Figure 3.44

and figure 3.45 show the yaw-rate responses for the uncontrolled and fully controlled vehicle while unladen and figure 3.46 and figure 3.47 show the same for the laden vehicle. Until the moment the brakes are applied, only the yaw-moment controller is operating. The controller again accurately tracks the desired yaw-rate in both conditions, ensuring the vehicle operates in the same manner, whether unladen or fully laden.

When the brakes are applied, the desired yaw-rate decreases as the vehicle speed decreases. It can be seen that in both the cases, the controller increases the stopping distance. This is the same effect noted during acceleration on a split-μ surface. As the wheel-slip angle increases, the peak longitudinal force moves closer to the locked wheel condition, resulting in the controller actually increasing stopping distances. By looking at figure 3.48 and figure 3.49 showing the side-slip angles, it is shown that the controller reduces side-slip angle as the lateral tyre forces are higher at the desired wheel-slip than when the wheels lock. In both cases the desired yaw-rate is tracked better with the controller activated.

This emphasises a trade off that must be made between longitudinal and lateral tyre force. Although shorter stopping distances are an ideal, in the case of combined cornering and braking, the lateral stability provided by the higher lateral tyre forces has a higher impact on driver safety.

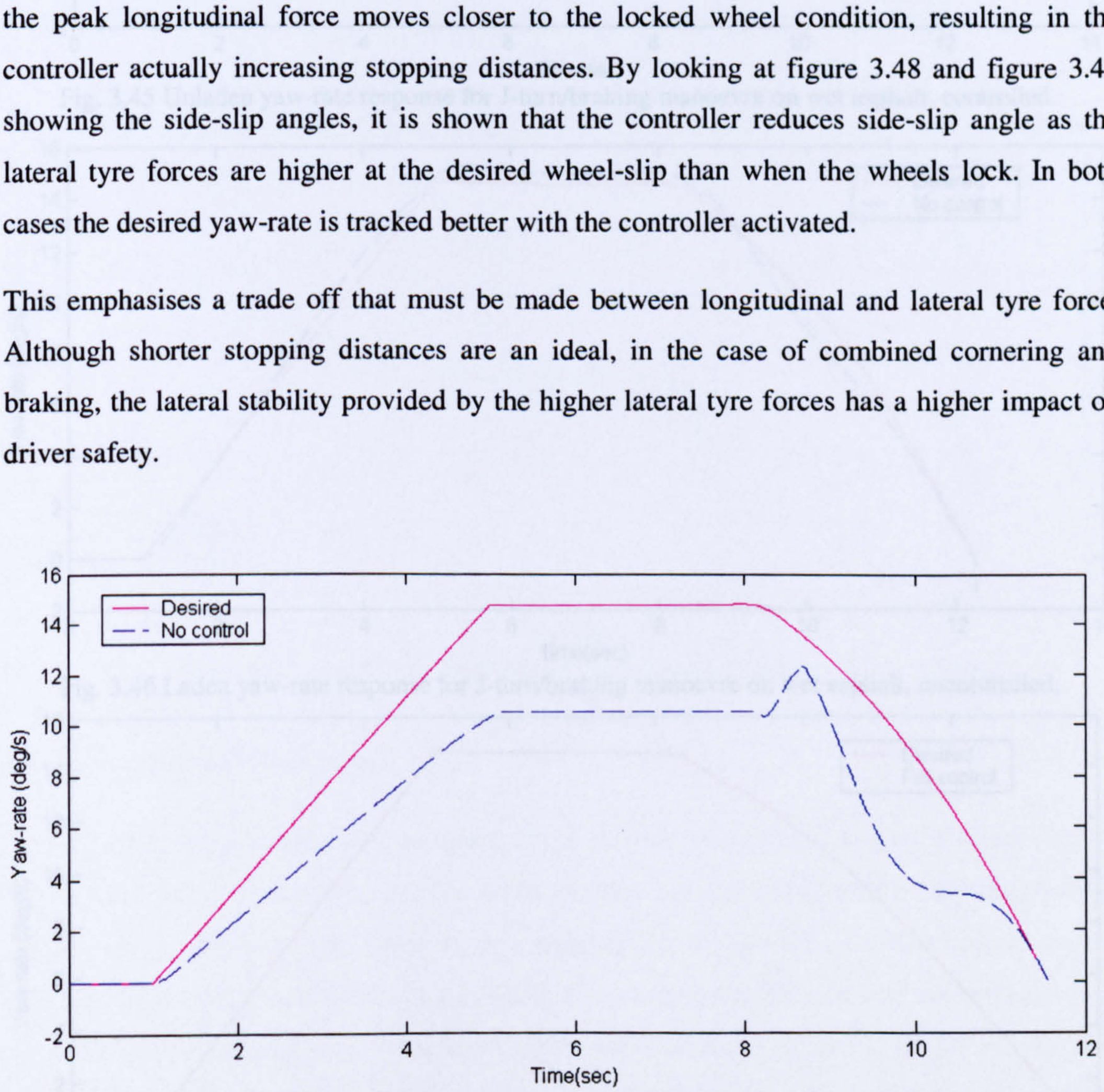

Fig. 3.44 Unladen yaw-rate response for J-turn/braking manoevre on wet asphalt, uncontrolled.

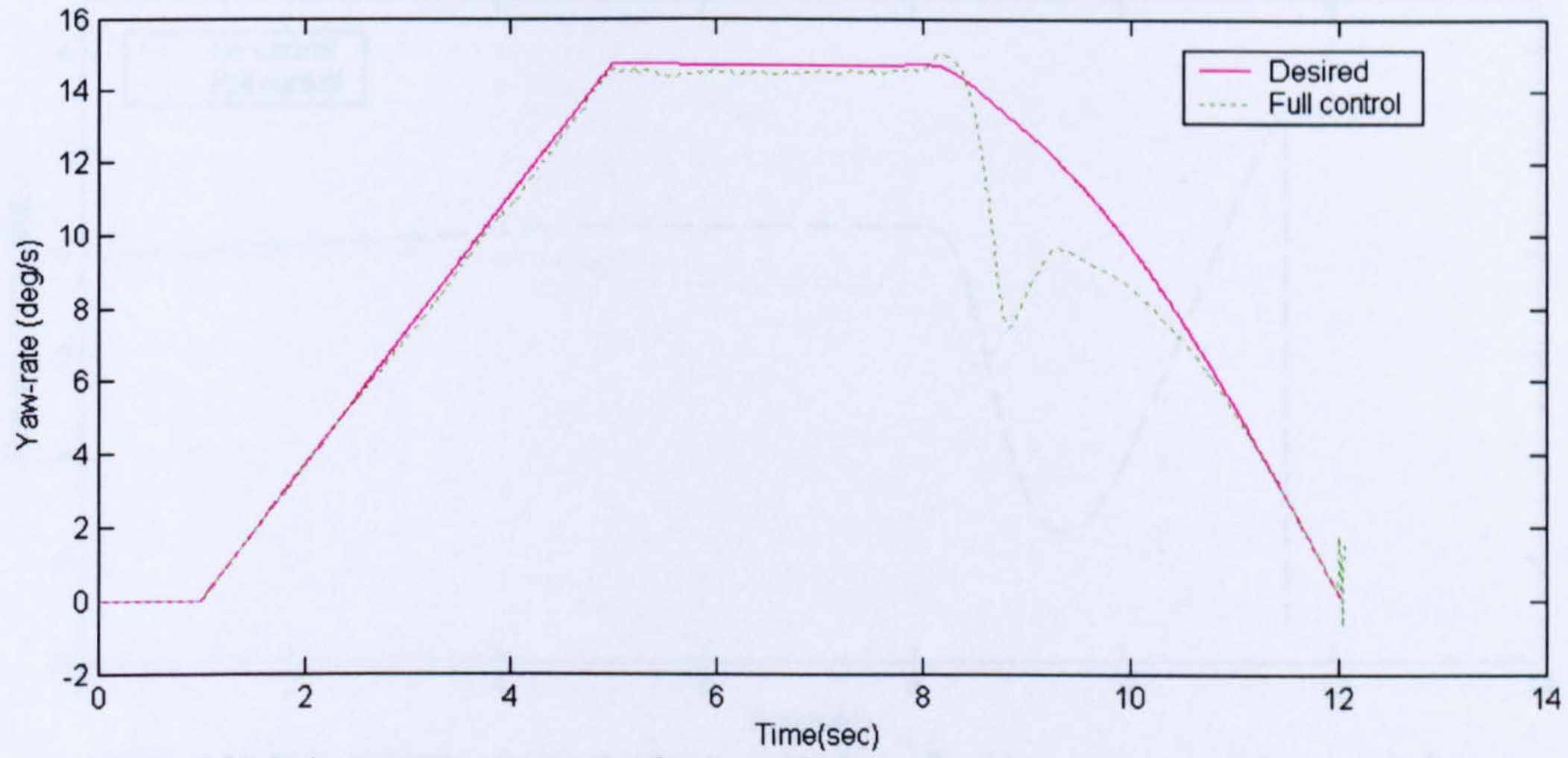

Fig. 3.45 Unladen yaw-rate response for J-turn/braking manoevre on wet asphalt, controlled.

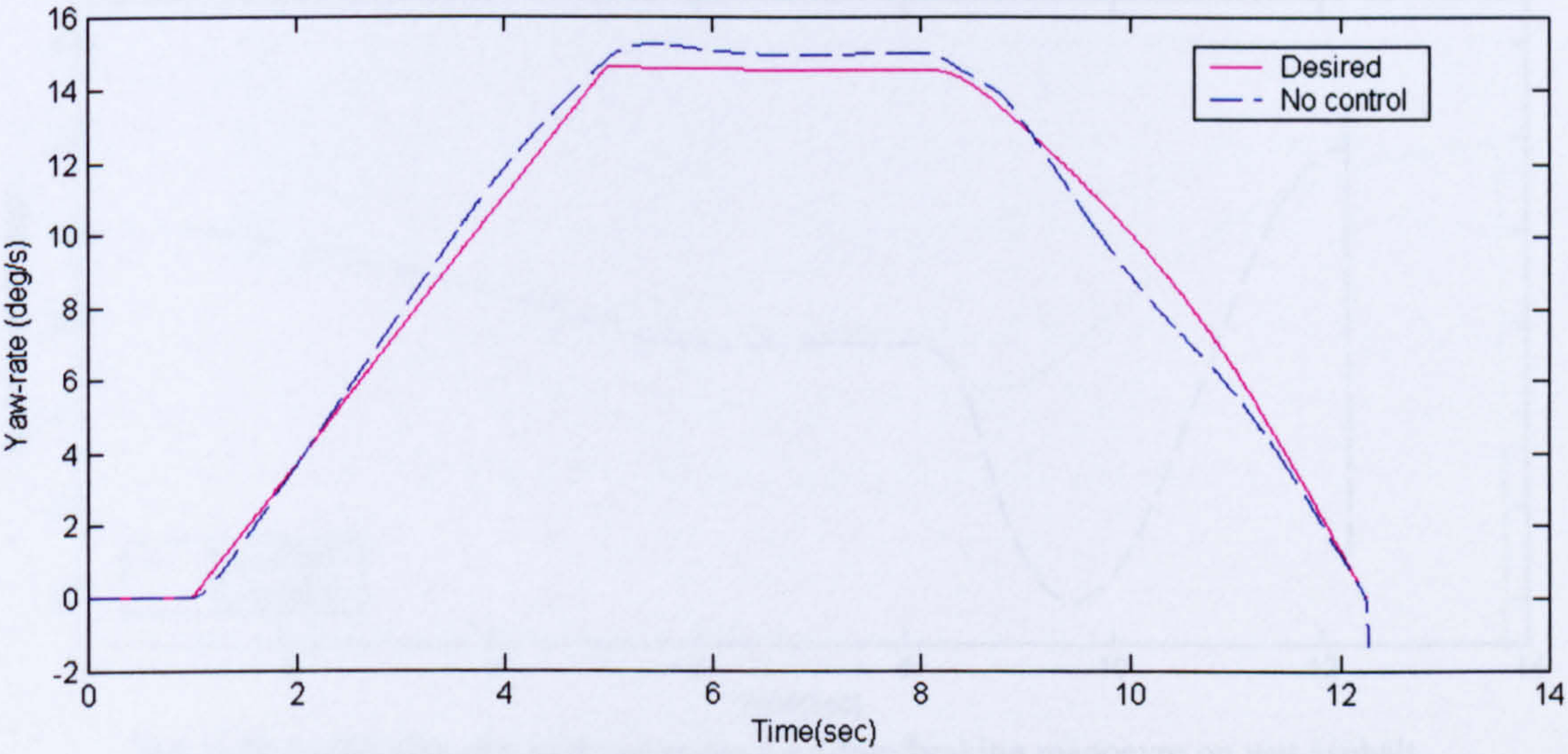

Fig. 3.46 Laden yaw-rate response for J-turn/braking manoevre on wet asphalt, uncontrolled.

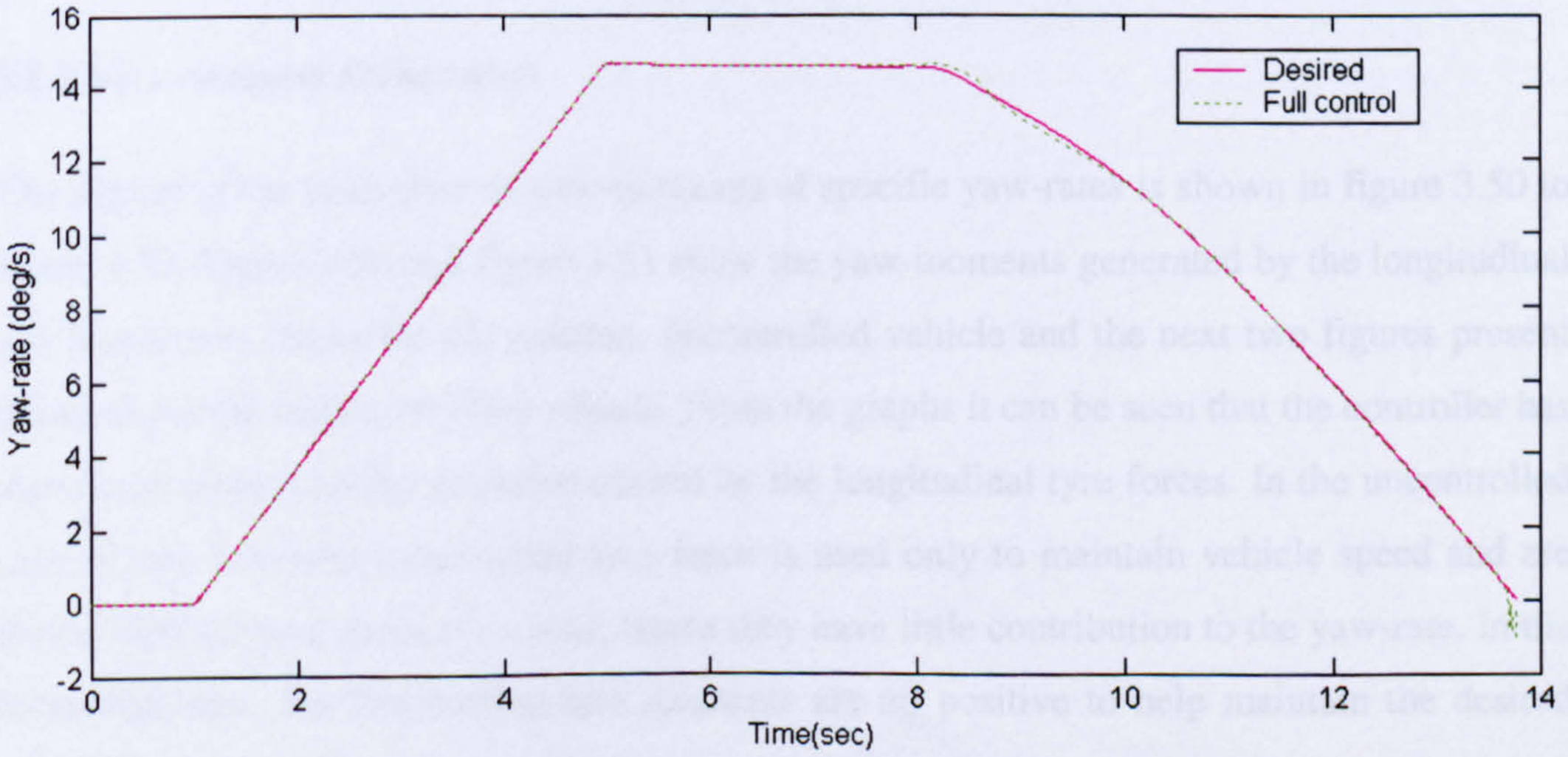

Fig. 3.47 Laden yaw-rate response for J-turn/braking manoevre on wet asphalt, controlled.

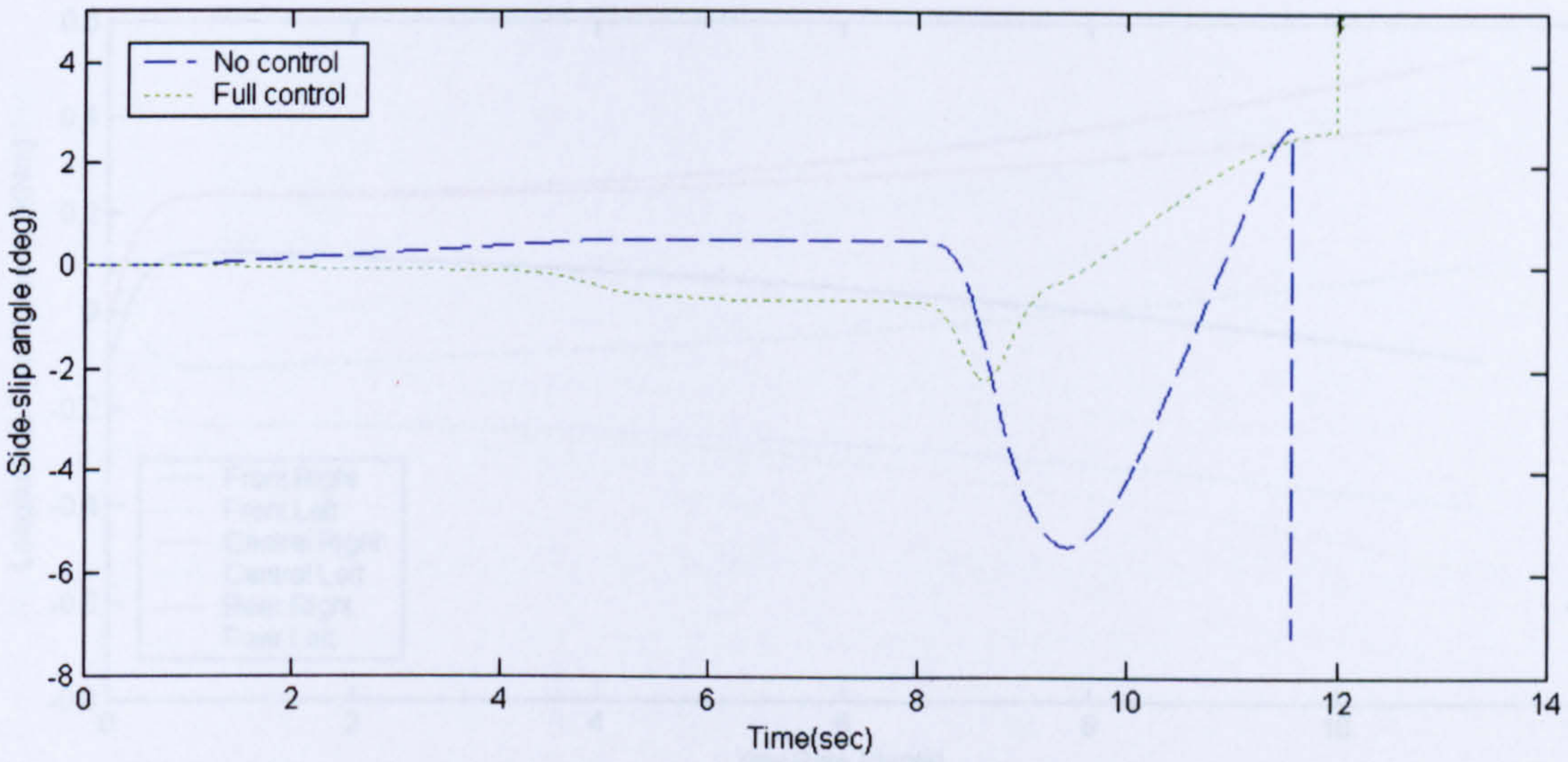

Fig. 3.48 Unladen side-slip angle response for J-turn/braking manoevre on wet asphalt.

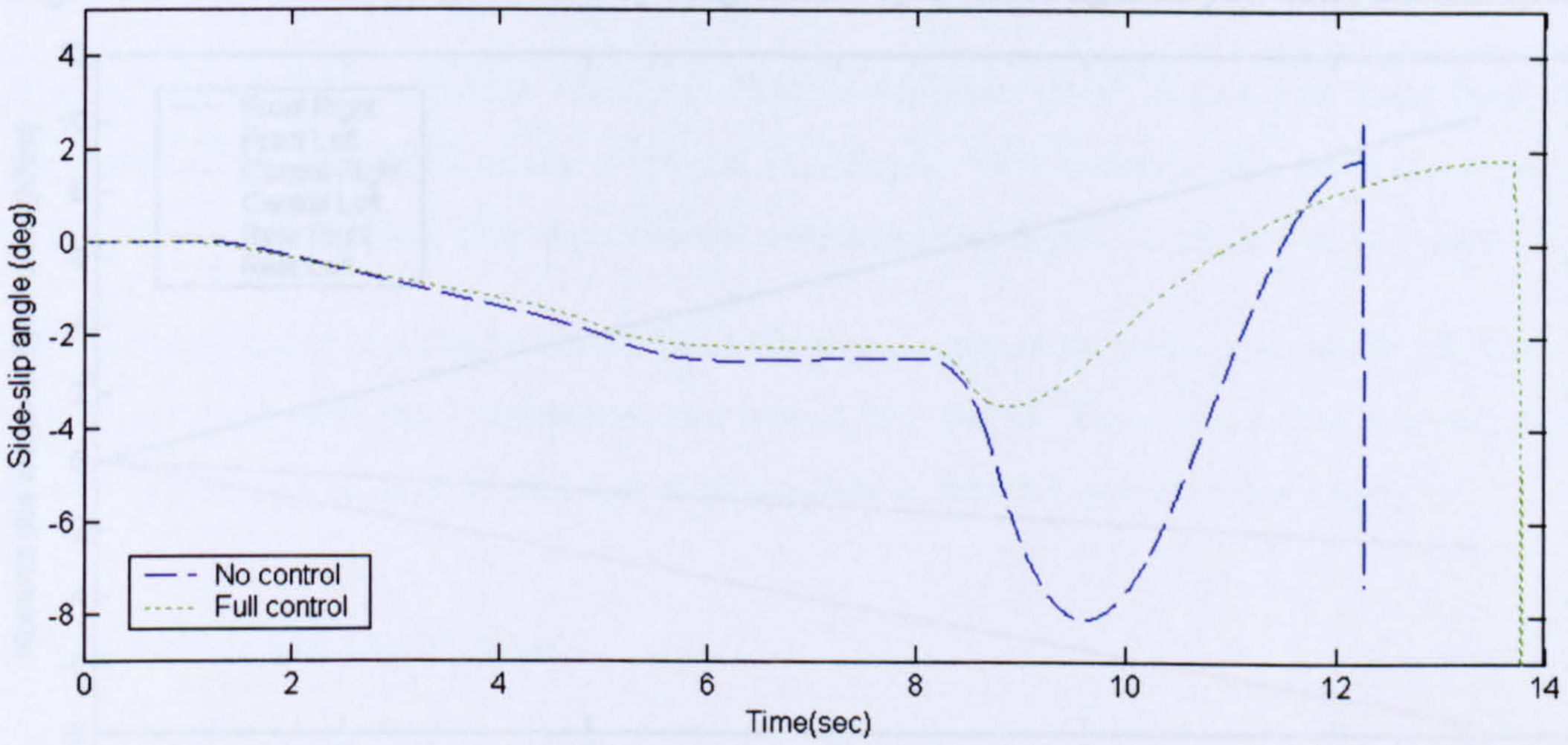

Fig. 3.49 Laden side-slip angle response for J-turn/braking manoevre on wet asphalt.

3.8.5 Yaw-moment Generation

The impact of the controller on yaw-moments at specific yaw-rates is shown in figure 3.50 to figure 3.53. Figure 3.50 and figure 3.51 show the yaw-moments generated by the longitudinal and lateral tyre forces for the unladen, uncontrolled vehicle and the next two figures present the same for the fully controlled vehicle. From the graphs it can be seen that the controller has significant impact on the moments caused by the longitudinal tyre forces. In the uncontrolled case (figure 3.50) the longitudinal tyre force is used only to maintain vehicle speed and are almost symmetrical about the x-axis, hence they have little contribution to the yaw-rate. In the controlled case, the longitudinal tyre moments are all positive to help maintain the desired yaw-rate.

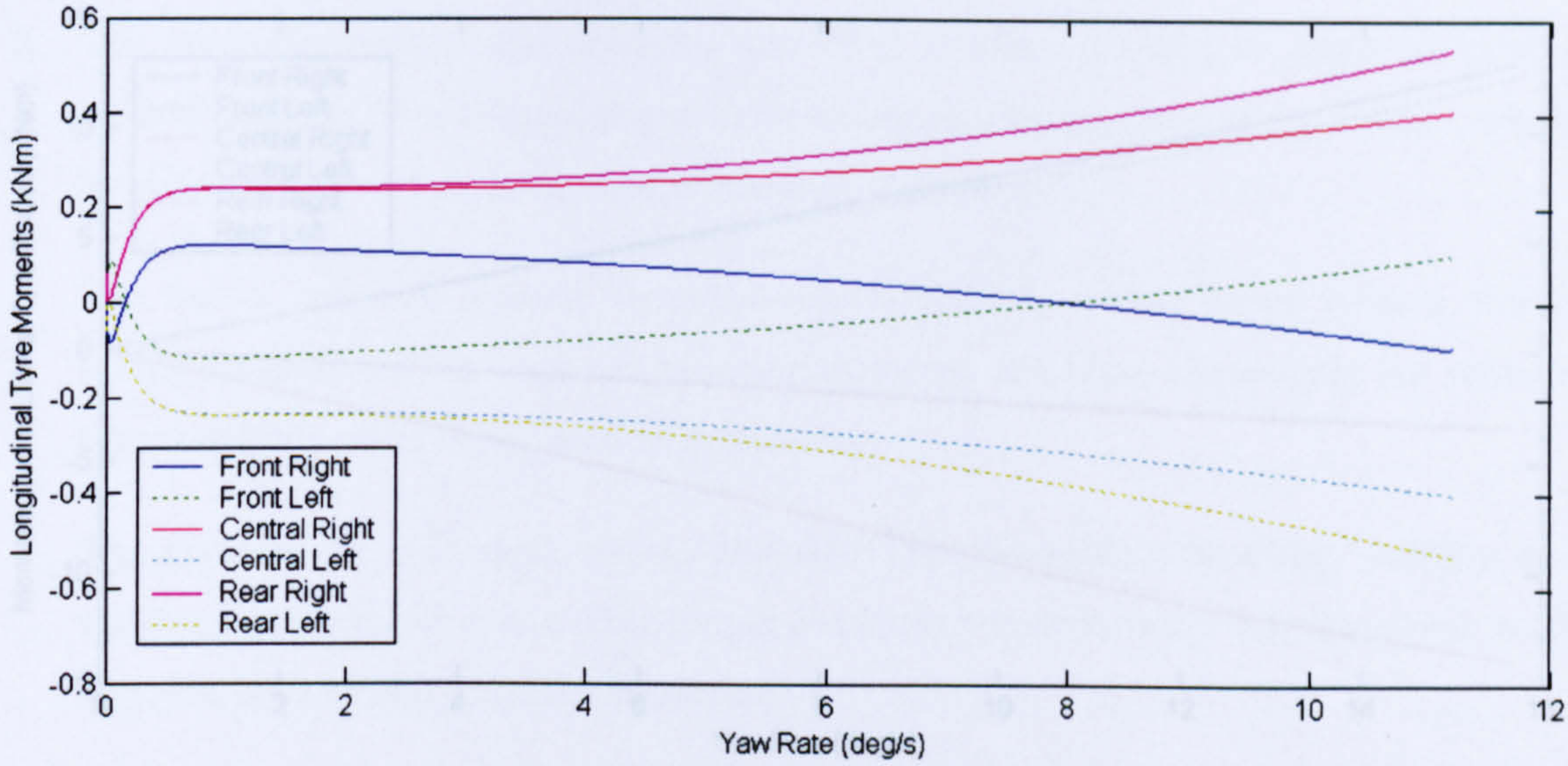

Fig. 3.50 Yaw-moments generated by longitudinal tyre forces against yaw-rate, uncontrolled

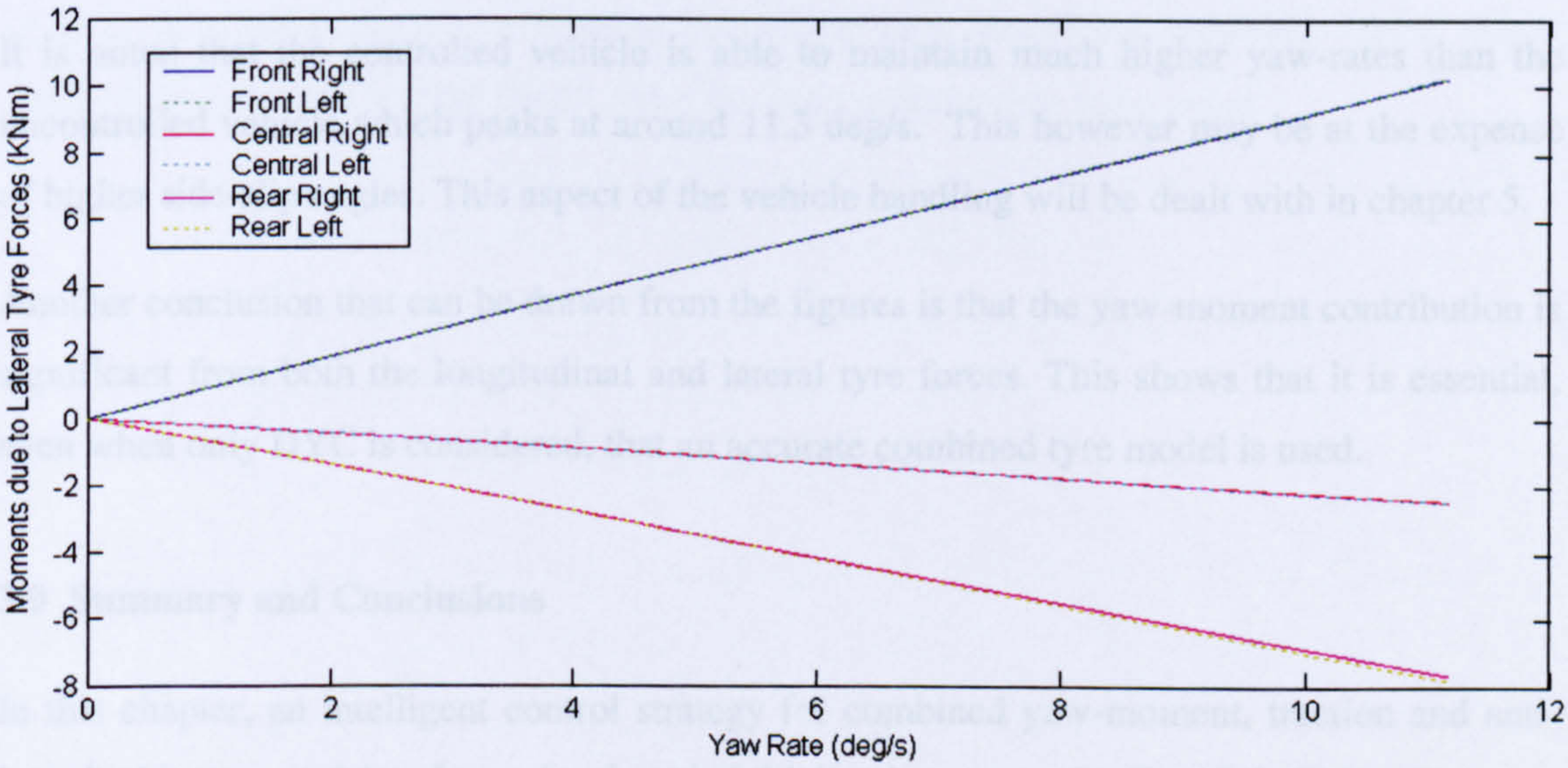

Fig. 3.51 Yaw-moments generated by lateral tyre forces against yaw-rate, uncontrolled

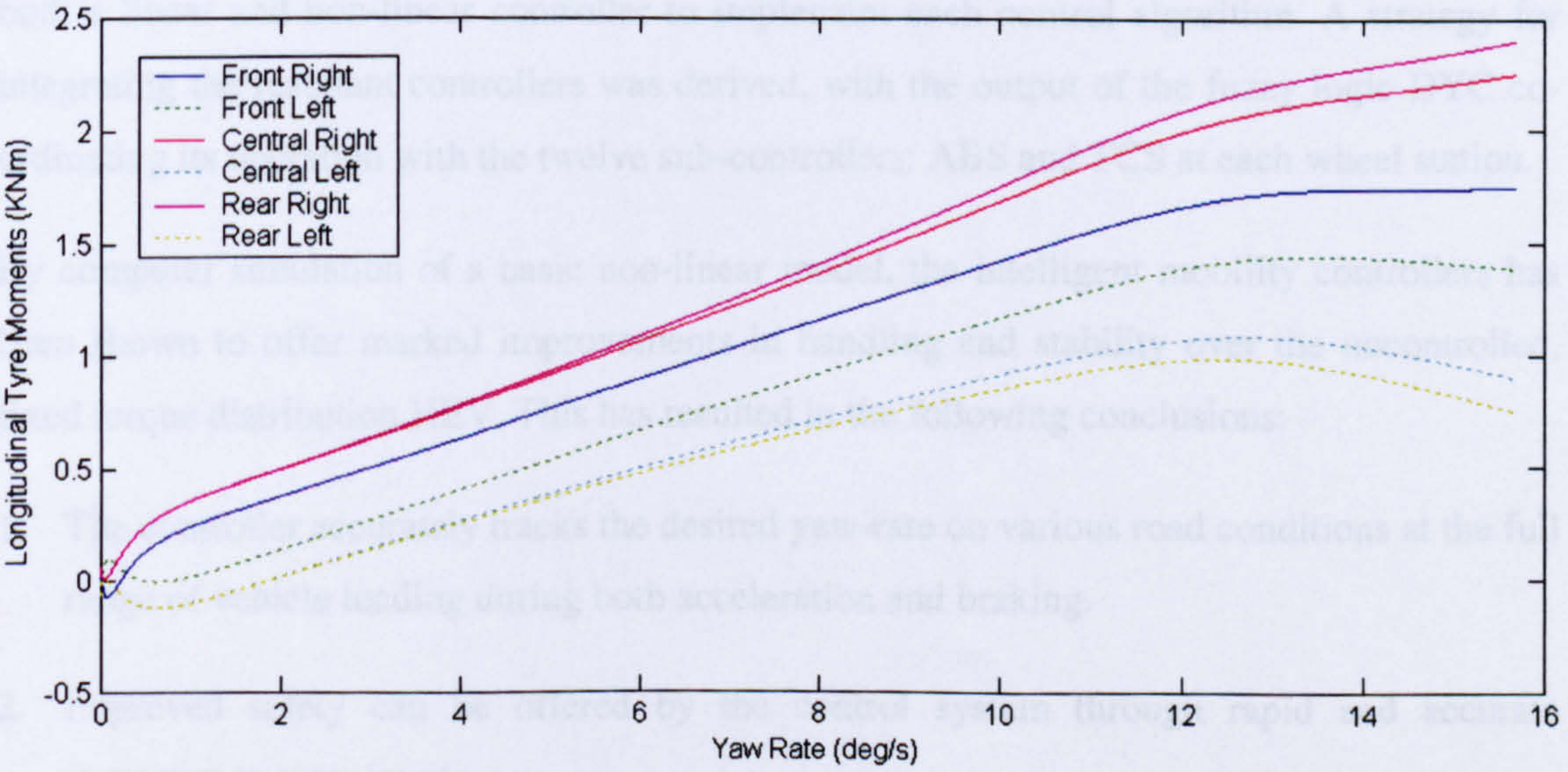

Fig. 3.52 Yaw-moments generated by longitudinal tyre forces against yaw-rate, controlled

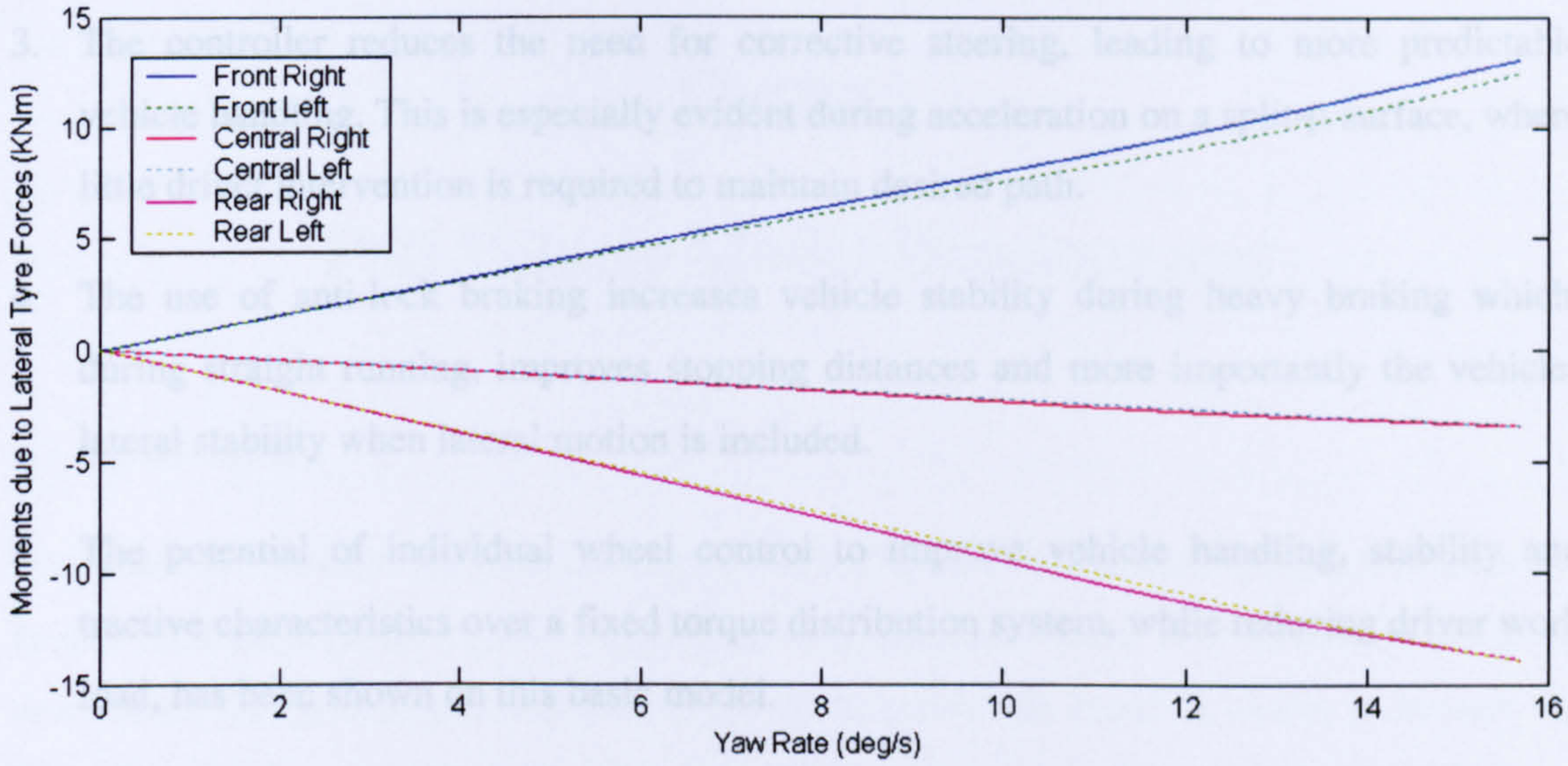

Fig. 3.53 Yaw-moments generated by lateral tyre forces against yaw-rate, controlled

It is noted that the controlled vehicle is able to maintain much higher yaw-rates than the uncontrolled vehicle which peaks at around 11.3 deg/s. This however may be at the expense of higher side-slip angles. This aspect of the vehicle handling will be dealt with in chapter 5.

Another conclusion that can be drawn from the figures is that the yaw-moment contribution is significant from both the longitudinal and lateral tyre forces. This shows that it is essential, even when only DYC is considered, that an accurate combined tyre model is used.

3.9 Summary and Conclusions

In this chapter, an intelligent control strategy for combined yaw-moment, traction and anti-lock braking control has been developed. Initially they were developed individually using both a linear and non-linear controller to implement each control algorithm. A strategy for integrating the resultant controllers was derived, with the output of the fuzzy logic DYC co-ordinating its operation with the twelve sub-controllers: ABS and TCS at each wheel station.

By computer simulation of a basic non-linear model, the intelligent mobility controllers has been shown to offer marked improvements in handling and stability over the uncontrolled, fixed torque distribution HEV. This has resulted in the following conclusions:

1. The controller accurately tracks the desired yaw-rate on various road conditions at the full range of vehicle loading during both acceleration and braking.

2. Improved safety can be offered by the control system through rapid and accurate responses to steer inputs.

3. The controller reduces the need for corrective steering, leading to more predictable vehicle handling. This is especially evident during acceleration on a split-μ surface, where little driver intervention is required to maintain desired path.

4. The use of anti-lock braking increases vehicle stability during heavy braking which, during straight running, improves stopping distances and more importantly the vehicles lateral stability when lateral motion is included.

5. The potential of individual wheel control to improve vehicle handling, stability and tractive characteristics over a fixed torque distribution system, while reducing driver work load, has been shown on this basic model.

These conclusions achieve the controller specifications laid out at the beginning of this chapter with the exception of limiting side-slip at high lateral accelerations, which will be dealt with on the full vehicle model, once the full controller has been tuned.

Chapter 4

Full Vehicle Model Development

4.1 Introduction

Now that the controller has been developed and tested on a basic handling model, in order for further validation of the control algorithms, it is necessary for a full vehicle model to be developed. This will be an extension of the basic non-linear handling model to include the following:

- The suspension system to include pitching and rolling motions along with vertical motion of the sprung and unsprung masses.
- Load transfer effects due to longitudinal and lateral accelerations.
- Conventional drivetrain components for comparison benefits.

This model should closely approximate the behaviour of the existing vehicle on road. By comparing simulation results to data provided by QinetiQ, taken from the conventional vehicle trials, it is possible to validate the vehicle model.

A simulation model, representing the conventional vehicle will also be developed. By including the conventional powertrain, and comparing its performance to the hybrid configuration, the advantages offered by the high torque capabilities of the hybrid-electric drivetrain will be apparent.

4.2 Full Vehicle Model

Now that the full vehicle model is to be developed, it is necessary to assess the required detail that the vehicle should exhibit in order to simulate the actual vehicle as closely as possible allowing validation against vehicle trial data for the existing vehicle. Work conducted by Shovlin (1999) included an assessment of the various extensions to the vehicle model and the relative impact they have on the simulation outputs of the conventional CSV on which this vehicle is based. The author conducts a fractional factorial[1] experiment, varying eight

---

[1] A factorial experiment with 8 extensions using parameter values of $\pm 20\%$ results in 2^8 simulations. Fractional factorial method runs only 16 simulations, sufficient to determine the impact of each extension.

different extensions to a basic linear handling model to assess the impact on the model undertaking a J-turn through peak lateral accelerations and yaw-rates, lateral acceleration rise times, steady state understeer gradient and roll gradient. Shovlin notes that the conclusions are only valid for on-road vehicle handling with this particular vehicle and hence, the conclusions presented are valid for the work conducted here. The investigation shows that the following extensions have a significant effect on the vehicle performance (the author notes that pitching motion has insignificant effect on handling, however, that is with the assumption of constant forward speed, which for the purpose of this work, is not the case):

- Non-linear tyre models
- Body bounce and pitch
- Tyre springs and dampers
- Steering system compliance
- Non-linear suspension components (referring to the bump stop / check forces)

In order to develop the full vehicle model, Shovlin (1999) notes from the fractional factorial experiments show that the following assumptions are valid:

- The suspension and tyre springs and dampers are assumed linear around a trim condition
- Suspension is independent at each wheel station
- Suspension geometry can be simplified to a scalar gain relation wheel force and displacement to suspension force and displacement
- Vehicle chassis is rigid
- Ackerman steer angles are ignored

The following additional assumptions are also:

- Tyres are constantly in contact with ground (not a valid assumption during off-road simulation, but made for the purpose of the work and simplicity of Simulink model)
- Tyre contact with ground is a point contact
- Tyre camber angle is zero (a lack of data meant that wheel camber was not included in the model)

4.2.1 Final Vehicle Co-ordinate System

The final coordinate system is shown in figure 4.1 (Note that F_s is positive on the body, Crolla *et al.* 1996, Huh *et al.* 2000). For reference, the 1st, 3rd and 5th wheels are considered the right set of tyres and the remaining tyres, the left set. By including the suspension system

to the model, it is possible to simulate in greater detail the handling and ride characteristics of the vehicle. The resulting model has eighteen degrees of freedom:

- Longitudinal, V_x
- Lateral, V_y
- Body bounce, V_z
- Yaw, ψ
- Pitch, θ
- Roll, ϕ
- Vertical motion of the six unsprung masses (wheels): $Z_{1\text{-}6}$
- Rotation of the six wheel, $\omega_{1\text{-}6}$

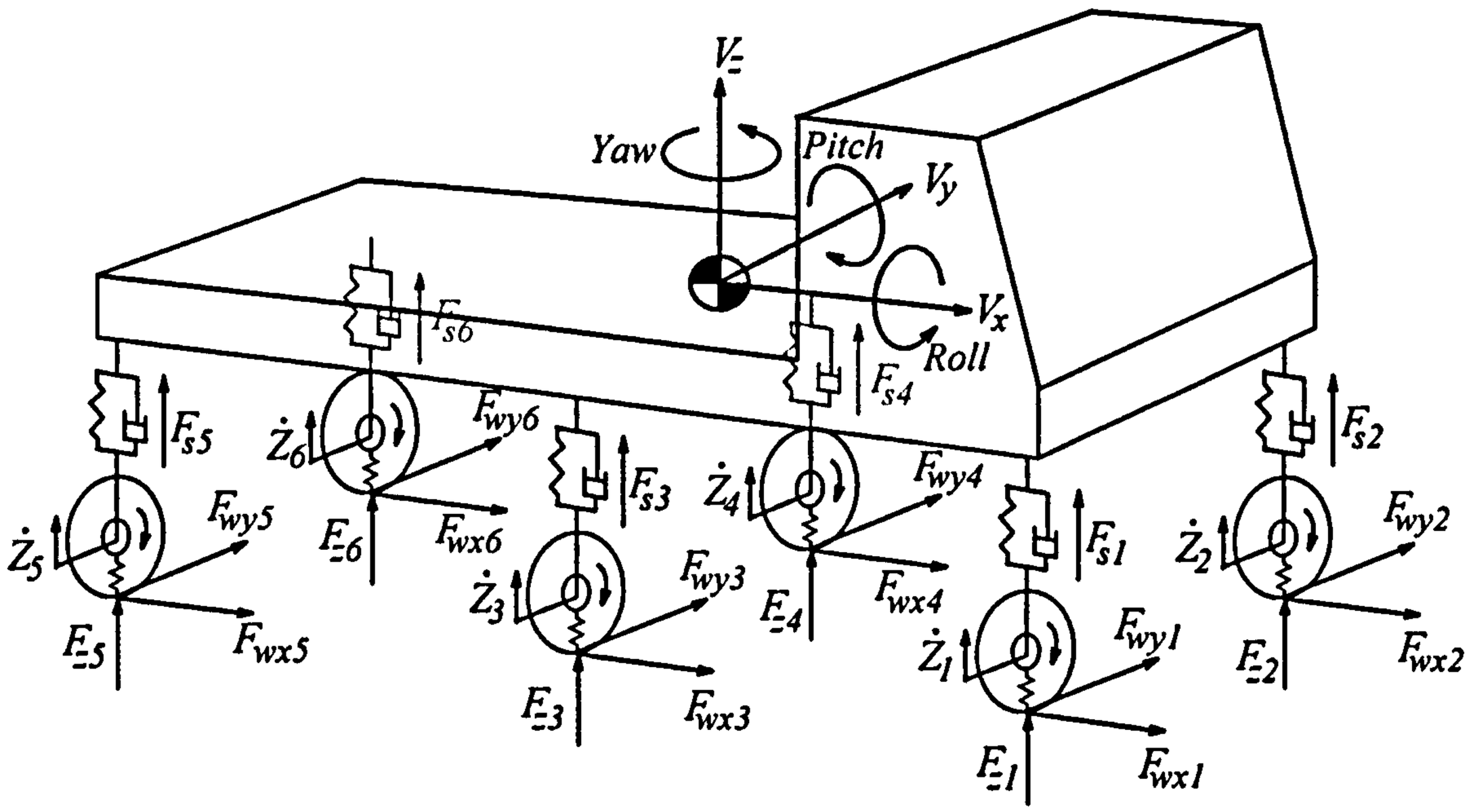

Fig. 4.1 Final 18 degree of freedom model

The equations for rolling and pitching and yawing motions are based on the Euler equations describing rotation of a rigid body around the three axis' (Meriam *et al.*, 2003 and Huh *et al.*, 2000). The six equations defining the motion of the vehicle body are presented in equations 4.1 to 4.6. For the vertical, rolling and pitching motions, the vertical suspension forces are the inputs to the system along with moments that are generated due to longitudinal and lateral acceleration and gravity as described by equations 4.7 and 4.8 and figure 4.2. A full set of vehicle parameters can be found in Appendix A.1.4

Longitudinal motion:

$$M(\frac{dV_x}{dt}+V_z\frac{d\theta}{dt}-V_y\frac{d\psi}{dt})=F_{wx1}+F_{wx2}+F_{wx3}+F_{wx4}+F_{wx5}+F_{wx6}-F_d \quad (4.1)$$

Lateral motion:

$$M(\frac{dV_y}{dt}+V_x\frac{d\psi}{dt}-V_z\frac{d\phi}{dt})=F_{wy1}+F_{wy2}+F_{wy3}+F_{wy4}+F_{wy5}+F_{wy6} \quad (4.2)$$

Vertical motion:

$$M(\frac{dV_z}{dt}+V_y\frac{d\phi}{dt}-V_x\frac{d\theta}{dt})=F_{s1}+F_{s2}+F_{s3}+F_{s4}+F_{s5}+F_{s6} \quad (4.3)$$

Rolling motion:

$$I_x\cdot\frac{d^2\phi}{dt^2}+(I_z-I_y)\cdot\frac{d\theta}{dt}\cdot\frac{d\psi}{dt}=t_s(-F_{s1}+F_{s2}-F_{s3}+F_{s4}-F_{s5}+F_{s6})+M_\phi \quad (4.4)$$

Pitching motion:

$$I_y\cdot\frac{d^2\theta}{dt^2}+(I_x-I_z)\cdot\frac{d\phi}{dt}\cdot\frac{d\psi}{dt}=-aF_{s1}-aF_{s2}-bF_{s3}-bF_{s4}+cF_{s5}+cF_{s6}+M_\theta \quad (4.5)$$

Yawing motion:

$$\begin{aligned}I_z\cdot\frac{d^2\psi}{dt^2}+(I_y-I_x)\cdot\frac{d\phi}{dt}\cdot\frac{d\theta}{dt}&=t(F_{wx1}-F_{wx2}+F_{wx3}-F_{wx4}+F_{wx5}-F_{wx6})\\&+aF_{wy1}+aF_{wy2}+bF_{wy3}+bF_{wy4}-cF_{wy5}-cF_{wy6}+M_z\end{aligned} \quad (4.6)$$

Moments due to lateral and longitudinal acceleration:

$$M_\varphi=M_bG(H_{cgB}-H_{rc})\sin\phi+M_bA_y(H_{cgB}-H_{rc})\cos\phi \quad (4.7)$$

$$M_\theta=M_bgH_{cgB}\sin\theta-M_bA_xH_{cgB}\cos\theta \quad (4.8)$$

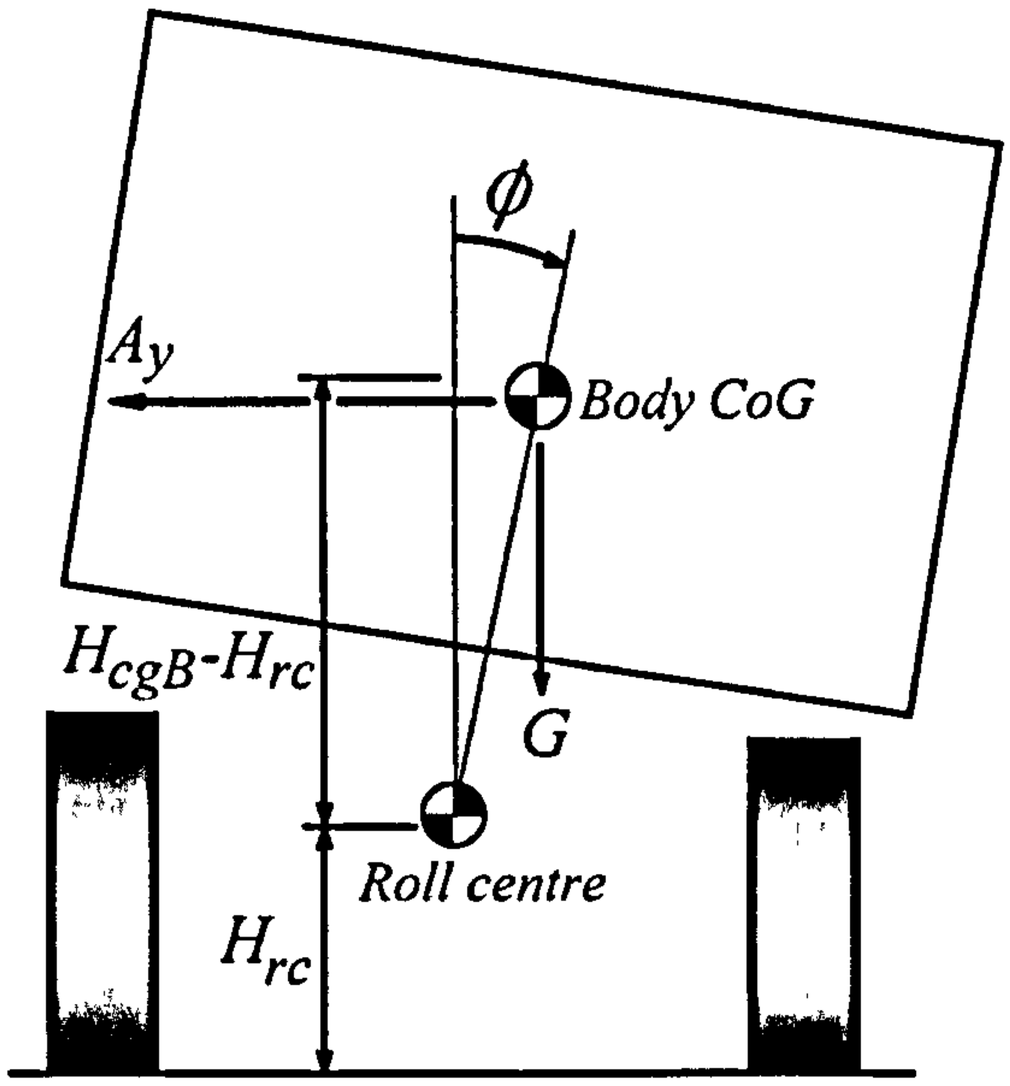

Fig 4.2 Roll motion and moments

4.2.2 Suspension System and Load Transfer Effects

The suspension of the passive CSV utilises a hydro-pneumatic strut at each wheel station, incorporating an oil filled damper. This is simplified to a parallel spring and damper combination to model the suspension at each wheel station. The same is also used to model the vertical forces in the tyre. The co-ordinate system for the suspension is shown in figure 4.3. There are various forces that come into play when modelling the vehicles suspension: vertical forces in the tyre and the suspension itself; the bump stop / check forces and the load transfer forces due to longitudinal and lateral acceleration. All of these forces need to be expressed and added to determine the motion of the sprung and unsprung masses along with the vertical tyre loading which has significant effect on vehicle handling.

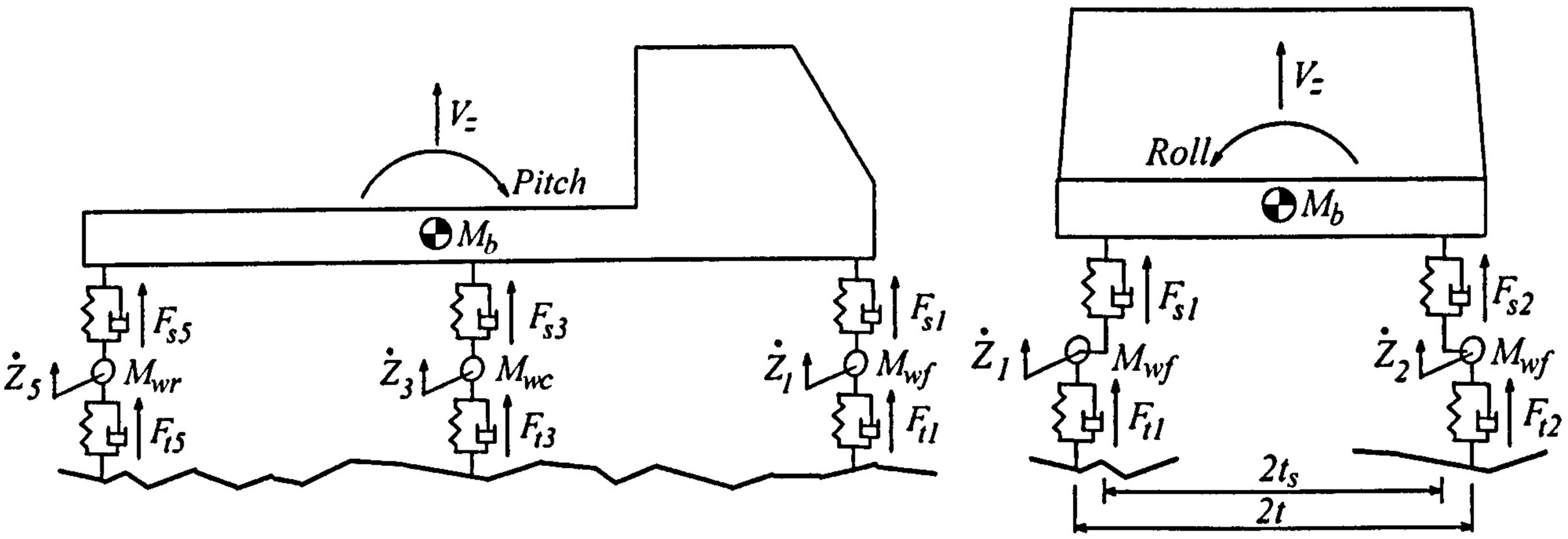

Fig. 4.3 Suspension co-ordinate system from right-hand side and front

Equations 4.9 and 4.10 present the forces in the linear representation of the suspension and tyre due to tension/relaxation of the parallel spring/damper combination. The suspension forces as seen by the vehicle body, F_{si} is expressed in equation 4.11 where the bump stop forces, F_{bi} are modelled by a look-up table of force against wheel position relative to body position and *BSF* relates force at bump stop to force at strut. It can be seen in figure 4.3 that the suspension works at a different position to the wheels in the y-axis. The values of t and t_s are used to represent these distances.

Suspension forces at strut:

$$F_{ssi} = K_{si}(Z_i - Z_{bi}) + C_{si}(\frac{dZ_i}{dt} - \frac{dZ_{bi}}{dt}) \quad (4.9)$$

Vertical tyre forces:

$$F_{ti} = K_{ti}(x_i - Z_i) + C_{ti}(\frac{dX_{oi}}{dt} - \frac{dZ_i}{dt}) \quad (4.10)$$

Suspension forces at strut:

$$F_{si} = F_{ssi} + F_{bi}BSF \quad (4.11)$$

The effects of longitudinal and lateral acceleration on the body, transfer through the suspension links from the equations for body roll and pitch (equation 4.7 and 4.8 respectively). There are two additional forces involved. These are changes in vertical force on the suspension and wheels themselves caused by the force acting on the unsprung mass due to lateral acceleration and also that from the sprung side force at the roll centre, termed the link load transfer (Dixon, 1991). Dixon also notes that longitudinal load transfer also takes place due to the same mechanisms, through the links and the unsprung masses. However, the exact height of the pitch centre is assumed to be at ground level, hence the link load transfer in longitudinal direction is zero. Equation 4.12 and equation 4.13 describe the effect.

$$F_{latacci} = \underbrace{\frac{M_{wi}H_{cgA}A_y}{t}}_{\text{due to unsprung mass}} + \underbrace{\frac{F_{zs}H_{rc}A_y}{gt}}_{\text{link load transfer}} \quad (4.12)$$

$$F_{longacci} = \underbrace{\frac{M_{wi}H_{cgA}A_x}{(a,b \text{ or } c)}}_{\text{due to unsprung mass}} \quad (4.13)$$

These forces combine to act on the vertical motion of the wheel. The suspension kinematics are simplified to two gains, used to convert forces at the suspension and bump stop to those at the wheel and vice versa, *SWF* (Shovlin, 1999).

$$M_{wi}\frac{dZ_i}{dt} = F_{ti} - F_{si}SWF \pm F_{latacci} \pm F_{longacci} \quad (4.14)$$

The equation to describe the motion of the vehicle body is a function of the rate of roll, pitch and body bounce and is calculated by equation 4.15 (which is altered depending on the wheel in question). The results can then be integrated and used as inputs to equation 4.9.

$$\frac{d^2Z_{bi}}{dt^2} = \frac{dV_z}{dt} \pm t_s\frac{d^2\phi}{dt^2} \pm (a,b \text{ or } c)\frac{d^2\theta}{dt^2} \quad (4.15)$$

The vertical tyre loading is determined by adding the vertical forces acting on the wheel (equation 4.13) to the static value for the particular vehicle loading resulting in equation 4.16.

$$F_{zi} = F_{zsi} + F_{si}SWF \pm F_{latacci} \pm F_{longacci} \quad (4.16)$$

A full list of the equations used are presented in Appendix A.1.4 along with the method of calculating vertical tyre load. By implementing these equations in the Simulink[tm] model, the full vehicle can be simulated. The actual ride responses of the vehicle are not of prime concern to this work, as it is the suspensions influence on the vehicle handling that is of most importance. The ride properties of the QinetiQ CSV have been dealt with in other literature (Shovlin, 1999 and Roberts, 2002) and the reader should refer to this work if more details of the suspension system and ride characteristics are required.

4.2.3 Compliant Steering System

The compliant steering system models the reaction at the road-wheel to a steer input at the hand-wheel. It is characterised by the stiffness and damping in the steering system itself as shown in Figure 4.4.

In Crolla *et al.* (1996) the steering system is presented. The resulting equation for the entire steering system as shown in Figure 4.4, including the steering ratio from front to central axis, the steer inertias of the four wheels and the ratio of road-wheel to hand-wheel, S_g, is presented in equation 4.17.

$$\ddot{\delta}_f = \frac{1}{(I_{wzf} + S_r I_{wzc})} * (S_g K_{ss}\delta_{hw} + E - C_{ss}\dot{\delta}_f - S_g^2 K_{ss}\delta_f) - \ddot{\psi} \quad (4.17)$$

E is the torque about the kingpin caused by the self-aligning moment and the castor angle:

$$E = M_{zf} + M_{zc} - r_w \tan\lambda_c (F_{wyf} + F_{wyc}) \quad (4.18)$$

As would be expected, it shows that the dynamics of the steering system are dependent on vehicle loading and lateral tyre forces. These equations are included in the model. Any values not available from the actual vehicle were taken from Crolla *et al.* (1996), where values are given for an off-road vehicle.

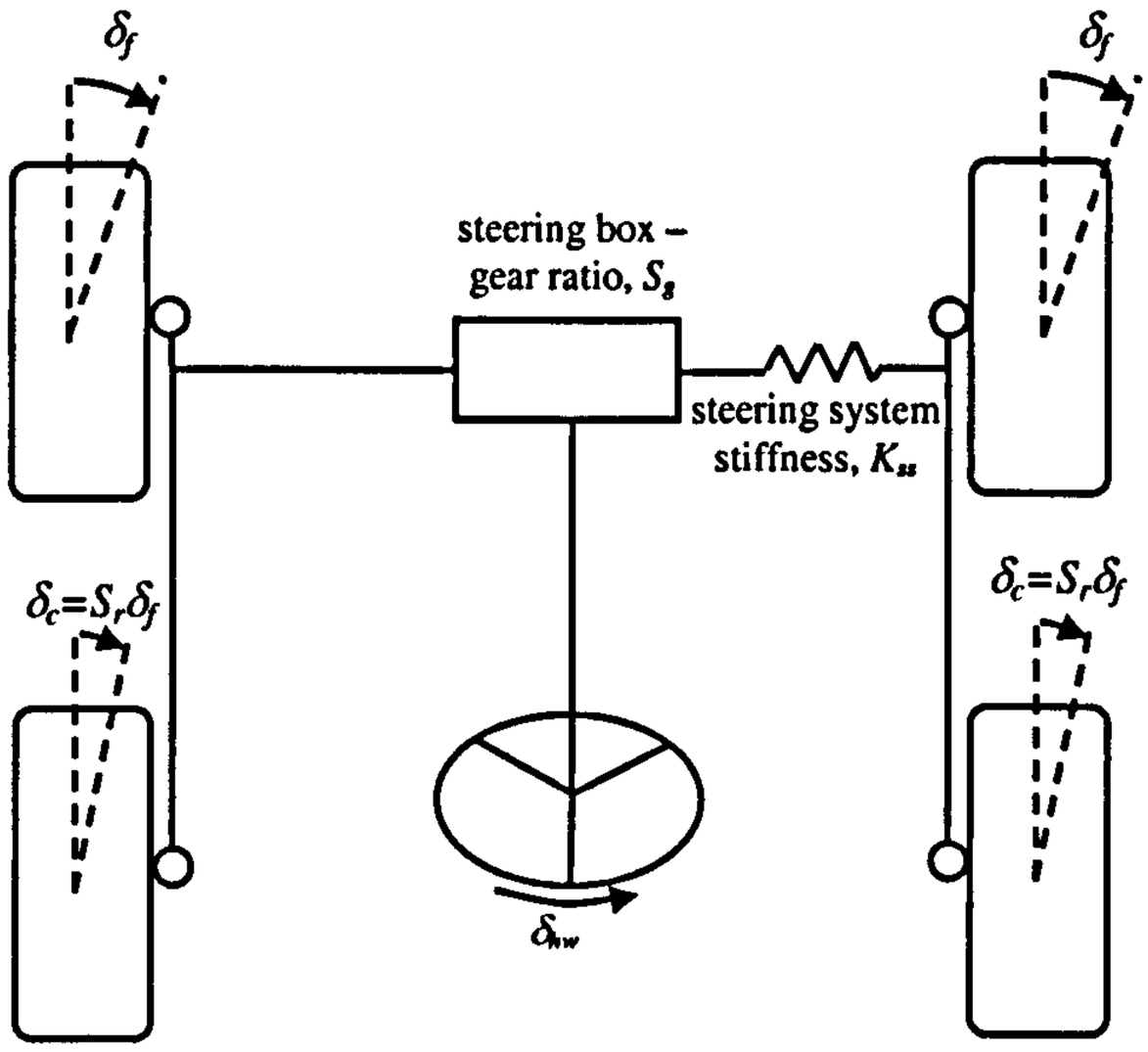

Fig. 4.4 Compliant steering system

4.2.4 Brake Force Distribution

In order to assess the performance of the ABS, it is necessary that the braking system against which it is being tested is representative of a conventional braking system where the brake force is distributed to each axle in fixed proportions to improve braking performance. For the conventional vehicle the maximum braking torque available is 52kNm, compared to 18.5kNm per wheel for the Hybrid-Electric Vehicle. This is distributed about the axles to aid braking and to help ensure that when wheel lock occurs, it aims to happen simultaneously on all axles. It is noted in Wong (1993) that this will occur when the proportion of braking force at each axle is the same as the distribution of vertical tyre loads from axle to axle. This brake force distribution is static and does not alter with loading, unless the vehicle is fitted with an Automatic Load-sensitive Braking-force meter (ALB). This infers that a compromise must be made to give good braking in both unladen and laden conditions. If rear tyres lock-up first, there will be a loss of directional stability, whereas locking of the front tyres results in a loss of directional control.

The performance of the braking system is optimised for a surface of $\mu = 0.8$. For the stationary vehicle in the unladen state, 50% of the vehicle weight is on the front axle and 25% on each of the remaining axles. When fully laden, this goes down to 28% on the front and 36% on the other two. As braking takes place there will be changes to this percentage due to load transfer. It is assumed that the maximum brake force at a given wheel before they lock is as expressed in its basic form in equation 4.19, while the total brake force for the vehicle is determined by the total load as in equation 4.20.

$$F_{\max} = \mu F_z \quad (4.19)$$

$$F_{t\max} = \mu(2F_{zsf} + 2F_{zsc} + 2F_{zsr}) \quad (4.20)$$

Where F_z includes the load transfer due to longitudinal deceleration. Therefore, the maximum brake force at each axle for a given deceleration is approximated as:

$$F_{\max f} = \mu(2F_{zsf} - 2K_{sf}a\theta) \quad (4.21)$$

$$F_{\max c} = \mu(2F_{zsc} - 2K_{sc}b\theta) \quad (4.22)$$

$$F_{\max r} = \mu(2F_{zsr} + 2K_{sr}c\theta) \quad (4.23)$$

Where the pitch angle is calculated from:

$$\frac{d^2\theta}{dt^2} = \frac{1}{I_y}(-2K_{sf}a^2\theta - 2K_{sc}b^2\theta - 2K_{sr}c^2\theta - M_b A_x H_{cgB}) \quad (4.24)$$

The maximum brake force at each axle is presented as a percentage of the total brake force for increasing deceleration as shown in figure 4.5. At zero deceleration, the static loading distribution is as above. The representation of the suspension as linear springs, means that the normal forces on the wheels vary in a linear manner with deceleration, resulting in a zero vertical tyre force for the rear axle above 0.72g in the laden case. Because of the large difference in loading of the unladen and laden vehicles, it can be seen that the peak brake force distribution between the unladen and laden vehicles varies greatly. From equation 4.20, the maximum braking torque allowed to prevent wheel locking is 45238Nm, which less than the brake torque available from both the conventional and hybrid braking systems. This means that if the full brake torque is applied, some or all of the wheels will lock, depending on the proportion sent to each wheel. To offer the optimal braking, the loss of directional control is preferred over loss of directional stability, hence, front lock-up occurring before rear lock-up. It is not possible to obtain a distribution that will satisfy the above in both laden and unladen cases. The following percentages for each axle were decided upon. These are not

optimised for all operating modes, but will prevent the rear wheels from locking up first until around 0.4g. Front: 55% Central: 30% Rear: 15%

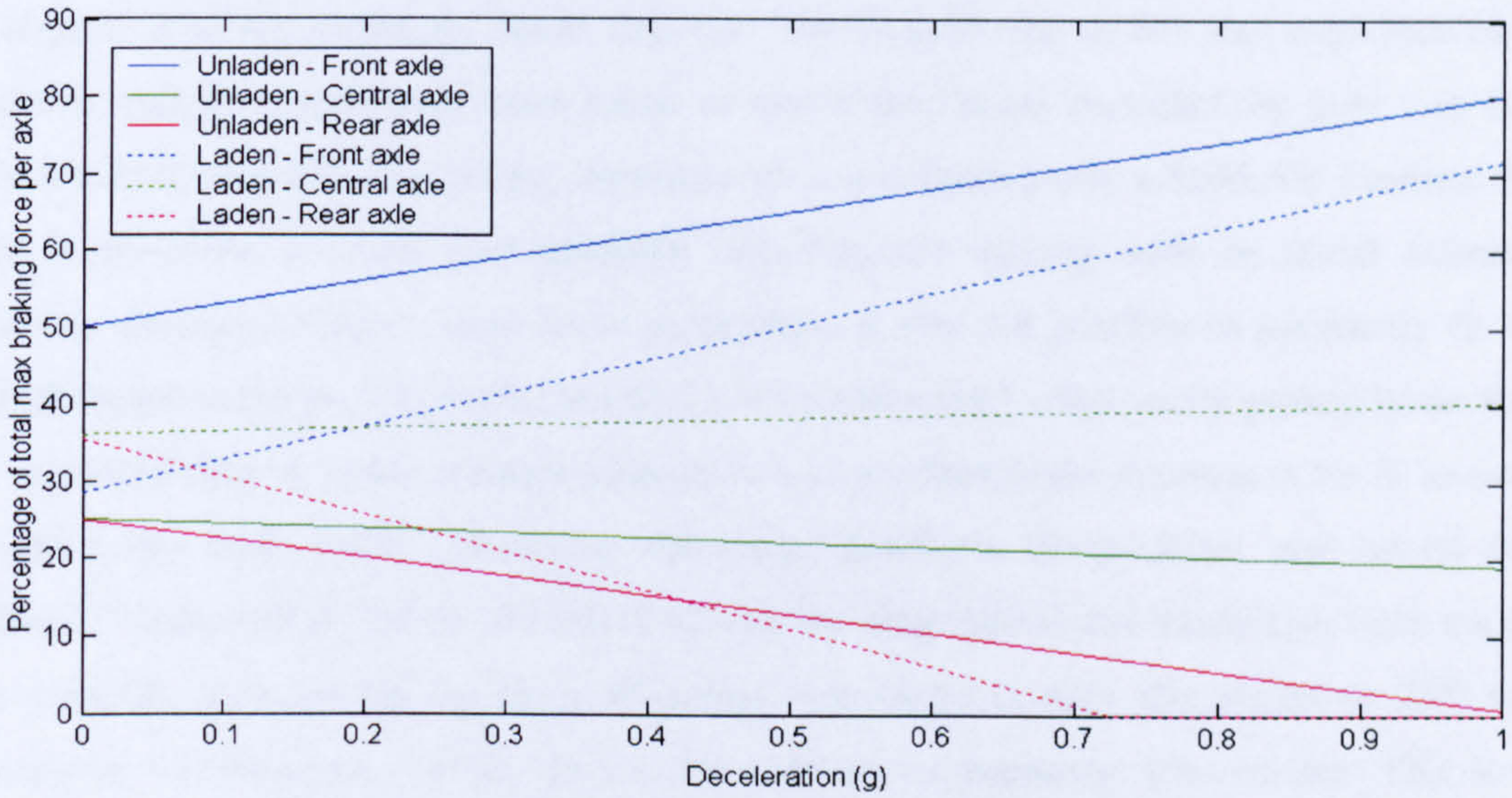

Fig. 4.5 Distribution of max braking force during deceleration

4.2.4 Tyre Model

In section 2.4 a Dugoff tyre model that was based on a similar tyre was used for the initial modelling work. Now that the full model is going to be validated, it is important that the tyre model is as accurate as possible. From literature it has been shown that the Pacejka model provides the most accurate capability of modelling tyre forces for a wide range of slip-angles and vehicle loads. Unfortunately, due to reluctance of the tyre company, full Pacejka coefficients for combined slip were not available. The only available data are some force / slip curves for pure longitudinal and pure lateral slip. As shown in section 3.6, it is necessary that a combined tyre model be used. Without actual Pacejka coefficients for a combined slip model, there is no way of determining such coefficients from the curves provided.

In Jansen *et al.* (1996) the necessity for accurate combined slip tyre characteristics in conjunction with good representation of the vehicle's suspension is outlined. Simulation tests are performed for combined braking and cornering manoeuvres while at the same time including the suspension system. Results show that the inclusion of the suspension characteristics and its accuracy have significant effect on the braking performance as is expected due to changes in vertical tyre load.

By utilising the Dugoff model and tuning the values of cornering stiffness, longitudinal stiffness and adhesion reduction coefficient, ε_r, to the provided curves, it should be possible to

implement a tyre model that has some degree of accuracy, especially at low values of wheel-slip and slip-angle. Obviously they can only be tuned to the pure longitudinal / lateral forces, but it was hoped that the Dugoff method of combining the forces would be sufficiently accurate to give the necessary detail required. The Dugoff tyre model was implemented in Simulink and the coefficients were tuned to match the curves provided for pure tyre data obtained from QinetiQ. The tuning algorithm used was fminsearch; a MatLAB function that aims to minimise a scalar user specified cost function starting with an initial estimate. However through tuning of only these parameters, it was not possible to accurately fit the Dugoff model to the provided tyre curves as the Dugoff model consistently peaked lower than the measured data. A scalar multiplication term was attached to the expression for X_i in order to match the peak forces. Obtaining the initial gradients (longitudinal and lateral tyre stiffness') was possible and decent fitting of both the longitudinal and lateral tyre force curves was possible, however the matching of lateral tyre forces at high slip-angles (> 25°) was inaccurate, but these are outside all but the most severe cornering manoeuvres. This is as would be expected; it is noted by Manning *et al.* (2002) that the Dugoff model is inaccurate at higher slip-angles and lateral accelerations. The results of the tyre fitting are shown in figure 4.6 and figure 4.7 for the longitudinal and lateral tyre forces respectively.

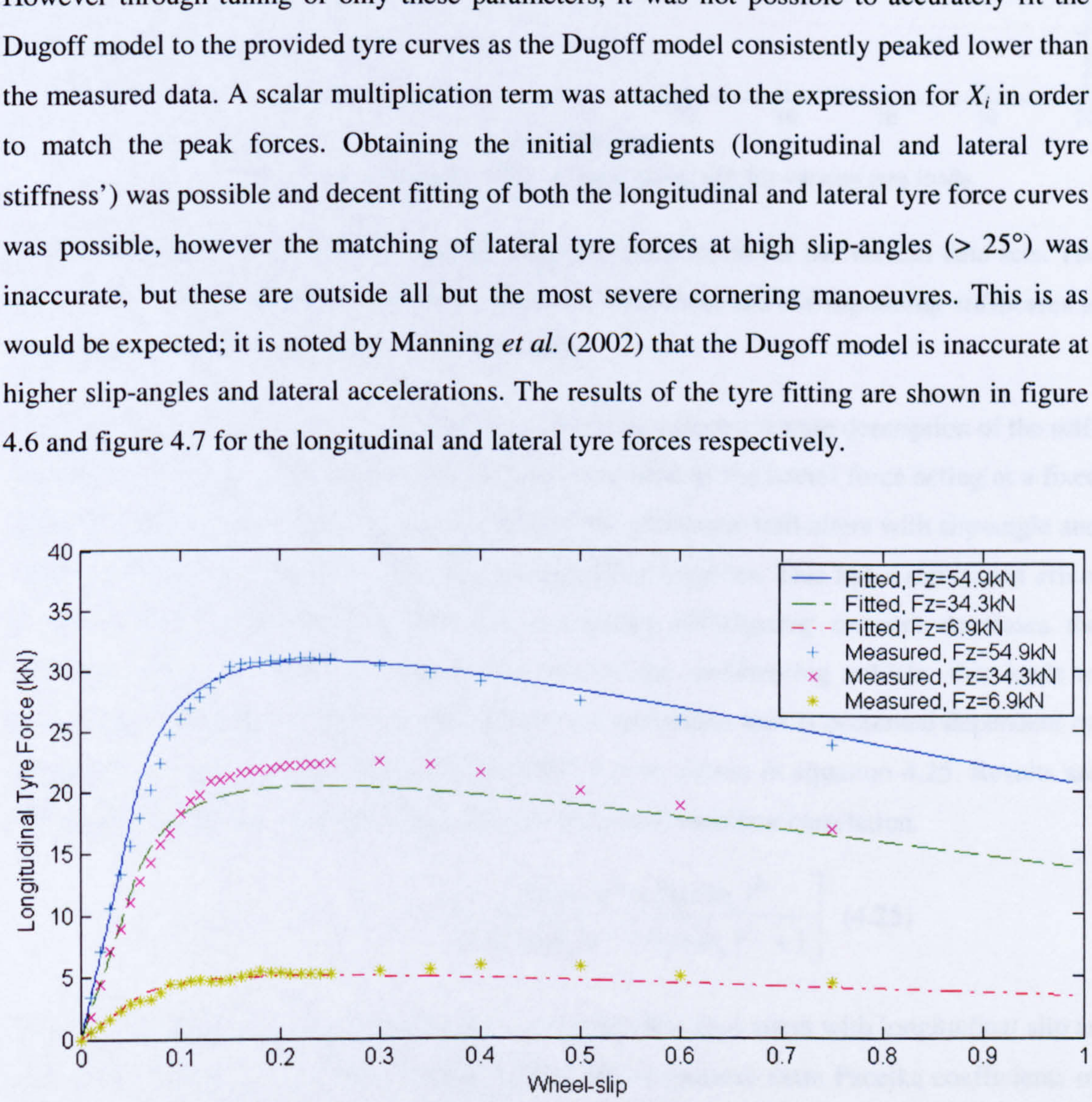

Fig. 4.6 Measured and fitted tyre data for pure longitudinal slip for various tyre loads.

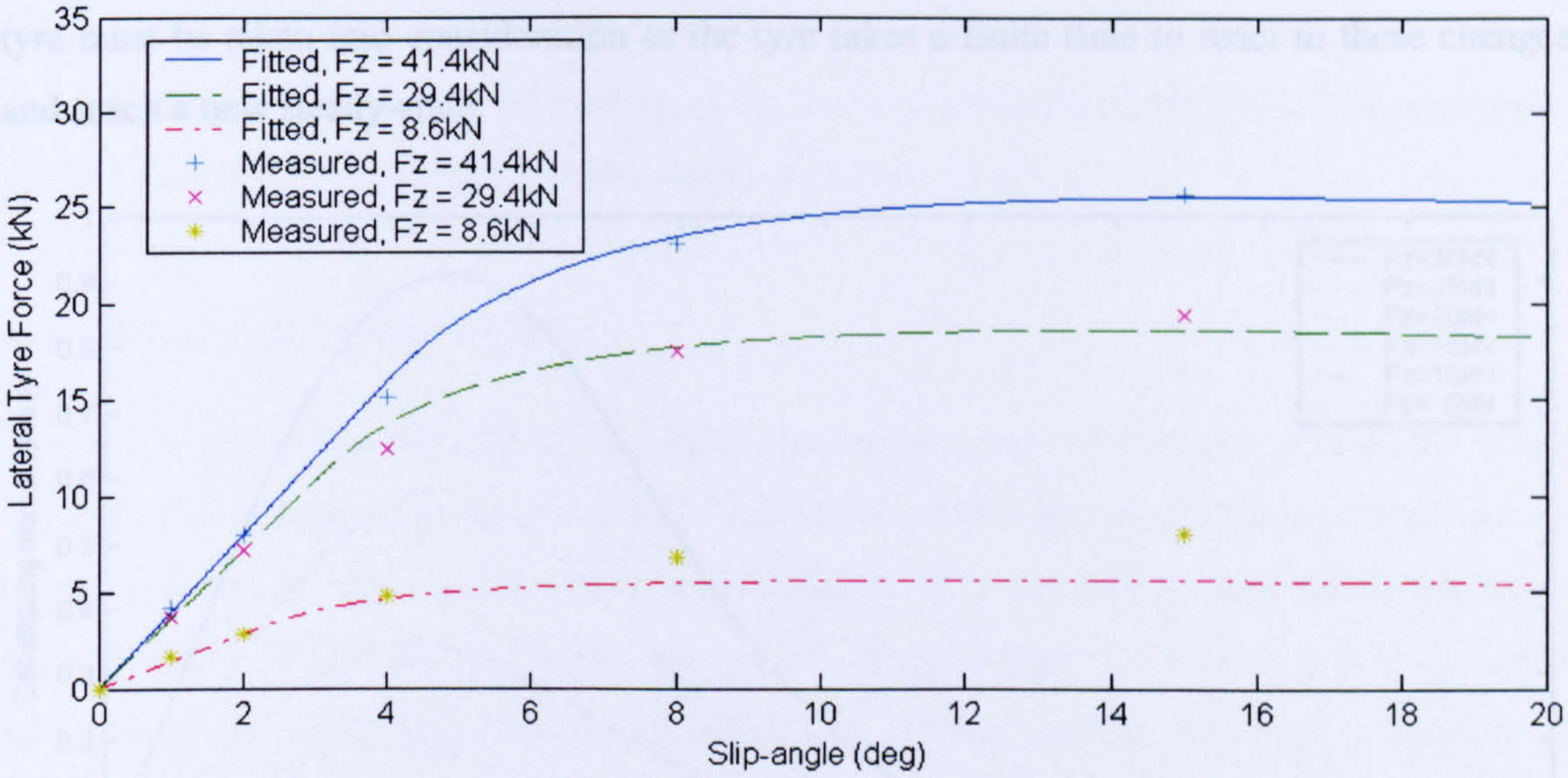

Fig. 4.7 Measured and fitted tyre data for pure lateral slip for various tyre loads.

Once the longitudinal and cornering stiffnesses had been found for the various data sets. The results were plotted against vertical tyre load and from these the corresponding stiffnesses at the vehicle's unladen and laden state were found.

Another improvement that is made to the tyre model is a more accurate description of the self-aligning moment. Until this point, this has been modelled as the lateral force acting at a fixed distance from the tyre centre, X_{trail}. In actual fact the pneumatic trail alters with slip-angle and vehicle loading, at high slip-angles, X_{trail} disappears all together. This has a significant effect on the vehicle at the handling limits, as a reduced self-aligning moment decreases the stabilising effect it contributes and in the case of the oversteering vehicle, this leads to instability. In Shovlin (1999) an expression for the pneumatic trail is presented dependent on slip-angle and vertical tyre loading for the CSV tyre as shown in equation 4.25. Results are calculated against the empirical magic formula and show excellent correlation.

$$X_{trail} = b_9(e^{(F_z b_8)} - 1)\left[\frac{\sin((b_4\alpha^2 + b_5\alpha)b_6)^{b_1}}{\cosh((b_4\alpha^2 + b_5\alpha)b_6)^{b_2} + 1}\right] \quad (4.25)$$

This model however is for pure lateral slip. The pneumatic trail alters with longitudinal slip as outlined in Bakker *et al.* (1987), but the method shown requires extra Pacejka coefficients of which none are available. Instead equation 4.25 will be used to model X_{trail}. Figure 4.8 shows the self-aligning moment when the equation is combined with the Dugoff tyre model.

The Dugoff tyre model is a steady-state model and has no transient ability. As noted in Pacejka (1979) steady-state tyre models are only accurate on steady or slow varying motions. When slip-angle and vertical tyre loads are varying quickly, then this transient effect on the

tyre must be taken into consideration as the tyre takes a finite time to react to these changes and reach a new steady-state.

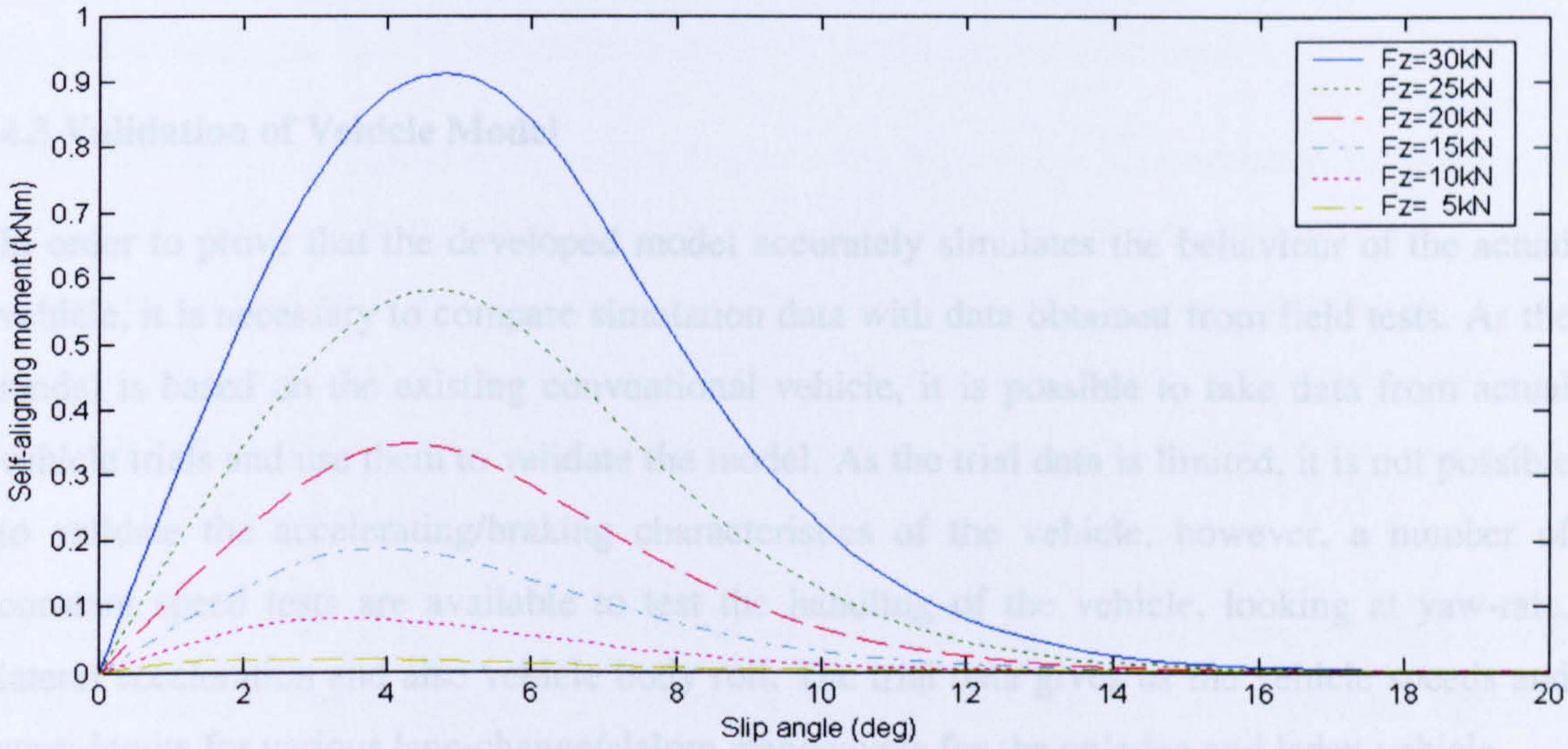

Fig. 4.8 Self-aligning moment with respect to slip-angle and vertical tyre loading

Crolla *et al.* (1996) notes that the first order lag is sufficient to model this effect. For lateral tyre force, the lag has a time constant equal to the time taken for the tyre to roll through a distance known as the lateral relaxation length, Rl_y. As expressed by Crolla (1996) and Dixon (1991) this is approximately equal to the tyre's rolling radius. The first order lag is expressed in equation 4.26 which can be utilised for longitudinal and lateral tyre forces.

$$F_{wy\_out} = \frac{1}{1 + \frac{Rl_y}{V_x} s} * F_{wy\_in} \quad (4.26)$$

Cooke (1996) also proposed that a first order lag is sufficient to model the transient response on a smooth road surface and utilises the method proposed by Segel (1982) (note: that Segel uses a relaxation length equal to the wheel diameter).

Clover and Bernard (1998) investigate the transient relaxation length for longitudinal tyre force, Rl_x. It is noted that as the tyres are stiffer in the longitudinal direction, the relaxation length is of lesser effect. They define longitudinal relaxation length to be the ratio of longitudinal slip stiffness to longitudinal carcass stiffness. As only slip stiffness is provided from the tyre data this equation is of limited use, however a value for longitudinal relaxation length is given as 0.091m for a 0.3m radius tyre, so for the 0.59 radius tyre a value of 0.18m will be used.

Without the accurate tyre data for the actual tyre, the validity of the vehicle model is always going to be questionable, but by looking at the model against actual data, it will be apparent if the tyre data is a good enough approximation of the real thing.

4.3 Validation of Vehicle Model

In order to prove that the developed model accurately simulates the behaviour of the actual vehicle, it is necessary to compare simulation data with data obtained from field tests. As the model is based on the existing conventional vehicle, it is possible to take data from actual vehicle trials and use them to validate the model. As the trial data is limited, it is not possible to validate the accelerating/braking characteristics of the vehicle, however, a number of constant speed tests are available to test the handling of the vehicle, looking at yaw-rate, lateral acceleration and also vehicle body roll. The trial data gives us the vehicle speeds and steer-inputs for various lane-change/slalom manoeuvres for the unladen and laden vehicle.

The vehicle model does not include a model of a differential for the purpose of validation; instead wheels are free to rotate depending on the radius of turn which acts very much like an open differential as each wheel, each receiving equal torque. Although the differential on the CSV has no limited-slip capabilities, because no differential device is ideal, there may be a slight torque bias, although the effects would be negligible. Therefore, is not thought that the omission of the differential will have a significant effect on the handling behaviour of the vehicle.

Six tests were used for comparison purposes: A slalom steer input for the unladen and laden vehicle at 35 and 40km/h respectively. A slalom steer input for the unladen and laden vehicle at 50km/h and a double lane-change steer input for both unladen and laden vehicle at 70km/h. The results for yaw rate, lateral acceleration and roll angle are compared for all six manoeuvres and are presented in figure 4.9 to figure 4.26.

It should be noted that the results for the actual vehicle give two readings for both lateral acceleration and roll angle. These readings represent the sensor outputs in the cab and in the body (exact positions of the sensors is unknown). Due to the nature of the simulation model, only one value is available, as the vehicle chassis is assumed rigid. This is taken from the centre of gravity that varies in the laden and unladen cases. The measured readings shown are the results for the lateral acceleration and roll angle of the vehicle body as this will be closer to the centre of gravity of the vehicle, especially in laden state also the readings at the cab were not available for all the vehicle trials. It should be noted that in the laden results at

70km/h (figure 4.24 to 4.26), there appears to be an offset in the simulated results for all quantities that develops in the first two seconds of the simulation. If this off-set, which can only be developed by a non-zero steer input, is removed, the roll-angle and yaw-rate would appear accurate, along with improved correlation for the lateral acceleration.

From the results for yaw-rate in unladen (figures 4.9, 4.15 and 4.21) and laden states (figures 4.12, 4.18 and 4.24) it can be seen in all the graphs that the unladen vehicle gives a more accurate response than in the laden case, which slightly overestimates the yaw-rate. In the unladen case, yaw-rate is accurate for positive values, but marginally underestimates for negative values. This is due to the symmetrical nature of the model, which is not necessarily the case for the real vehicle.

In the same manner as the yaw-rate comparison, the roll angle of the laden vehicle shows a slight overestimation (figures 4.14, 4.20 and 4.26) while the unladen case shows the opposite to be true (figures 4.11, 4.17 and 4.23). As roll angle is dependent on lateral acceleration, which in turn relies on yaw-rate, it stands to reason that an underestimation of yaw-rate would result in a similar underestimation of roll-angle.

Another point of note is that the simulated and measured data for lateral acceleration in both the unladen (figures 4.10, 4.16 and 4.22) and laden states (figures 4.13, 4.19 and 4.25) show there is a phase difference between the two. A contribution to this phase difference lies in the positioning of the accelerometer on the vehicle. By looking at figure 4.27, which shows the lateral acceleration responses at the cab and at the body, it can be seen that the phase of the cab is slightly ahead of that of the body. If the sensor is behind that of the combined centre of gravity then there will be a phase difference between the two.

From the graphs it can be seen that the simulated responses are of the same shape and in the most part magnitude as those of the actual vehicle although the results appear less accurate at higher speeds. From this, it is possible to conclude that the model is a valid representation of the actual vehicle undertaking these manoeuvres. With no data to validate acceleration or brake responses of the vehicle further validation is not possible however the inclusion of roll-angle shows that some aspect of the suspension system is accurately modelled.

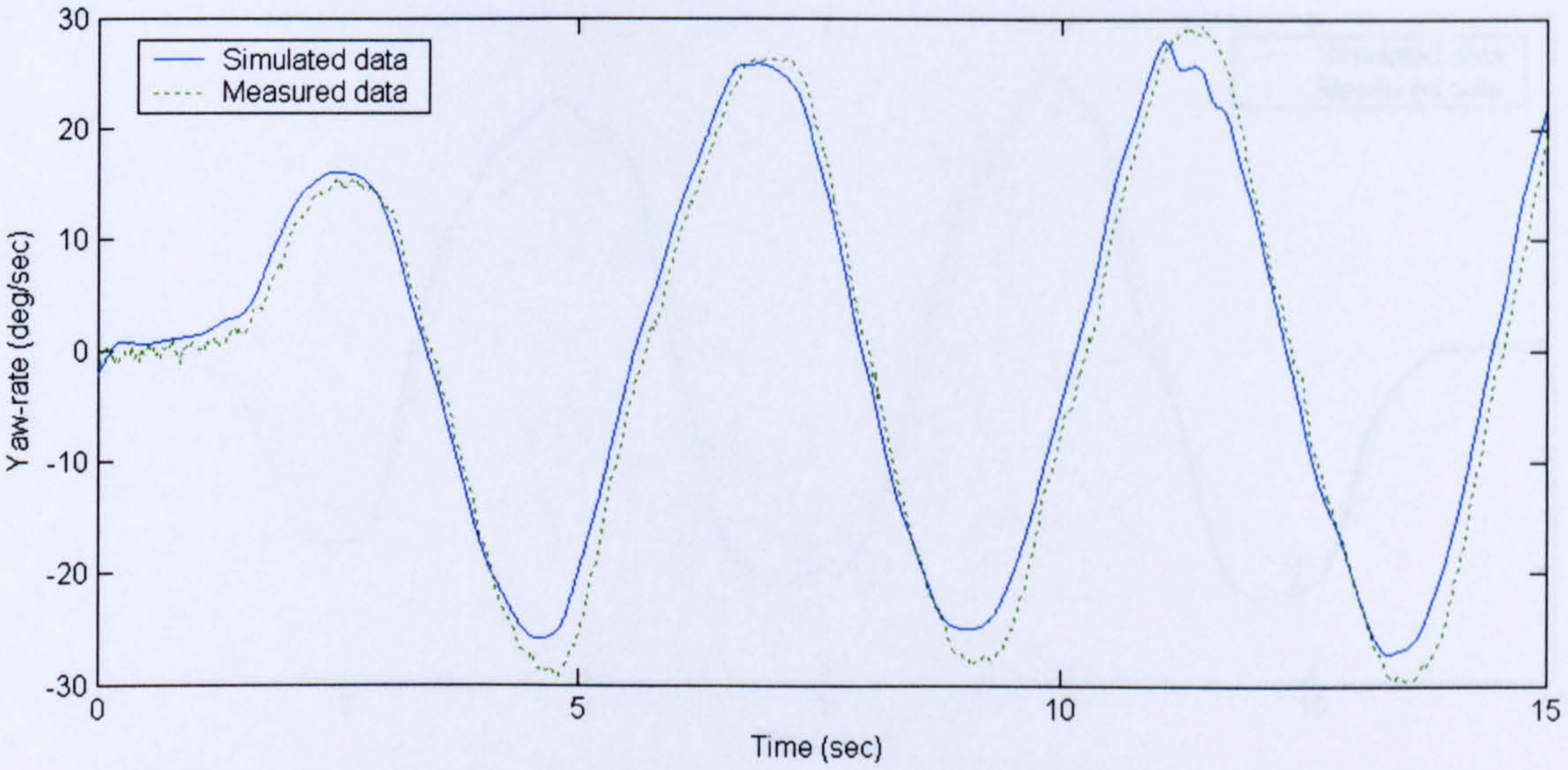

Fig 4.9 Yaw-rate of actual and simulated unladen vehicle for double lane change at 35km/h

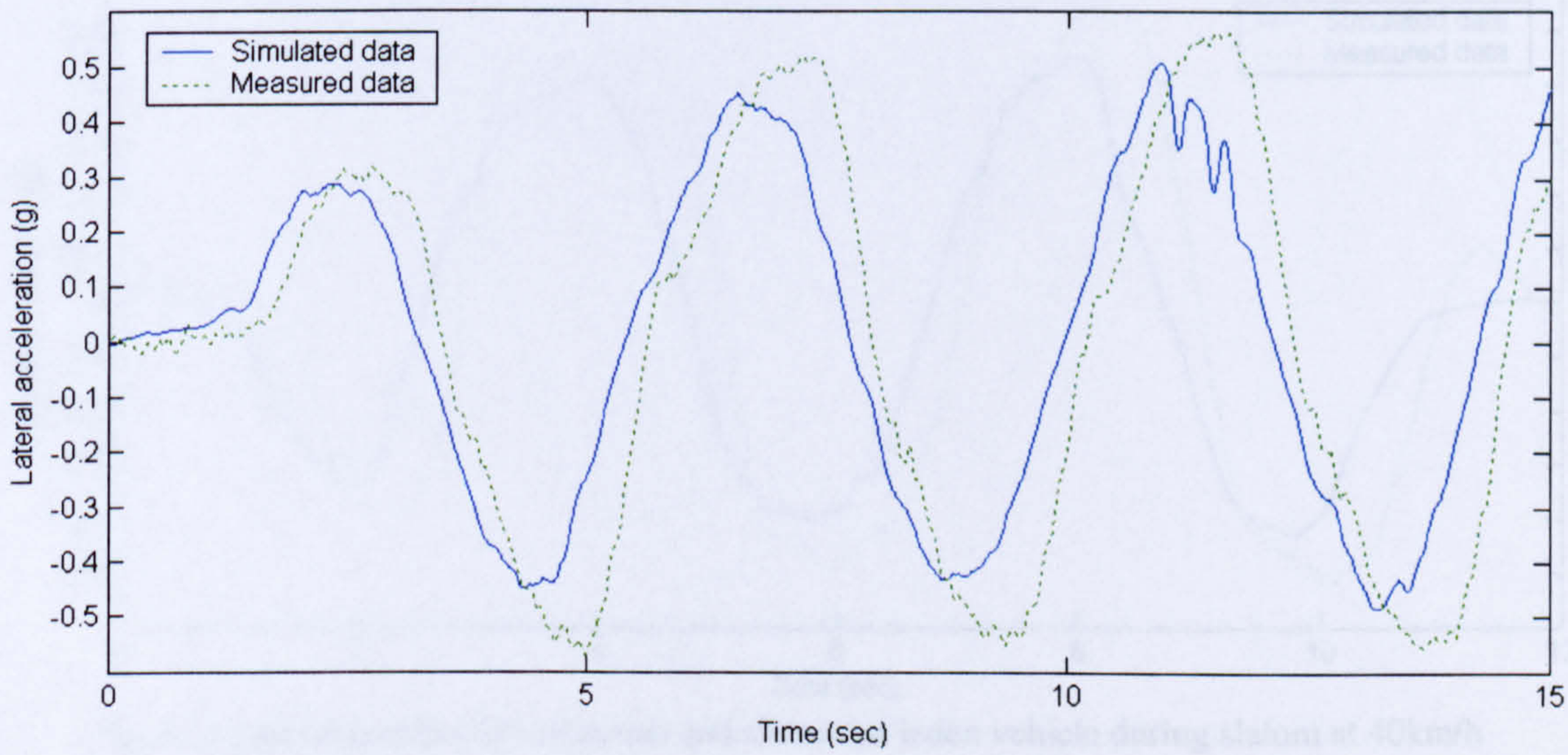

Fig 4.10 Lateral acceleration of actual and simulated unladen vehicle during slalom at 35km/h

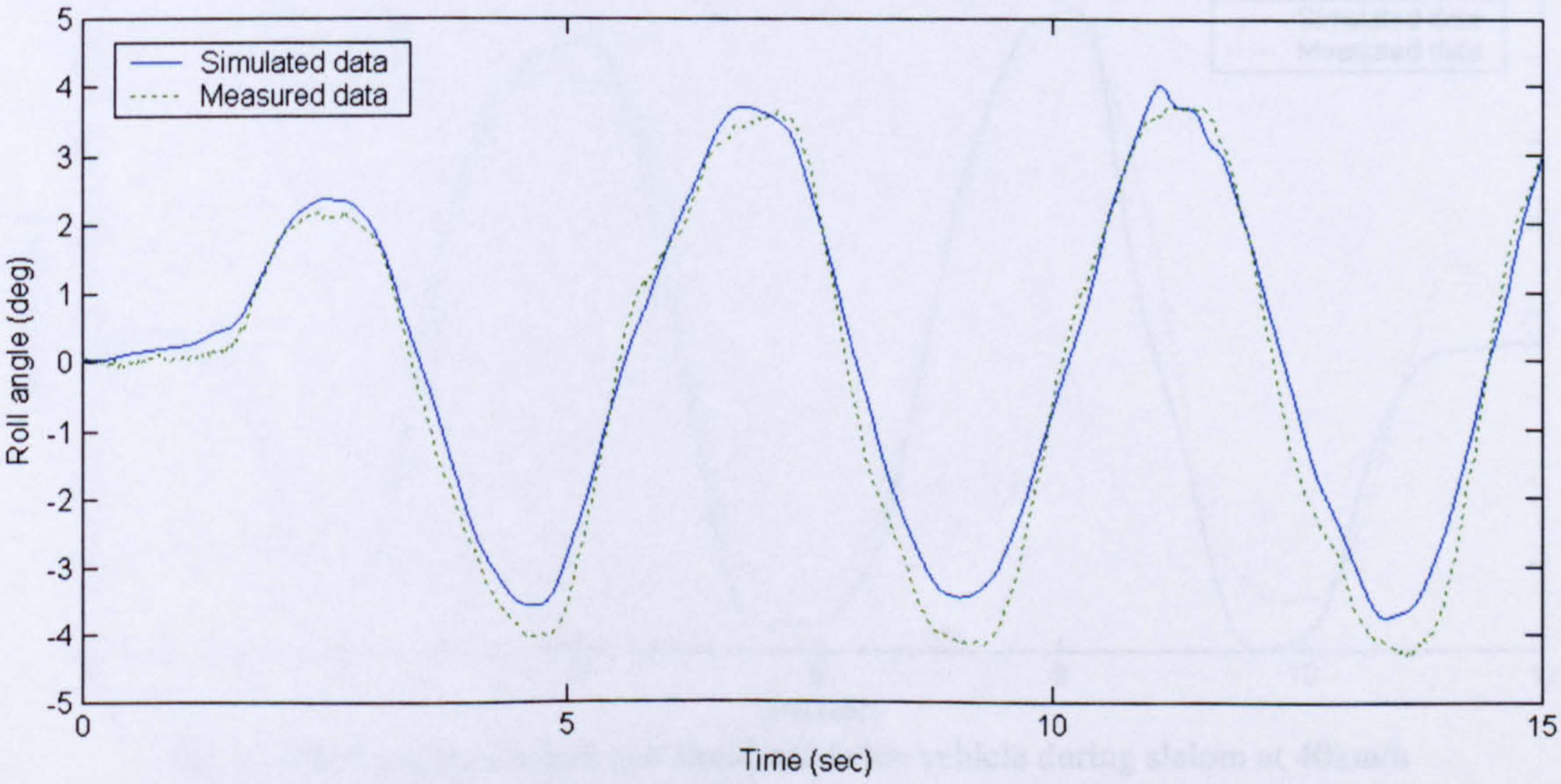

Fig 4.11 Roll angle of actual and simulated unladen vehicle during slalom at 35km/h

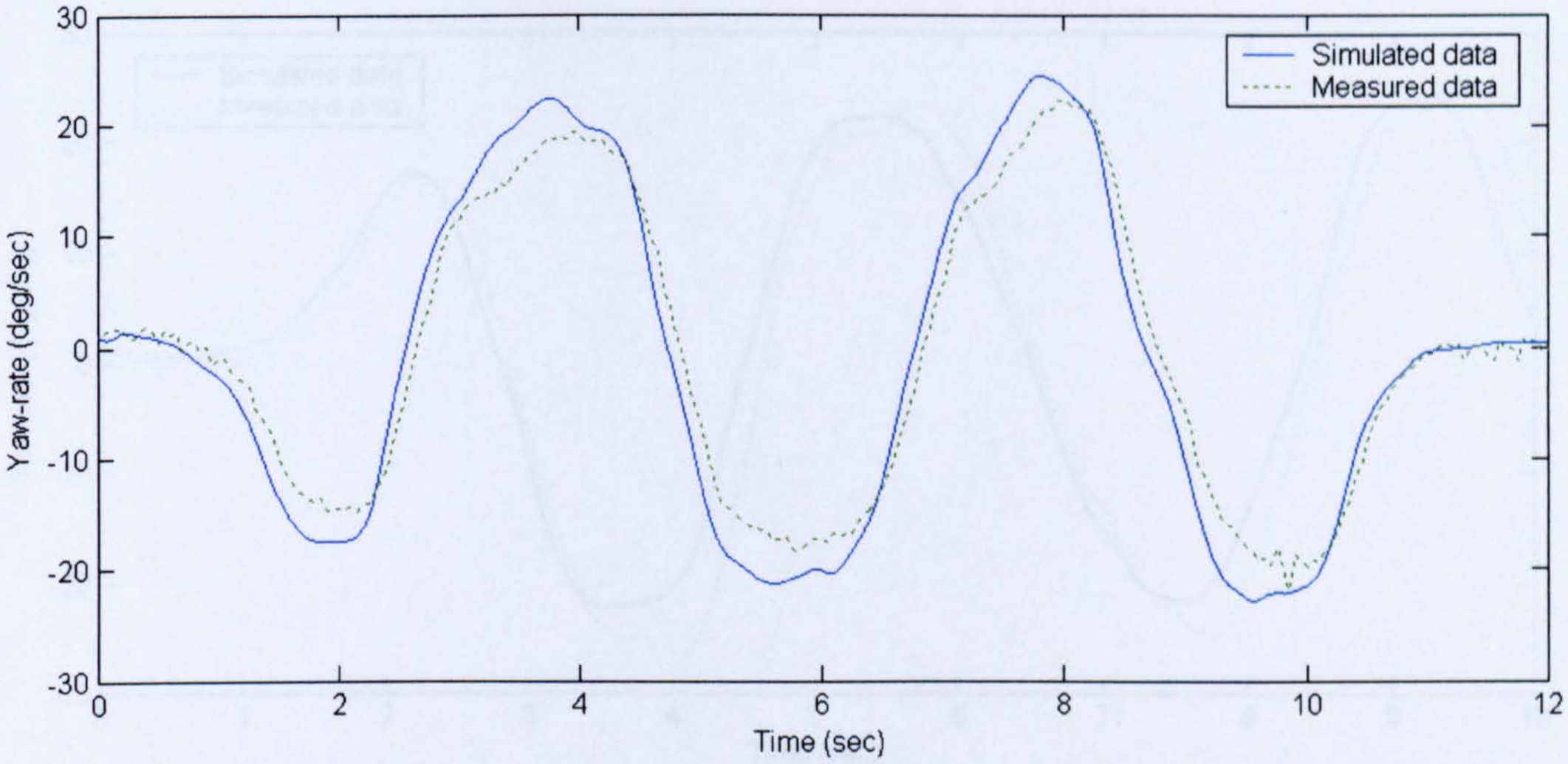

Fig 4.12 Yaw rate of actual and simulated laden vehicle during double lane change at 40km/h

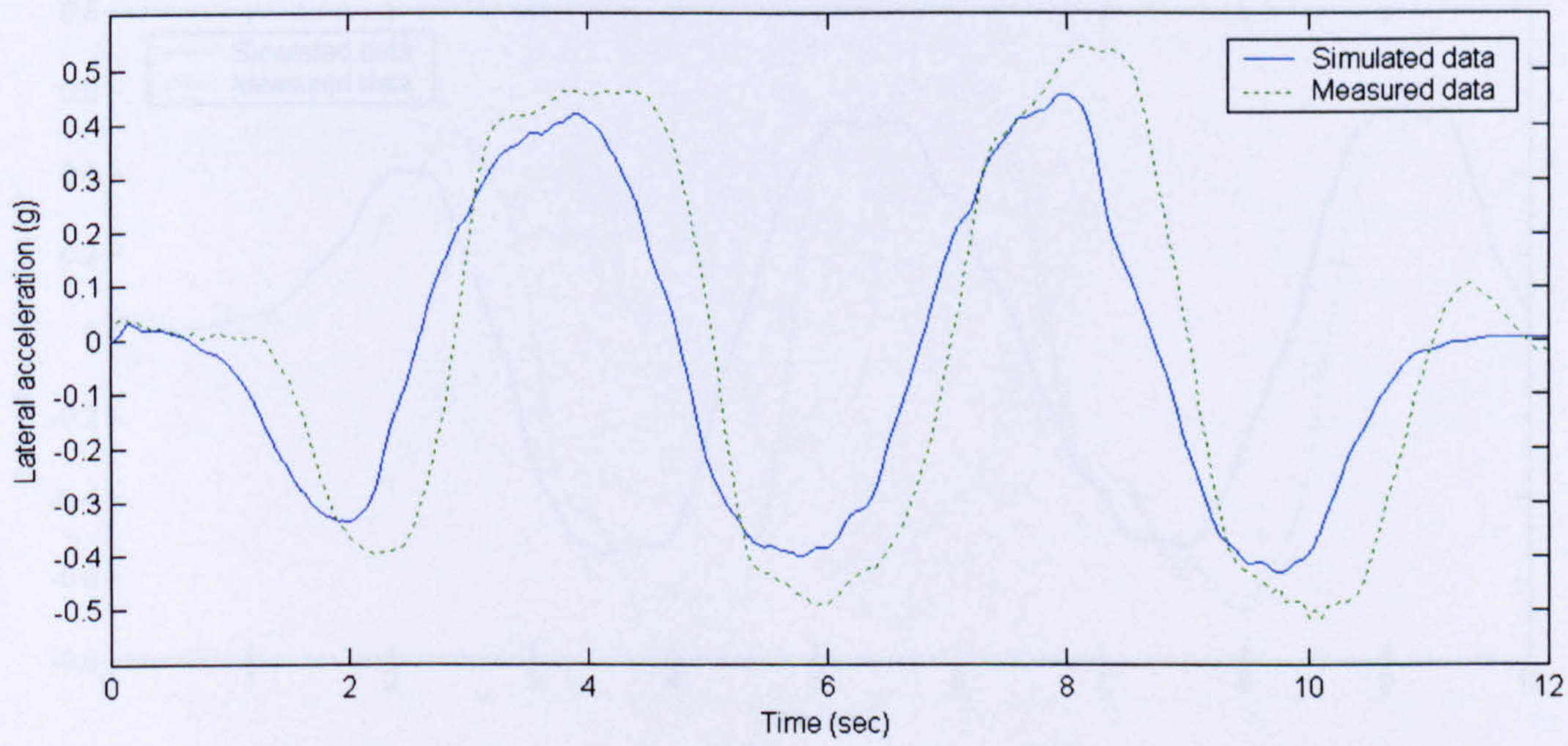

Fig 4.13 Lateral acceleration of actual and simulated laden vehicle during slalom at 40km/h

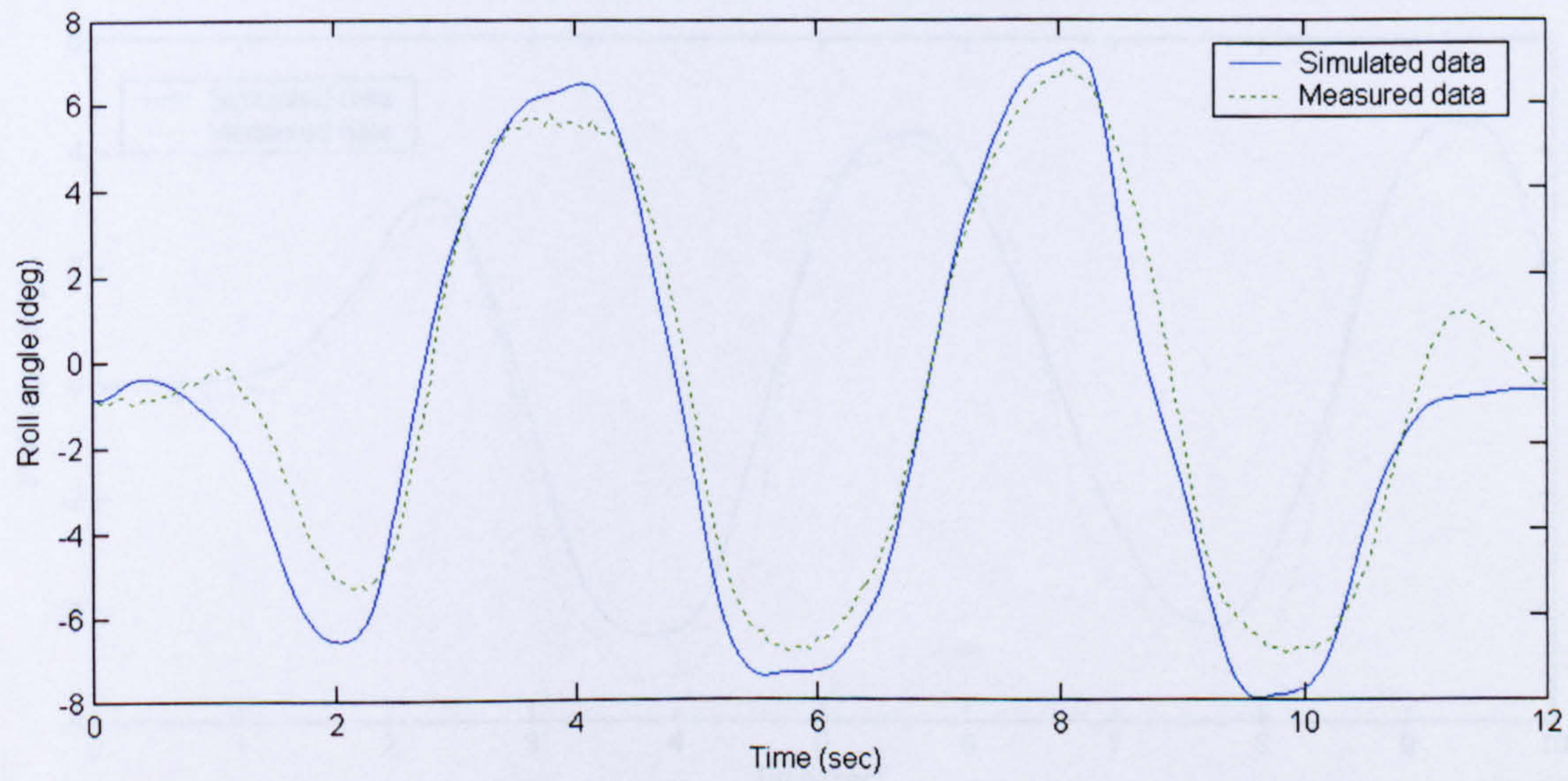

Fig 4.14 Roll angle of actual and simulated laden vehicle during slalom at 40km/h

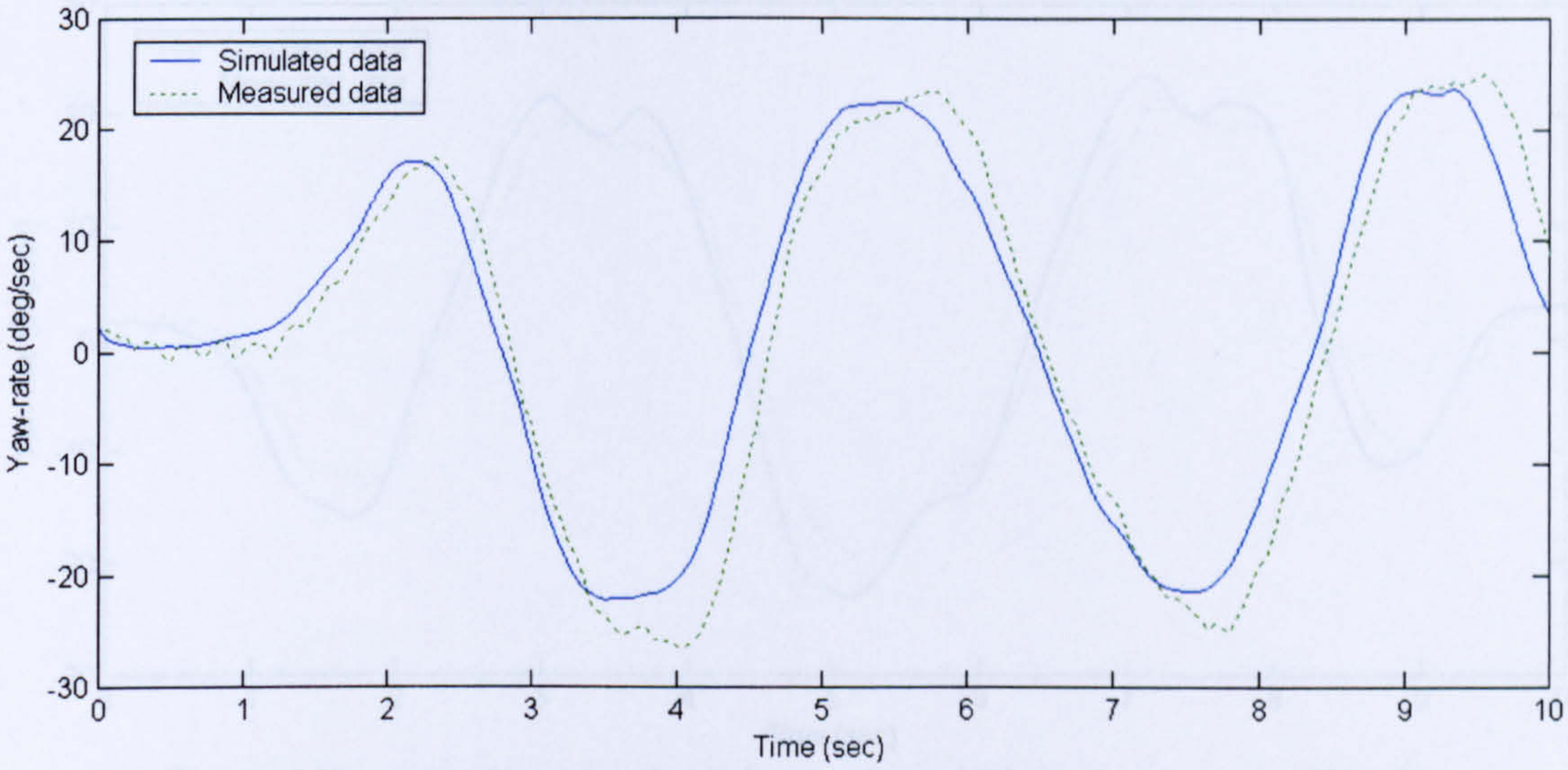

Fig 4.15 Yaw rate of actual and simulated unladen vehicle during slalom at 50km/h

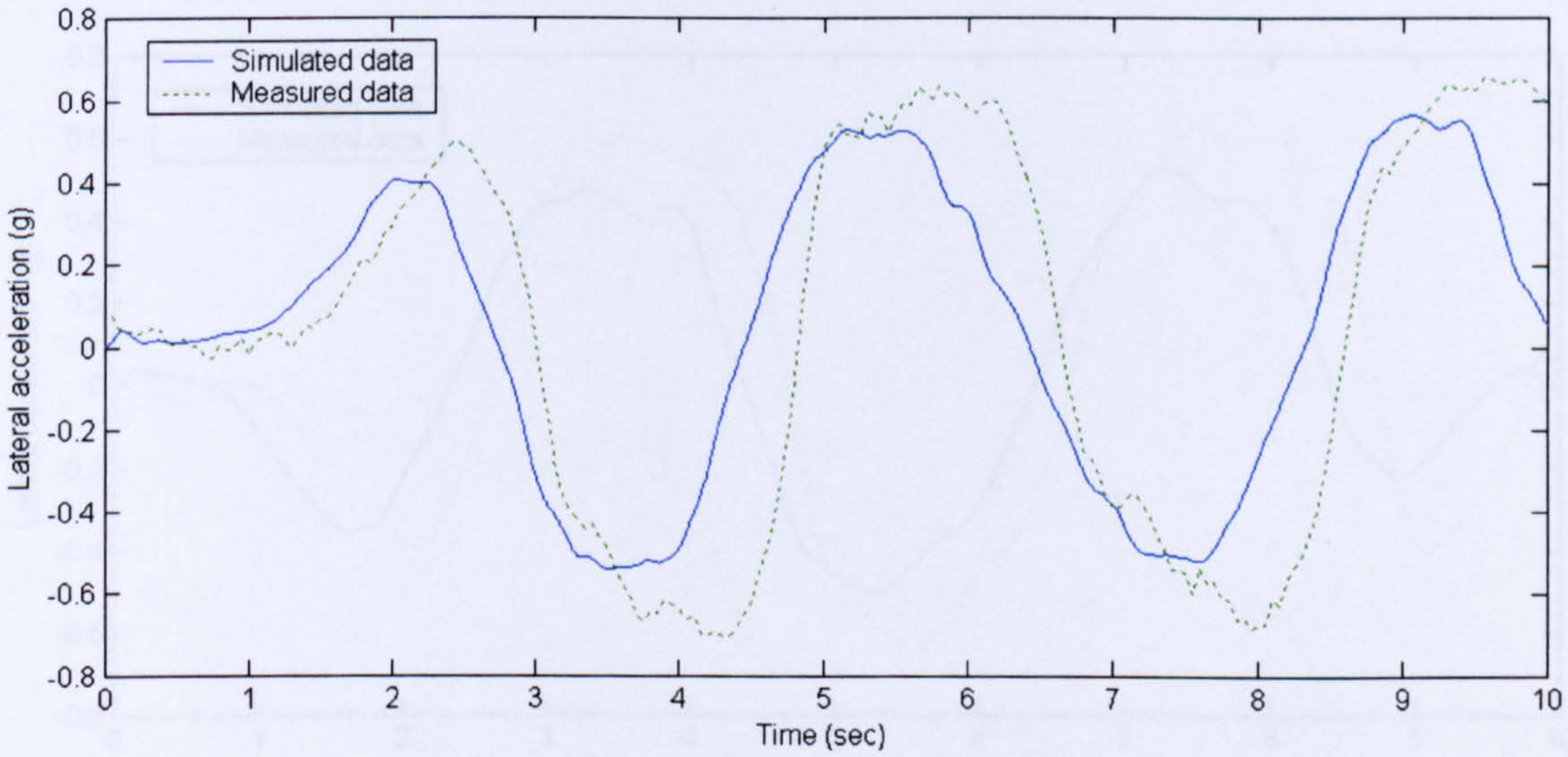

Fig 4.16 Latacc of actual and simulated unladen vehicle during slalom at 50km/h

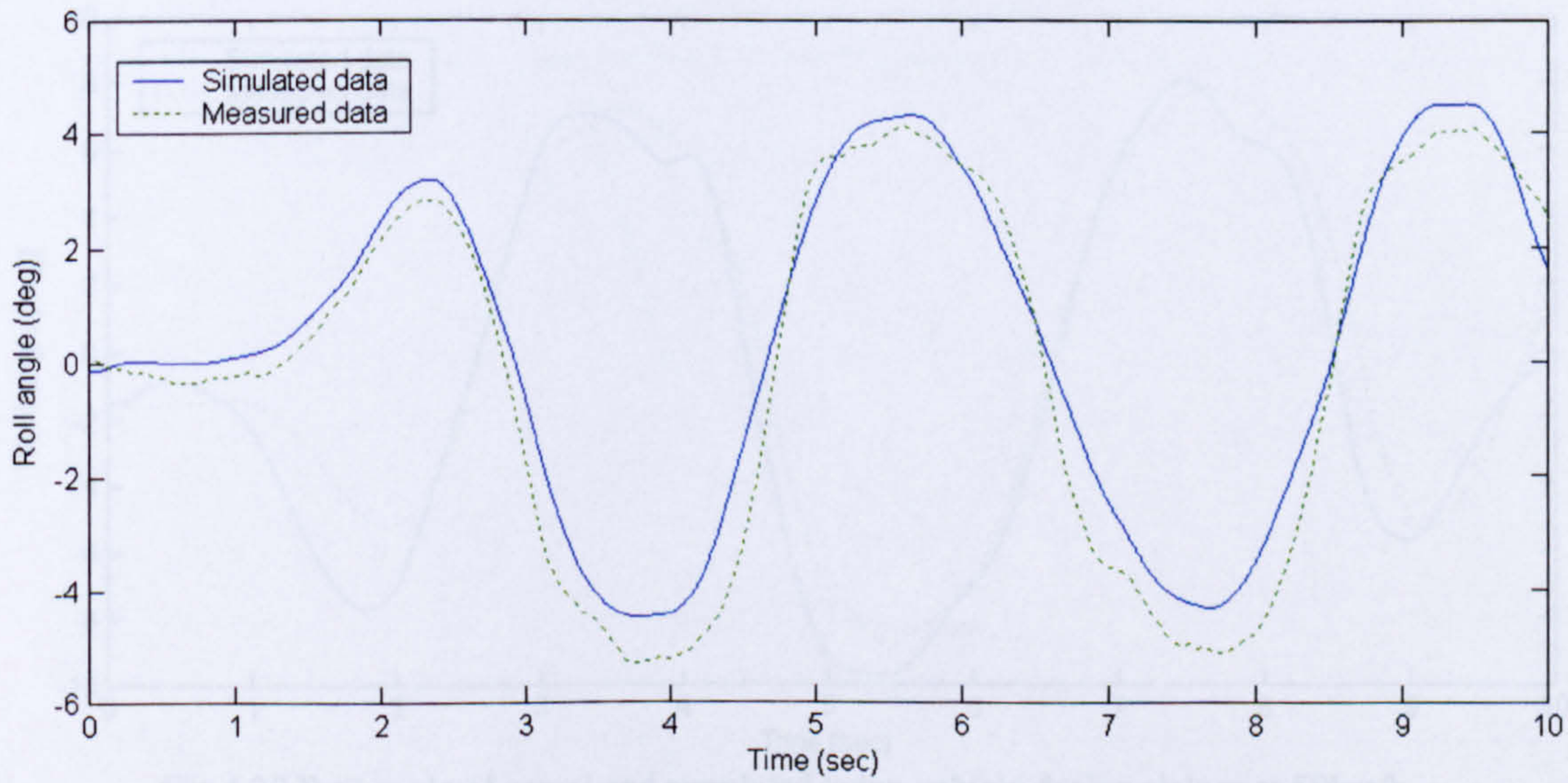

Fig 4.17 Roll angle of actual and simulated unladen vehicle during slalom at 50km/h

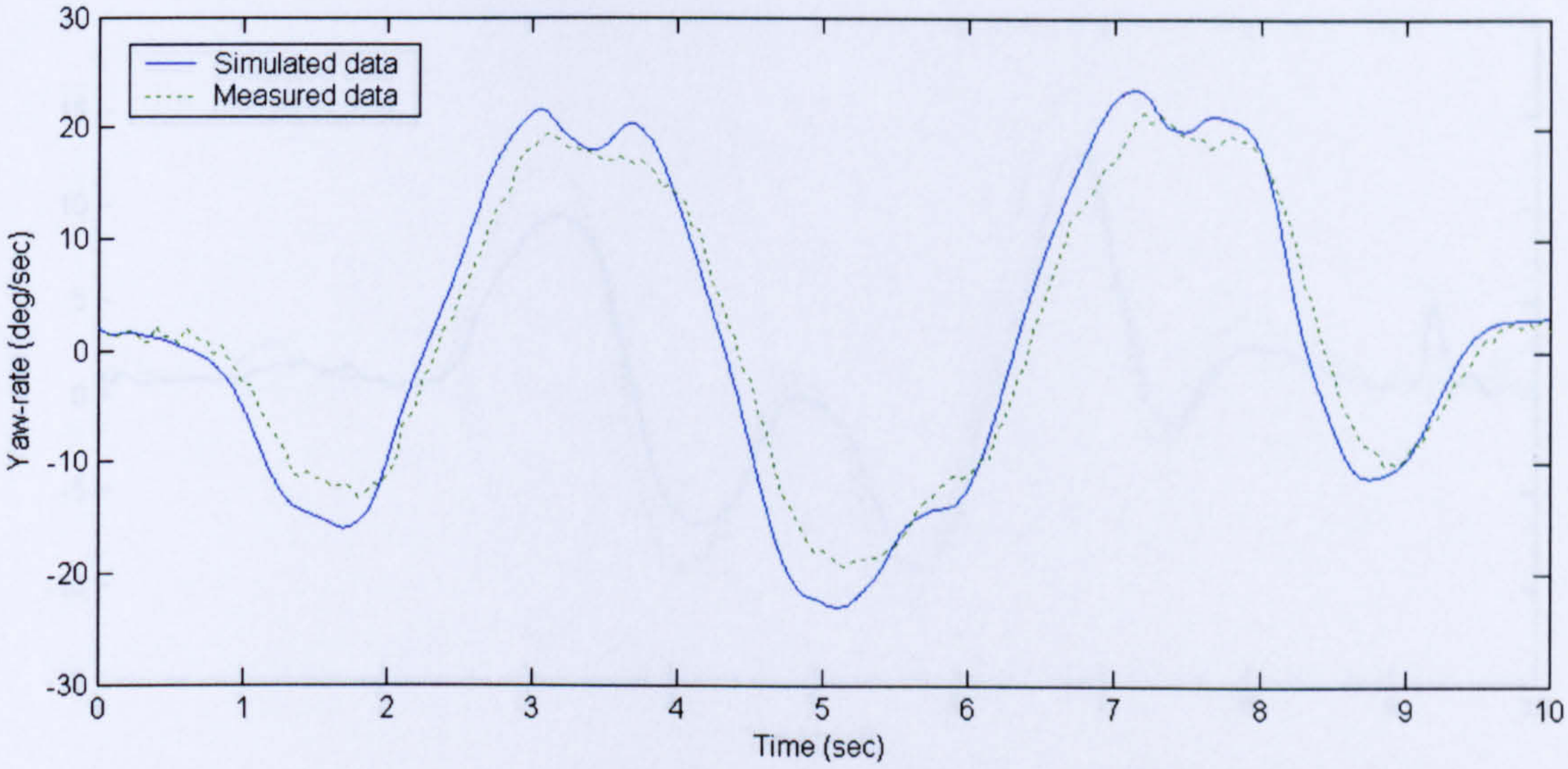

Fig. 4.18 Yaw rate of actual and simulated laden vehicle during slalom at 50km/h

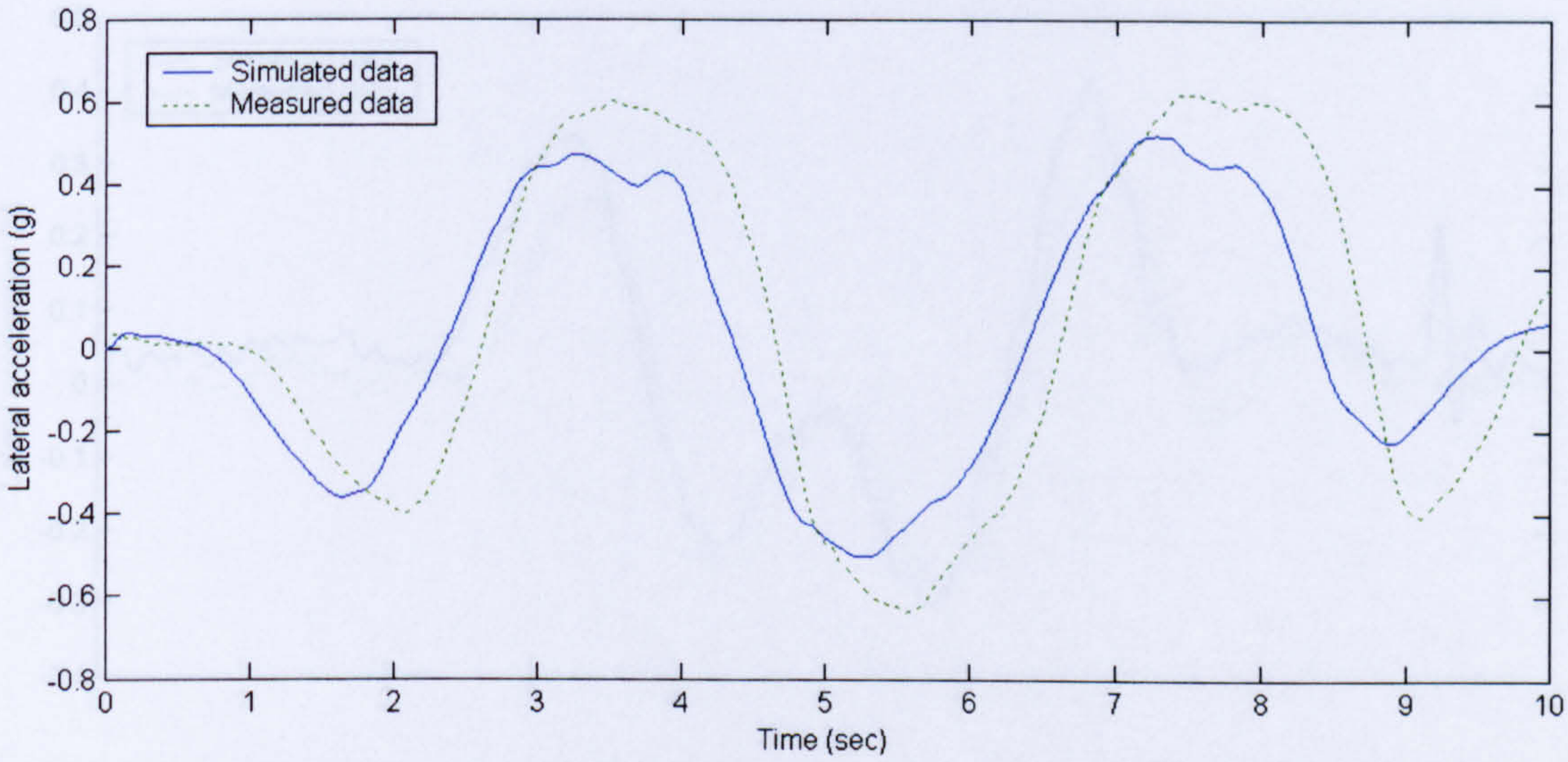

Fig 4.19 Latacc of actual and simulated laden vehicle during slalom at 50km/h

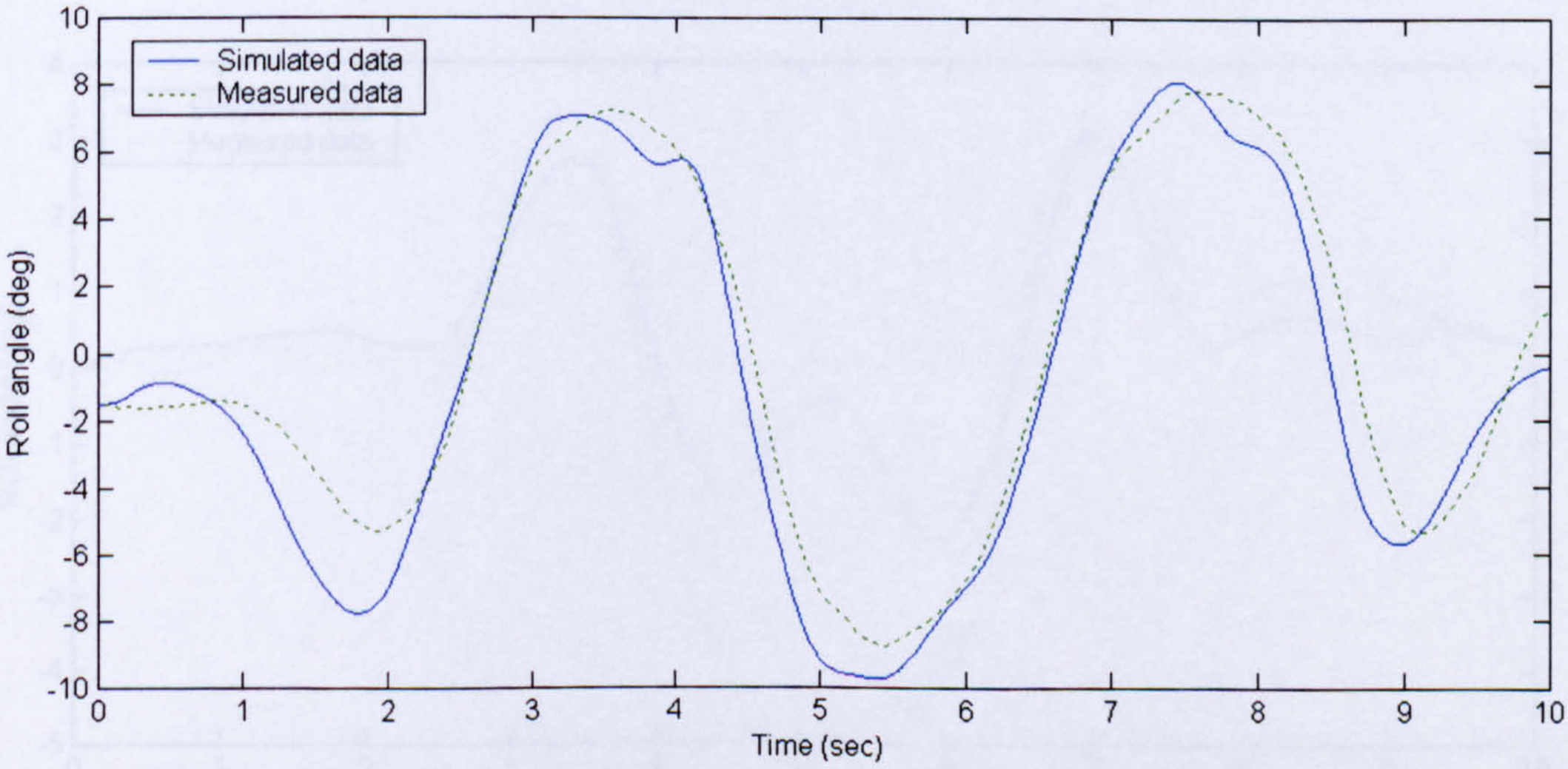

Fig 4.20 Roll angle of actual and simulated laden vehicle during slalom at 50km/h

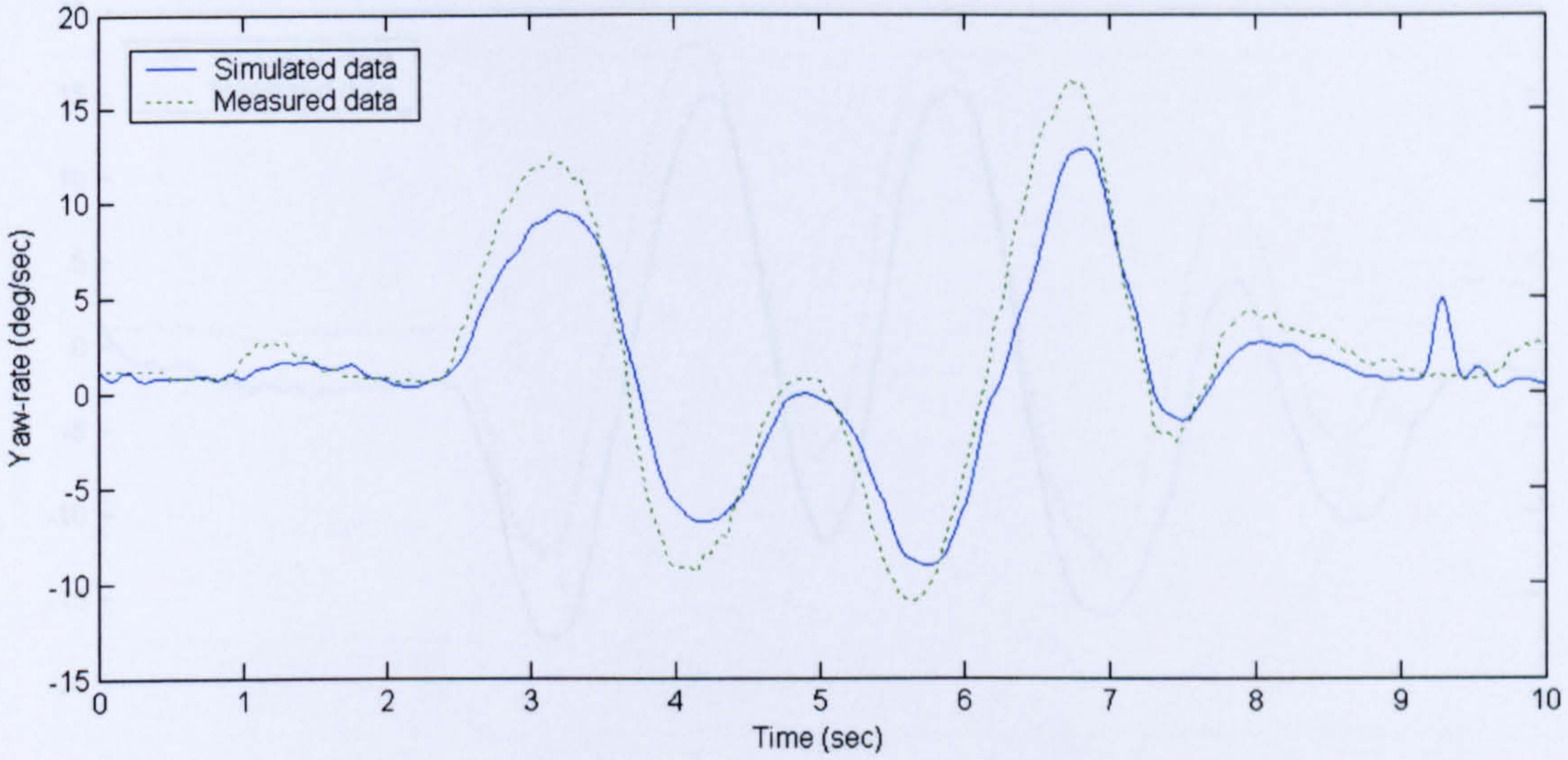

Fig 4.21 Yaw-rate of actual and simulated unladen vehicle for double lane change at 70km/h

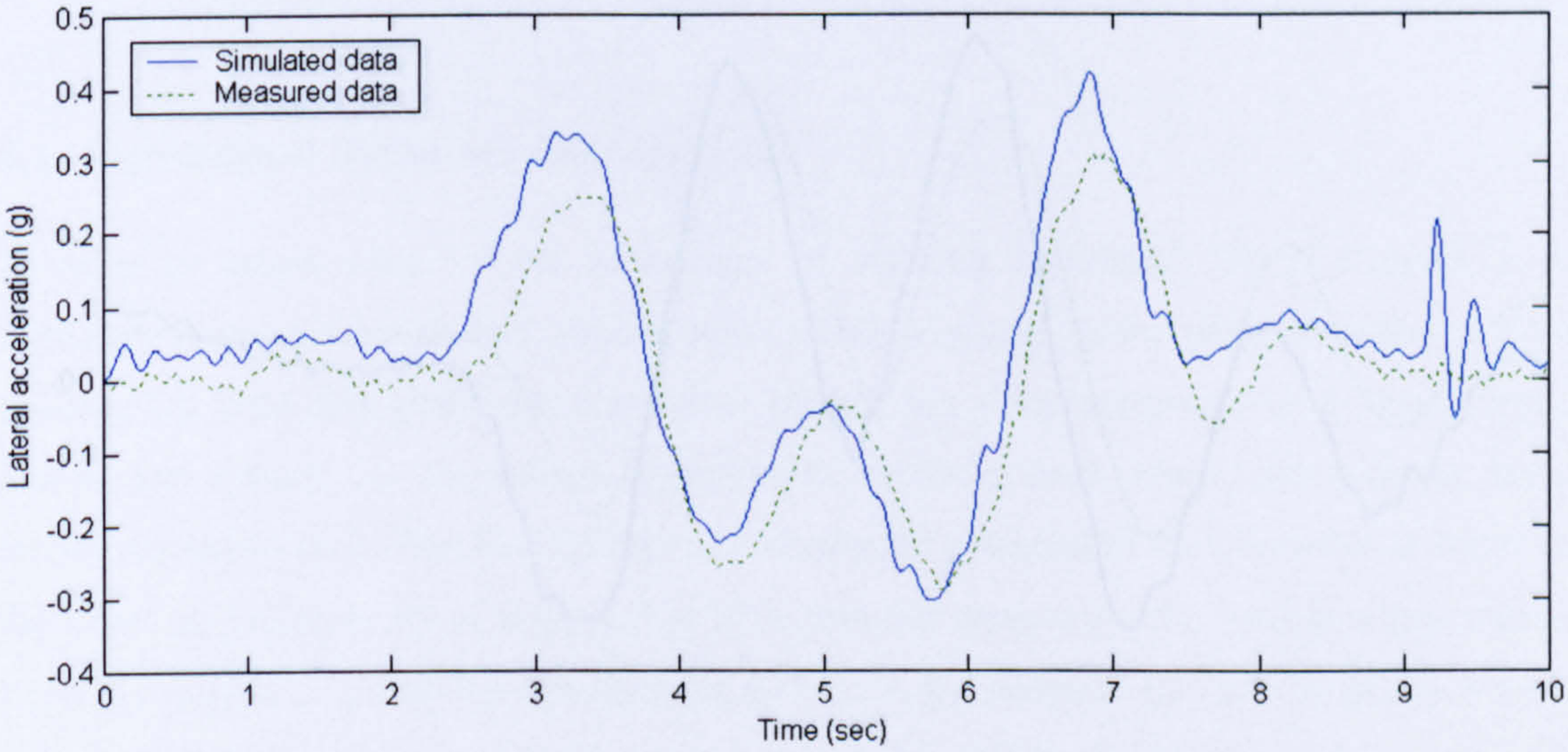

Fig 4.22 Lateral acceleration of actual and simulated unladen vehicle for double lane change at 70km/h

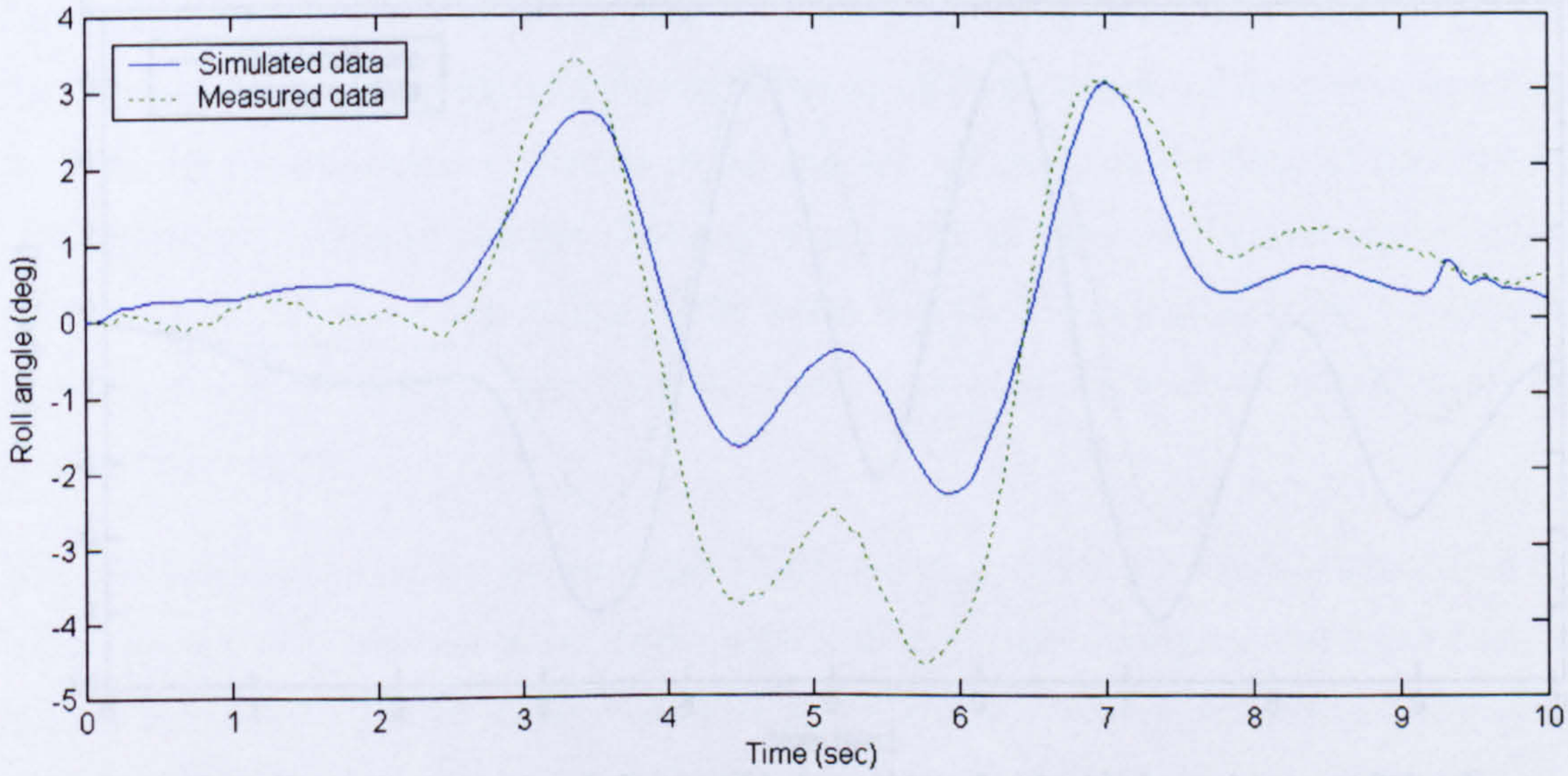

Fig 4.23 Roll angle of actual and simulated unladen vehicle for double lane change at 70km/h

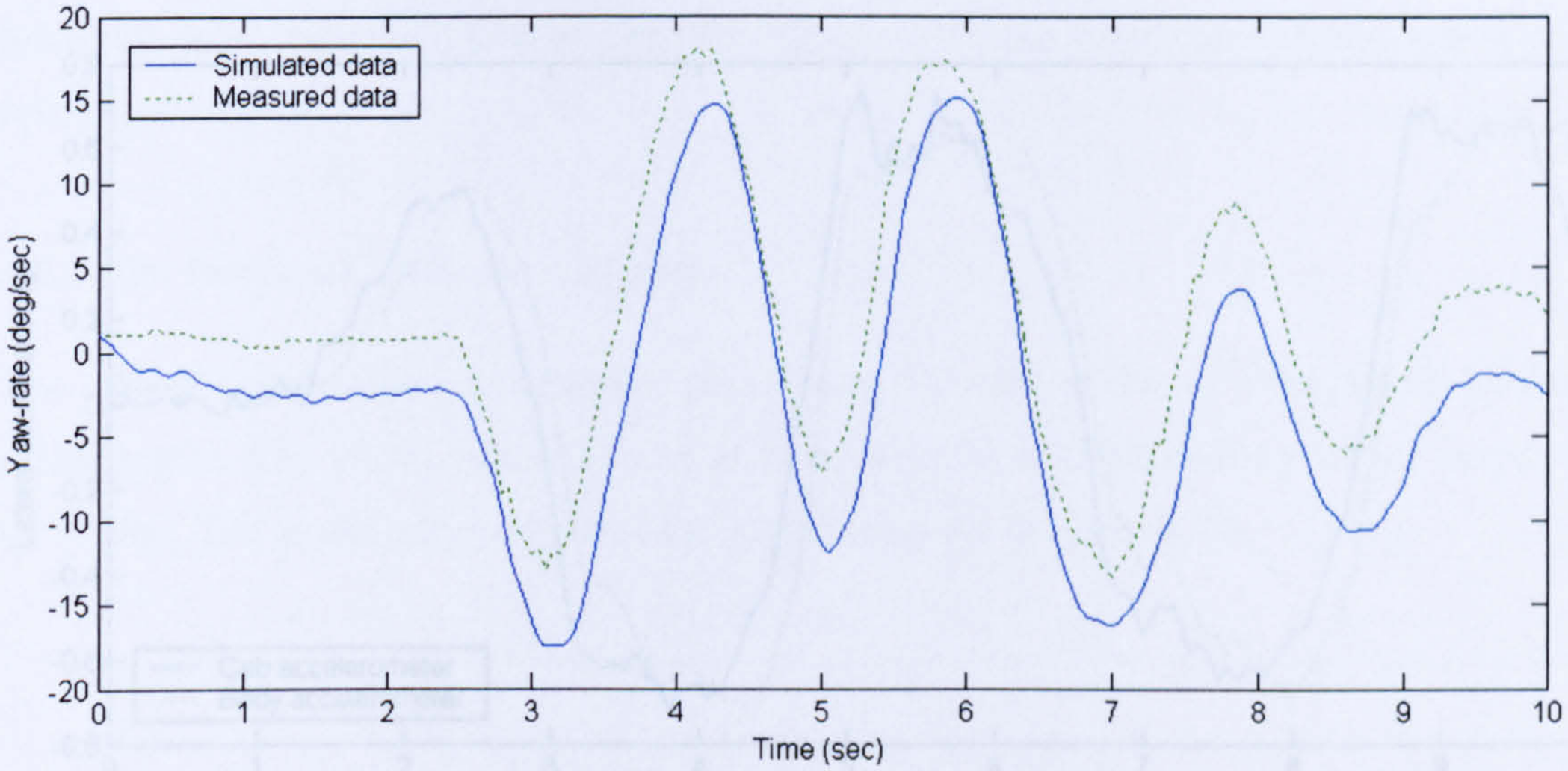

Fig 4.24 Yaw-rate of actual and simulated laden vehicle for double lane change at 70km/h

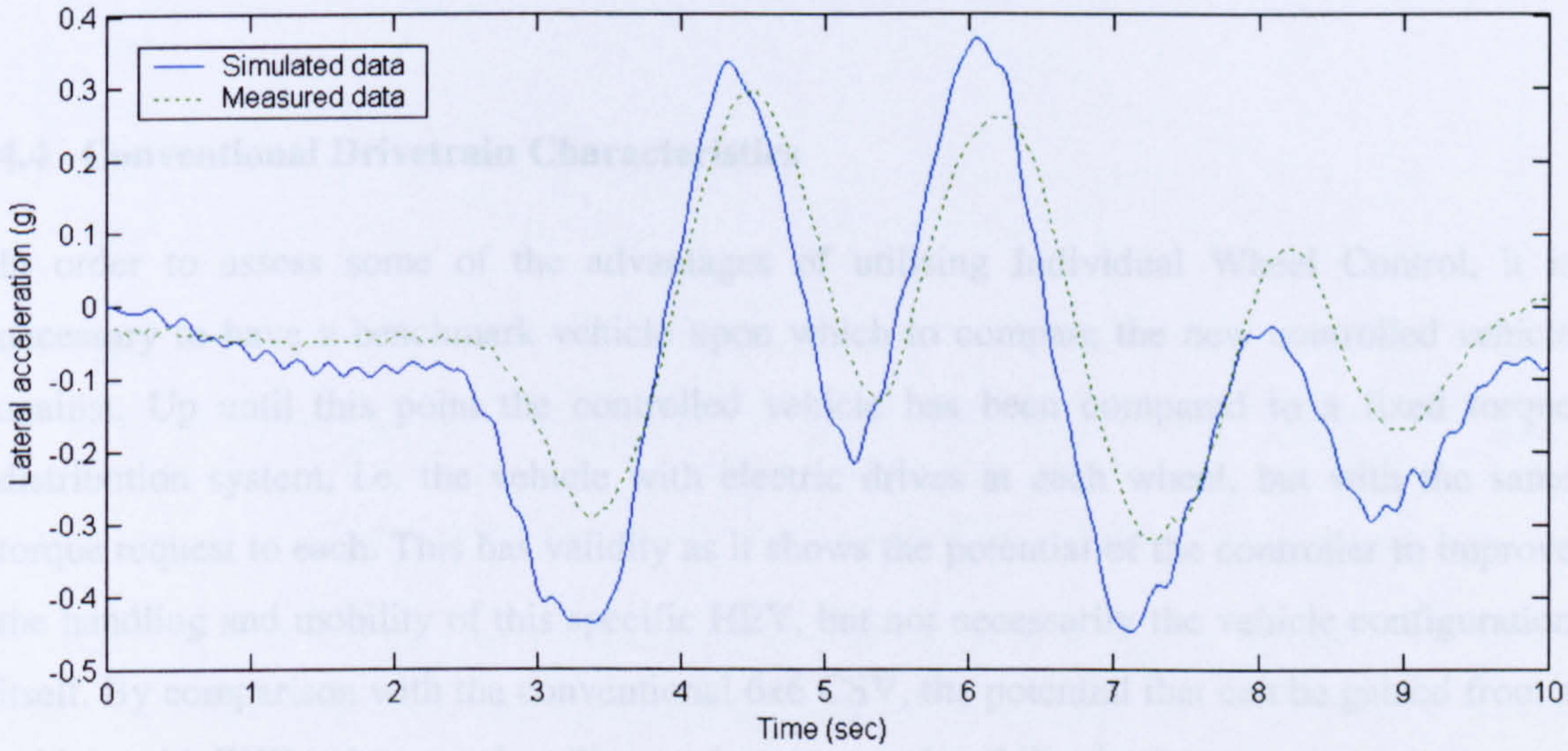

Fig 4.25 Lateral acceleration of actual and simulated laden vehicle for double-lane change at 70km/h

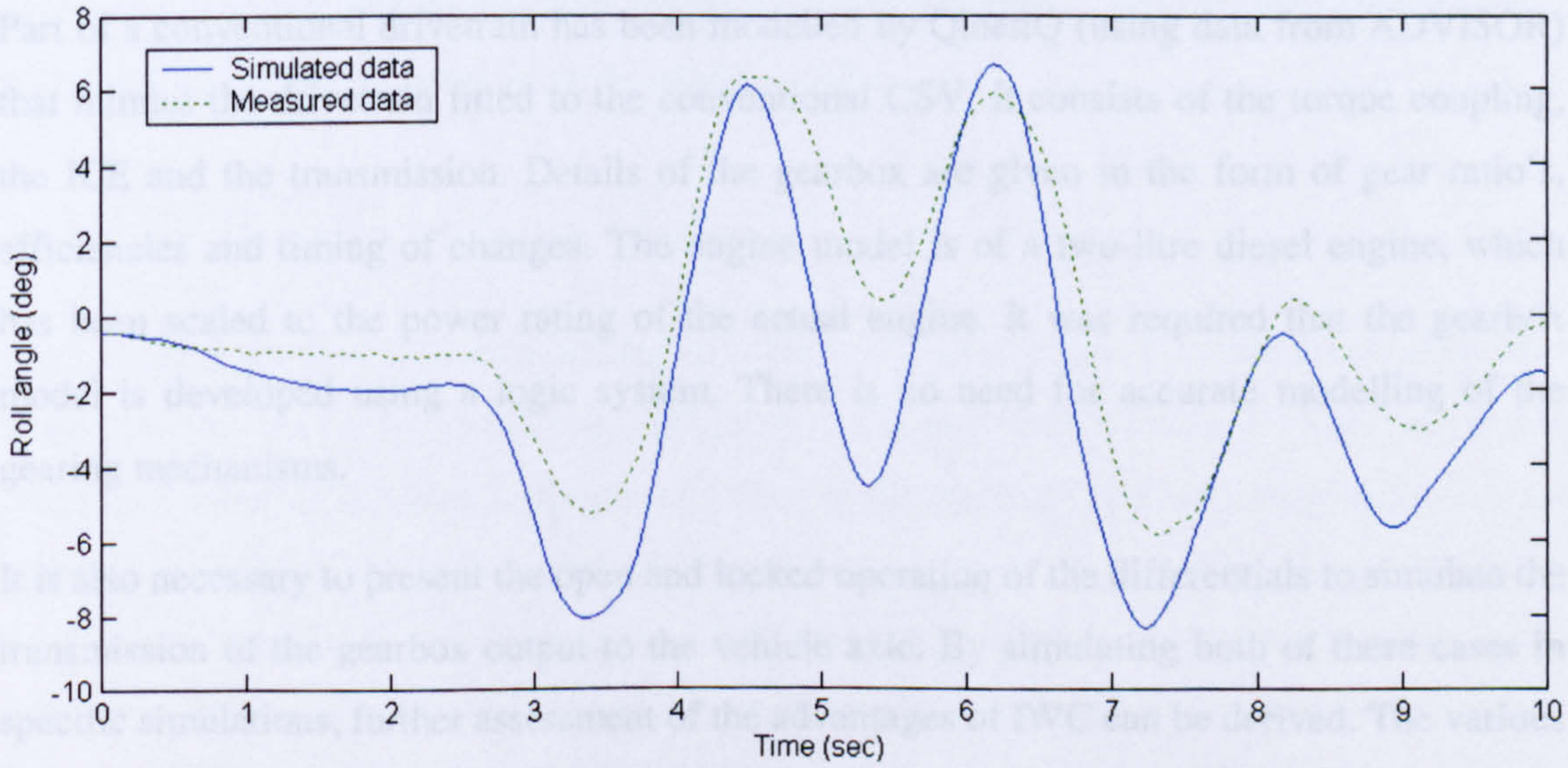

Fig 4.26 Roll angle of actual and simulated laden vehicle for double lane change at 70km/h

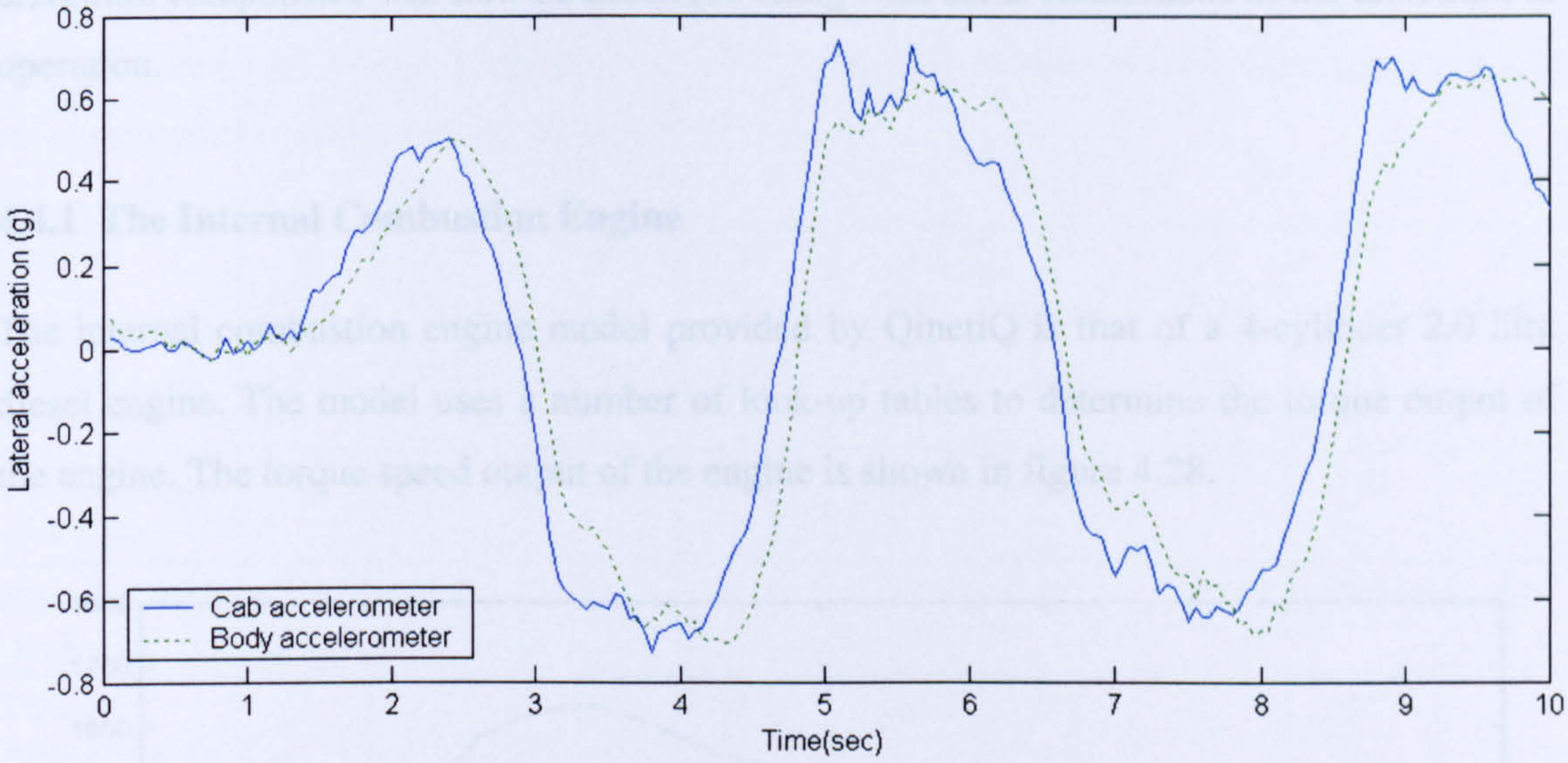

Fig 4.27 Unladen lateral acceleration of cab and body during slalom at 50km/h

4.4 Conventional Drivetrain Characteristics

In order to assess some of the advantages of utilising Individual Wheel Control, it is necessary to have a benchmark vehicle upon which to compare the new controlled vehicle against. Up until this point the controlled vehicle has been compared to a fixed torque distribution system, i.e. the vehicle with electric drives at each wheel, but with the same torque request to each. This has validity as it shows the potential of the controller to improve the handling and mobility of this specific HEV, but not necessarily the vehicle configuration itself. By comparison with the conventional 6x6 CSV, the potential that can be gained from a vehicle with IWC to improve handling performance and mobility is shown.

Part of a conventional drivetrain has been modelled by QinetiQ (using data from ADVISOR) that mimics the drivetrain fitted to the conventional CSV. It consists of the torque coupling, the ICE and the transmission. Details of the gearbox are given in the form of gear ratio's, efficiencies and timing of changes. The engine model is of a two-litre diesel engine, which has been scaled to the power rating of the actual engine. It was required that the gearbox model is developed using a logic system. There is no need for accurate modelling of the gearing mechanisms.

It is also necessary to present the open and locked operation of the differentials to simulate the transmission of the gearbox output to the vehicle axle. By simulating both of these cases in specific simulations, further assessment of the advantages of IWC can be derived. The various

drivetrain components will now be described along with some simulations of the drivetrain in operation.

4.4.1 The Internal Combustion Engine

The internal combustion engine model provided by QinetiQ is that of a 4-cylinder 2.0 litre diesel engine. The model uses a number of look-up tables to determine the torque output of the engine. The torque speed output of the engine is shown in figure 4.28.

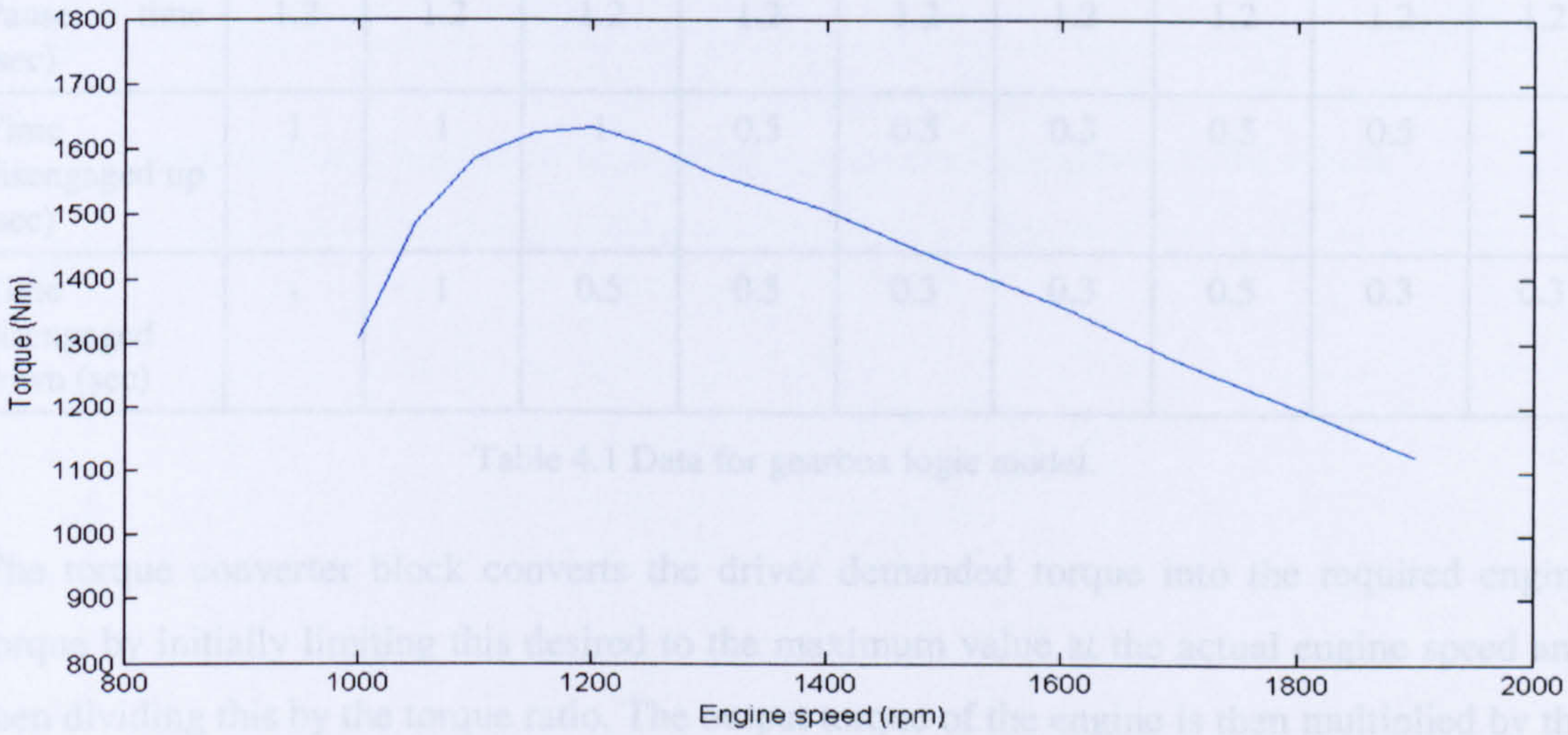

Fig. 4.28 Torque / speed curve for the 2.0 litre deisel engine

A demand torque and the gearbox speed are used as inputs to an engine control block, which determines the correct fuel rate. The fuelling is cut off depending on whether the vehicle is changing gear or braking. The engine brake torque is determined from a look-up table taking engine rpm and rate of fuel injection, leading to an output torque. The torque is then scaled to mimic the larger engine present on the existing CSV.

4.4.2 The Gearbox and Torque Converter

A nine-speed gearbox is to be modelled in order to transmit torque from the torque converter through to the drive axle. The data on the gearbox was provided in the form of gear ratios and efficiency maps. In addition to these, a number of timing properties with respect to the gear changes were used. A logic model was developed in Simulink to mimic the gear-changes made by a driver when accelerating or decelerating. The gearbox logic data is presented in table 4.1. Time pause is a minimum time between gear changes and the time disengaged represents the time that the gearbox is disengaged from the engine. There also must be a

maximum rate at which the torque changes as the clutch engages, as full torque cannot be delivered instantaneously. A simple rate-limit is applied to simulate the disengagement and re-engagement of the clutch by the driver.

	1st Gear	2nd Gear	3rd Gear	4th Gear	5th Gear	6th Gear	7th Gear	8th Gear	9th Gear
Change up revs (rpm)	1900	1903	1905	1906	1955	2001	2015	2017	-
Change down revs (rpm)	-	657	800	802	818	781	741	782	785
Pause time (sec)	1.2	1.2	1.2	1.2	1.2	1.2	1.2	1.2	1.2
Time disengaged up (sec)	1	1	1	0.5	0.5	0.3	0.5	0.5	-
Time disengaged down (sec)	-	1	0.5	0.5	0.3	0.3	0.5	0.3	0.3

Table 4.1 Data for gearbox logic model.

The torque converter block converts the driver demanded torque into the required engine torque by initially limiting this desired to the maximum value at the actual engine speed and then dividing this by the torque ratio. The output torque of the engine is then multiplied by the torque ratio to determine the torque input to the gearbox. The torque converter also changes the engine output speed by the speed ratio of the torque converter.

Figure 4.29 and figure 4.30 show the gear number and vehicle speed respectively for the vehicle accelerating from 5 to 100km/h in unladen and laden states. The torque outputs of the conventional and hybrid vehicle are shown in figure 4.31 outlining the increased torque capability offered by the hybrid vehicle providing the power requirements can be met.

As can be seen from the graphs, the acceleration performance of the conventional vehicle is much less than the vehicle equiped with electric drives. This difference in tractive performance should mean that the conventional vehicle will have a greatly reduced tendancy to wheel-spin during acceleration. However, this is not necessarily the case, as when a gear change takes place, the torque to the wheel from the driveline drops to zero. If the clutch re-engages quickly, there is a sudden increase in torque, causing a change in wheel speed resulting in wheel spin on low friction surfaces when differentials are unlocked. Traction control, either through engine control or brake actuation can relieve such problems, but these are beyond the scope of this work

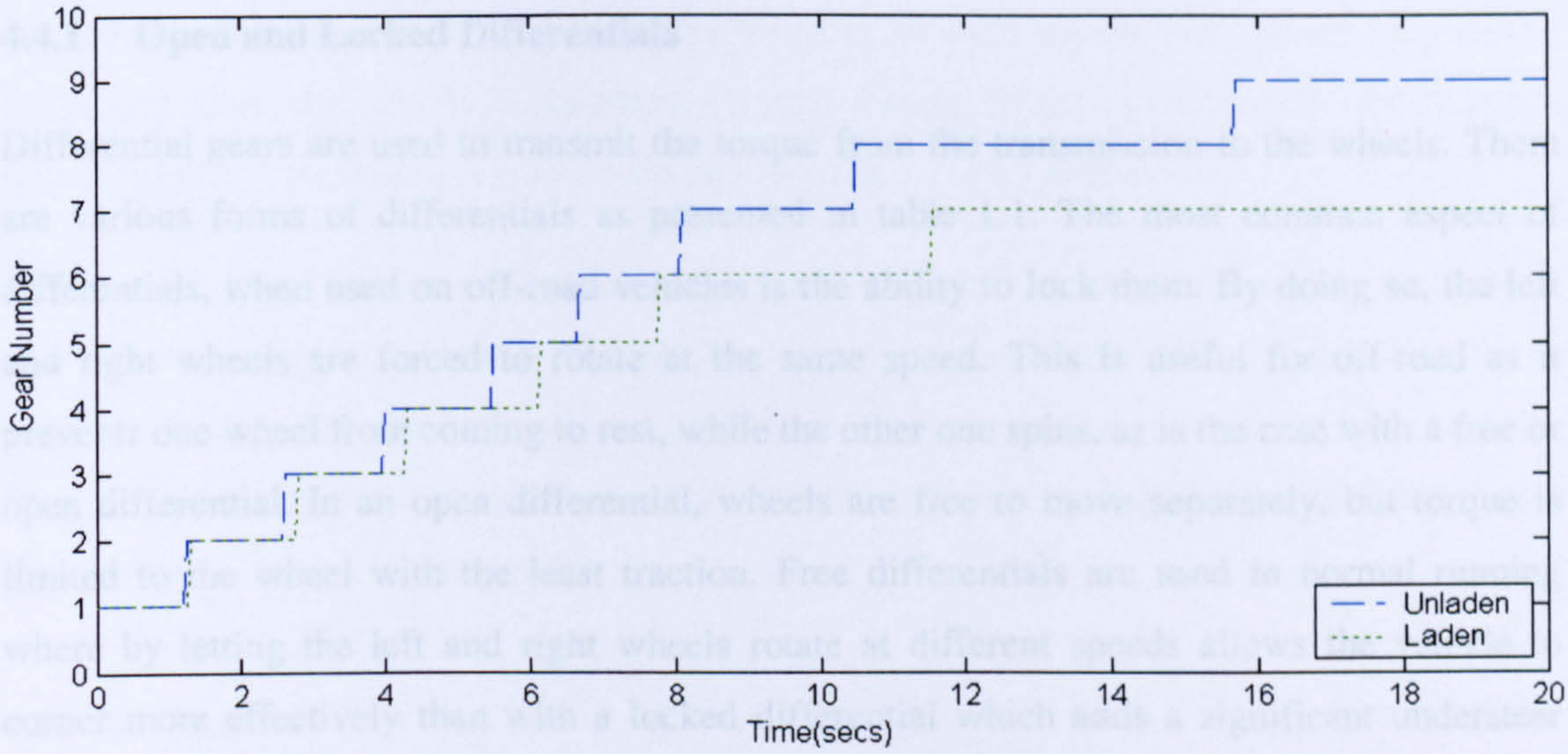

Fig. 4.29 Gear number for accelerating unladen and laden conventional vehicle

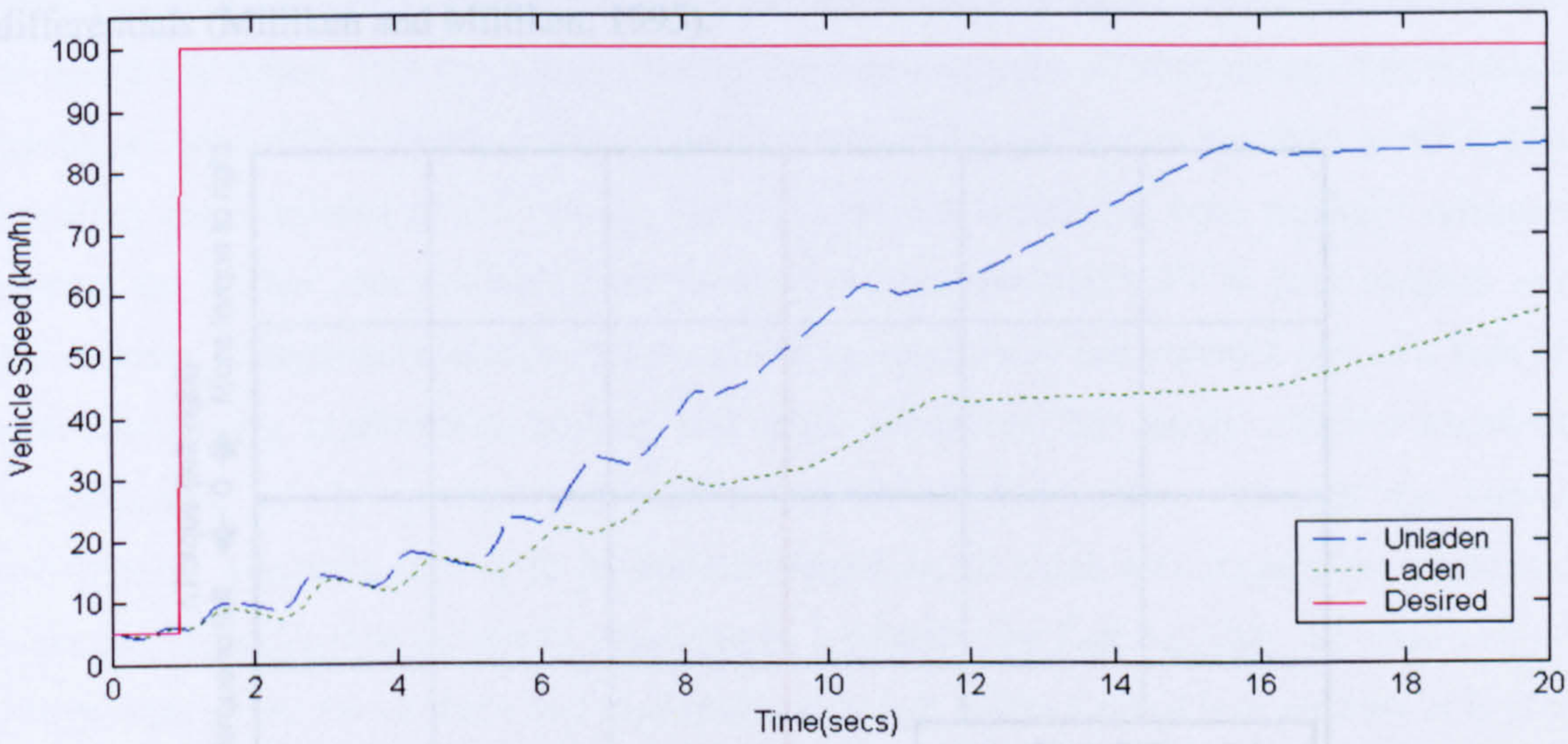

Fig. 4.30 Vehicle speed for accelerating unladen and laden conventional vehicle

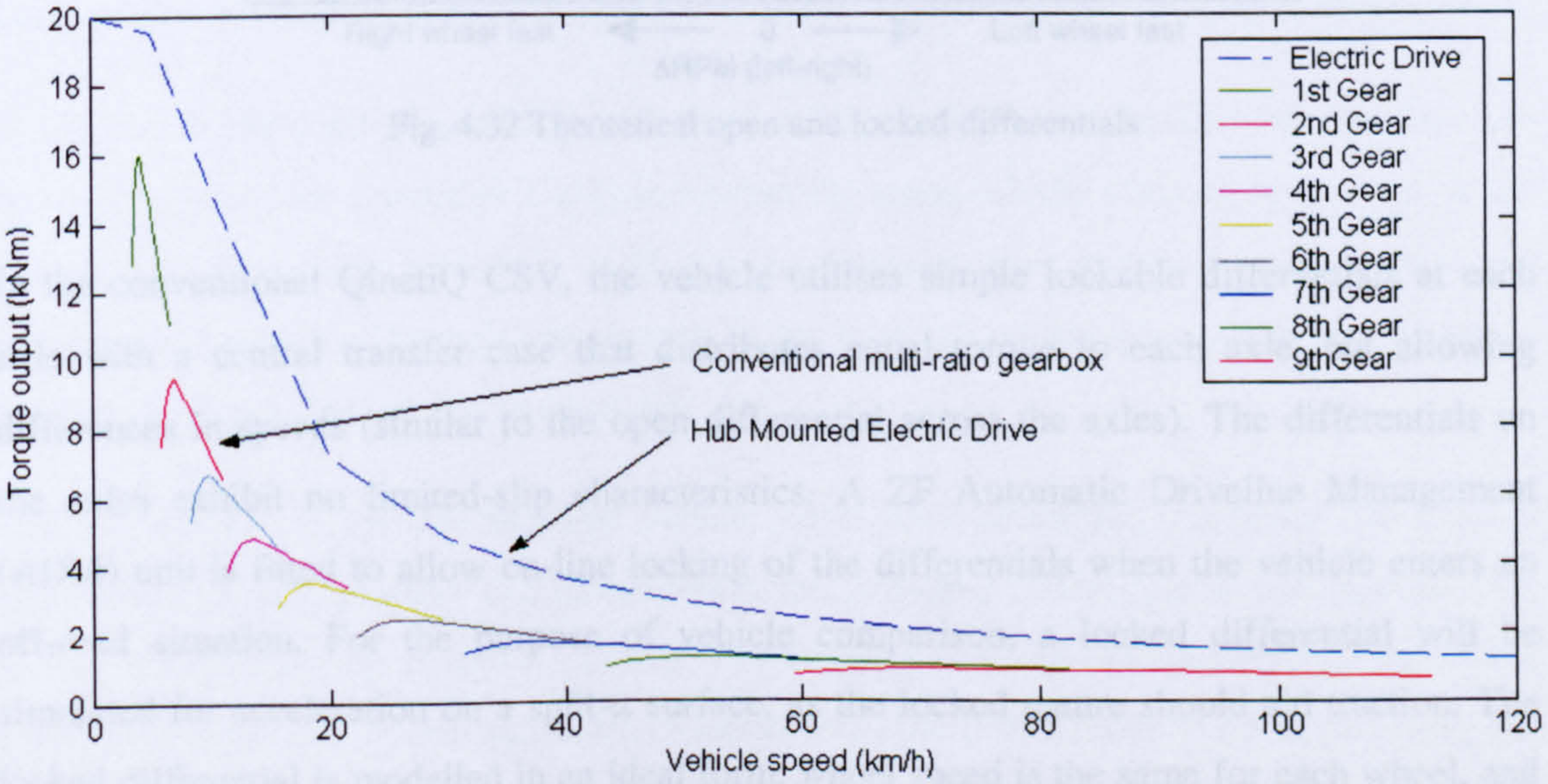

Fig. 4.31 Torque / speed outputs for conventional and hybrid drivetrains

4.4.1 Open and Locked Differentials

Differential gears are used to transmit the torque from the transmission to the wheels. There are various forms of differentials as presented in table 1.1. The most common aspect of differentials, when used on off-road vehicles is the ability to lock them. By doing so, the left and right wheels are forced to rotate at the same speed. This is useful for off-road as it prevents one wheel from coming to rest, while the other one spins, as is the case with a free or open differential. In an open differential, wheels are free to move separately, but torque is limited to the wheel with the least traction. Free differentials are used in normal running where by letting the left and right wheels rotate at different speeds allows the vehicle to corner more effectively than with a locked differential which adds a significant understeer effect. Figure 4.32 shows the idealised operation characteristics of locked and open differentials (Milliken and Milliken, 1995).

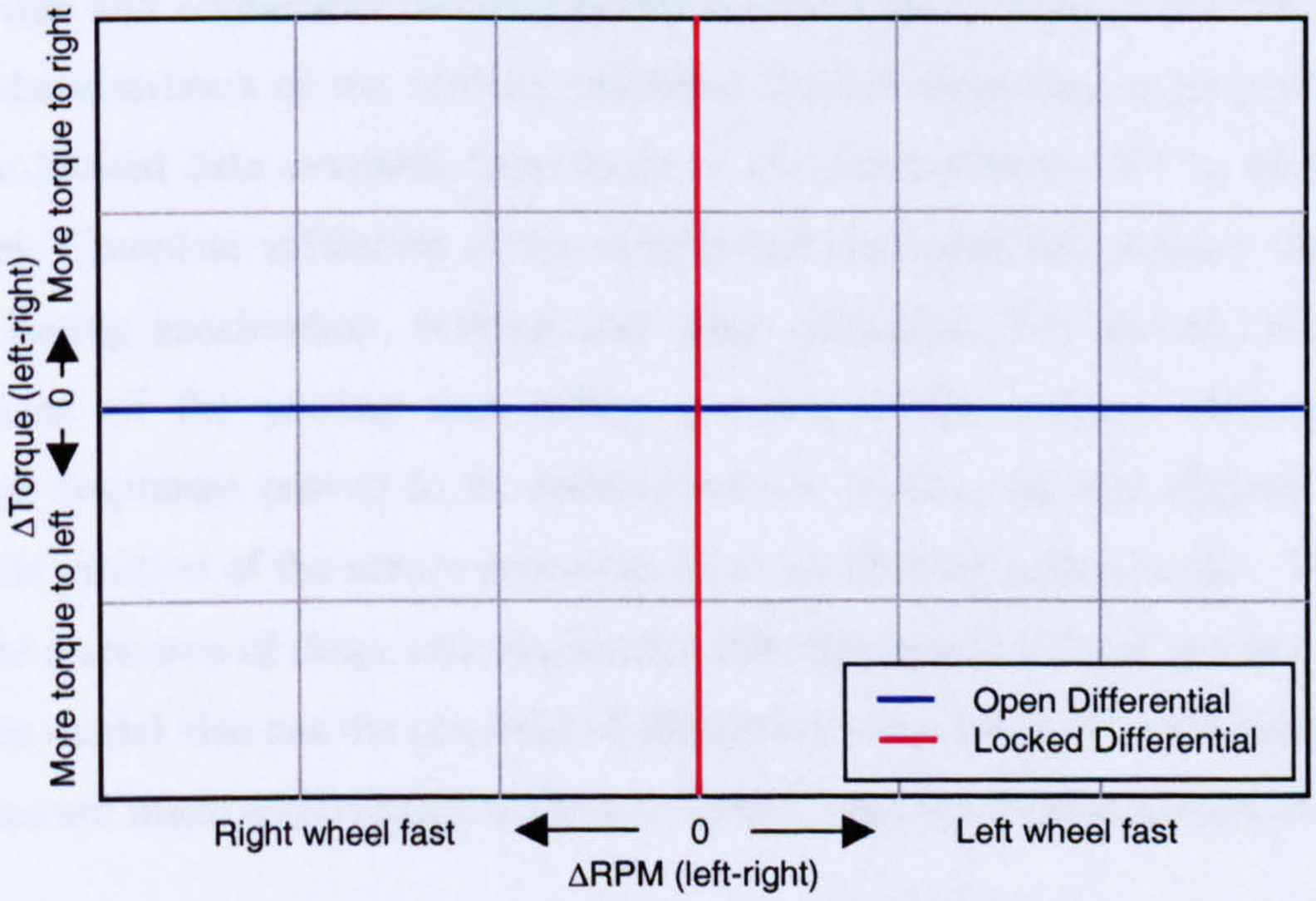

Fig. 4.32 Theoretical open and locked differentials

In the conventional QinetiQ CSV, the vehicle utilises simple lockable differentials at each axle with a central transfer case that distributes equal torque to each axle, but allowing differences in speeds (similar to the open differential across the axles). The differentials on the axles exhibit no limited-slip characteristics. A ZF Automatic Driveline Management (ADM) unit is fitted to allow on-line locking of the differentials when the vehicle enters an off-road situation. For the purpose of vehicle comparison, a locked differential will be simulated for acceleration on a split-μ surface, as the locked nature should aid traction. The locked differential is modelled in an ideal form, wheel speed is the same for each wheel, and

is generated by using the sum of the torques acting on each wheel. This should help reduce wheel-slip when the vehicle is simulated on split-μ surfaces as it prevents the wheel on the low friction side from spinning as would happen with an open differential.

For constant speed manoeuvres, actual vehicle trial data will be used to show the variation of yaw-rate with respect to vehicle loading. The operation of the open differential means that at constant speed, where the drivetrain only provides sufficient torque to maintain vehicle speed, the conventional vehicle should operate in a similar manner to the HEV with fixed torque distribution as shown in Section 4.3.

4.5 Summary

In this chapter the final vehicle model has been developed onto which the final controller can be tested and tuned. This complex model has eighteen degrees of freedom and can simulate handling, ride and acceleration/braking performance of the vehicle in the time domain. The handling characteristics of the vehicle, including the roll dynamics, were partially validated against the limited data available from trials of the conventional CSV in both unladen and laden states. Complete validation of the vehicle however, was not possible due to a lack of trial data during acceleration, braking and other excitation. The model exhibits excellent representation of the yawing and rolling motions of the vehicle although the lateral acceleration responses proved to be underestimated in all cases and slightly out of phase, however the position of the sensor proved to be a contributing factor to this. All results show comparable responses of shape and magnitude, although results proved less accurate at higher speeds. The model also has the potential of simulating some basic off-road behaviour, if some assumptions are made with regards to the tyre model, which will be discussed in Chapter 6.

In Chapter 3, the controlled vehicle was simulated against the uncontrolled vehicle. This can be used to prove the controller's impact against the same vehicle without the control. If the potential of the vehicle drivetrain itself is to be assessed, then it must be compared to the conventional vehicle. Through comparison of the two, the advantages gained by the use of Individual Wheel Control can be assessed.

Various aspects of the conventional vehicle have been presented, including the internal combustion engine, gearbox and torque converter. A locked differential is also modelled for testing acceleration on a split-μ surface. For braking tests, the torque capabilities of the conventional braking system and those available from the HMED will be compared using the brake force distribution stipulated in section 4.2.4.

The simulation of the engine and drivetrain show that the torque capabilities of the conventional vehicle are significantly less than the hybrid vehicle and the need for gear changes further hampers the vehicles tractive performance. From this it can be concluded that the hybrid vehicle will possess better acceleration and an increased potential for control, however, the high torque capabilities of the HEV also make it more prone to wheel-slip and increased lateral instability. This further necessitates the need for control of the hybrid drivetrain.

Chapter 5

Final Controller Design

5.1 Introduction

The previous chapter presented the full vehicle model and validated it against actual vehicle trial data. By including the suspension characteristics and loads transfer effects, the vehicle dynamics have altered from those presented in Chapter 2, especially during mid to high lateral accelerations. The controller developed in Chapter 3 will now be implemented on the full vehicle model. Although the general format of the controller will remain the same, given that the vehicle will still behave in fundamentally the same manner, it must be tuned to optimise its performance on the now more complex model. The controller will be tuned through the use of two different tuning algorithms implemented in MatLAB, fminsearch (Mathworks Inc., 1996) and DIRECT (Jones *et al.*, 1992). By tuning the operation of the controller under a wide range of conditions, a balanced control algorithm can be deduced. It is essential that this controller is robust to changing parameters, both internal and external. It is also hoped that this robustness will allow the controller to perform equally well in off-road conditions where external vehicle parameters vary constantly.

An additional safety feature will also be added to the controller to limit the side-slip angle at the handling limits of the vehicle, which vary depending on loading and road friction coefficient. This will be implemented as a separate controller by limiting the desired yaw-rate used by the full mobility controller.

5.2 Tuning of Control Parameters

In order to optimise the operation of the controller presented in Chapter 3, it must be tuned to offer the optimal results. In order to do this effectively, it must be tuned under a number of conditions to ensure the controllers robustness. As the TCS and ABS controllers operate independently from the DYC, they can be tuned first. Once these have been tuned, the co-ordinated yaw-moment controller will need to be tuned. In order to get a robust control algorithm, it will be necessary to tune the controller using a number of simulations covering a range of the vehicle behaviour.

Prior to the tuning process, it was noticed that during the operation of the sub-controllers, the yaw-rate tracking exhibited an undesired amount of oscillation. This was deemed to be caused by the large torque demands generated at the wheels with good traction, attempting to generate the yaw-moment that would usually be developed using both sets of tyres combined with the slower rate of change of torque permitted by the HMED's. A number of methods were investigated to help alleviate the oscillations. The most effective method proved to be an additional weighting of the DYC output while either of the sub-controllers were operating. This is expressed in table 5.1.

Wheel-slip state	Effect on DYC demand signal
-3	No reduction in torque on any wheel : DYC signal * 0.5
-2	No reduction in torque on left wheels : DYC signal * 0.5
-1	No reduction in torque on right wheels : DYC * 0.5
0	No effect
1	No increase in torque on right wheels : DYC signal * 0.8
2	No increase in torque on left wheels : DYC signal * 0.8
3	No increase in torque on any wheels : DYC signal * 0.8

Table 5.1 Revised control integration logic

5.2.1 Tuning TCS and ABS

Fminsearch is a MatLAB® function used to minimise a user determined cost function. The cost function is designed to minimise the overshoot of the controller and reduce the time that wheel-slip is above the required value, vehicle speed and stopping distances will also be included for each controller respectively. There will be 6 values that will be tuned for both Traction Control and Anti-lock Braking. These represent the proportional (K_{ap} and K_{bp}) and derivative gains (K_{ad} and K_{bd}) at each axle. Due to load transfers and various loading states, it will be necessary to simulate the vehicle in unladen and fully laden states and on a couple of different surfaces in order to achieve robust control.

For Traction Control, the vehicle is simulated 4 times to calculate the cost function. These are unladen and laden on ice and wet road surfaces. The cost function is a combination of the final vehicle speed after 6 seconds and also the integral of wheel-slip error (only when actual wheel-slip is greater than desired). Fminsearch minimises the cost function. For the Anti-lock Braking, the vehicle is simulated braking hard while on wet asphalt and ice in both unladen and laden states. Cost function is derived from the integral of wheel-slip error and also the vehicle speed.

The final values are for the controller gains for the traction controllers at front central and rear axles are:

K_{apf}= 199590, K_{adf}= 4620, K_{apc} = 198770, K_{adc} = 3800, K_{apr} = 198770, K_{adr} = 14510

The final values are for the controller gains for the Anti-lock braking controllers at front central and rear axles are:

K_{bpf}= 196310, K_{bdf}= 18157, K_{bpc} = 196310, K_{bdc} = 16683, K_{bpr} = 188940, K_{bdr} = 18894

Due to the brake force distribution as set out in Chapter 4, the ABS control proportional coefficient is slightly lower at the rear of the vehicle as the braking forces are lower. It should be noted that the gains presented are very high. Boundaries used in the tuning algorithm prevented any higher values. Due to the rate limiter on the torque production, there is a limit to the rate at which the control signals can take effect, hence the large values are presented. These large control torque demands will never results in torques of such large magnitudes due to the rate limit on torque production. If the demand signal was taken into account in the cost function, smaller gains could be expected with an insignificant impact on performance.

5.2.3 Full Algorithm Tuning

Now that the TCS and ABS controllers have been tuned, it is necessary for the yaw-moment controller to be tuned. As it is a fuzzy logic controller, there are constraints that must be placed on the tuneable variables. Fminsearch does not allow for any constraints and so it not applicable for this controller. So instead, a tuning algorithm called Direct was used, developed by Jones *et al.* (1992) and presented in Bjorkman and Holstrom (1999). Direct solves constrained, mixed-integer, global optimisation problems using both a global and local search method, which means the algorithm will find the global optimum within the constraints, without settling in a local minima. First it was necessary to derive a cost function to minimise and also determine which variables to alter to tune the fuzzy logic controller. It is known that the membership functions will be symmetrical as the vehicle will behave the same whether turning left or right, which halves the number of parameters that require tuning. The tuneable parameters, x(1-5), are shown in figure 5.1. In order for good all round performance of the controller, it is necessary to tune the control parameters while the vehicle undertakes a number of manoeuvres. These manoeuvres are designed to show the full range of vehicle behaviour, including operation of all the sub- controllers and also performance during subtle and severe steer inputs. The following tests were decided upon:

- Laden J-turn at 20km/h.
- Laden J-turn at 60km/h.
- Laden lane-change starting at 5km/h accelerating up to 40km/h.
- Laden acceleration on a split-μ surface starting from 5 km/h.
- Laden heavy braking on a split-μ surface starting from 80 km/h to 0km/h.
- Unladen J-turn at 20km/h.
- Unladen lane-change starting at 40km/h accelerating up to 80km/h.
- Unladen acceleration on a split-μ surface starting from 5 km/h.
- Unladen heavy braking on a split-μ surface starting from 80 km/h to 0km/h.

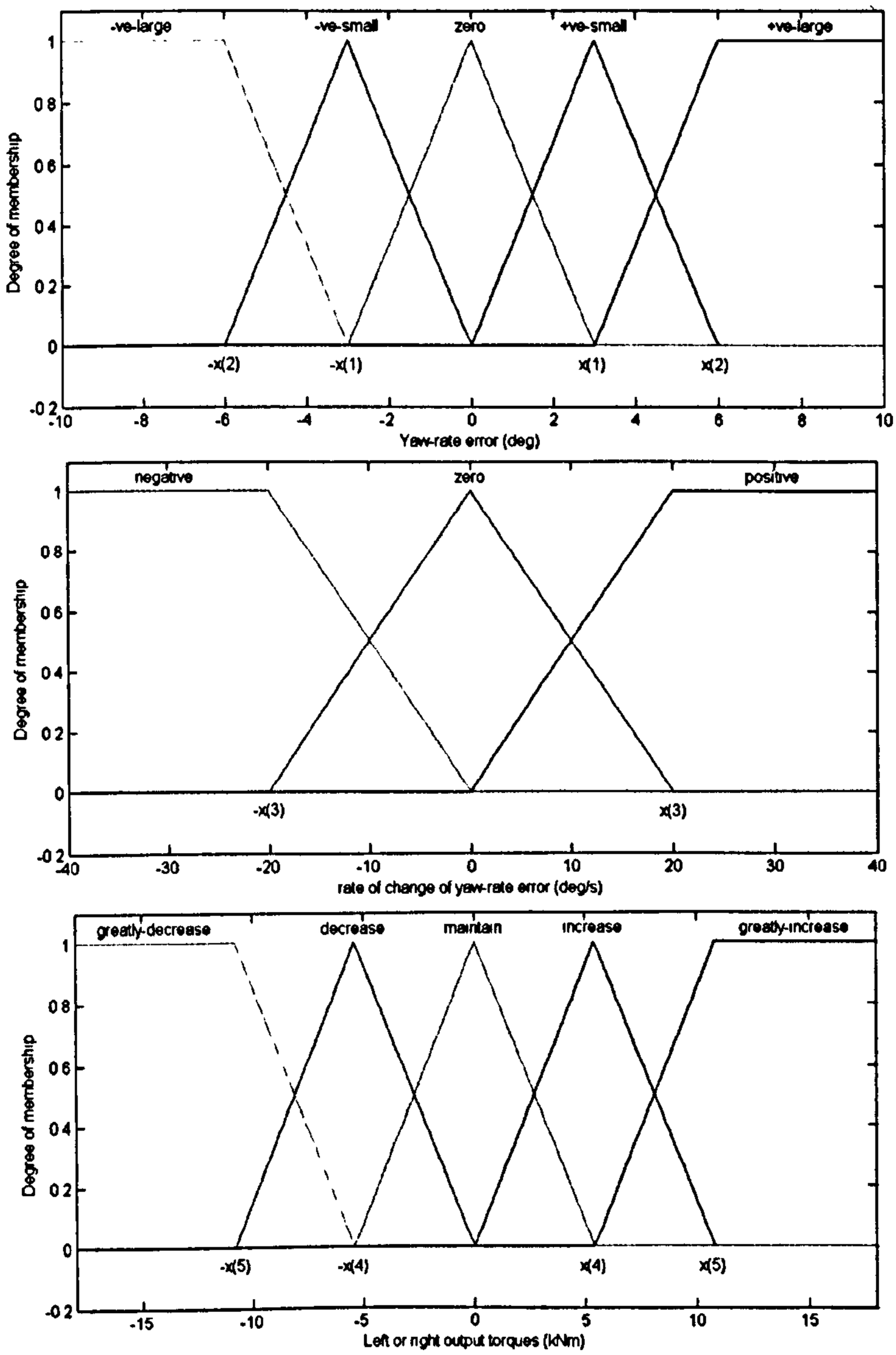

Fig. 5.1 Tunable parameters (x) for fuzzy logic controller for yaw-rate error, rate of change of yaw-rate error and output torques (identical for left and right)

Cost functions were determined for all the above simulations. The aim of the final controller is to reduce yaw-rate error and wheel-slip resulting in increased safety and decreased driver workload. Selection of the cost function is an iterative process and must be altered in order to give each simulation a roughly equal rating as unequal values for the different simulations would promote controller bias towards a particular manoeuvre at the expense of its performance on another. For the acceleration on split-μ surfaces, the peak error was given a high cost to help remove the initial yaw-rate spike developed. The final cost function that DIRECT aims to reduce is the sum of the costs from each simulation.

The controller was tuned on two different computers at the same time, each with slightly different cost functions and the best parameters from each simulation were then compared to give the final control values. The final values for x are given as:

$$x(1) = 2.1653 \quad x(2) = 4.5981 \quad x(3) = 36.759 \quad x(4) = 11909 \quad x(5) = 15185$$

Again, as exhibited during the tuning of the traction control and anti-lock braking controller gains, the final 2 values representing the controller torque demands are upwards of 10kN. This is again due to the rate limit of the HMEDs with the actual torque demands from the controller never reaching such large values.

5.3 Extension of Controller to Limit Side-slip

When the vehicle is approaching the limits of the vehicle performance, the side-slip increases as the lateral tyre force saturates. This leads to lateral instability. Another result of high lateral accelerations is the danger posed by body roll. As the controller imposes a desired yaw-rate on the vehicle, there is no safety mechanism to prevent this yaw-rate from reaching a value which would result in the vehicle rolling or sliding out of control. There are two methods of intervening with the controller to restrict vehicle operation to safe values of lateral acceleration or side-slip angles. The first is by including the side-slip angle into the fuzzy logic controller as an additional input, to set boundaries on the side-slip angle, preventing the controller outputting torque demands that are dangerous to the vehicle. The second method is to limit the desired yaw-rate itself when the side-slip angle goes beyond a predefined value.

A form of DYC similar to this is presented in Manning *et al.* (2000). Here, yaw-moments are produced through differential braking depending on the position of the vehicle in the β phase plane (β against dβ/dt) to maintain the vehicle stability during high lateral accelerations. Results show that side-slip angles are greatly reduced, improving lateral stability.

In Abe *et al.* (2001) yaw-rate control by DYC and side-slip control by DYC are compared. Results show that on a low friction surface, yaw-rate control by DYC shows larger side-slip angles than the side-slip control method as would be expected. It is noted that the latter control method has greater potential for compensating against unstable vehicle motion caused by tyre force saturation.

The uncontrolled vehicles lateral acceleration responses to increasing steer angle for the unladen and laden vehicle on a number of road surfaces at 30 and 60km/h are shown in figure 5.2 and figure 5.4 respectively. The vehicles side-slip angle responses to increasing steer input for the same are shown in figure 5.3 and figure 5.5. From figures 5.2 and 5.4, it can be seen that the limit of the linear region varies greatly with loading and road friction coefficient, where as vehicle speed has little effect on the end of the linear region with respect to the lateral acceleration. In the linear region there is no need for any intervention from a limit controller, as the primary concern at the low to mid lateral accelerations (up to around 0.3-0.4g) is yaw-rate tracking as vehicle stability is ensured. However, when the vehicle gets further into the non-linear region, the need for limit control is increased and the need to follow a desired yaw-rate gives way to maintaining vehicle stability.

From the results, it is possible to see that the uncontrolled vehicle has two distinct limits, one occurs for the understeering vehicle and the other for the oversteering steering. When unladen (understeering), there comes a point where yaw-rate ceases to change with increasing steer-angle, yet the vehicle remains stable, however changes in steer-angle cease to have an effect on vehicle heading. In the case of the laden oversteering vehicle, as the steer angle increases the vehicle becomes unstable even at relatively low steer-angles and the side-slip angle increases massively. In the case of the laden vehicle at 60km/h, the vehicle becomes unstable when the steer-angle reaches 6-11° depending on the road surface.

It has already been shown on the basic non-linear handling model, that the controller helps maintain the vehicle stability when laden. By starting to impose boundaries on the side-slip angle as it gets above +/- 4° the vehicle stability should be ensured.

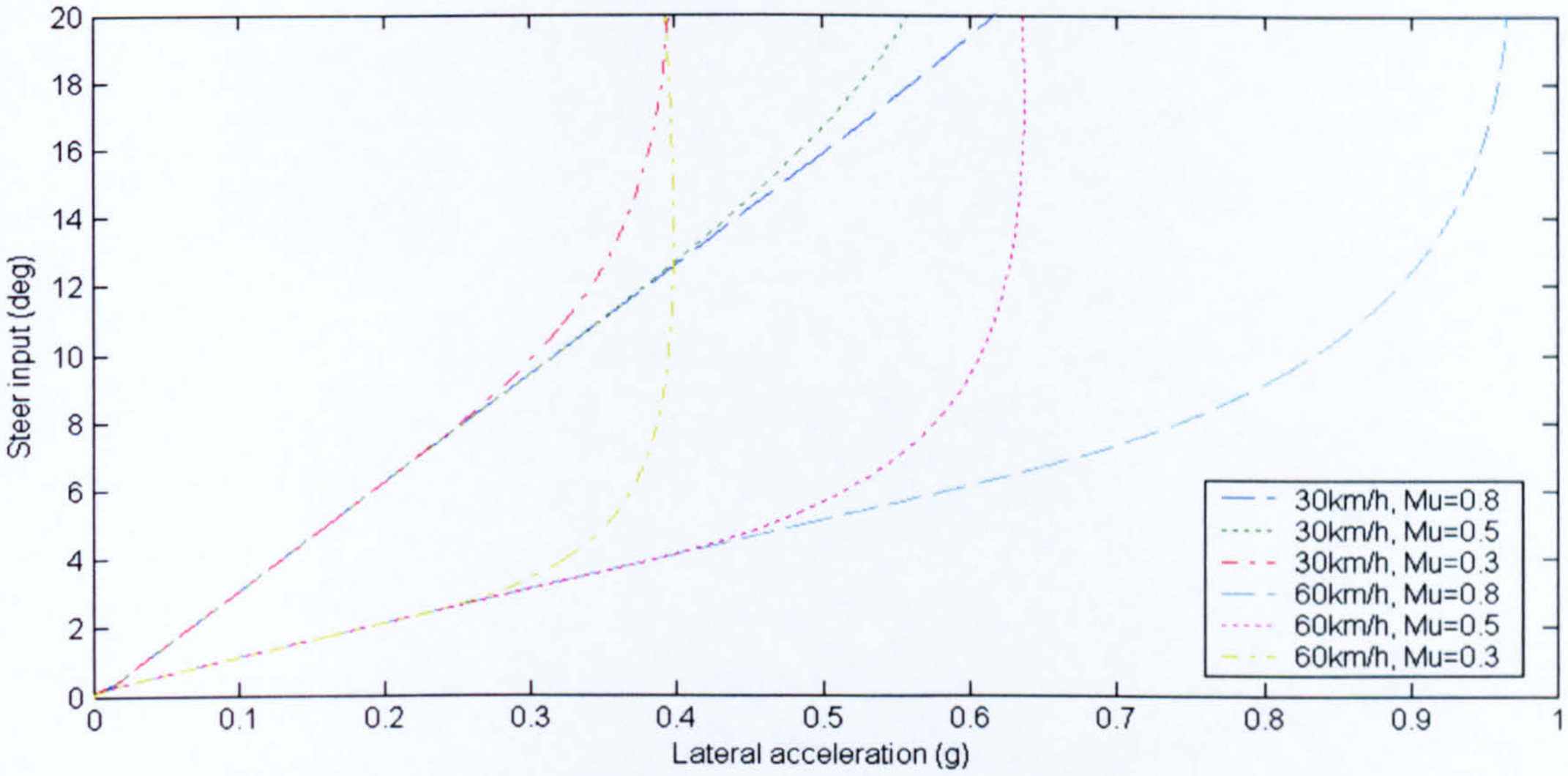

Fig. 5.2 Lateral acceleration response to steer-input for unladen vehicle, uncontrolled

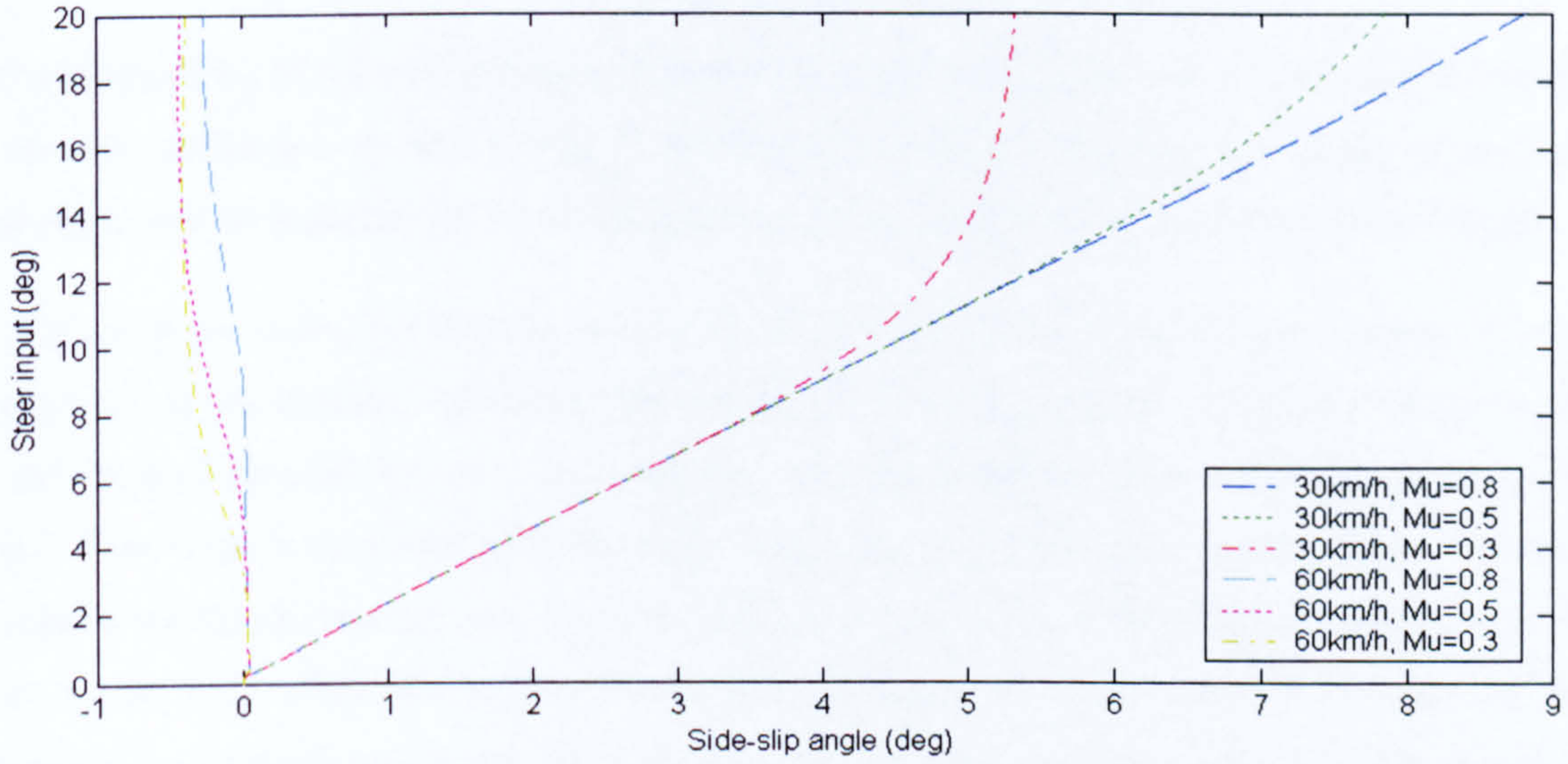

Fig. 5.3 Side-slip angle response to steer input for unladen vehicle, uncontrolled

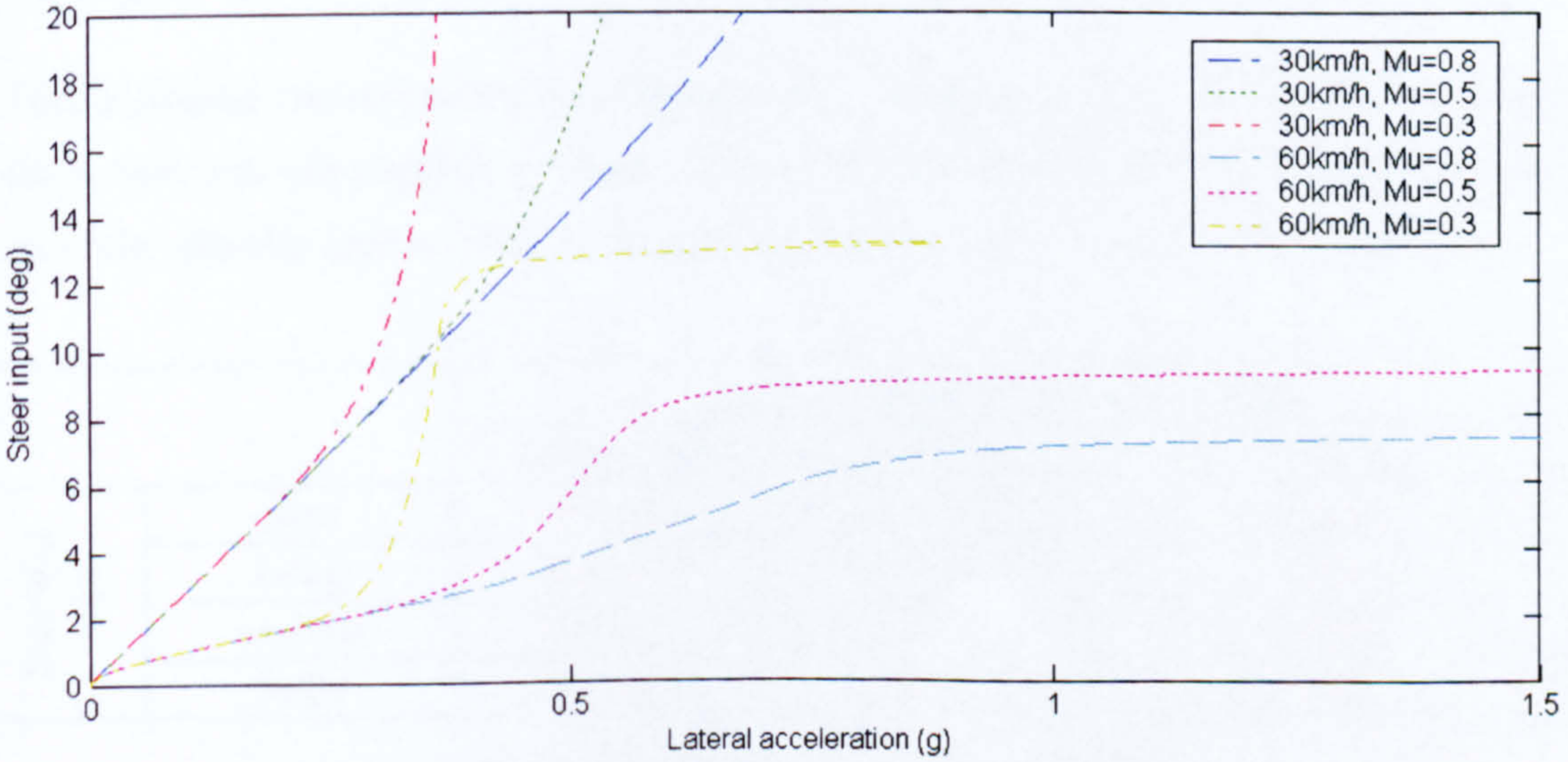

Fig. 5.4 Lateral acceleration response to steer-input for laden vehicle, uncontrolled

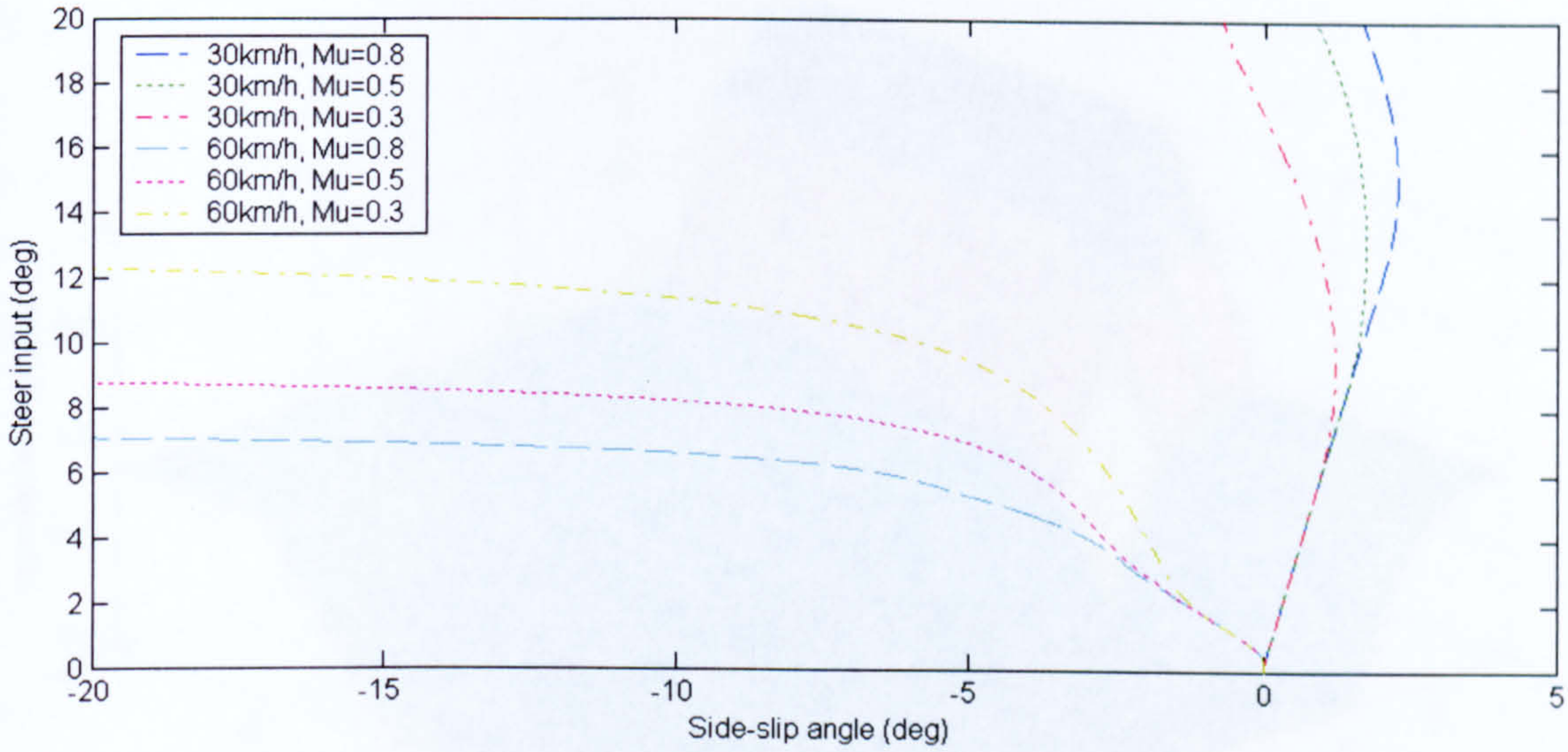

Fig. 5.5 Side-slip angle response to steer input for laden vehicle, uncontrolled

As the mobility controller has been shown to be adept at following the desired yaw-rate under various conditions, by intervening in the desired yaw-rate when side-slip angle, β, gets too large, it will be possible for the vehicle to remain in a stable region regardless of steer input.

A fuzzy logic controller will be used to impose this control which will be redundant for the majority of the vehicles operation. The controller takes the absolute value of side-slip angle and the derivative of that value and outputs a yaw-rate reduction value which ranges from 1 to 0.2. This value is then multiplies the desired yaw-rate to give the new desired value. The rules used in the fuzzy controller are given in table 5.2. The surface of the fuzzy controller is shown in figure 5.6. When the yaw-rate and side-slip angle are both positive or negative the controller output is set as one, as in these cases, reducing yaw-rate leads to increasing side-slip angles.

This additional control feature fits into the control structure as shown in figure 5.7 relying on the vehicle side-slip angle as an input. As with all the controllers developed, the performance on of the side-slip limiter relies on accurate estimation or sensing of external parameters.

		Rate of change of side-slip angle		
		Decreasing	maintaining	increasing
Side-slip angle	zero	Maintain	maintain	reduce
	small	Reduce	reduce	limit
	medium	Reduce	limit	limit
	large	Limit	limit	limit

Table 5.2 Fuzzy logic rules for side-slip limiter

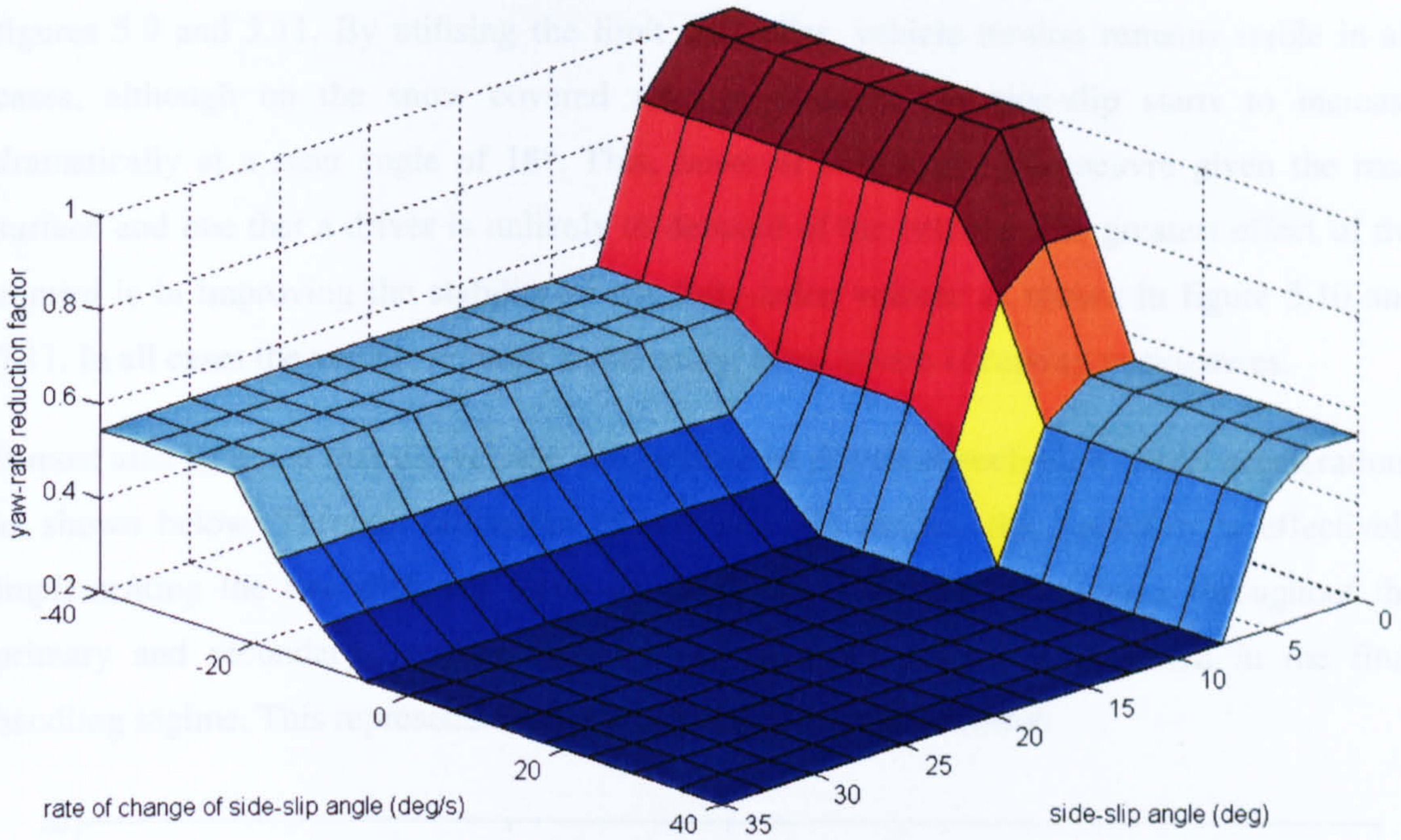

Fig. 5.6 Fuzzy surface for side-slip limiter

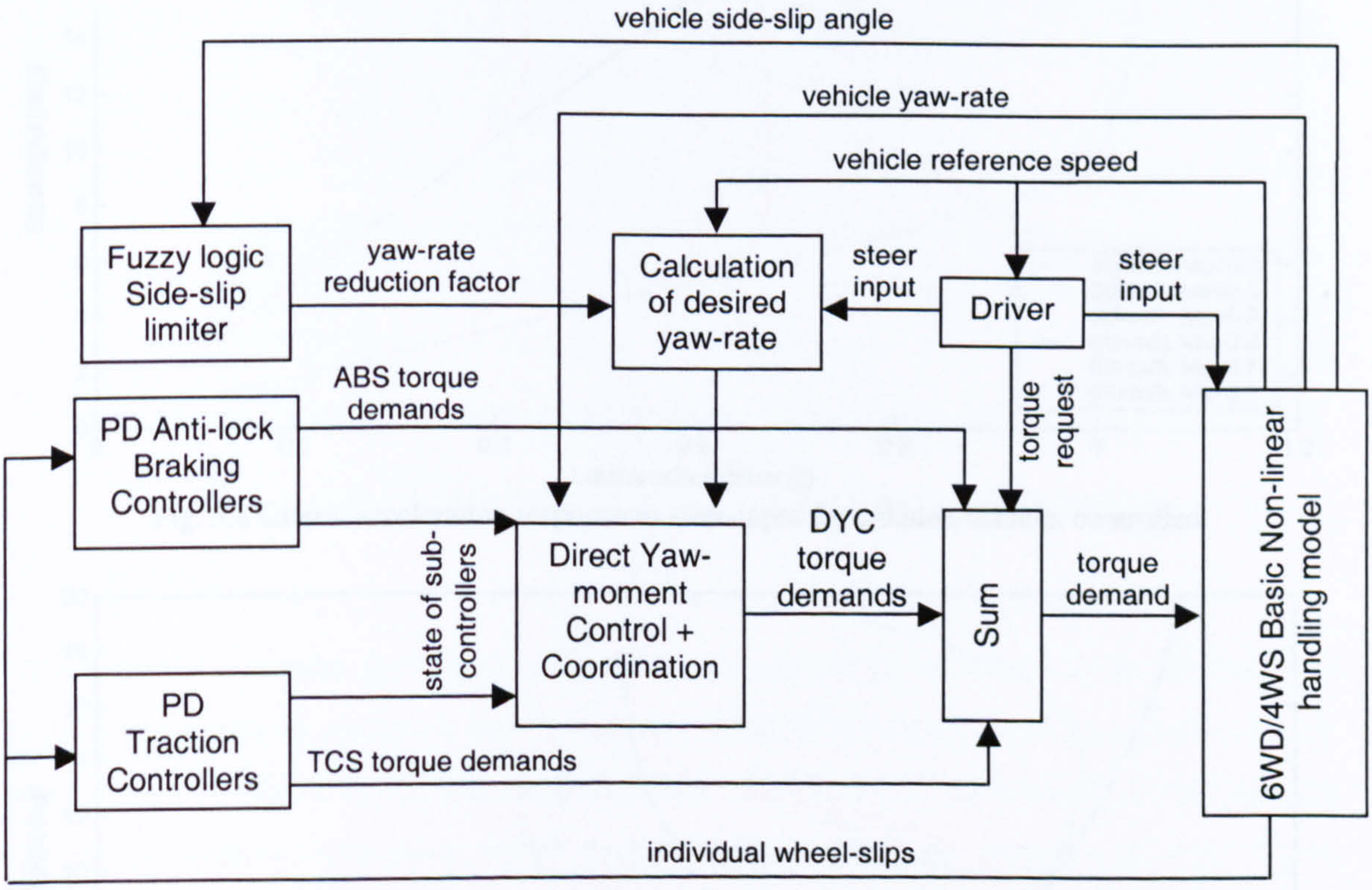

Fig. 5.7 Control system layout

The constant speed tests for increasing steer inputs as presented above for the uncontrolled vehicle are performed by the controlled vehicle with the yaw-rate limiter. The results for lateral acceleration are shown in figures 5.8 and 5.10 and the results for side-slip angle in

figures 5.9 and 5.11. By utilising the limit controller, vehicle motion remains stable in all cases, although on the snow covered road at 60km/h, the side-slip starts to increase dramatically at a steer angle of 18°. This, however is a severe manoeuvre given the road surface and one that a driver is unlikely to demand of the vehicle. The greatest effect of the control is in improving the stability of the fully-laden vehicle as shown in figure 5.10 and 5.11. In all cases the vehicle remains stable under these severe cornering manoeuvres.

It must also be noted that the vehicle will seldom be driven at such high lateral accelerations as shown below. Through utilisation of this side-slip limiter, the controller is effectively implementing the two different forms of DYC. Yaw-rate tracking occurs throughout the primary and secondary handling regimes and side-slip control in executed in the final handling regime. This represents a complete form of handling control.

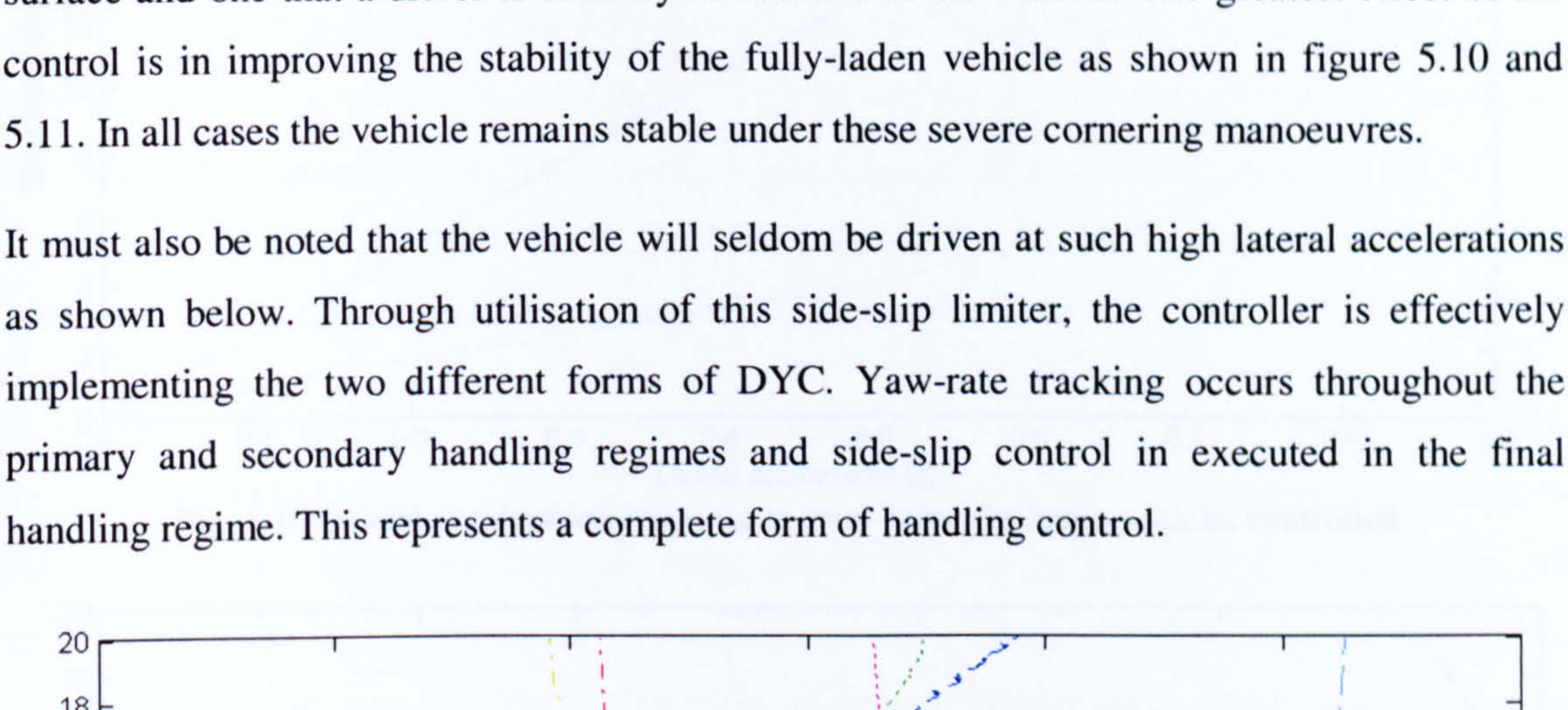

Fig. 5.8 Lateral acceleration response to steer-input for unladen vehicle, controlled

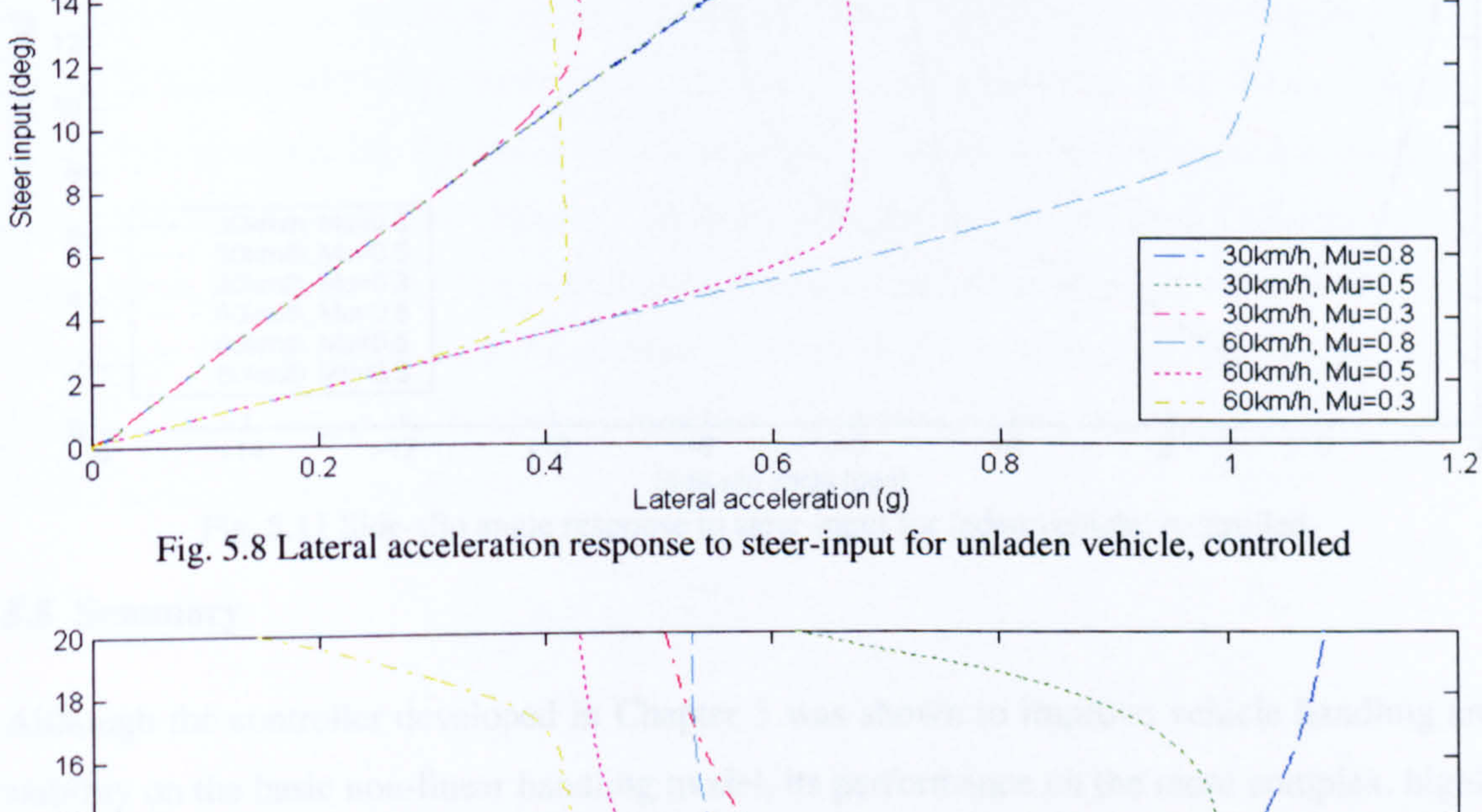

Fig. 5.9 Side-slip angle response to steer-input for unladen vehicle, controlled

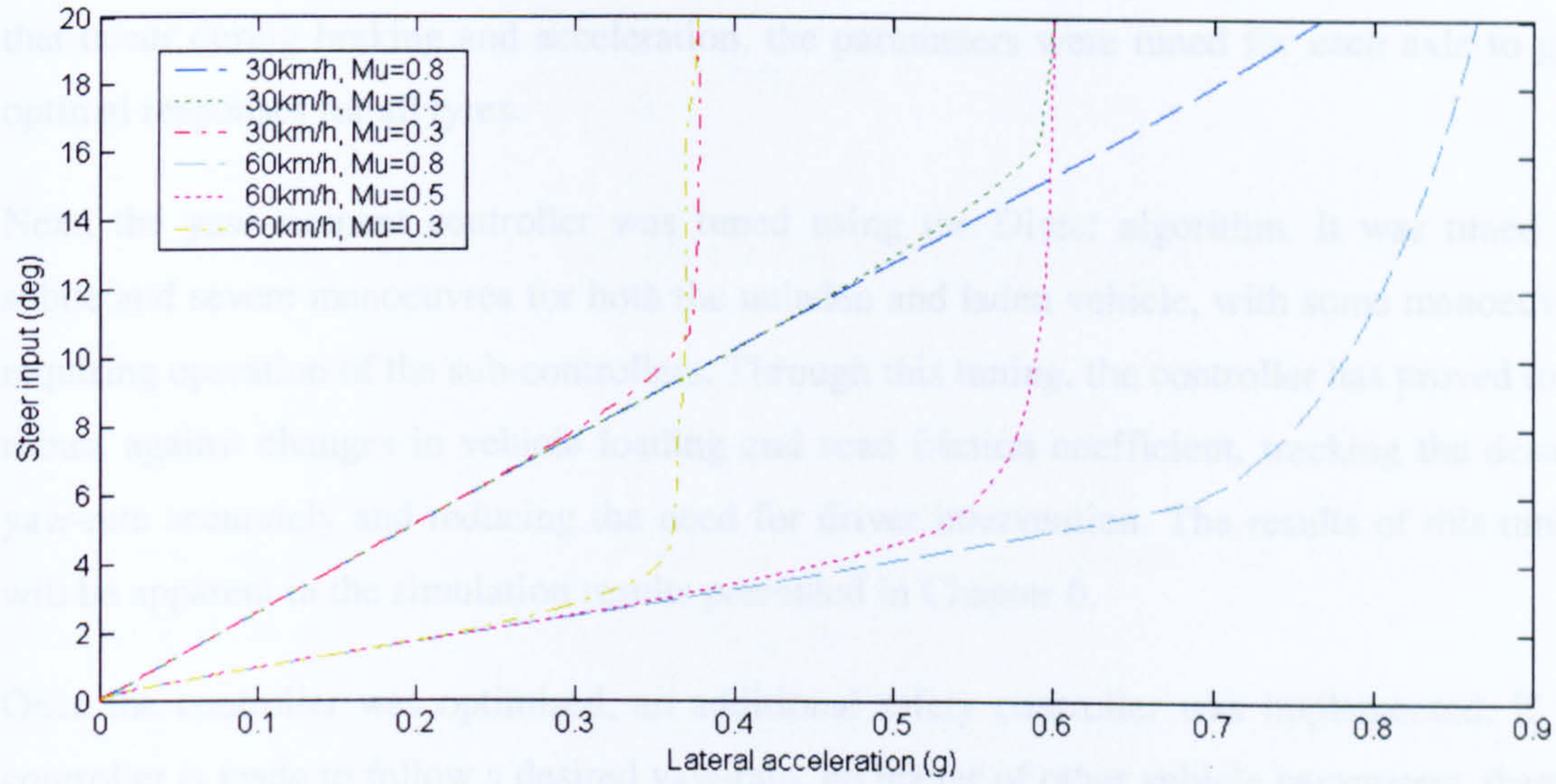

Fig. 5.10 Lateral acceleration response to steer-input for laden vehicle, controlled

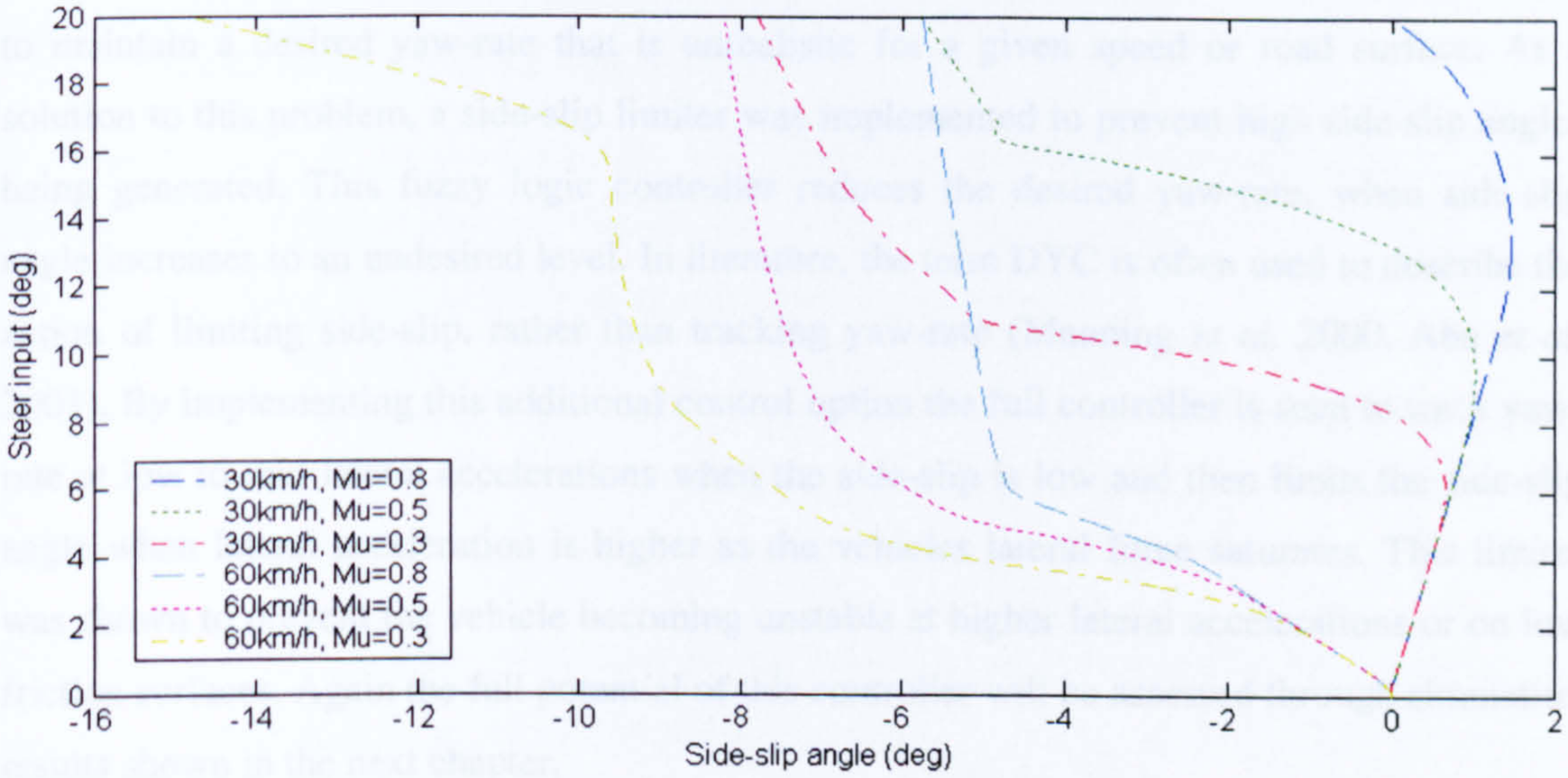

Fig. 5.11 Side-slip angle response to steer-input for laden vehicle, controlled

5.5 Summary

Although the controller developed in Chapter 3 was shown to improve vehicle handling and stability on the basic non-linear handling model, its performance on the more complex, highly non-linear full vehicle model was not guaranteed. This is due to the addition of load transfer and suspension characteristics, which have significant effect on vertical tyre load. These increase the transient nature of the tyre and have a dramatic effect on the available tyre forces.

In this chapter, the controller has been tuned to optimise its performance for various aspects of vehicle use on the full vehicle model. Initially the sub-controllers were tuned using a gradient search algorithm, in order to optimise the TCS and ABS. Due to the load transfers

that occur during braking and acceleration, the parameters were tuned for each axle to give optimal responses for all tyres.

Next, the yaw-moment controller was tuned using the Direct algorithm. It was tuned for subtle and severe manoeuvres for both the unladen and laden vehicle, with some manoeuvres requiring operation of the sub-controllers. Through this tuning, the controller has proved to be robust against changes in vehicle loading and road friction coefficient, tracking the desired yaw-rate accurately and reducing the need for driver intervention. The results of this tuning will be apparent in the simulation results presented in Chapter 6.

Once the controller was optimised, an additional safety controller was implemented. If the controller is made to follow a desired yaw-rate, no matter of other vehicle parameters, there is the potential for a high side-slip angle being produced. This occurs as the controller attempts to maintain a desired yaw-rate that is unrealistic for a given speed or road surface. As a solution to this problem, a side-slip limiter was implemented to prevent high side-slip angles being generated. This fuzzy logic controller reduces the desired yaw-rate, when side-slip angle increases to an undesired level. In literature, the term DYC is often used to describe the action of limiting side-slip, rather than tracking yaw-rate (Manning *et al.* 2000, Abe *et al,* 2001). By implementing this additional control option the full controller is seen to track yaw-rate at low to mid lateral accelerations when the side-slip is low and then limits the side-slip angle when lateral acceleration is higher as the vehicles lateral force saturates. This limiter was shown to prevent the vehicle becoming unstable at higher lateral accelerations or on low friction surfaces. Again the full potential of this controller will be assessed through simulation results shown in the next chapter.

Chapter 6

Assessment of Individual Wheel Control

6.1 Introduction

In this chapter, the performance of both the controller and the HEV will be assessed. The simulation work will be used to answer two questions.

1. If the Hybrid-Electric Vehicle is built, what are the benefits that can be gained from Individual Wheel Control?
2. What are the potential benefits that the Hybrid-Electric Vehicle will have over the existing QinetiQ conventional vehicle?

In order to answer the first question the intelligent mobility controlled vehicle will be compared to the Hybrid-Electric Vehicle with a fixed torque distribution. This will show the benefits of utilising IWC on the particular drive configuration.

To answer the second, the performance of the controlled HEV will be compared against that of the existing conventional vehicle, partially by use of the conventional drivetrain developed in Section 4.4 and partially using actual vehicle test data.

Both on-road and off-road testing will be performed in order to validate the operation and benefits of the intelligent mobility controller developed.

6.2 Comparison of On-road Responses

As with the preliminary testing conducted on the basic non-linear handling model, the tuned intelligent mobility controller with side-slip limiter will now be tested with respect to the on-road responses of the vehicle. Various manoeuvres will be tested with the aim of showing controller performance under a wide range of conditions, showing again the robustness inherent in the fuzzy logic control algorithms and the method of co-ordination. Due to the success of the partial validation of the vehicle model, it can be assumed that the on-road behaviour of the controller will be representative of its performance on an actual vehicle, especially during constant speed handling manoeuvres.

As before, the HEV model, with and without control, will be simulated to show the benefits of the controlled vehicle over the passive vehicle. In addition to this, the conventional vehicle will also be included in a number of simulations using either actual data from vehicle trials or through the use of the conventional drivetrain modelled in Chapter 4.

6.2.1 Split-μ Acceleration

The vehicle accelerates from 5 to 80km/h while the left set of tyres rest on a snow covered surface and the right set on dry asphalt. The conventional vehicle model with the locked differential and the HEV with and without control are all simulated undertaking the same manoeuvre. The results for yaw-rate are shown for the unladen and laden vehicle in figure 6.1 and 6.4 respectively. The vehicle paths and speeds responses are also presented (figures 6.2, 6.3, 6.5 and 6.6).

Results show that the controller is effective at reducing the yaw-rate error produced by the split-μ surface. Compared to the uncontrolled HEV, the controller reduces peak yaw-rate error by approximately 62% in the laden case and 73% in the unladen case. This results in reducing the corrective steering that the driver will need to apply to maintain the desired course. Although there is oscillation in the results for the unladen case, its effect on both forces felt by the driver is likely to be negligible compared to those felt through longitudinal acceleration.

Looking at the responses for the conventional vehicle, there is a surprising amount of yaw generated, considering the reduced torque capabilities of the driveline and the locked differential action. In fact, wheel-slip remains relatively low throughout the vehicle acceleration as the wheel on the low friction surface is prevented from spinning due to the effect of the locked differential. The yaw-rate is caused mainly by the difference in available tractive force at each wheel. A peak occurs each time the clutch is engaged after a gear change, as there is a large change in the torque applied to the wheels.

As would be expected, considering the torque capabilities of the conventional and hybrid-electric driveline, the acceleration performance of the HEV is much greater than that of the conventional vehicle as shown in figures 6.3 and 6.6. However, it should be noted that the gear change timing data provided by QinetiQ may not be representative of the vehicle in heavy acceleration. Despite the disruption of torque due to the gear change, reducing the vehicle acceleration performance, the torque capabilities of the conventional vehicle are not nearly as high as that of the HMED (see figure 4.30).

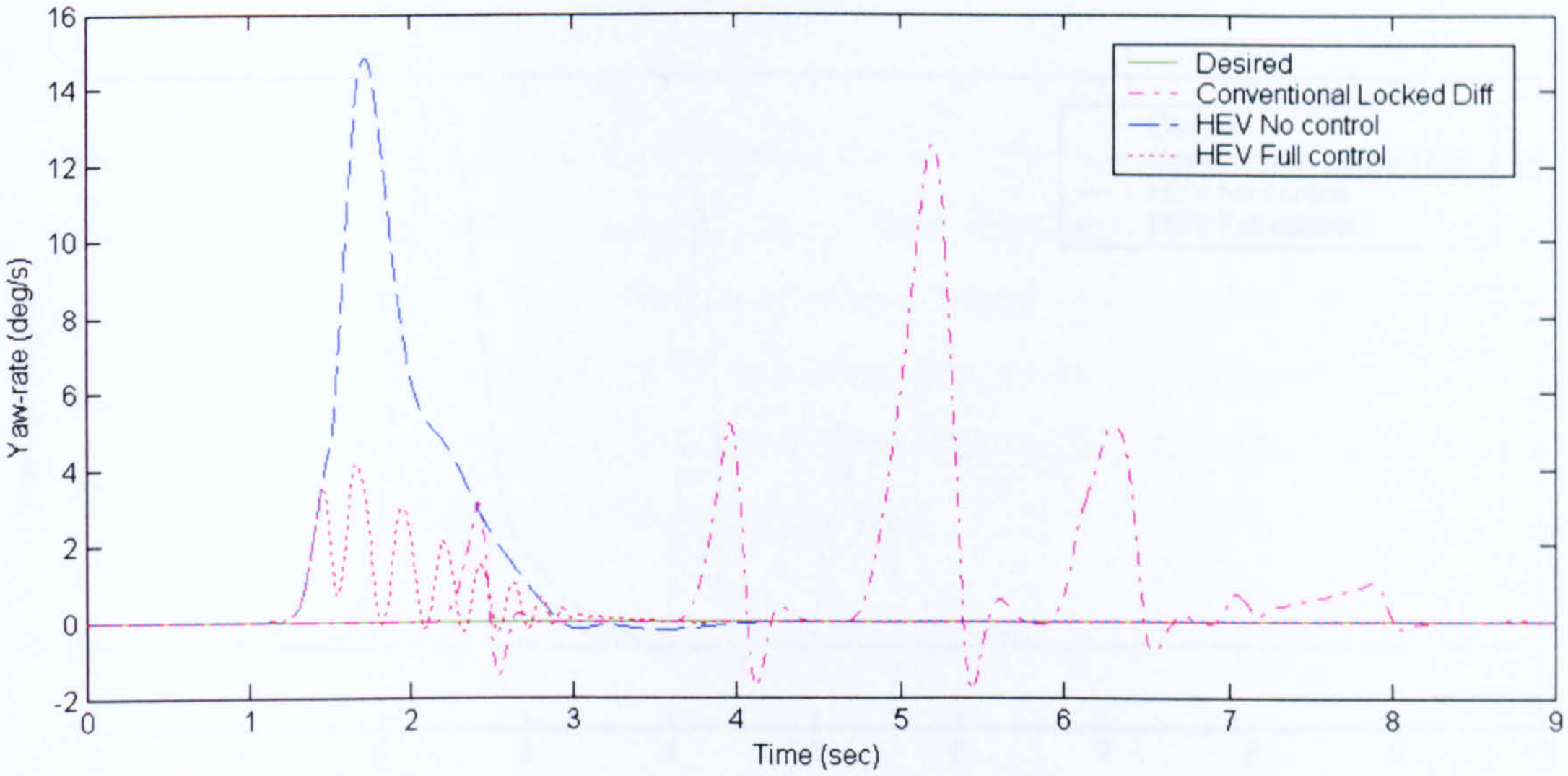

Fig. 6.1 Unladen yaw-rate response for acceleration on a split-μ surface

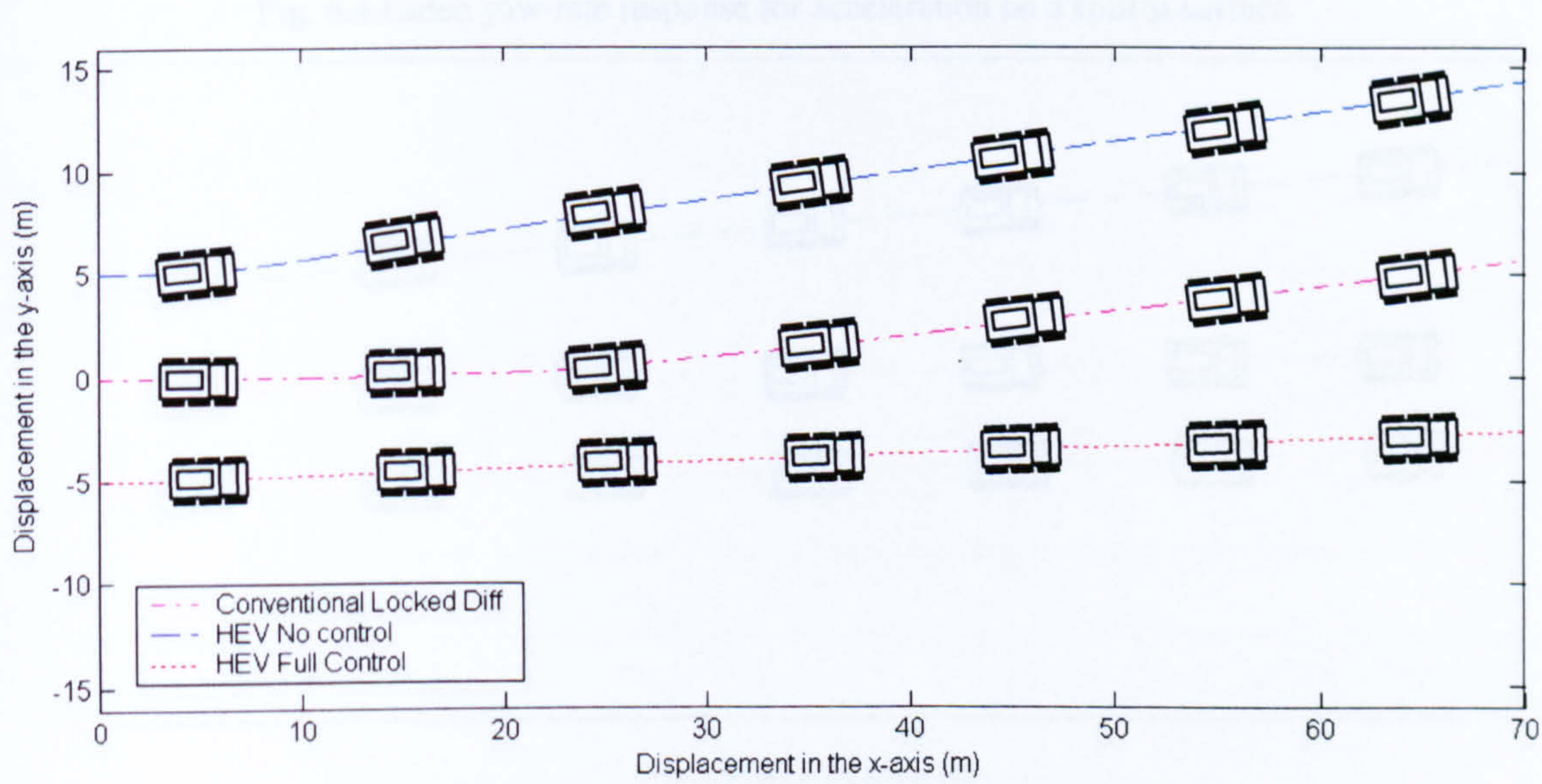

Fig. 6.2 Unladen vehicle path for acceleration on a split-μ surface

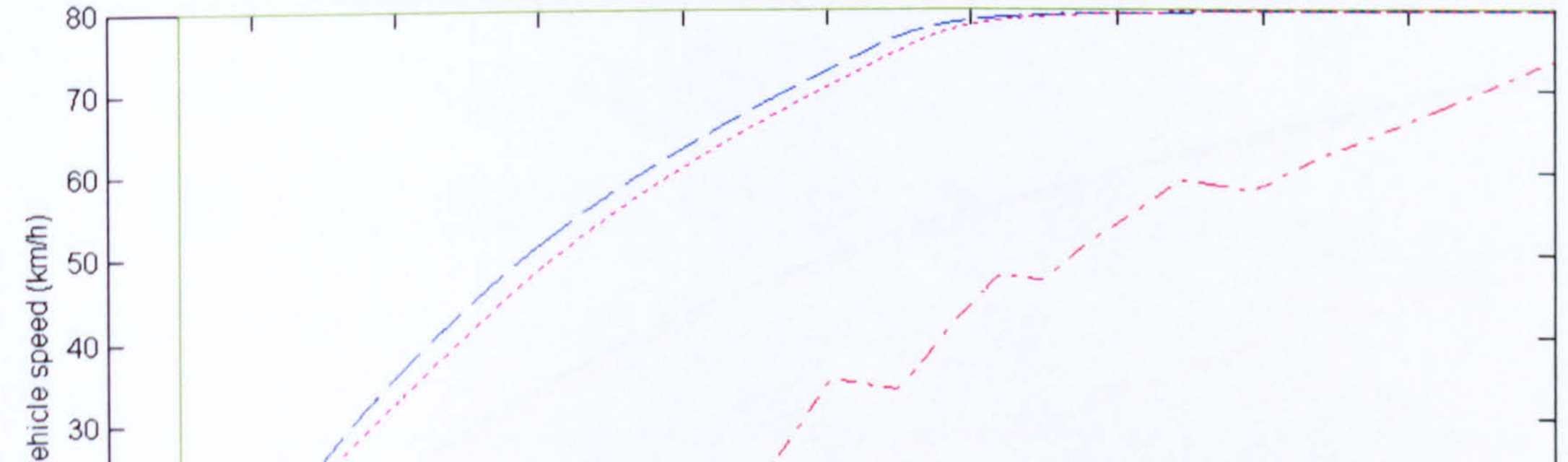

Fig. 6.3 Unladen vehicle speed response on split-μ surface

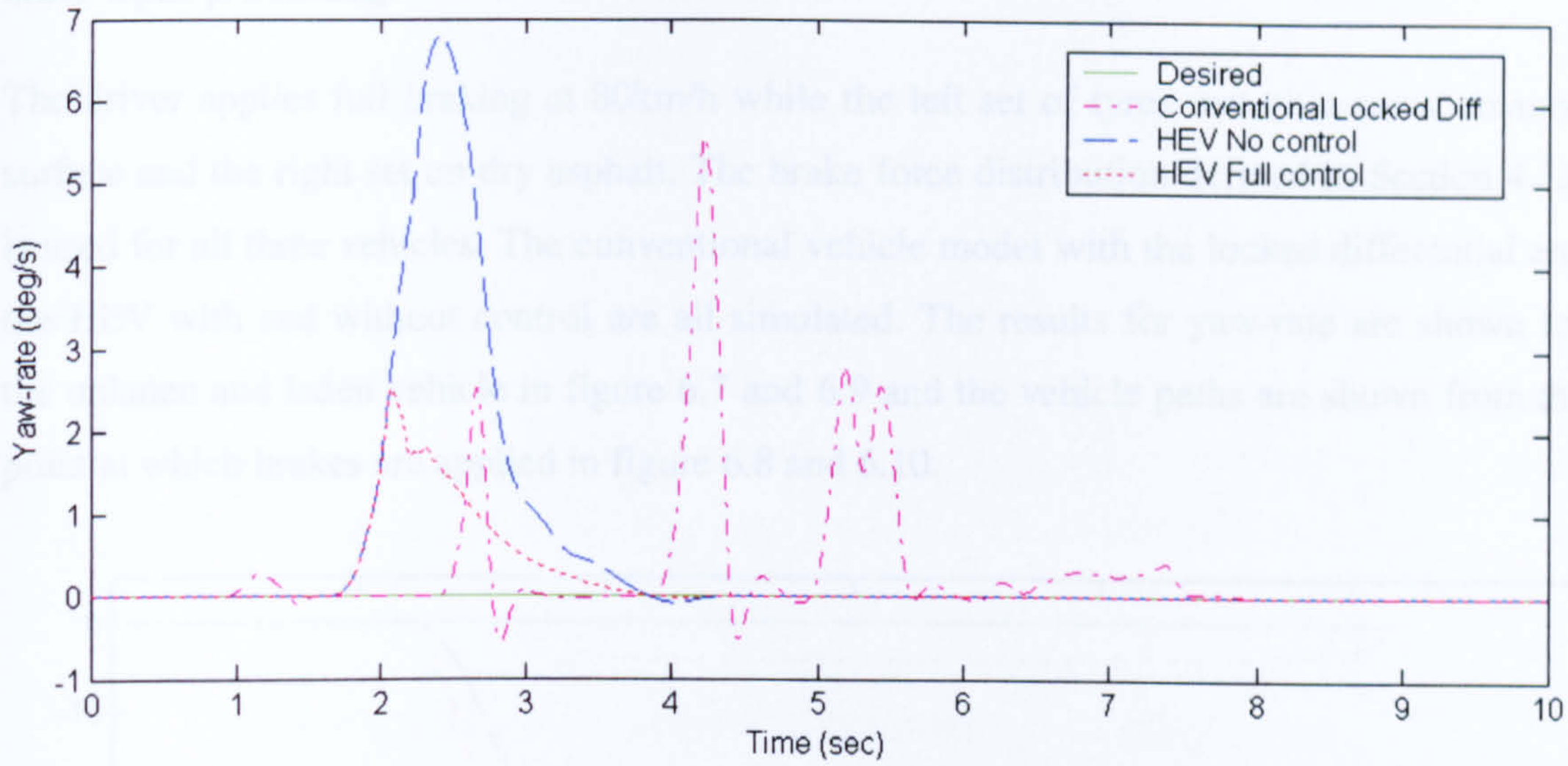

Fig. 6.4 Laden yaw-rate response for acceleration on a split-μ surface

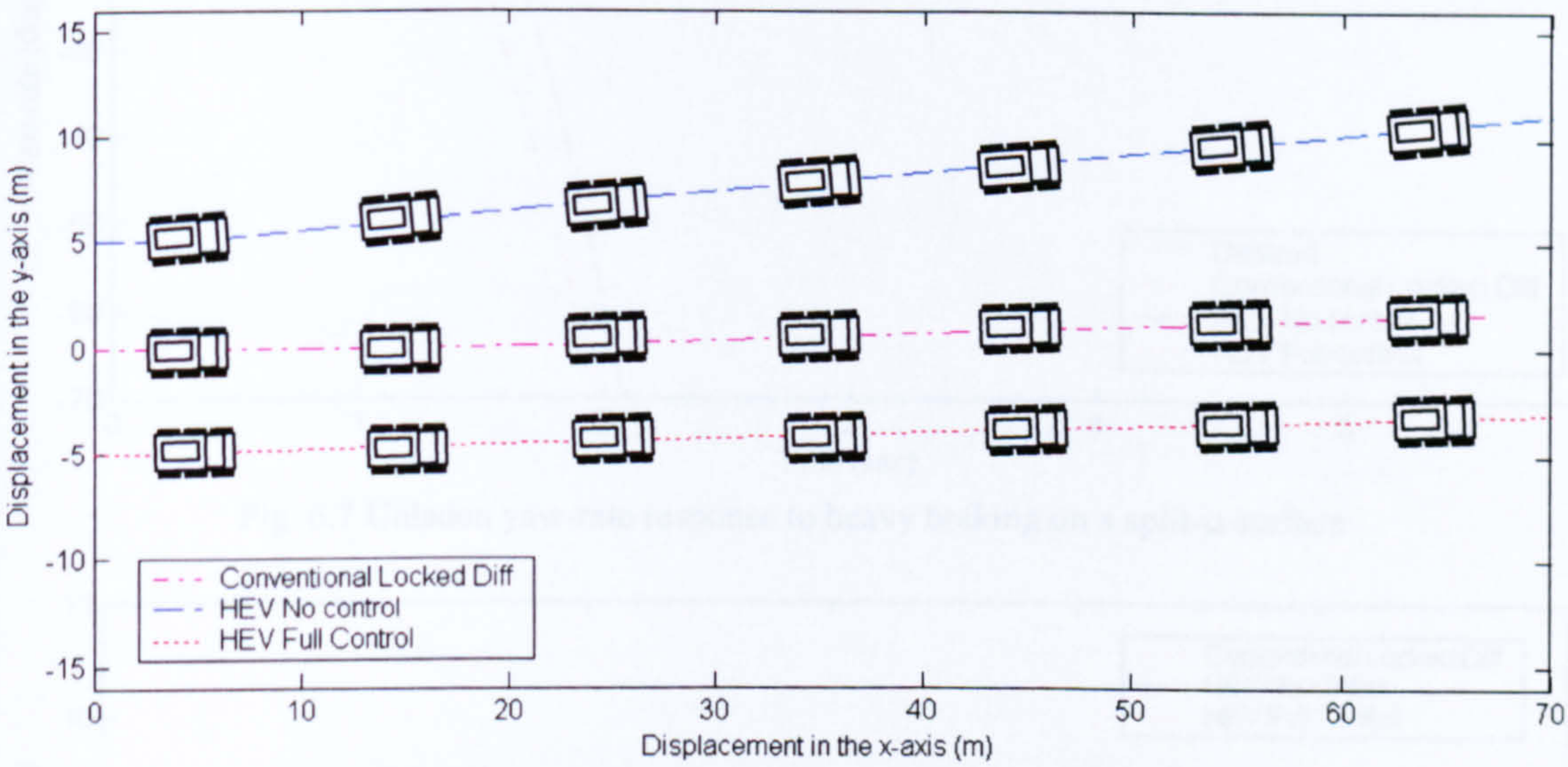

Fig. 6.5 Laden vehicle path for acceleration on a split-μ surface

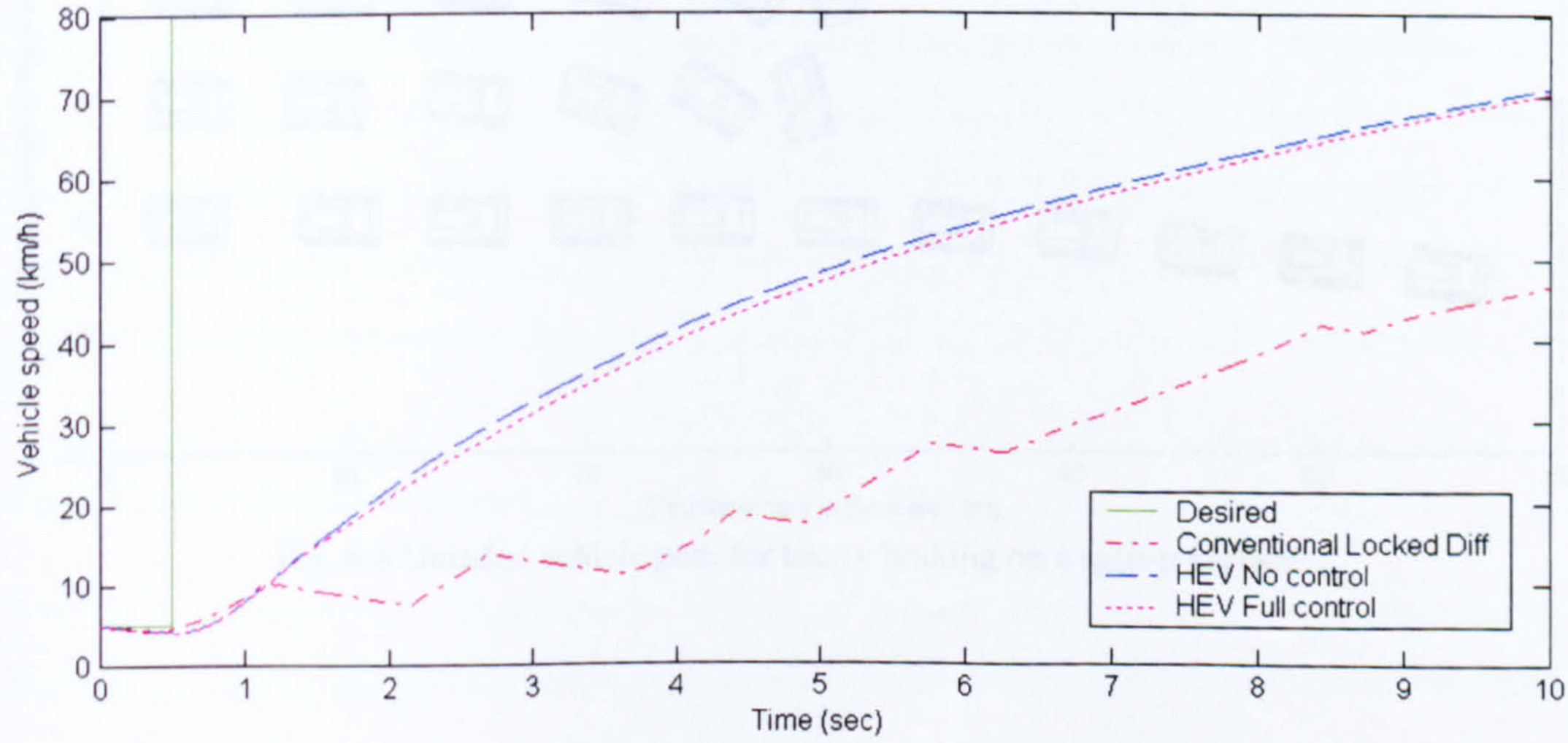

Fig. 6.6 Laden vehicle speed response on split-μ surface

6.2.2 Split-μ Braking

The driver applies full braking at 80km/h while the left set of tyres rest on a snow covered surface and the right set on dry asphalt. The brake force distribution derived in Section 4.2.4 is used for all three vehicles. The conventional vehicle model with the locked differential and the HEV with and without control are all simulated. The results for yaw-rate are shown for the unladen and laden vehicle in figure 6.7 and 6.9 and the vehicle paths are shown from the point at which brakes are applied in figure 6.8 and 6.10.

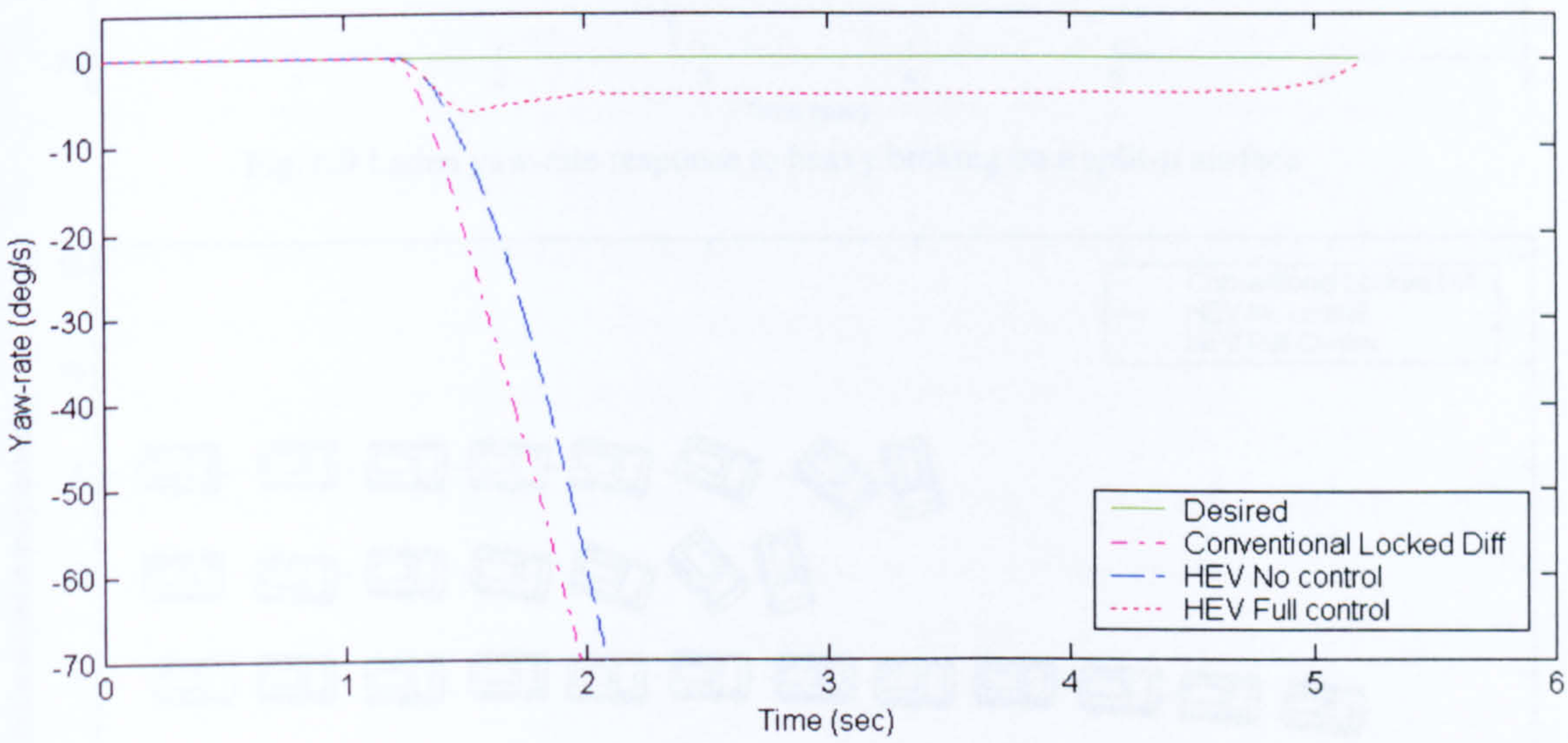

Fig. 6.7 Unladen yaw-rate response to heavy braking on a split-μ surface

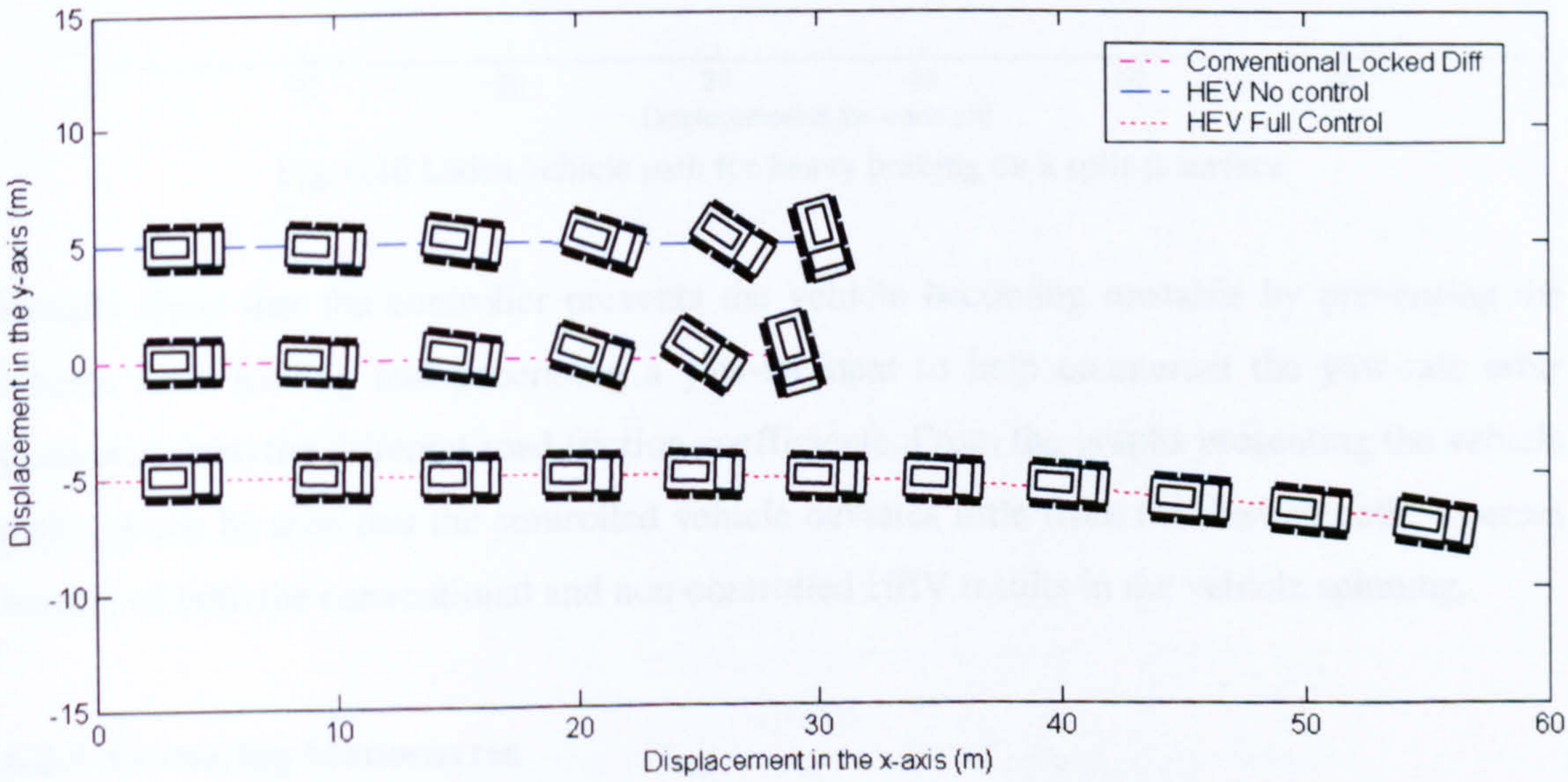

Fig. 6.8 Unladen vehicle path for heavy braking on a split-μ surface

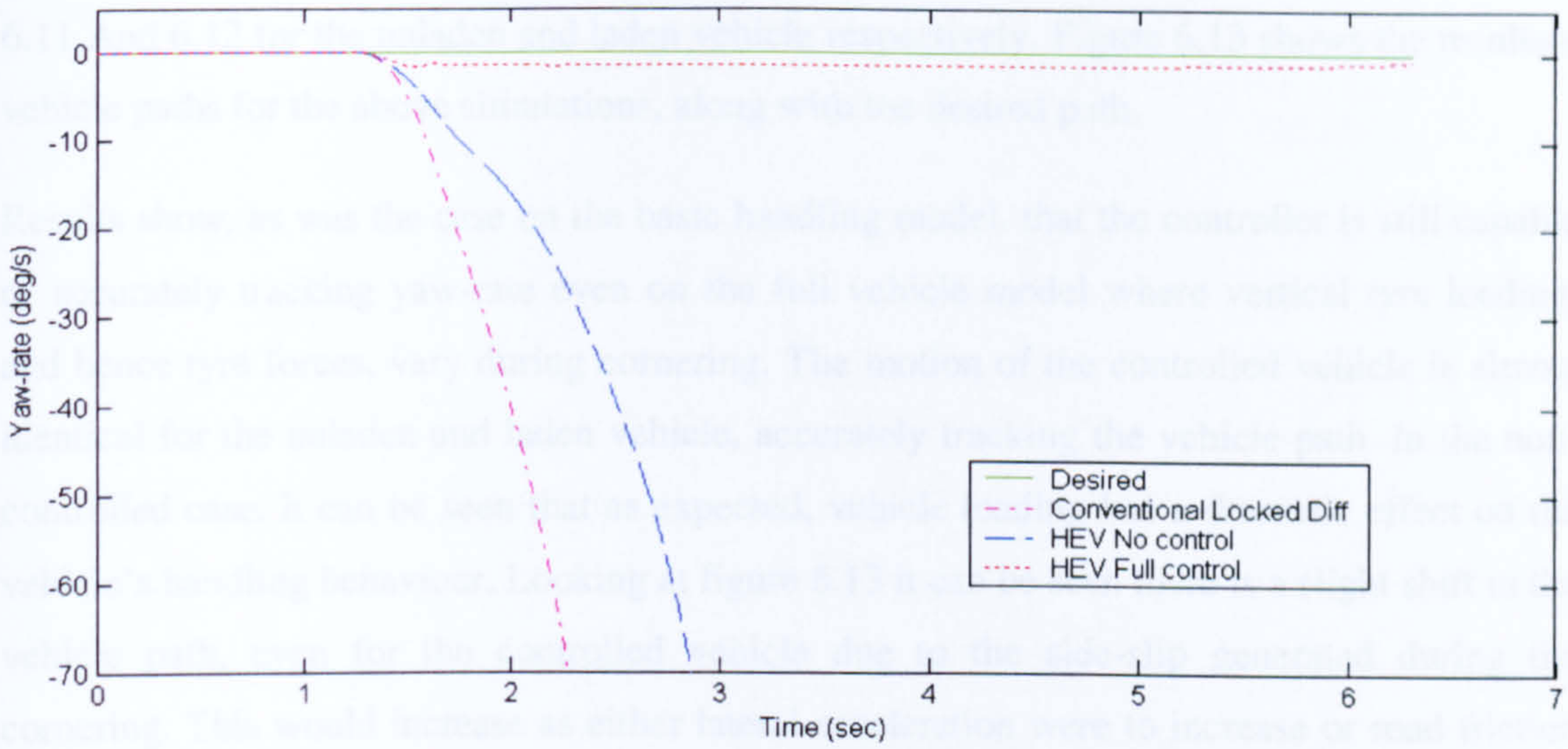

Fig. 6.9 Laden yaw-rate response to heavy braking on a split-μ surface

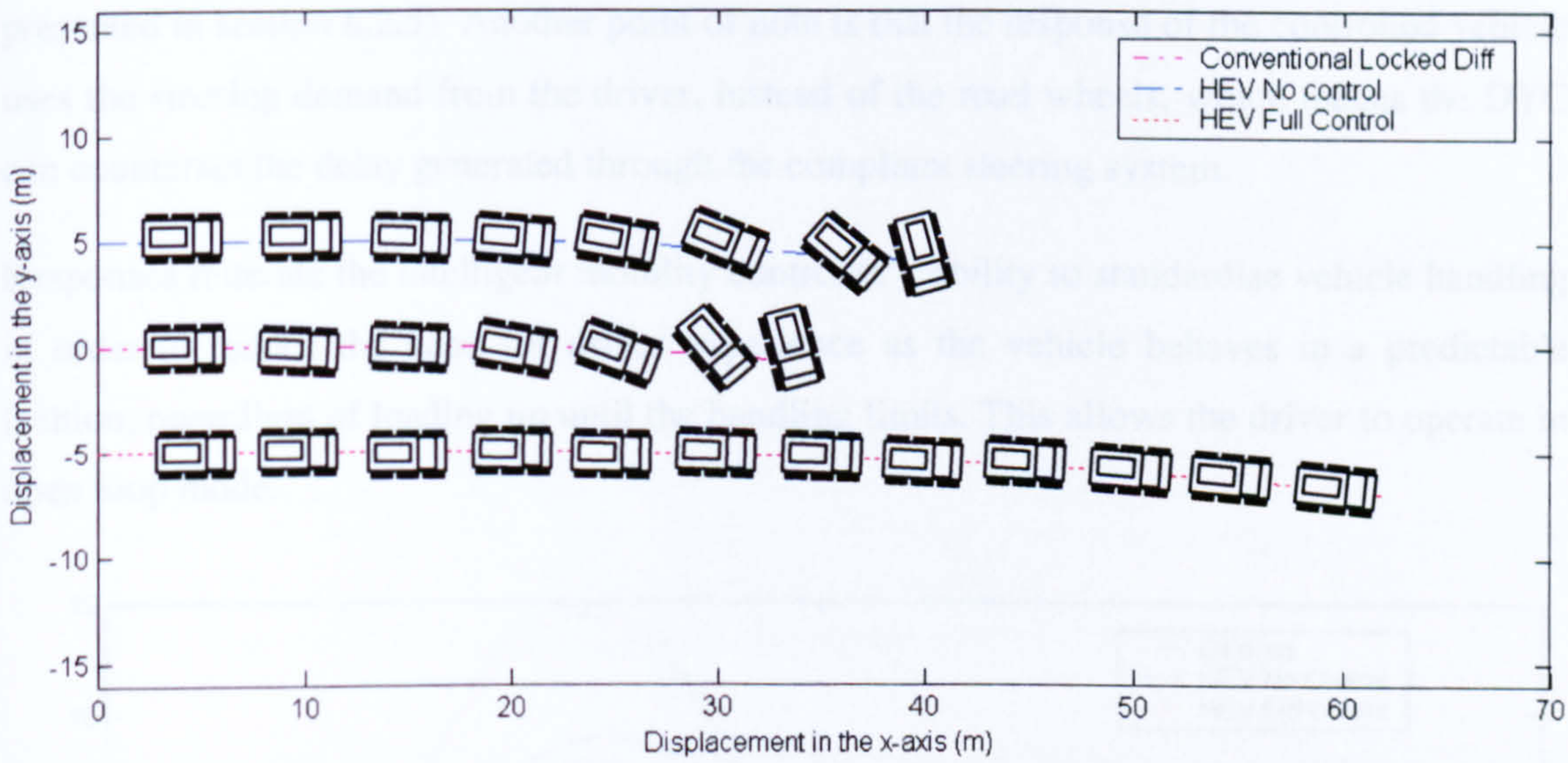

Fig. 6.10 Laden vehicle path for heavy braking on a split-μ surface

Results show that the controller prevents the vehicle becoming unstable by preventing the wheels from locking and generating a yaw-moment to help counteract the yaw-rate error generated from the different road friction coefficients. From the graphs presenting the vehicle paths, it can be seen that the controlled vehicle deviates little from the desired path, whereas motion of both the conventional and non-controlled HEV results in the vehicle spinning.

6.2.3 Cornering Manoeuvres

Firstly the uncontrolled and controlled HEV is simulated undertaking a single lane-change manoeuvre on dry asphalt at a speed of 80km/h. The yaw-rate responses are shown in figure

6.11 And 6.12 for the unladen and laden vehicle respectively. Figure 6.13 shows the resultant vehicle paths for the above simulations, along with the desired path.

Results show, as was the case on the basic handling model, that the controller is still capable of accurately tracking yaw-rate even on the full vehicle model where vertical tyre loading, and hence tyre forces, vary during cornering. The motion of the controlled vehicle is almost identical for the unladen and laden vehicle, accurately tracking the vehicle path. In the non-controlled case, it can be seen that as expected, vehicle loading has a dramatic effect on the vehicle's handling behaviour. Looking at figure 6.13 it can be seen there is a slight shift in the vehicle path, even for the controlled vehicle due to the side-slip generated during the cornering. This would increase as either lateral acceleration were to increase or road friction reduce up to a limit, at which point the yaw-rate limiter would take effect (as will be presented in section 6.2.5). Another point of note is that the response of the controlled vehicle uses the steering demand from the driver, instead of the road wheels, which means the DYC can counteract the delay generated through the compliant steering system.

Responses reiterate the intelligent mobility controller's ability to standardise vehicle handling in order to reduce the need for driver experience as the vehicle behaves in a predictable fashion, regardless of loading up until the handling limits. This allows the driver to operate in open loop mode.

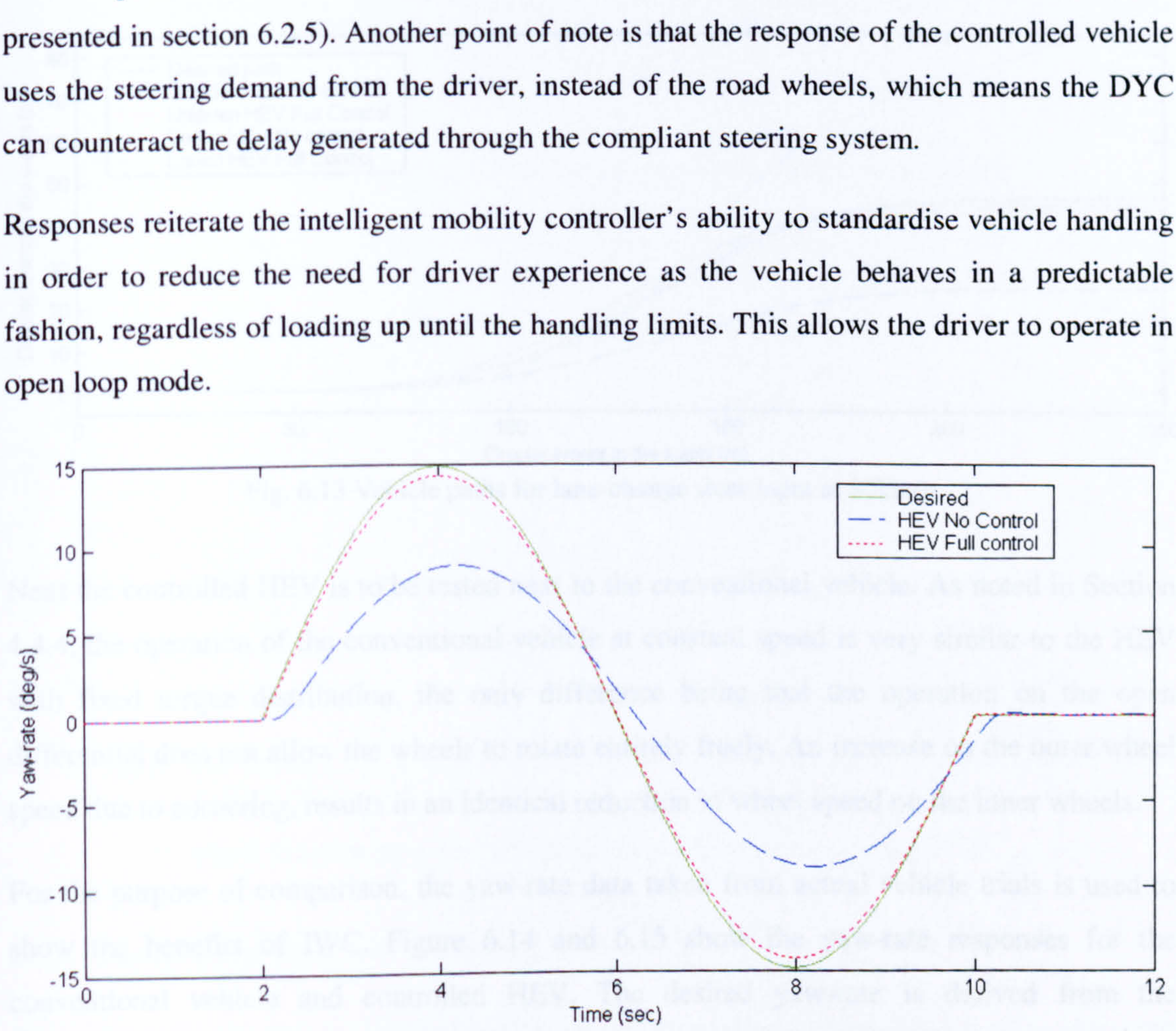

Fig. 6.11 Unladen yaw-rate response to lane-change steer input at 80km/h

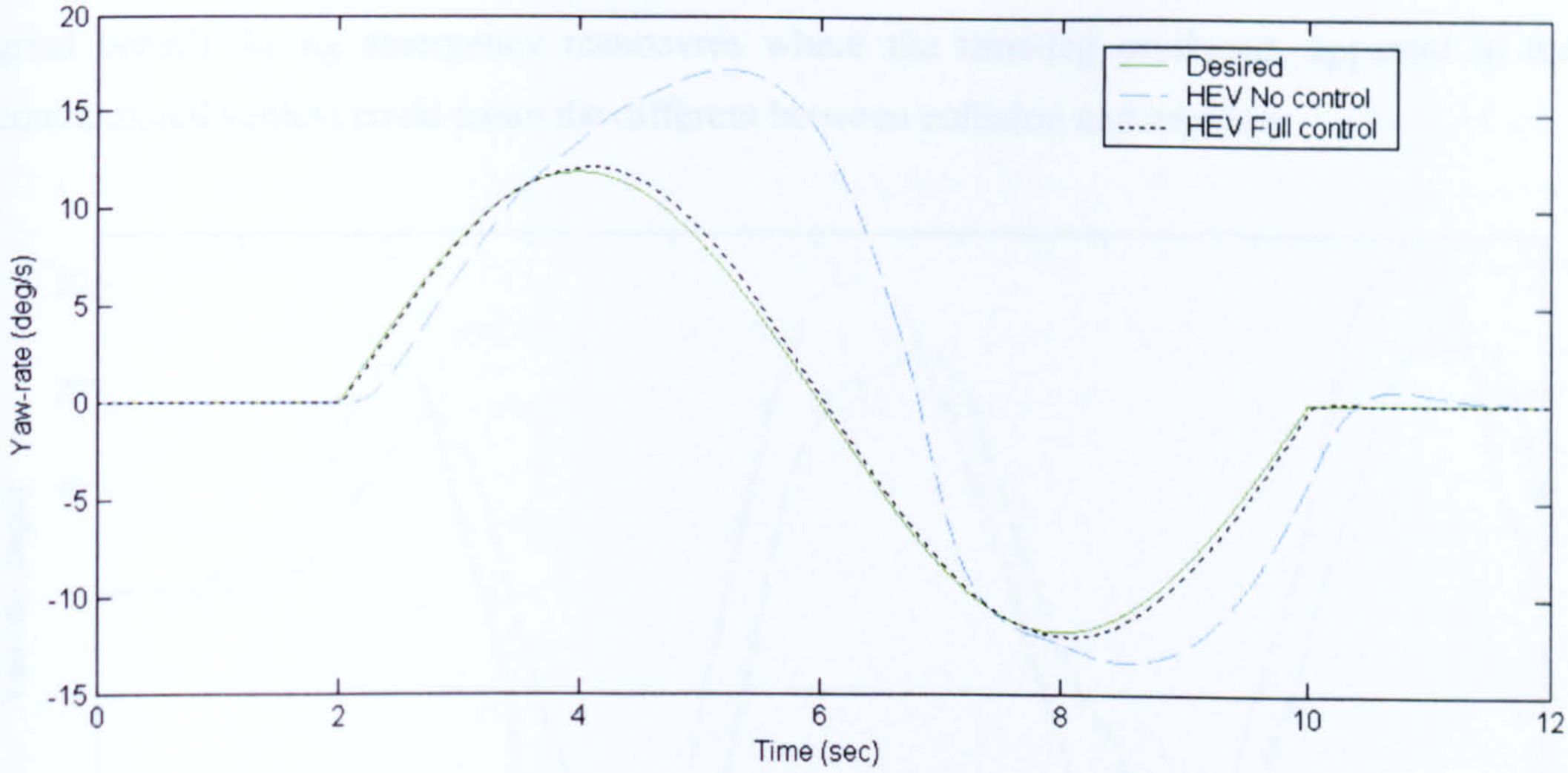

Fig. 6.12 Laden yaw-rate response to lane-change steer input at 80km/h

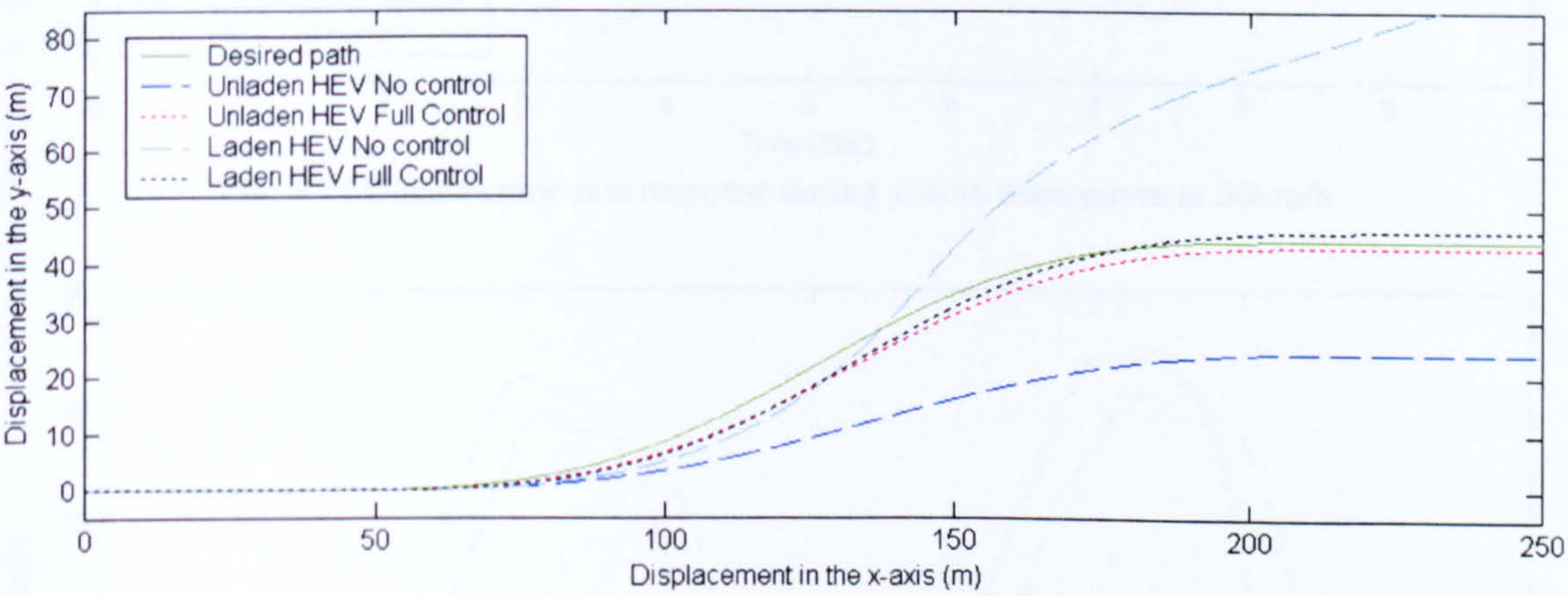

Fig. 6.13 Vehicle paths for lane-change steer input at 80km/h

Next the controlled HEV is to be tested next to the conventional vehicle. As noted in Section 4.4.4, the operation of the conventional vehicle at constant speed is very similar to the HEV with fixed torque distribution, the only difference being that the operation on the open differential does not allow the wheels to rotate entirely freely. An increase on the outer wheel speed due to cornering, results in an identical reduction in wheel speed on the inner wheels.

For the purpose of comparison, the yaw-rate data taken from actual vehicle trials is used to show the benefits of IWC. Figure 6.14 and 6.15 show the yaw-rate responses for the conventional vehicle and controlled HEV. The desired yaw-rate is derived from the handwheel steer input and the vehicle speed. Again it can be seen that the controller allows the vehicle to react rapidly to driver steer inputs and is able to track desired yaw-rate regardless of vehicle loading. This gives increased driver control over the vehicle and is of

great benefit during emergency manoevres where the time-lag produced, apparent in the conventional vehicle could mean the different between collision and evasion.

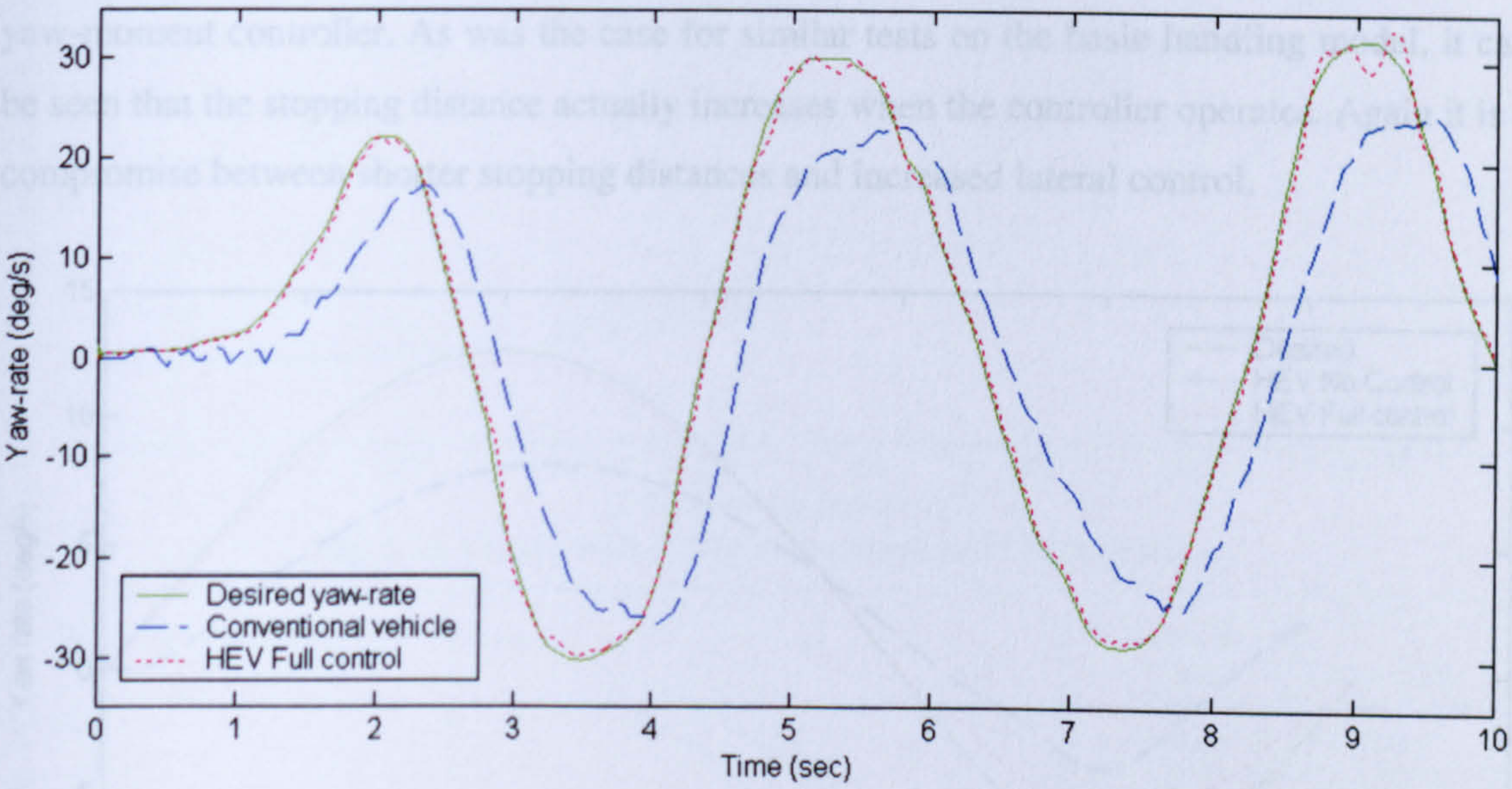

Fig. 6.14 Unladen yaw-rate response during slalom manoeuvre at 50km/h

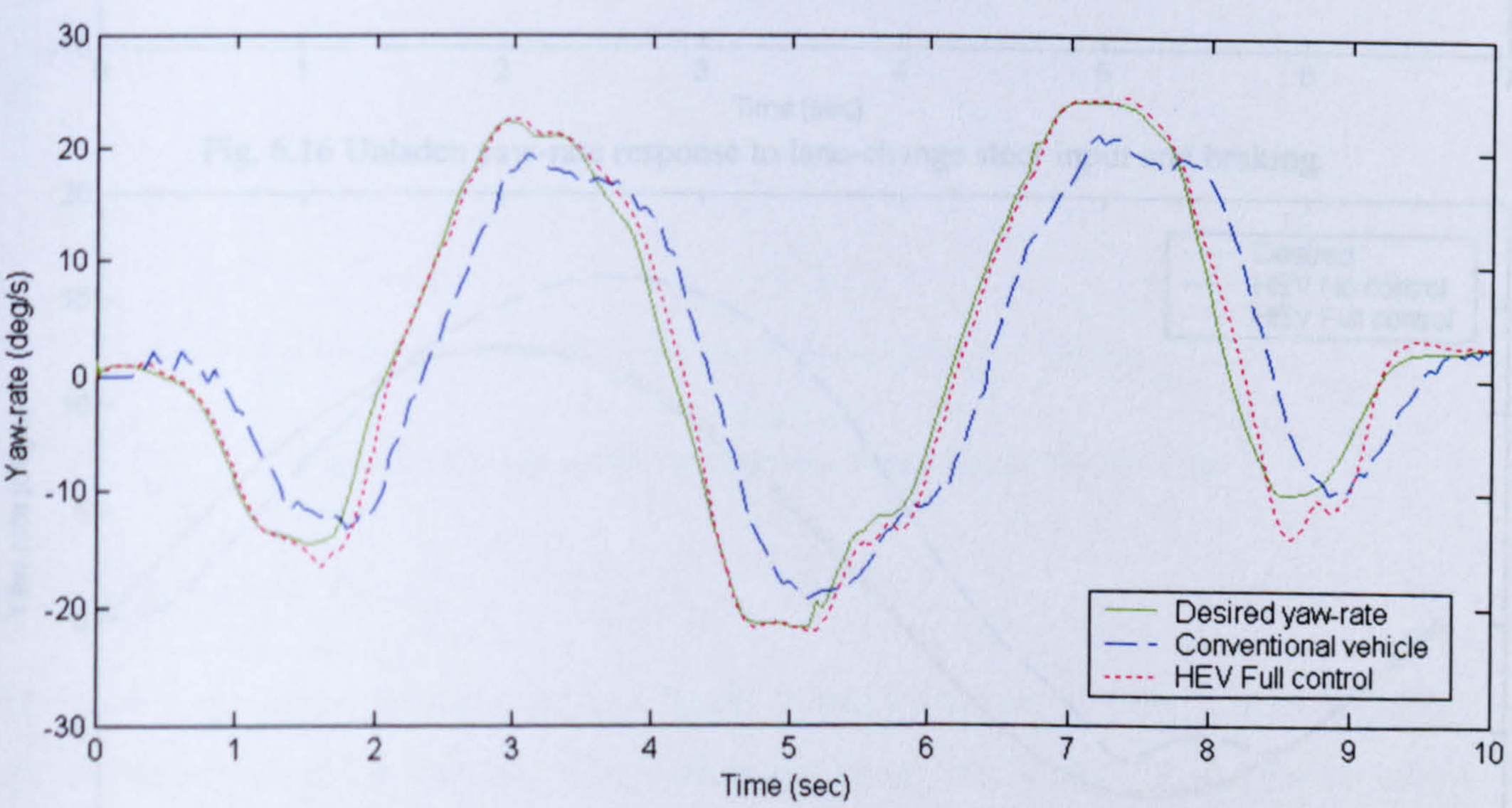

Fig. 6.15 Laden yaw-rate response during slalom manoeuvre at 50km/h

6.2.4 Combined Braking and Cornering

The vehicle is simulated undertaking a lane-change manoeuvre at 60km/h on a dry road surface when the full brakes are applied half way through the manoeuvre. Both the uncontrolled and the controlled HEV are simulated. The yaw-rate results are shown in figure 6.16 and 6.17. The vehicle paths are shown in figure 6.18 and the resultant vehicle speeds in figure 6.19.

Simulations show that even under the severe braking conditions, the controller can achieve good yaw-rate tracking, this is especially evident for the laden vehicle. The controller allows the desired path to be followed, showing the collaboration between the ABS systems and the yaw-moment controller. As was the case for similar tests on the basic handling model, it can be seen that the stopping distance actually increases when the controller operates. Again it is a compromise between shorter stopping distances and increased lateral control.

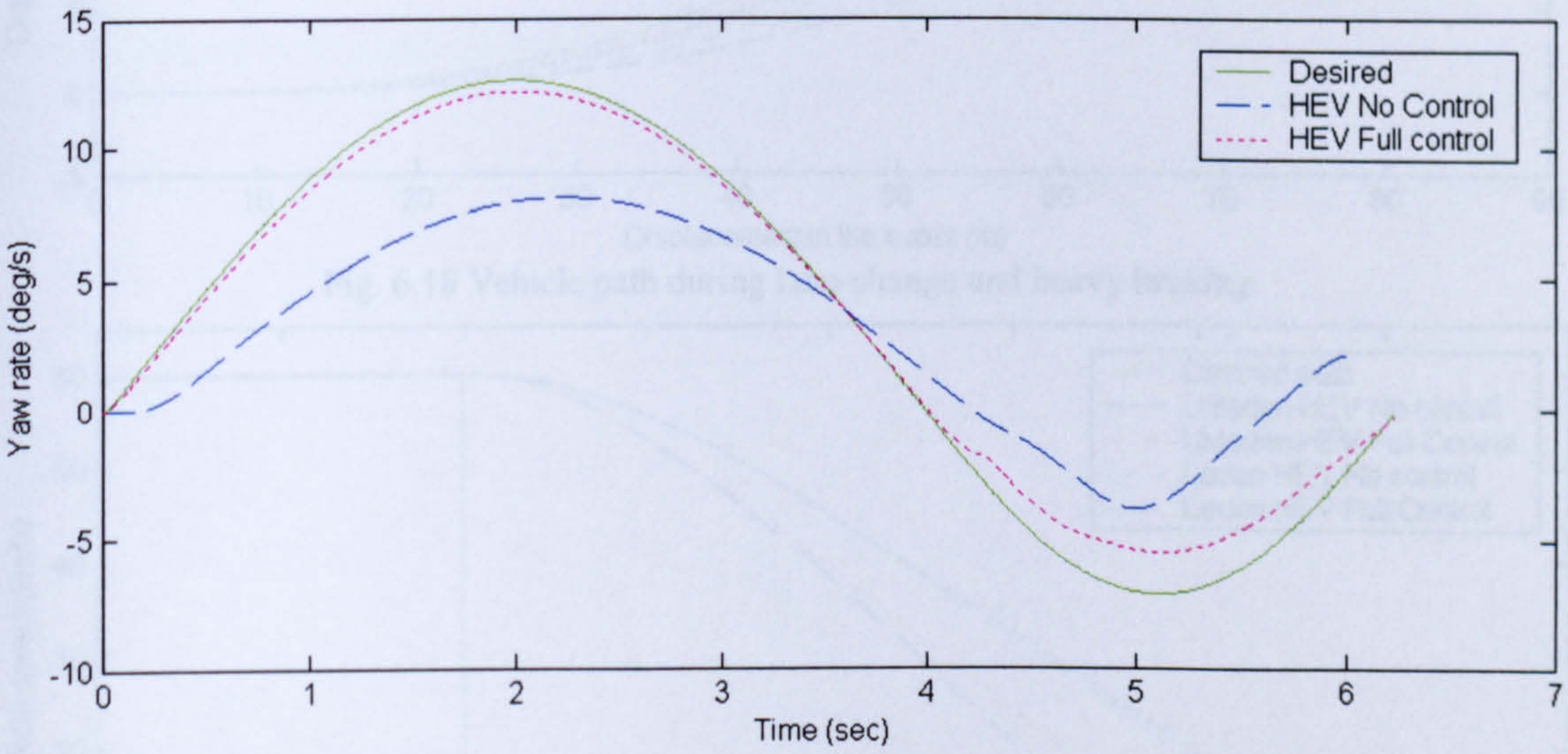

Fig. 6.16 Unladen yaw-rate response to lane-change steer input and braking

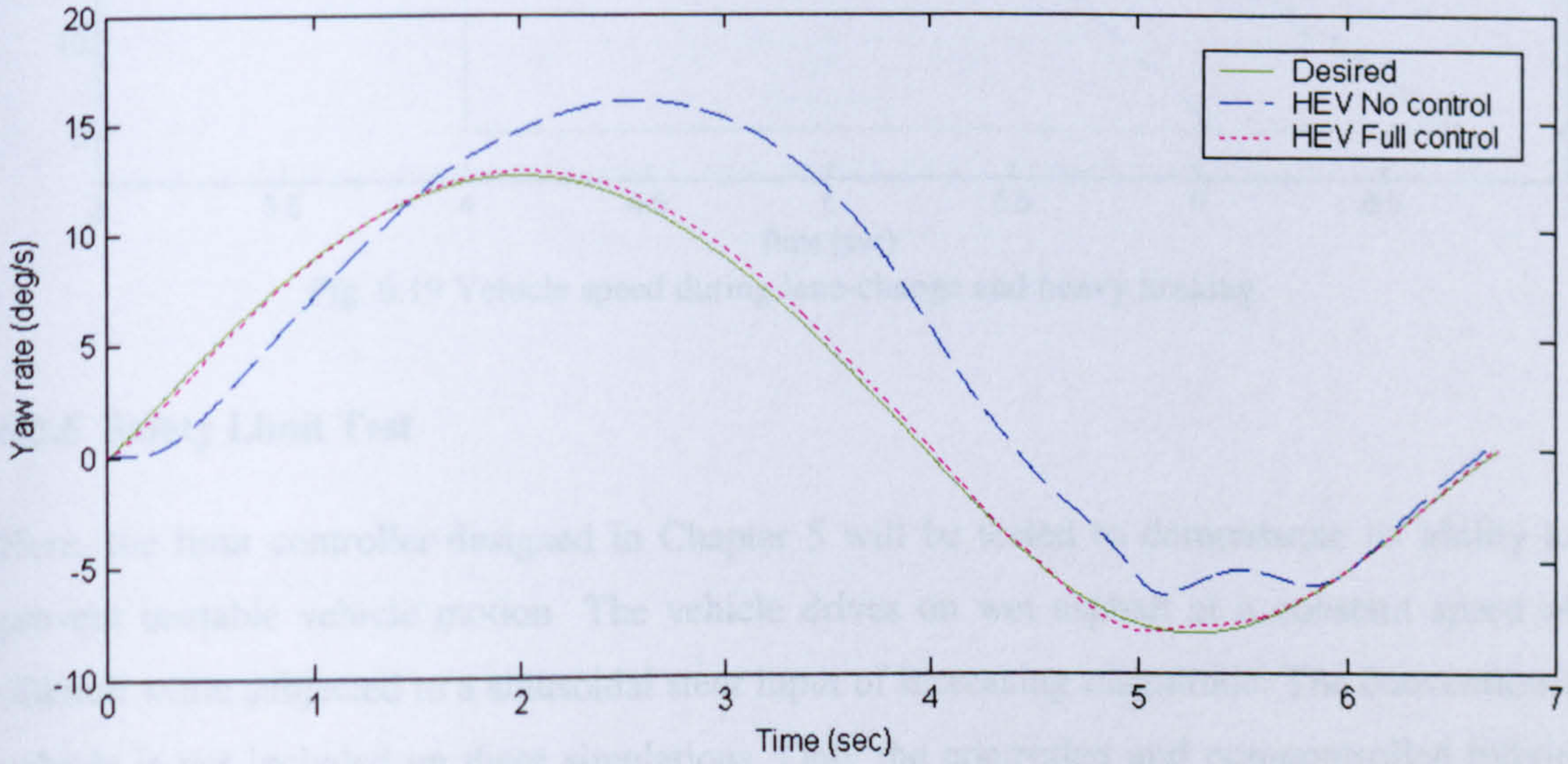

Fig. 6.17 Laden yaw-rate response to lane-change steer input and braking

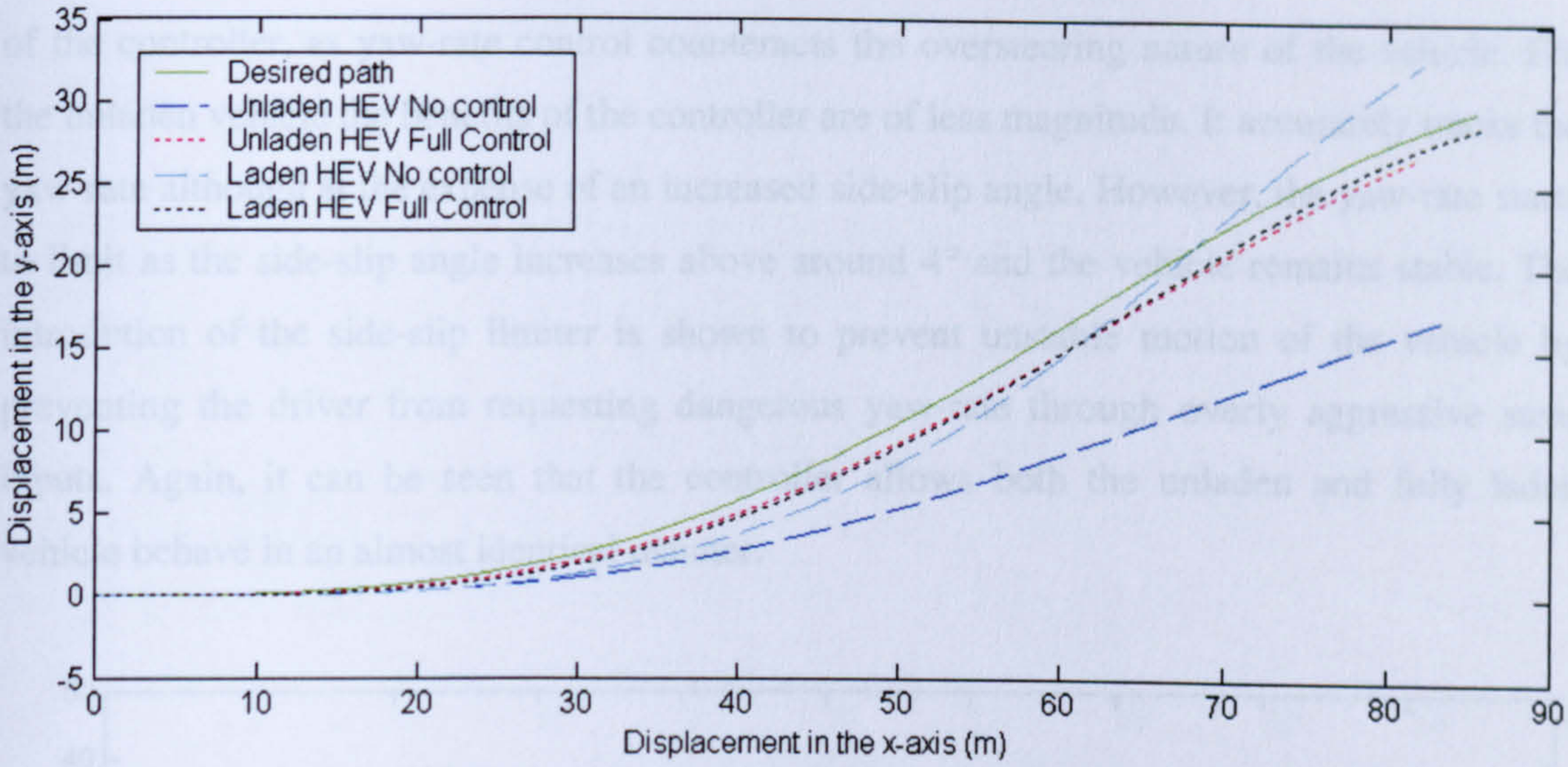

Fig. 6.18 Vehicle path during lane-change and heavy braking

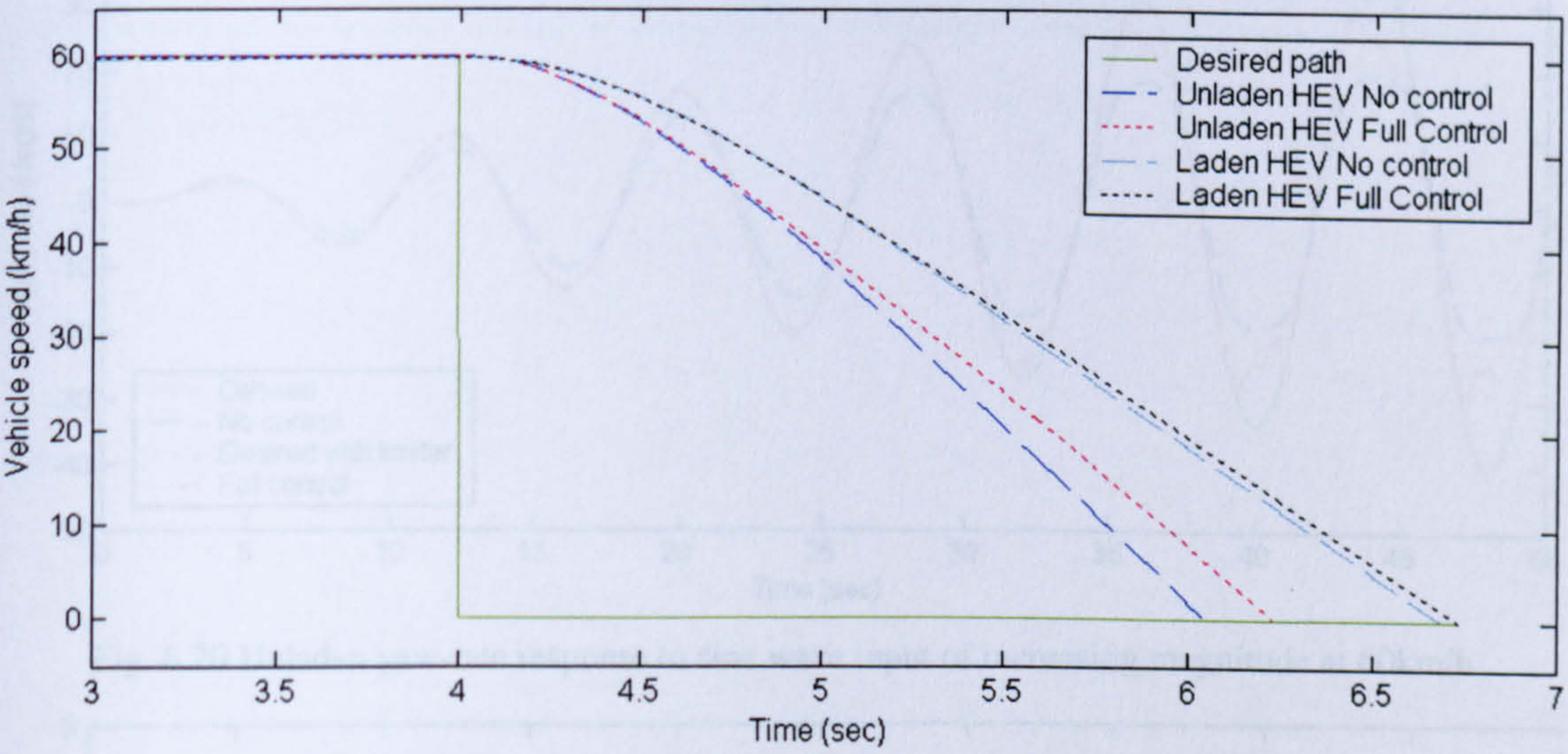

Fig. 6.19 Vehicle speed during lane-change and heavy braking.

6.2.5 Safety Limit Test

Here, the limit controller designed in Chapter 5 will be tested to demonstrate its ability to prevent unstable vehicle motion The vehicle drives on wet asphalt at a constant speed of 60km/h while subjected to a sinusoidal steer input of increasing magnitude. The conventional vehicle is not included on these simulations. Only the controlled and non-controlled hybrid vehicle are simulated as the handling limits during constant speed are relatively unaffected by the drivetrain. Figure 6.20 and 6.22 show the yaw-rate responses and figure 6.21 and 6.23 show the side-slip angle responses for the unladen and laden vehicle respectively.

In both cases it can be seen that the controller follows the desired yaw-rate up until the side-slip angle reaches its boundaries conditions. Again the laden case shows the greater potential

of the controller, as yaw-rate control counteracts the oversteering nature of the vehicle. For the unladen vehicle the benefits of the controller are of less magnitude. It accurately tracks the yaw-rate although at the expense of an increased side-slip angle. However, the yaw-rate starts to limit as the side-slip angle increases above around 4° and the vehicle remains stable. The introdution of the side-slip limiter is shown to prevent unstable motion of the vehicle by preventing the driver from requesting dangerous yaw-rate through overly aggressive steer inputs. Again, it can be seen that the controller allows both the unladen and fully laden vehicle behave in an almost identical manner.

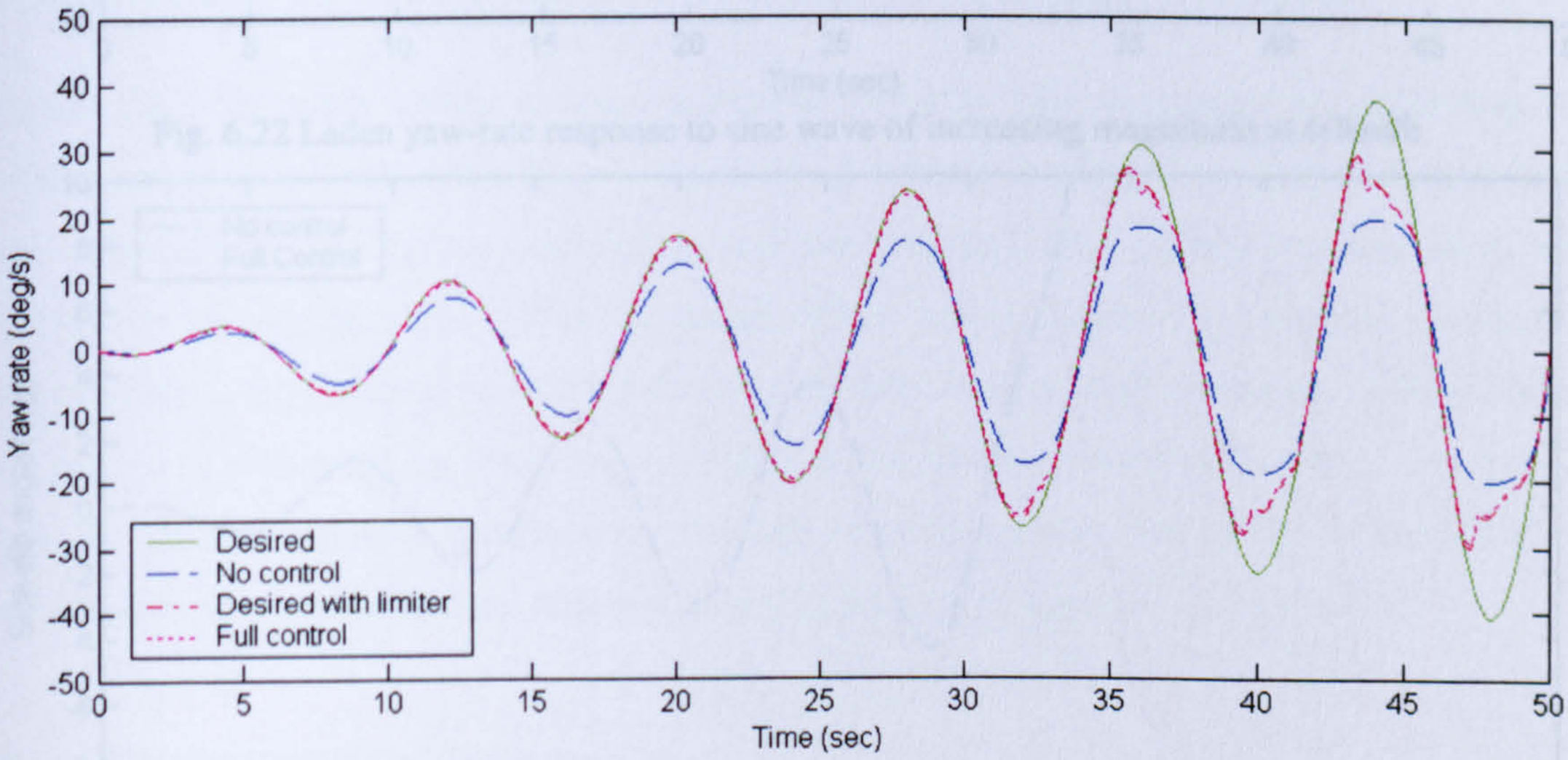

Fig. 6.20 Unladen yaw-rate response to sine wave input of increasing magnitude at 60km/h

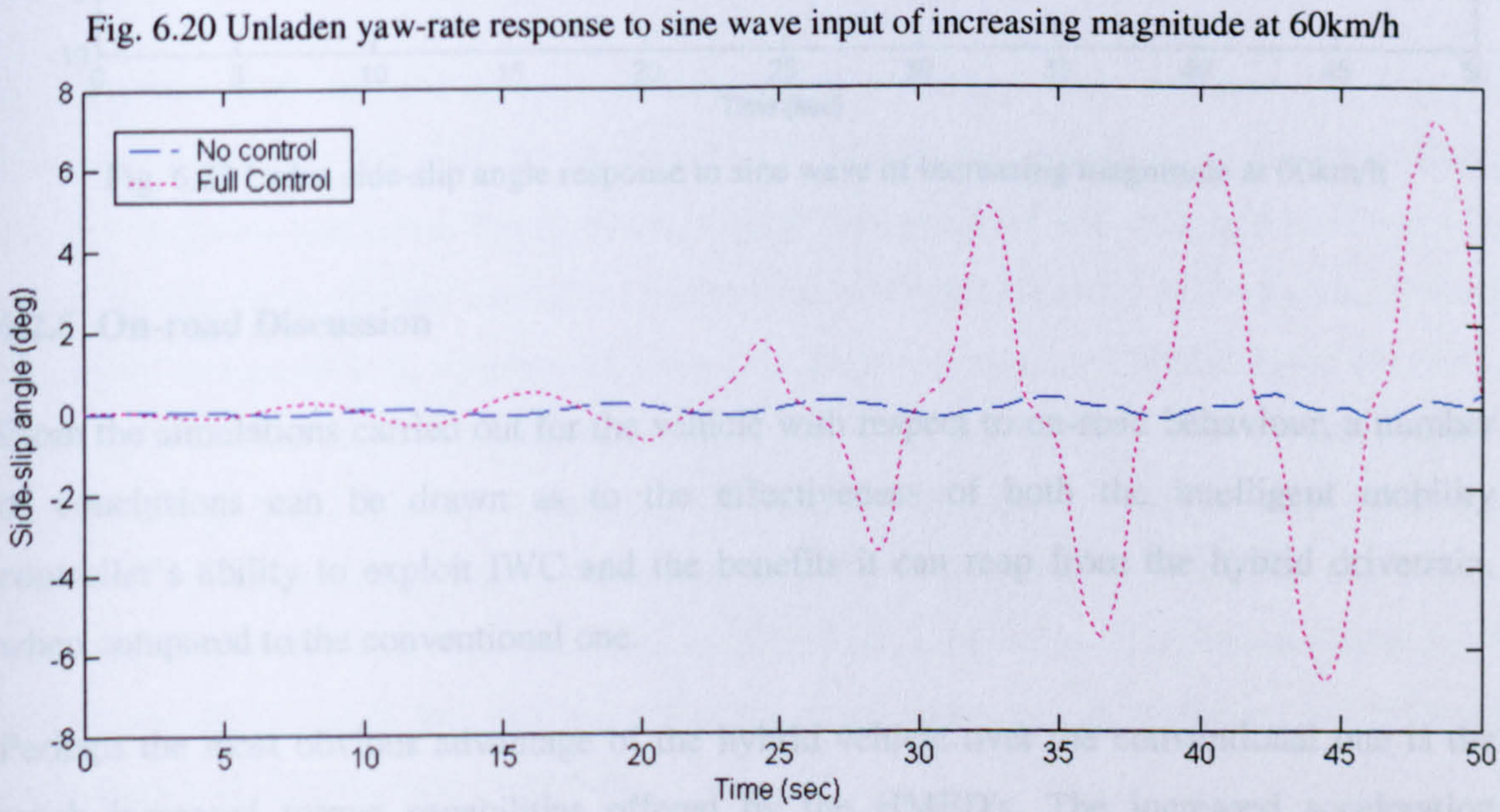

Fig. 6.21 Unladen side-slip angle response to sine wave of increasing magnitude at 60km/h

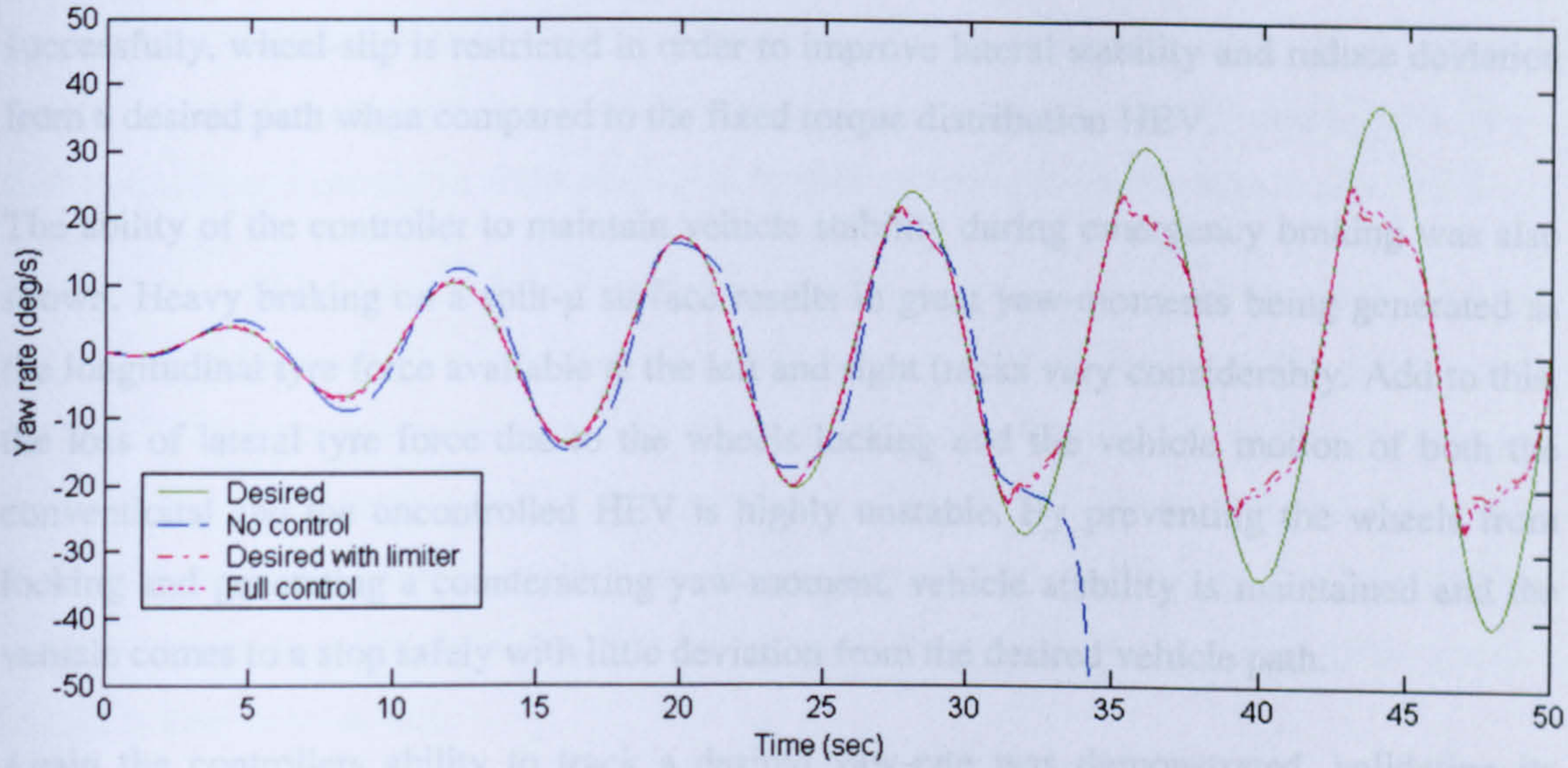

Fig. 6.22 Laden yaw-rate response to sine wave of increasing magnitude at 60km/h

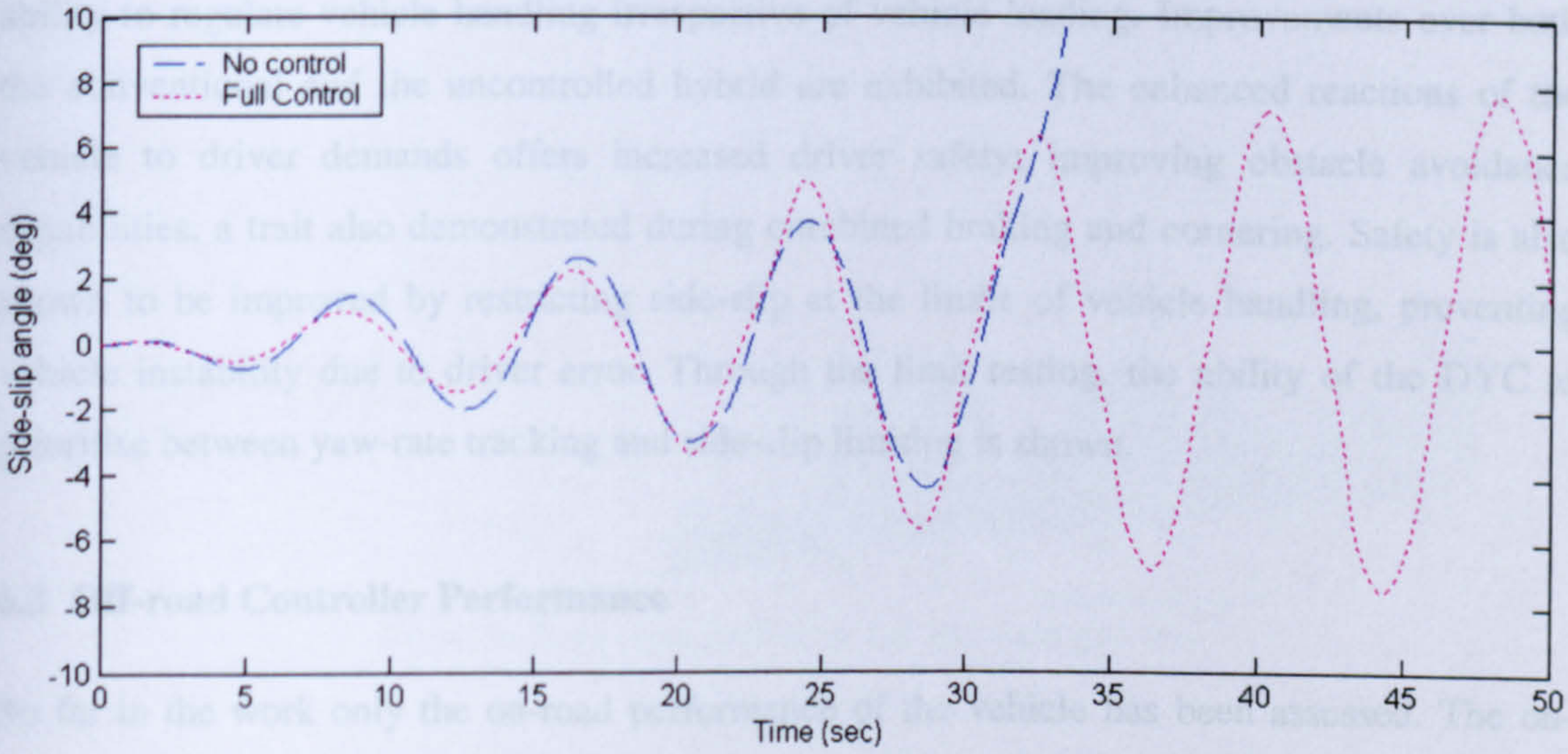

Fig. 6.23 Laden side-slip angle response to sine wave of increasing magnitude at 60km/h

6.2.6 On-road Discussion

From the simulations carried out for the vehicle with respect to on-road behaviour, a number of conclusions can be drawn as to the effectiveness of both the intelligent mobility controller's ability to exploit IWC and the benefits it can reap from the hybrid drivetrain, when compared to the conventional one.

Perhaps the most obvious advantage of the hybrid vehicle over the conventional one is the much increased torque capabilities offered by the HMED's. The increased acceleration performance gives the HEV a greater potential for logistics support over the ICE powered vehicle, reducing time taken to get from A to B. By regulating this torque capability

successfully, wheel-slip is restricted in order to improve lateral stability and reduce deviation from a desired path when compared to the fixed torque distribution HEV.

The ability of the controller to maintain vehicle stability during emergency braking was also shown. Heavy braking on a split-μ surface results in great yaw-moments being generated as the longitudinal tyre force available at the left and right tracks vary considerably. Add to this, the loss of lateral tyre force due to the wheels locking and the vehicle motion of both the conventional and the uncontrolled HEV is highly unstable. By preventing the wheels from locking and generating a counteracting yaw-moment, vehicle stability is maintained and the vehicle comes to a stop safely with little deviation from the desired vehicle path.

Again the controllers ability to track a desired yaw-rate was demonstrated, validating its ability to regulate vehicle handling irrespective of vehicle loading. Improvements over both the conventional and the uncontrolled hybrid are exhibited. The enhanced reactions of the vehicle to driver demands offers increased driver safety; improving obstacle avoidance capabilities, a trait also demonstrated during combined braking and cornering. Safety is also shown to be improved by restricting side-slip at the limits of vehicle handling, preventing vehicle instability due to driver error. Through the limit testing, the ability of the DYC to prioritise between yaw-rate tracking and side-slip limiting is shown.

6.3 Off-road Controller Performance

So far in the work only the on-road performance of the vehicle has been assessed. The on-road test procedures are outlined in section 2.2. Due to the intended use of the vehicle, offering logistics support to the frontline, a good percentage of the vehicle's time spent in operation will be in off-road situations. As has been outlined previously in the thesis, off-road behaviour is impossible to simulate with any great degree of accuracy. Modelling of the tyre's interaction with the earth is at present, extremely limited, especially during combined traction and cornering. Other than implementing the controller on the actual vehicle and recording objective and subjective data from the sensors and driver, there is no way to fully validate the controller's operation in an off-road environment. There is, however a certain amount of basic vehicle simulation work that can be carried out to go some way to validating the off-road performance of the proposed controller.

In Takahashi and Pacejka (1987) the tyre response to uneven road surfaces during cornering is investigated it is noted that there is loss in side force available at the tyre due to the effect of the time-varying relaxation length, which is dependent of vehicle load. This variation is

modelled as a third order polynomial. Unfortunately, in order to model this variation in relaxation length, empirical data must be retrieved from testing, which is unavailable for the tyre in question. Instead, the fixed relaxation lengths are used as outlined in Section 4.2.5.

The vehicle will be simulated undertaking various manoeuvres while subjected to a random road input and time varying road friction coefficients. A method similar to that conducted by Cooke (1996) for combined assessment of handling and ride. Road input profiles are shown in figure 6.24 and the varying values of μ are shown in figure 6.25 for the left and right tracks. Note that the lower friction coefficients tend to occur when road height is lowest and the greatest values occur on the higher parts of the surface, potentially simulating rocks sticking out from mud or loose dirt.

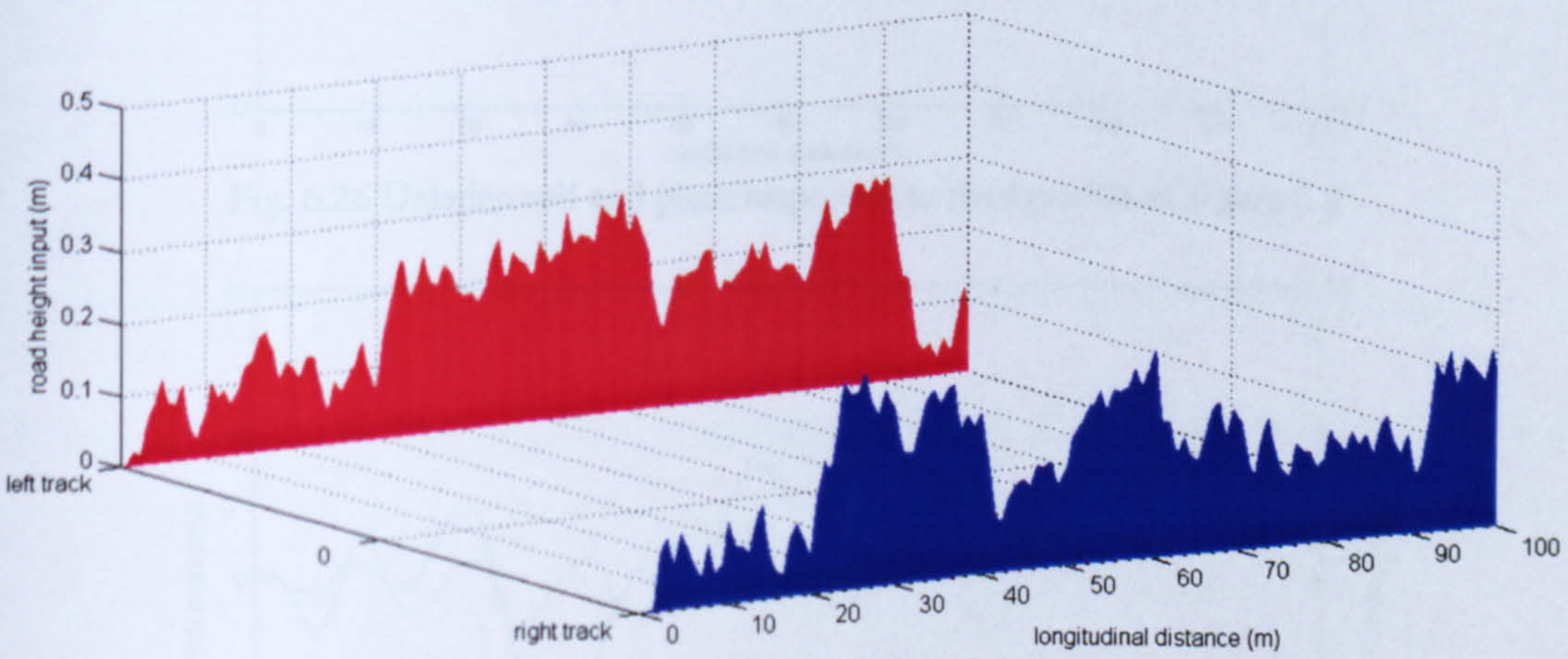

Fig. 6.24 Road input profile for left and right tyre sets

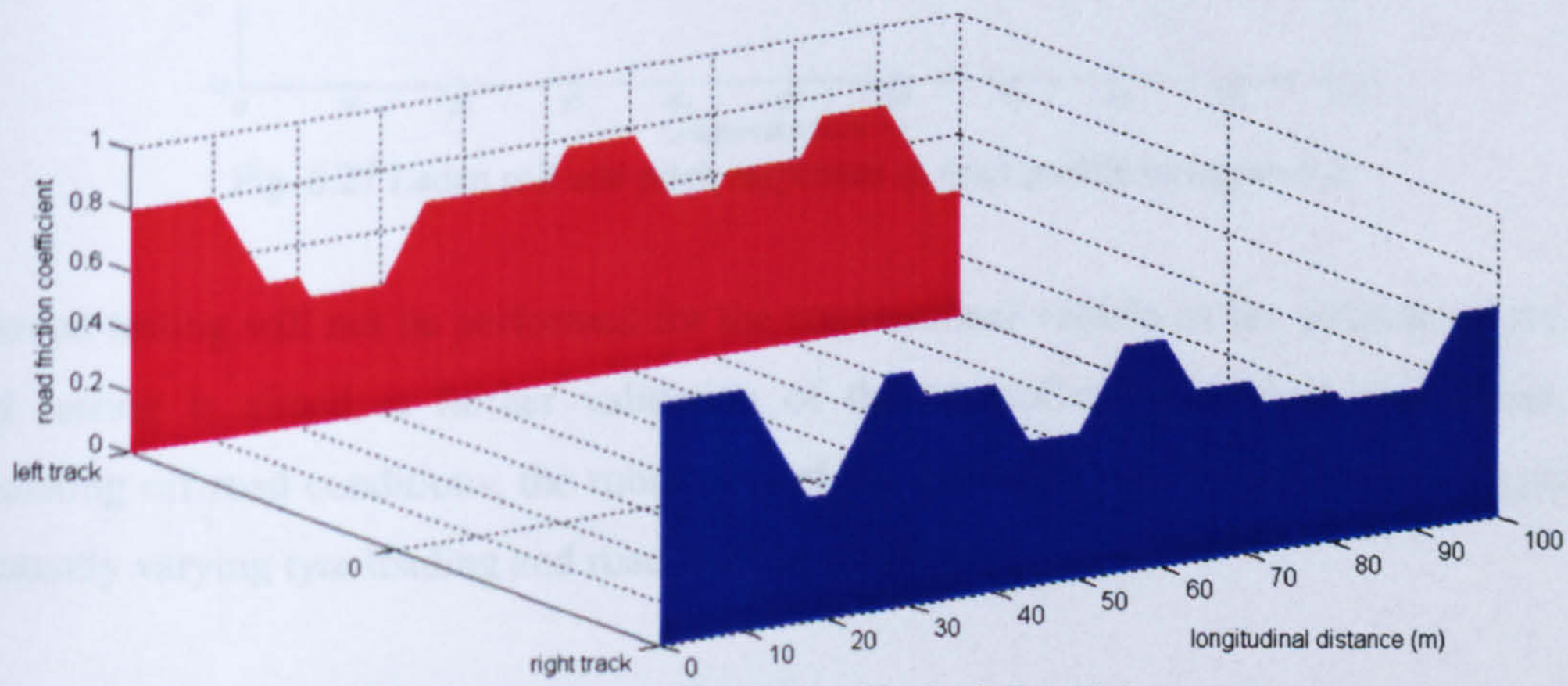

Fig. 6.25 Road friction coefficient profile for left and right tyre sets

Figure 6.26 and figure 6.27 show the roll and pitch motions for the vehicle when driving along the road surface at 60km/h for the unladen and laden vehicle respectively. As would be expected the laden response is much more damped than the unladen one, due to the larger

inertia's involved. Comparison of these responses with some presented in Huh *et al.* (2000) for a similar sized vehicle traversing a road surface of roughly the same magnitude, shows that the roll and pitch angles are of the scale that would be expected from the vehicle under such conditions.

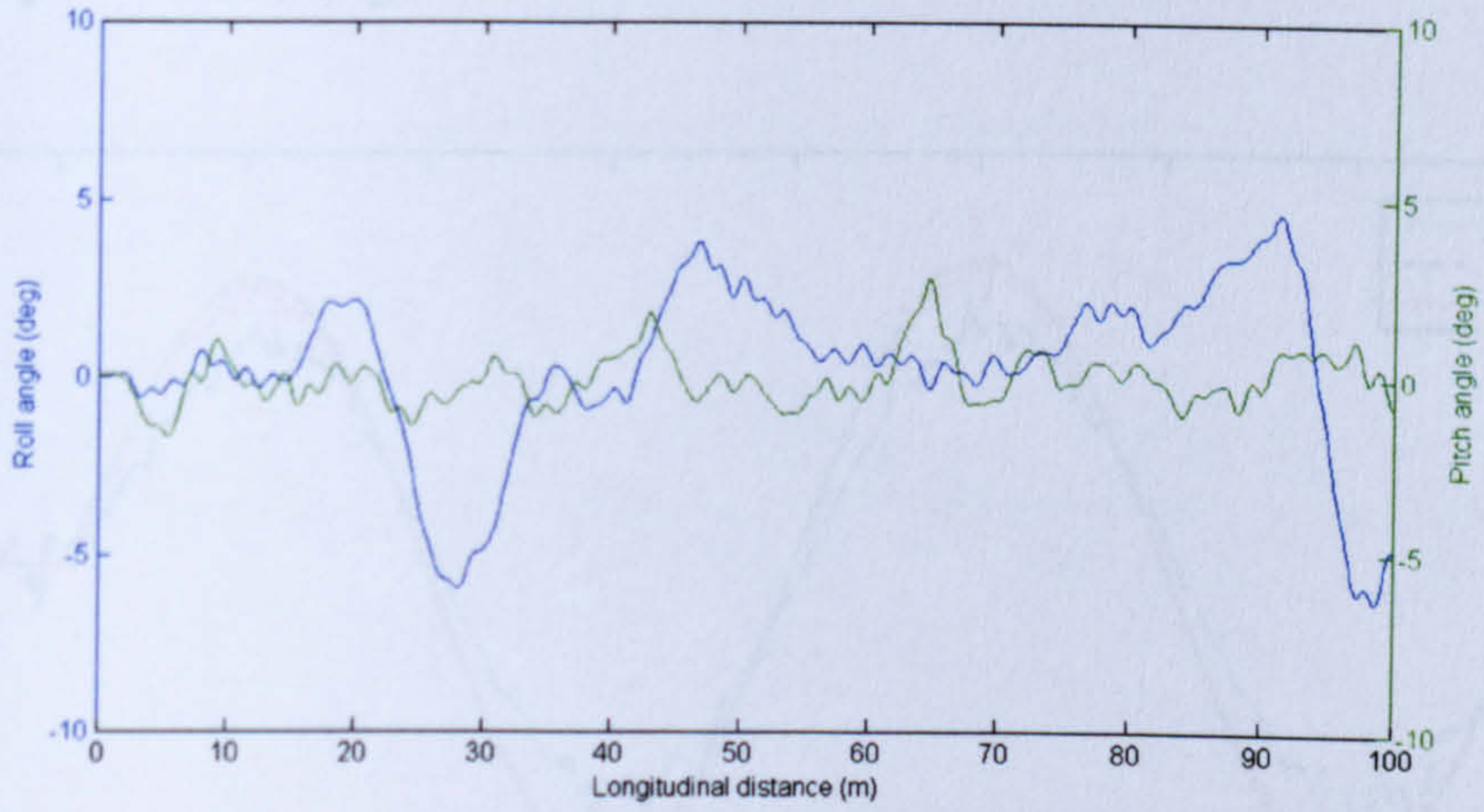

Fig. 6.26 Unladen roll and pitch responses to road profile in figure 6.2

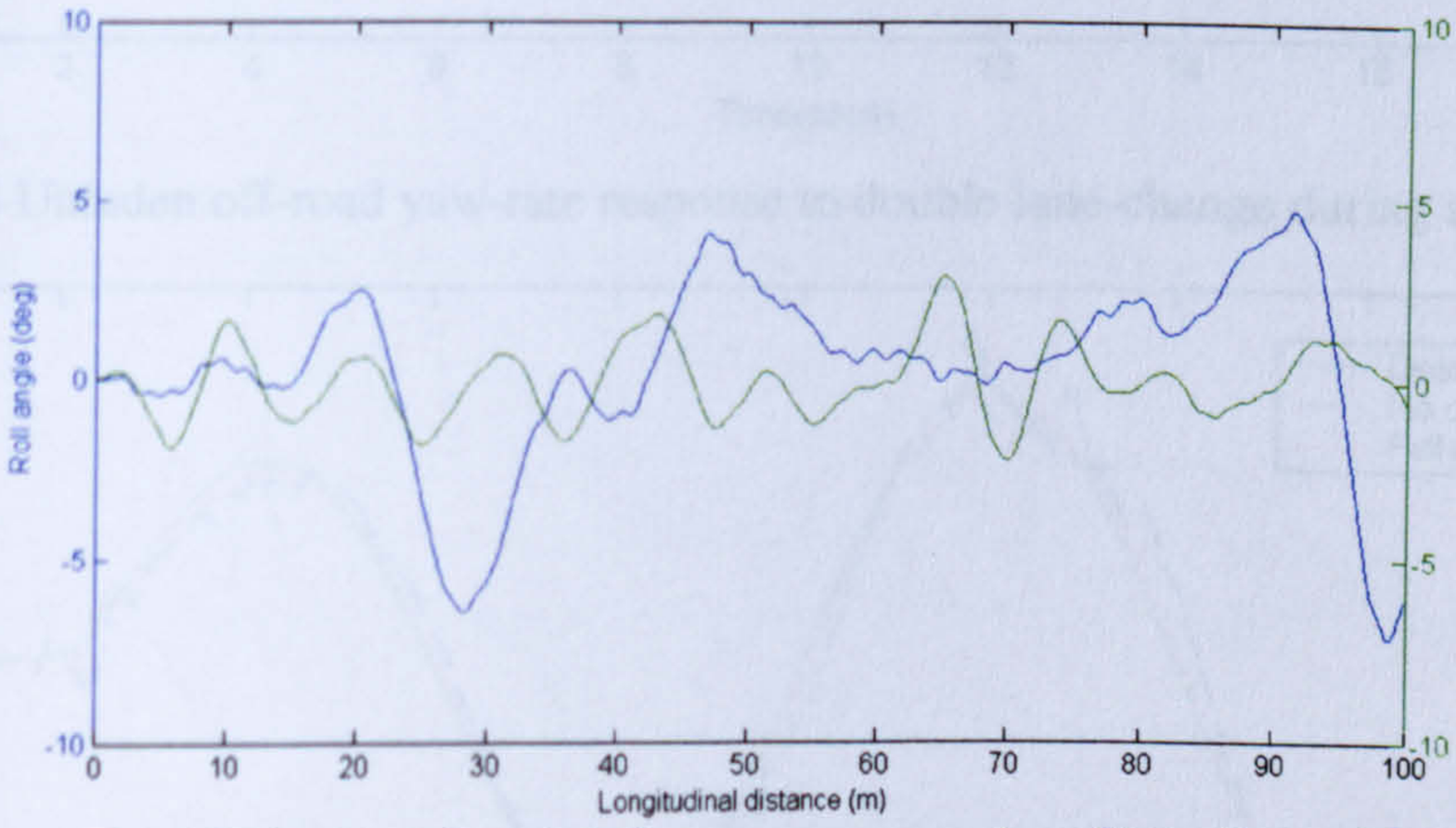

Fig. 6.27 Laden roll and pitch responses to road profile in figure 6.2

Off-road testing will not be performed for the conventional vehicle as the purpose of the off-road testing is aimed at further validation of the controller under such conditions. By simulating off-road conditions, the robustness of the controller will be tested with respect to constantly varying tyre loading and road friction coefficient.

6.3.1 Double Lane-change Manoeuvre

The vehicle is simulated off-road undertaking a double lane-change while accelerating from 5 to 60km/h. The yaw-rate responses are shown in figure 6.28 and 6.29 for the unladen and laden vehicle respectively.

Results show that the severe road surface has little effect on the vehicles ability to track the desired yaw-rate. As with the on-road condition, the controlller is robust to changes in vehicle load, again showing accurate yaw-rate tracking. It is demonstrated that despite the constant and uneven changes in μ and the road height, the yaw-rate tracking of the controller is robust enough to cope with the changes.

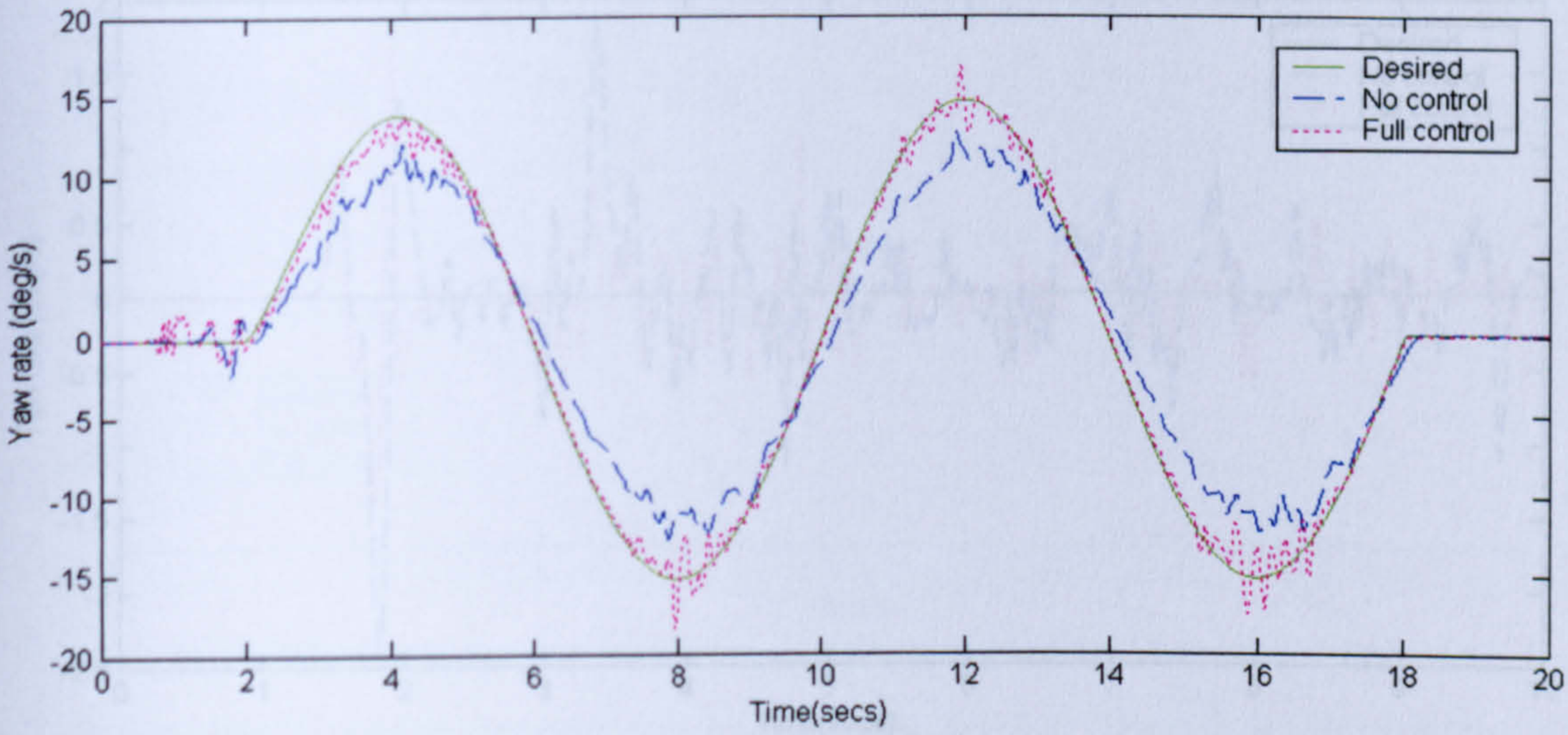

Fig. 6.28 Unladen off-road yaw-rate response to double lane-change during acceleration

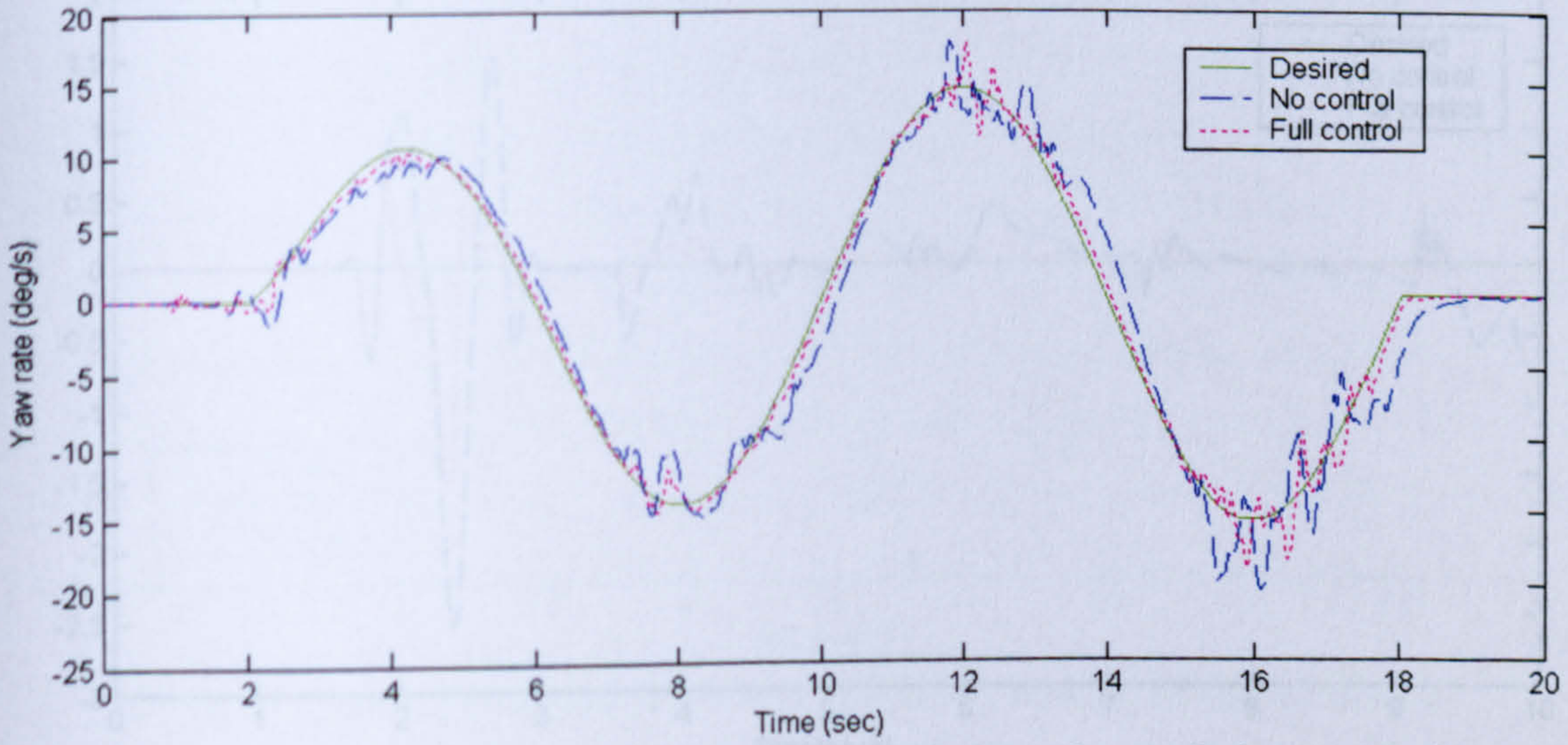

Fig. 6.29 Laden off-road yaw-rate response to double lane-change during accleration

6.3.2 Off-road Acceleration on Split-μ Surface

Given that the road friction coefficient is varying all the time, a bias is placed on the right track so its average μ is 1.6 times greater than the left track. The vehicle is accelerated from 5km/h up to 80km/h and the responses for the yaw-rate are shown in figure 6.30 and 6.31 for the unladen and laden vehicle respectively.

Results show that due to the dominant effect of the varying vertical tyre loads, the changes in the road friction coefficient have little effect on the yaw-rates generated. The peak yaw-rate for the uncontrolled vehicle is shown to be around 2°/s which is much lower than the same experiment on-road. The controller however, does show a slight reduction of the peak values over the uncontrolled responses.

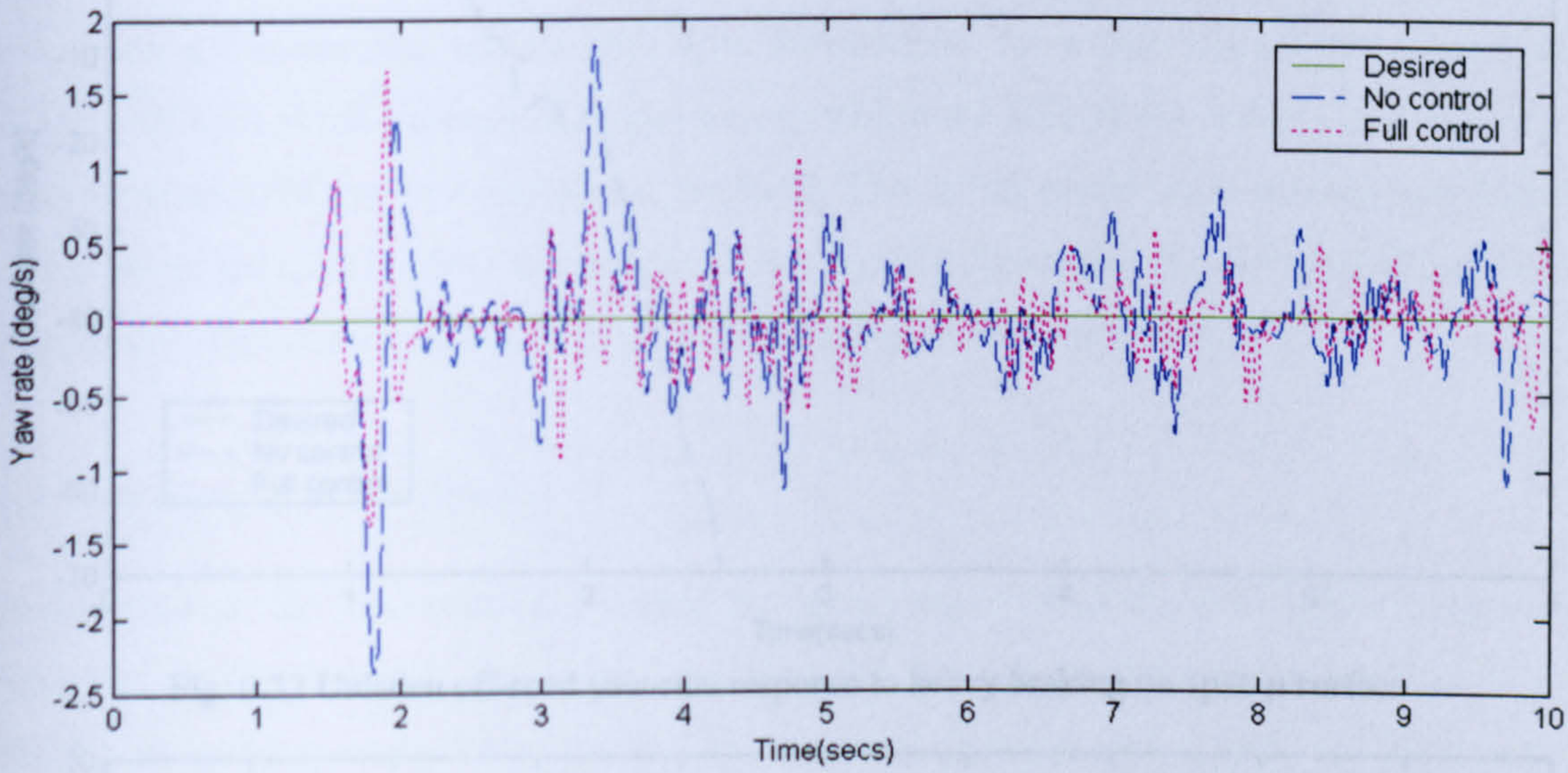

Fig. 6.30 Unladen off-road yaw-rate response to acceleration on a split-μ surface

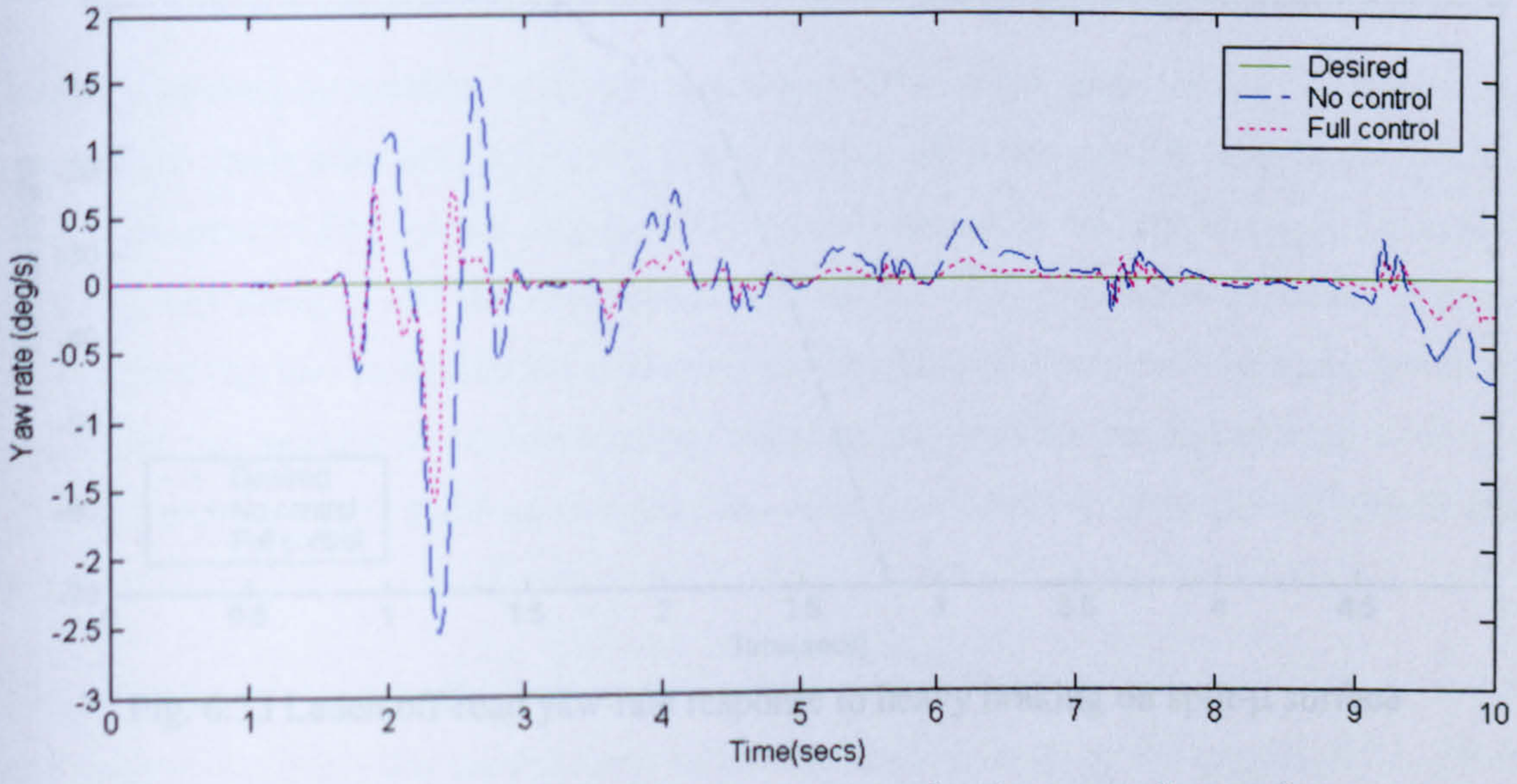

Fig. 6.31 Laden off-road yaw-rate response to acceleration on a split-μ surface

6.3.3 Off-road Heavy Braking on a Split-μ Surface

The same road surface as above is utilised to simulate the heavy braking of the unladen and laden vehicle as it decelerates from 60 to 0km/h. The yaw-rate responses are shown in figure 6.32 and 6.33. The results show that in the case of braking, the intelligent mobility controller

still has significant effect on vehicle stability, even during this simulated off-road behaviour. The uncontrolled vehicle spins out of control, while the controlled vehicle prevents wheel lock and limits the yaw-rate error produced, preventing vehicle instability.

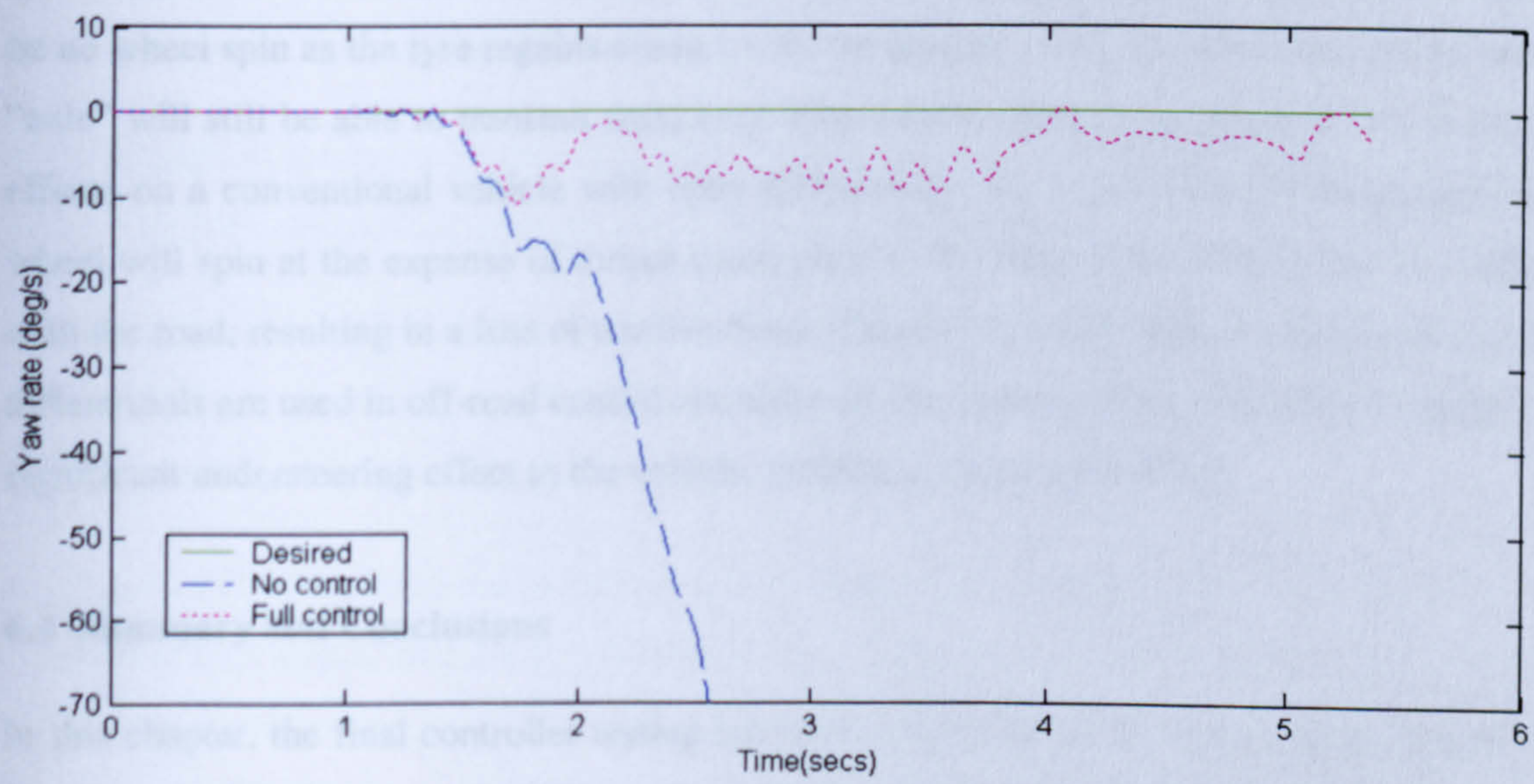

Fig. 6.32 Unladen off-road yaw-rate response to heavy braking on split-μ surface

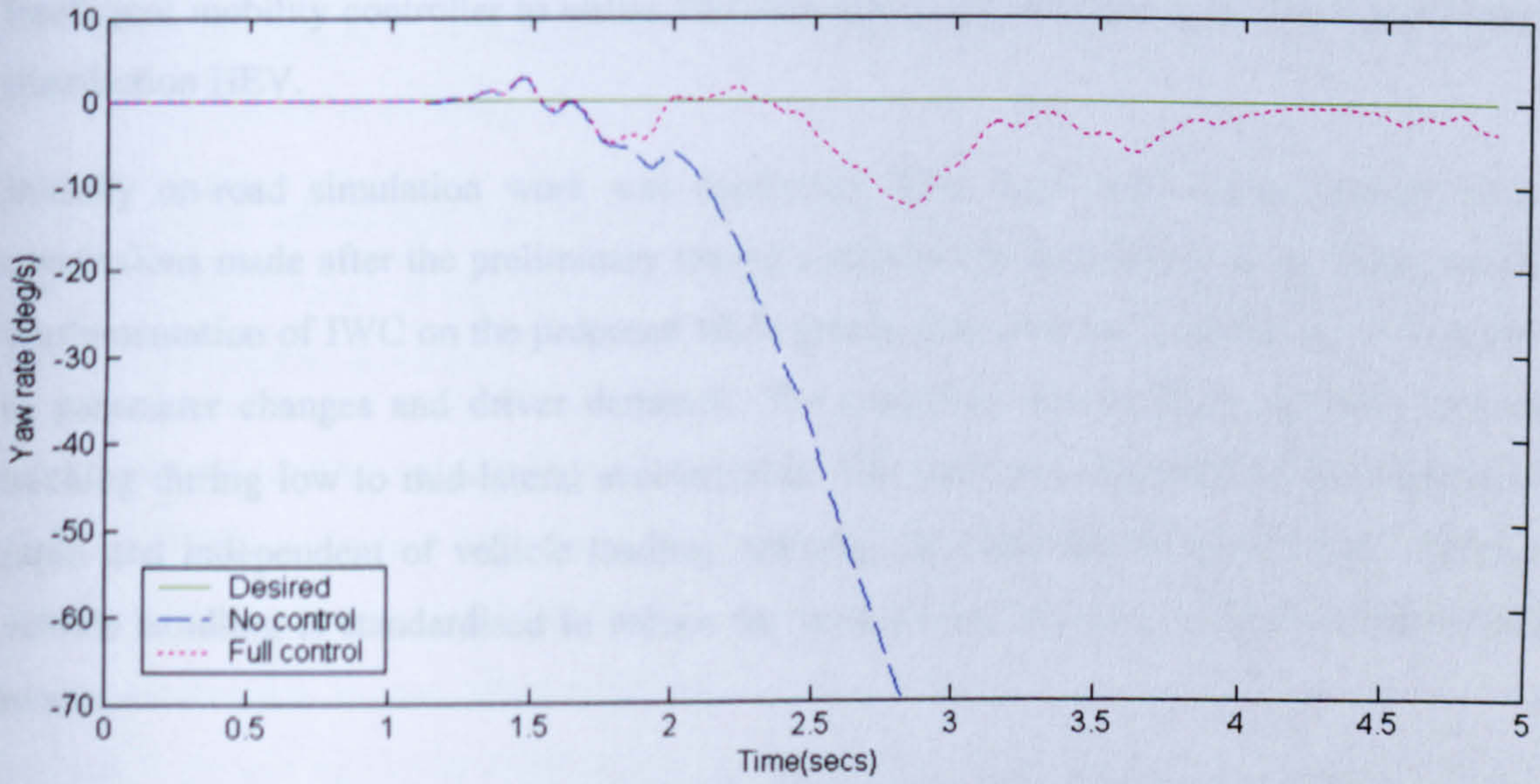

Fig. 6.33 Laden off-road yaw-rate response to heavy braking on split-μ surface

6.3.4 Off-road Discussion

In this section, some basic off-road simulation work has been conducted. Although, as has been noted previously, no solid conclusions can be drawn from the results shown, due to the over simplified representation of the off-road tyre / ground interaction, the work would suggest that the controller remains stable to the external excitation caused by varying road height and μ values.

In the acceleration tests, the results show that in the off-road conditions shown, traction control is of limited effect. However, one of the advantages of the control is that during tyre lift off, when opposing wheel torque becomes zero, the wheel speed will not run up to full speed as traction controller will limit it to 20% higher than vehicle speed. This means there'll be no wheel spin as the tyre regains contact with the ground. Also, the other tyre on the same "axle" will still be able to transmit maximum torque to the road. This situation has negative effects on a conventional vehicle with open differentials. As a tyre lifts off the ground, the wheel will spin at the expense of torque transmitted to the side of the vehicle still in contact with the road, resulting in a loss of tractive force. This is one of the main reasons why locked differentials are used in off-road conditions, although the locking of the differential imposes a significant understeering effect to the vehicle, limiting its manoeuvrability.

6.4 Summary and Conclusions

In this chapter, the final controller testing has been conducted on the full eighteen-degree of freedom model. Through simulation, the potential gained by the implementation of the intelligent mobility controller to utilise IWC has been demonstrated against the fixed torque distribution HEV.

Initially on-road simulation work was conducted. This work adds further weight to the conclusions made after the preliminary testing conducted in Section 3.9. It is shown that the implementation of IWC on the proposed HEV greatly improves the robustness of the vehicle to parameter changes and driver demands. The controller still exhibits excellent yaw-rate tracking during low to mid-lateral accelerations. The yaw-rate responses to steer inputs are rapid and independent of vehicle loading, reducing the need for an experienced driver, as vehicle handling is standardised to reduce the need for the driver to operate in closed loop mode.

The inclusion of the side-slip limit controller adds an extra level of safety for both the driver and vehicle. It ensures that the full range of vehicle handling is under the control of the driver, and greatly reduces the chances of unstable motion while undertaking cornering manoeuvres.

The operation of the Traction Control and Anti-lock Braking Systems counteract wheel spin and wheel-lock respectively, preventing a loss in lateral tyre forces, which aid vehicle stability, especially during heavy braking. This is demonstrated on the split-μ surface and during combined cornering and braking manoeuvres.

Through simplified off-road testing, an insight into the possible performance that the controller can provide off-road has been presented. The controller is shown to continue tracking yaw-rate even on a severe road surface where the tyre forces generated are varying constantly with time. From this it is noted that operation of the controller is equally advantageous for both on and off-road conditions.

With regards to the comparison between the performance of the existing and the theoretical HEV with IWC, the following conclusions have been reached:

- The acceleration performance of the HEV is substantially better than that provided by the conventional drivetrain and with the implemented controller, this increased power is regulated to offer improved road holding.

- The use of IWC allows the proposed vehicle to react with minimal delay and uniformly to hand-wheel inputs, making the proposed vehicle much more agile that the conventional vehicle.

- With the implementation of ABS, the stability of the HEV is greatly increased, even during emergency manoeuvres. Without such control on the conventional vehicle, its stability cannot be assured.

Although these advantages have been demonstrated in the simulation work, further validation against a greater range of trial data could further bring to light the limitations that are imposed by the conventional drivetrain.

From the simulation work presented in this chapter the potential benefits offered by Individual Wheel Control have been shown with respect to both a fixed torque distribution HEV and the conventional QinetiQ CSV. The culmination of these benefits results in greatly increased mobility for the off-road vehicle, leading to reduced time taken from A to B and increased vehicle agility to avoid obstacles and reject disturbances caused by non-uniform surfaces.

Chapter 7

Conclusions

The Hybrid Electric Vehicle has received an increasing amount of interest from both academia and industry over the past decade. A number of passenger cars and commercial vehicles have taken advantage of the potential benefits that can be gained from the use of hybrid technology, such as reduced emissions, increased efficiency and improved torque capability. One particular area that has received less attention is their use in off-road vehicles. This is likely due the higher cost of HEV production and the limited commercial potential of full off-road vehicles. However, their use for military vehicles has obvious advantages. Of all the hybrid configurations possible, perhaps the most promising for off-road vehicles is the series hybrid with in-wheel motors. The separation of the ICE from the driveline, makes silent running an option without the range restrictions imposed by a pure EV. Also, the high torque capabilities of the electric drive make it ideal for powering the vehicle over rough surfaces and obstacles in order to offer logistics support to the frontline.

Through implementation of individual electric drives at each wheel station as part of a series hybrid or electric drivetrain, a greater level of vehicle control can be utilised than is possible with a conventional drivetrain. Herein lies the potential of Individual Wheel Control. This increased control gives rise to a number of well-known mobility control systems that can be implemented more effectively on such a vehicle. The systems which could benefit most from IWC are Traction Control, Anti-lock Braking and Direct Yaw-moment Control. In the literature, the use of these systems on passenger cars with in-wheel motors has been shown to be of great benefit.

Analysis of this previous work led to the objectives outlined in section 1.8. In order for these to be met, the following work was conducted and the relevant conclusions drawn.

Initial work focused on developing basic models in Simulink to simulate the dynamic responses of the proposed vehicle. The vehicle models were based on the conventional, 6WD Combat Support Vehicle developed by QinetiQ (formerly DERA). The conventional drivetrain was replaced by individual Hub Mounted Electric Drives at each wheel station to simulate the proposed HEV. All other vehicle parameters remained the same. The preliminary modelling included analysis of the fundamental vehicle handling characteristics through the

use of the linear bicycle model and development of two vehicle models that include the necessary complexity on which to design and test the individual mobility control systems. These models were the single wheel model for development of the Traction Control and Anti-lock Braking Systems and a basic non-linear handling model on which to implement Direct Yaw-moment Control. A physically based Dugoff tyre model was utilised to model the combined-slip characteristics of the tyre under quasi steady-state conditions.

Control strategies for implementing the various mobility controllers have been reviewed. Through simulation work using the relevant vehicle model, both linear and non-linear control systems were developed and tested. This resulted in three individual control options; linear PD controllers for the implementation of both TCS and ABS and a non-linear fuzzy logic controller for the DYC. The PD controllers were chosen due to their robustness and simplicity, as the vehicle will implement 12 individual PD controllers to run TCS and ABS at each wheel station. The fuzzy logic controller provides an ideal method for controlling the yaw-moment control of the vehicle due to its robustness to increasing model complexity and its intuitive nature.

A new controller co-ordination strategy was developed in order to realise the full intelligent mobility controller. Through preliminary simulation of the controller on the basic non-linear handling model, some initial conclusions as to the benefits of Individual Wheel Control were drawn. Results demonstrated the ability of the controller to track a desired yaw-rate with quick and accurate responses to driver steer demands, regardless of vehicle loading and road conditions. The ABS and TCS were shown to reduce stopping distances and acceleration performance respectively during straight running and improve lateral stability during combined cornering and braking. The combined operation of the controllers during acceleration/braking on split-μ surfaces to reduce wheel-slip and maintain vehicle heading was also evaluated and showed promising results. This all resulted in a reduced driver workload as the vehicle behaves predictably under a wide range of circumstances.

In order to allow greater validation of the controller, an eighteen-degree of freedom full *vehicle model was developed*. This model included the effects caused by the suspension system and load transfers in order to accurately model the *vehicle's on-road behaviour. The* Dugoff tyre model was tuned to match curves for pure-slip provided for the actual tyre and transient effects were included to increase the accuracy of the model. The full vehicle model was partially validated for on-road handling against the limited trial data provided for the conventional CSV and showed accurate representation of yaw-rate, lateral acceleration and

roll-angle, especially in the unladen state. This model offers a simulation tool that is simple to run and analyse results. It is easily altered to represent 4WD or even 8WD vehicles and has great potential for future vehicle handling simulation work.

The model also allows some basic off-road simulation to be conducted with respect to handling manoeuvres, acceleration and braking. By inputting a rough road input and varying the road friction coefficient, an insight into the controller performance off-road can be gained. It should be noted however, that this method is of limited validity and that the only way to accurately assess the off-road performance of the vehicle is through actual vehicle trials.

A conventional vehicle model was also developed, to include the drivetrain of the existing vehicle. The drivetrain includes the ICE, gearbox, torque converter and transmission. A locked differential was also modelled. This model was used to quantify the benefits that are offered by the HEV over the existing vehicle, especially with respect to Individual Wheel Control.

Once the full model was developed, the final controller was implemented and tuned to offer optimum operation for the specific vehicle under a wide range of vehicle operating conditions, ensuring robustness to both internal and external parameter changes.

Work previous to this point had assumed that the vehicle operates in the primary or secondary-handling regime during low to mid-lateral accelerations. However, the implementation of yaw-rate tracking to aggressive steer inputs can result in substantial side-slip as the vehicle aims to maintain a yaw-rate that will impair vehicle stability. In order to prevent such conditions, an additional fuzzy logic controller was developed to limit the side-slip angle as the vehicle enters the final handling regime, maintaining vehicle stability. This novel control method imposes limits on the desired yaw-rate as the side-slip angle approaches boundaries defined by the controller. This extension to the mobility control acts as an additional safety feature to maintain vehicle stability under a greater range of driver demands.

Results for the intelligent mobility controller on the full vehicle model further validated the conclusions drawn from the preliminary testing. Through comparison with the fixed torque distribution hybrid and the conventional vehicle on a number of test procedures, the potential of IWC to standardise vehicle handling and to reduce driver workload has been shown. The inclusion of the side-slip limit controller is also shown to maintain vehicle stability at high lateral accelerations or on low friction surfaces, increasing driver safety. Basic off-road testing shows that the performance of the controller is stable on rough surfaces of varying

friction coefficient, showing that the controller can still track the desired yaw-rate and maintain stability under such conditions. Previously conducted work on IWC has focused almost solely on on-road behaviour for passenger cars under limited conditions. Here, an integrated mobility controller for a 6WD vehicle has been developed that can offer control over almost the entire range of vehicle handling while also inferring suitability for off-road applications.

With respect to the objectives in section 1.8 the following has been achieved:

1. Detailed vehicle models were derived and the full model was partially verified against trial data provided by QinetiQ for the conventional 6x6 on which the proposed vehicle is based.

2. A robust mobility control system has been developed, integrating TCS, ABS and DYC along with a side-slip limiter. This controller has full control of the vehicle to provide control in the three regions of vehicle handling and improve road holding during acceleration and braking.

3. *The controller* was optimised to improve vehicle handling in all loading conditions, both on and off-road. The braking and acceleration performance of the vehicle has been shown to offer improvements over both a fixed torque distribution HEV and the conventional vehicle. The acceleration response of the HEV offers great improvement over the conventional vehicle through the use of electric drives, with the controller ensuring this increased torque capability is taken advantage of. The controller is shown to adapt to a number of driving situations to offer stability during a greatly increased range of operating conditions.

4. The benefits of IWC have been shown both with respect to a fixed torque distribution hybrid and also the conventional vehicle. IWC allows vehicle handling to be tailored to a desired response, providing torque distribution to aid vehicle stability.

In conclusion this work has presented a novel method of controlling motion of a large, off-road vehicle through the use of Individual Wheel Control to offer improvements in vehicle handling and safety both on and off-road. The operating conditions in which the vehicle remains stable have been greatly increased, resulting in greater mobility and performance.

Further Work

Here are some possible avenues for further work that would be of benefit to the work included in this thesis.

Results in chapter 6 show that the controller developed has excellent potential for improving both vehicle handling in the linear range, but also vehicle safety at the limits of vehicle handling. However, in order for effective implementation of the controller, there must be a great degree of confidence in the various parameters used by the controller. These parameters are outlined in section 1.5, which shows that they have been the subject of a great deal of research. Without accurate readings of vehicle speed, yaw-rate or side-slip angle, the performance of the controller cannot be guaranteed.

Perhaps the largest area for future work lies in off-road assessment of the controller. As has been noted the most effective way of assessing a vehicles off-road performance is through actual vehicle trials. In order for this work to be fully concluded, implementation of the controller on an actual vehicle platform must be an eventual goal. Through the combination of the mobility control with active suspension systems, there is the possibility of removing the trade off that is often made between desired handling and ride behaviour.

References

Abe M., Kano Y., Suzuki K., Shibahata Y., Furukawa Y. "Side-slip control to stabilise vehicle lateral motion by direct yaw moment". *JSAE Review 22, pp 413-419,* 2001.

Atkin G. Storey J. "Electric vehicles: Prospects for battery, fuel cell and hybrid powered cars". Financial Times publishing, 1999.

Austin L., Morrey D. "Recent advances in anti-lock braking systems and traction control systems". *Proceedings of IMechE part D Vol. 214, pp 625-638,* 2000.

Bakker E., Pacejka H.B., Lidner.L. "A new tire model with an application in vehicle dynamic studies". *SAE paper no. 890087,* 1989.

Bauer M., Tomizuka M., "Fuzzy logic traction controllers and their effect on longitudinal vehicle platoon systems". *Vehicle system dynamics, Vol. 25, pp. 277-303,* 1996.

Baumann B., Rizzoni G., Washington G. "Intelligent control of Hybrid vehicles using Neural Networks and Fuzzy logic". *SAE paper no. 981061,* 1998.

Bevley D.M., Gerdes J.C., Wilson C., Zhang G. "The use of GPS based velocity measurements for improved vehicle state estimation", *Proceedings of American Control Conference,* June 2000.

Bjorkman M., Holmstrom K. "Global optimization using the DIRECT algorithm in Matlab". *Advanced modelling and optimization, Vol. 1, no. 2,* 1999.

Cheok K.C., Hoogterp F.B., Fales W.K. "Fuzzy logic traction control design". *SAE paper no. 960957,* 1996.

Chumsamutr R., Fujioka T. "Improvement of electric vehicle's cornering performance by direct yaw-moment control". *Proceedings of AVEC,* 2000.

Clover C.L., Bernard J.E. "Longitudinal tyre Dynamics". *Vehicle System Dynamics Vol. 29 pp 231-259,* 1998.

Crolla D.A., Firth G. and Horton D. "An introduction to vehicle dynamics", University of Leeds, School of mechanical engineering, 1996.

Cooke R. "The interaction between ride and handling behaviour of an actively suspended vehicle". PhD Thesis, University of Leeds, School of mechanical engineering, 1996.

Dixon J.C. "Tyres, Suspension and Handling". Cambridge University Press, 1991.

Dorf R.C., Bishop R.H. "Modern Control Systems". Eighth edition, Addison Wesley Longman, Inc, 1998.

Drakunov S.V., Ashrafi B., Rosiglioni A. "Yaw control algorithm via sliding mode control", *Proc. American Control Conference*, June 2000.

Drakunov S.V., Ozguner U., Dix P., Ashrafi B. "ABS control using optimum search via sliding modes". *IEEE Transactions on control systems technology, Vol. 3, No. 1*, March 1995.

Dugoff H., Fancher P.S. and Segel L. "An analysis of tire traction properties and their influence on vehicle dynamic performance", *SAE paper no. 700377*, 1970.

El-Gindy M., Mikulcik E.C. "Sensitivity of vehicles's yaw rate response: three-axle truck". *Int. Journal of Vehicle Design, Vol. 14, no. 4*, 1993.

Esmailzadeh E., Goodarzi A., Vossoughi G.R. "Optimal yaw moment control law for improved vehicle handling". *Mechatronics 13, pp 659-675*, 2003.

Franklin G.F, Powell J.D., Workman M. "Digital control of dynamic systems". Third edition, Addison Wesley Longman, Inc, 1998.

Friedland B. "Advanced control system design". Prentice-Hall International Ltd. 1996.

Fukada Y. "Slip-angle estimation for vehicle stability control". *Vehicle system dynamics, Vol. 32 pp. 375-388*, 1999.

Gunter D.D. "Modeling and simulation of a 6x6 military Troop/cargo transport vehicle". *SAE paper no. 980224*, 1998.

Gustafsson F. "Monitoring Tire Road friction Using the Wheel slip". *IEEE control systems*, August 1998.

Hac A., Simpson M.D. "Estimation of vehicle side slip angle and yaw rate". *SAE paper no. 2000-01-0696*, 2000.

Holzwarth R.K., May K.A. "Analysis of traction control systems augmented by limited slip differentials". SAE paper no. 940831, 1994.

Hori Y., Toyoda Y., Tsuruoka Y. "Traction control of electric vehicle: Basic experimental results using the test EV "OUT Electric March"". *IEEE Transactions on industry applications, Vol. 34 No. 5,* September/October 1998.

Horowitz.R., de Wit C.C. "Observer for tire/road contact friction using only wheel angular velocity information". *Proc. of the 38th conference on Decision and Control,* Dec 1999.

Hosomi K., Nagae A., Yamamoto Y. "Development of Active Traction Control System". *SAE paper no. 2000-01-1636,* 2000.

Huh K., Kim J. and Hong J. "Handling and driving characteristics for six-wheeled vehicles". *Proc. ImechE Vol. 214 Part D, pp 159-170,* 2000.

Jansen T.H., Van Oosten J.J.M., Pauwelussen J.P., Pacejka H.P. "Sensitivity of vehicle handling to combined slip tyre characteristics". *Proceedings of AVEC,* 1996.

Jones D.R., Perttunen C.D., Stuckman B.E. "Global Optimization: Beyond the Lipschitzian Model". *Proceedings of IEEE,* 1992.

Jung H.S., Kwak B.H, Park Y.J. "Development of traction control system". *Seoul 2000 FISITA automotive conference,* 2000.

Jung H., Kwak B., Park Y. "Improved directional stability in traction control system" *Proceedings of AVEC,* 2000.

Kawabe T., Nakazawa M., Notsu I., Watanabe Y. "A sliding mode controller for wheel slip ratio control system". *Vehicle system dynamics, Vol. 27, pp. 393-408,* 1997.

Kimbrough S., Datla K. "An effective means for implementing wheel-slip control without a ground speed sensor". Vehicle System Dynamics, 25: 327-339, Suppl. S 1996.

de Koker P.M., J. Gouws J., Pretorius L. "Fuzzy control algorithm for Automotive Traction Control Systems". *Electro-technical Conference,* 1996.

Kachroo P., Unsal C. "Sliding mode measurement feedback control for anti-lock braking systems". *IEEE transactions on control systems technology, Vol. 7 No. 2,* March 1999.

Lyshevski S.E., Sinha A.S.C., Rizkalla M., El-Sharkawy M., Nazarov A., Cho P.C., Wylam W., Mitchell J., Friesen M. "Analysis and control of hybrid-electric vehicles with individual wheel brushless traction motors". *Proc. American Control Conference*, June 2000.

Maclaurin E.B. "The effects of limited slip differentials on the handling and traction properties of off-road vehicles". *Proc. ISTVS 6th European Conf. Austria*, 1994.

Madni A.M., Wan L.A., Layton M.R. "A miniature yaw rate sensor for intelligent chassis control". *IEEE Conference on Intelligent Transportation System*, 1997.

Manning W.J., Crolla D.A., Brown M.D., Selby M.A. "IVMC: Intelligent Vehicle Mobility Control". *SAE paper 02P-337*, 2002.

Mathworks Inc. "Optimization toolbox for use with Matlab". The Mathworks Inc, 1999.

Meriam J.L., Kraige L.G. "Engineering mechanics. Vol.2, Dynamics". John Wiley and sons, 2003.

Milliken W.F., Milliken D.L. "Race Car Vehicle Dynamics". SAE publications, 1995.

Motoyama S. Uki H., Isoda K., Yuasa H. "Effect of traction force distribution control on vehicle dynamics". *Vehicle System Dynamics Vol. 22 pp 455-464*, 1993.

MSC Software. "MSC.ADAMS". *http://www.mscsoftware.com/*, 2000.

Nagai M., Hirano Y., Yamanaka S. "Integrated control of active rear wheel steering and direct yaw moment control". *Vehicle system dynamics, 27 pp.357-370*, 1997.

Pacejka H.B. "Tyre factors and vehicle handling". *Int. Journal of Vehicle Design, Vol. 1, no.1*, 1979.

Pacejka H.B. "Tyres and vehicle dynamics". Butterworth-Heinemann, 2002.

Pacejka H.B., Besselink I.J.M. "Magic formula tyre model with transient properties". *Supplement to Vehicle system dynamics, Vol. 27, pp234-249*, 1997.

Park J.H., Kim C.Y., "Wheel slip control in traction control system for vehicle stability". *Vehicle system dynamics, Vol. 31, pp. 263-278*, 1999.

Park M.K., Suh I.H., Byoun S.J., Oh.S.R. "An intelligent co-ordinated control system for steering and traction of electric vehicle". *Proc. of the IEEE IECON 22nd Int.Conference on Industrial Electronics, Control, and Instrumentation,* 1996.

Plummer A.R., Brown M.D "Course notes Intelligent digital control". University of Leeds, 1999a.

Plummer A.R., Brown M.D "Course notes Machine intelligence". University of Leeds, 1999b.

Ray L.R. "Non-linear tire force estimation and road friction identification: Simulation and experiments". *Automatica, Vol. 33 No. 10 pp. 1819-1833,* 1997.

Roberts S.A. "The design and implementation of a semi-active suspension system for an off-road vehicle". PhD thesis. School of Mechanical Engineering, University of Leeds, 2002.

Sado H., Sakai S.I., Hori Y. "Road Condition Estimation for traction control in electric vehicle". *Proc. of the IEEE International Symposium on Industrial Electronics, Page(s): 973 -978 vol.2,* 1999.

Saeks R., Cox C. "Design of an adaptive control system for a hybrid electric vehicle". *Proc. of IEEE,* 1999.

Sakia S., Sado H., Hori Y. "Motion Control in an Electric Vehicle with Four Independently Driven In-Wheel Motors". *IEE/ASME Transactions on mechatronics, Vol. 4, No. 1,* March 1999.

Saraf S., Tomizuka M. "Slip-angle estmiation for vehicles on Automated highways". *Proceedings of the American Control Conference,* 1997.

Segel L. "Basic linear theory of handling and stability of automobiles". *International Centre for Transportation Studies, Vol. IV,* 1982.

Senger R.D., Merkle M.A., Nelson D.J. "Validation of ADVISOR as a simulation tool for a series hybrid electric vehicle", *SAE paper no. 981133 sp-1331,* 1998.

Sharp R.S. "On the accurate representation of tyre shear forces by a multi-radial-spoke model", *Vehicle system design, Vol. 18 supplement,* 1989.

Shino M., Wang Y.Q. and Nagai M. "Motion Control of Electric Vehicles Considering Vehicle Stability". *Proceedings of AVEC*, 2000.

Shovlin A. "A body attitude controller of an off-road vehicle". PhD Thesis, School of Mechanical Engineering, University of Leeds, 1999.

Sigl A., Demel H. "ASR-Traction control, state of the art and some prospects". *SAE paper no. 900204*, 1990.

Song J.B, Kim B.C., Chang H.W. "Slip control systems based on Engine Throttle control approach". *Proceedings of AVEC*. 1998.

Song J.B. Byun K.S. "Throttle actuator control system for vehicle control". *Mecahtronics, Vol. 9 pp 477-495*, Aug 1999.

Szostak H.T., Allen R.W., Rosenthal T.J. "Analytical modeling of driver response in crash avoidance maneuvering volume II: An interactive tire model for driver/vehicle simulation". *U.S. DOT report no. DOT HS 807 271*, 1988.

Tahami F., Kazemi R., Farhanghi S. "A novel driver assist stability system for All-Wheel-Drive Electric Vehicles". *IEEE transactions on Vehicular Technology, Vol. 52, pp 683-692*, 2003.

Takahashi T., Pacejka H.B. "Cornering on uneven roads" *10th IAVSD symposium on Dynamics of Vehicles on roads and tracks*, June 1987.

Thompson R.W. "Hub Mounted Electric Drive project at DERA and MST (UK)", *All Electric Combat Vehicle Conference*, 1999.

Tsiotras P., de Wit C.C. "On the optimal braking of wheeled vehicles". *Proc. American Control Conference*, June 2000.

Vehicle Systems Analysis. "ADVISOR". http://www.ctts.nrel.gov/analysis/. 2003.

Wakefield E.H. "History of the electric automobile: Hybrid electric vehicles". SAE publications, 1998.

Wipke K.B., Cuddy M.R. "Analysis of the fuel economy benefit of drivetrain hybridization". *SAE paper no. 970289, sp-1243*, 1997.

Wong J.Y. "Theory of ground vehicles". John Wiley and sons, Inc, 1993.

Wouk V. "Hybrid electric vehicle". *American scientific,* October 1997.

Yoshimura T., Uchida H., Nasu H., Hino J., Ueno R. "Traction force control of an electric vehicle in 2WS-4WD mode using fuzzy reasoning". *Int. J of Vehicle Design, Vol. 18, No. 5,* 1997.

ZF Friedrichshafen "ZF Limited-Slip Differentials". *Commercial product information, ZF Friedrichshafen,* 1999.

Appendix A

Vehicle Modelling

A.1 Modelling Equations

Here are the modelling equations that are used to implement the vehicle models in Simulink[tm].

A.1.1 Dugoff Tyre Model

Unresolved Longitudinal Tyre Forces:

$$F_{wx1} = \frac{C_{\lambda f}\lambda_1}{1-\lambda_1} X_1(2-X_1) \qquad F_{wx2} = \frac{C_{\lambda f}\lambda_2}{1-\lambda_2} X_2(2-X_2)$$

$$F_{wx3} = \frac{C_{\lambda r}\lambda_3}{1-\lambda_3} X_3(2-X_3) \qquad F_{wx4} = \frac{C_{\lambda r}\lambda_4}{1-\lambda_4} X_4(2-X_4)$$

$$F_{wx5} = \frac{C_{\lambda r}\lambda_5}{1-\lambda_5} X_5(2-X_5) \qquad F_{wx6} = \frac{C_{\lambda r}\lambda_6}{1-\lambda_6} X_6(2-X_6)$$

Unresolved Lateral Tyre Forces:

$$F_{wy1} = \frac{C_{\alpha f}\tan\alpha_1}{1-\lambda_1} X_1(2-X_1) \qquad F_{wy2} = \frac{C_{\alpha f}\tan\alpha_2}{1-\lambda_2} X_2(2-X_2)$$

$$F_{wy3} = \frac{C_{\alpha r}\tan\alpha_3}{1-\lambda_3} X_3(2-X_3) \qquad F_{wy4} = \frac{C_{\alpha r}\tan\alpha_4}{1-\lambda_4} X_4(2-X_4)$$

$$F_{wy5} = \frac{C_{\alpha r}\tan\alpha_5}{1-\lambda_5} X_5(2-X_5) \qquad F_{wy6} = \frac{C_{\alpha r}\tan\alpha_6}{1-\lambda_6} X_6(2-X_6)$$

Wheel-slip:

$$\lambda_1 = \begin{cases} 1-\dfrac{V_x}{r_w\omega_1} & if\ r_w\omega_1 \le V_x\ \ (in\ acceleration) \\ -1+\dfrac{r_w\omega_1}{V_x} & if\ r_w\omega_1 > V_x\ \ (in\ braking) \end{cases}$$

$$\lambda_2 = \begin{cases} 1-\dfrac{V_x}{r_w\omega_2} & if\ r_w\omega_2 \le V_x\ \ (in\ acceleration) \\ -1+\dfrac{r_w\omega_2}{V_x} & if\ r_w\omega_2 > V_x\ \ (in\ braking) \end{cases}$$

$$\lambda_3 = \begin{cases} 1 - \dfrac{V_x}{r_w \omega_3} & if\ r_w \omega_3 \le V_x\ \ (in\ acceleration) \\ -1 + \dfrac{r_w \omega_3}{V_x} & if\ r_w \omega_3 > V_x\ \ (in\ braking) \end{cases}$$

$$\lambda_4 = \begin{cases} 1 - \dfrac{V_x}{r_w \omega_4} & if\ r_w \omega_4 \le V_x\ \ (in\ acceleration) \\ -1 + \dfrac{r_w \omega_4}{V_x} & if\ r_w \omega_4 > V_x\ \ (in\ braking) \end{cases}$$

$$\lambda_5 = \begin{cases} 1 - \dfrac{V_x}{r_w \omega_5} & if\ r_w \omega_5 \le V_x\ \ (in\ acceleration) \\ -1 + \dfrac{r_w \omega_5}{V_x} & if\ r_w \omega_5 > V_x\ \ (in\ braking) \end{cases}$$

$$\lambda_6 = \begin{cases} 1 - \dfrac{V_x}{r_w \omega_6} & if\ r_w \omega_6 \le V_x\ \ (in\ acceleration) \\ -1 + \dfrac{r_w \omega_6}{V_x} & if\ r_w \omega_6 > V_x\ \ (in\ braking) \end{cases}$$

Non-dimensional slip coefficient:

$$X_i = \begin{cases} X_i & if\ \ X_i \le 1 \\ 1 & if\ \ X_i > 1 \end{cases}$$

Where:

$$X_i = \frac{\mu_i F_{zi}(1 - s_i)(1 - \varepsilon_r) V_x \sqrt{s_i + \tan^2 \alpha_i)}}{2 \cdot \sqrt{C_t^{\,2} s_i^2 + C_\alpha^{\,2} \tan^2 \alpha_i}}$$

A.1.2 Single Wheel Model

In addition to the Dugoff Tyre Model.

Wheel Motion:

$$I_w \frac{d\omega}{dt} = T - r_w F_{wx} - r_w RR$$

Vehicle Motion:

$$\frac{M_b}{6} \frac{dV_x}{dt} = F_{wx}$$

A.1.3 Basic Non-linear Handling Model

In addition to Dugoff tyre model.

Resolved tyre forces:

$$F_{wx1} = F_{wx1}\cos\delta_f - F_{wy1}\sin\delta_f \qquad F_{wx2} = F_{wx2}\cos\delta_f - F_{wy2}\sin\delta_f$$

$$F_{wx3} = F_{wx3}\cos\delta_c - F_{wy3}\sin\delta_c \qquad F_{wx4} = F_{wx4}\cos\delta_c - F_{wy4}\sin\delta_c$$

$$F_{wx5} = F_{wx5} \qquad F_{wx6} = F_{wx6}$$

$$F_{wy1} = F_{wy1}\cos\delta_f + F_{wx1}\sin\delta_f \qquad F_{wy2} = F_{wy2}\cos\delta_f + F_{wx2}\sin\delta_f$$

$$F_{wy3} = F_{wy3}\cos\delta_c + F_{wx3}\sin\delta_c \qquad F_{wy4} = F_{wy4}\cos\delta_c + F_{wx4}\sin\delta_c$$

$$F_{wy5} = F_{wy5} \qquad F_{wy6} = F_{wy6}$$

Longitudinal motion:

$$M_b(\frac{dV_x}{dt} - V_y\frac{d\psi}{dt}) = F_{wx1} + F_{wx2} + F_{wx3} + F_{wx4} + F_{wx5} + F_{wx6} - F_d$$

Lateral motion:

$$M_b(\frac{dV_y}{dt} + V_x\frac{d\psi}{dt}) = F_{wy1} + F_{wy2} + F_{wy3} + F_{wy4} + F_{wy5} + F_{wy6}$$

Yawing motion:

$$I_z\frac{d^2\psi}{dt^2} = t(F_{wx1} - F_{wx2} + F_{wx3} - F_{wx4} + F_{wx5} - F_{wx6})$$
$$+aF_{wy1} + aF_{wy2} + bF_{wy3} + bF_{wy4} - cF_{wy5} - cF_{wy6} + M_z$$

Self-aligning Moment:

$$M_{z1} = -X_{trail}F_{wy1} \qquad M_{z2} = -X_{trail}F_{wy2}$$

$$M_{z3} = -X_{trail}F_{wy3} \qquad M_{z4} = -X_{trail}F_{wy4}$$

$$M_{z5} = X_{trail}F_{wy5} \qquad M_{z6} = X_{trail}F_{wy6}$$

$$M_z = M_{z1} + M_{z2} + M_{z3} + M_{z4} + M_{z5} + M_{z6}$$

Wheel Rotation:

$$I_{wf}\frac{d\omega_1}{dt} = T_1 - r_wF_{wx1} - r_wRR \qquad I_{wf}\frac{d\omega_2}{dt} = T_2 - r_wF_{wx2} - r_wRR$$

$$I_{wc}\frac{d\omega_3}{dt} = T_3 - r_w F_{wx3} - r_w RR \qquad I_{wc}\frac{d\omega_4}{dt} = T_4 - r_w F_{wx4} - r_w RR$$

$$I_{wr}\frac{d\omega_5}{dt} = T_5 - r_w F_{wx5} - r_w RR \qquad I_{wr}\frac{d\omega_6}{dt} = T_6 - r_w F_{wx6} - r_w RR$$

Wheel-slip angle:

$$\tan\alpha_1 = \frac{V_y + a\dfrac{d\psi}{dt}}{V_x + t\dfrac{d\psi}{dt}} - \delta_f \qquad \tan\alpha_2 = \frac{V_y + a\dfrac{d\psi}{dt}}{V_x - t\dfrac{d\psi}{dt}} - \delta_f$$

$$\tan\alpha_3 = \frac{V_y + b\dfrac{d\psi}{dt}}{V_x + t\dfrac{d\psi}{dt}} - \delta_c \qquad \tan\alpha_4 = \frac{V_y + b\dfrac{d\psi}{dt}}{V_x - t\dfrac{d\psi}{dt}} - \delta_c$$

$$\tan\alpha_5 = \frac{V_y - c\dfrac{d\psi}{dt}}{V_x + t\dfrac{d\psi}{dt}} \qquad \tan\alpha_6 = \frac{V_y - c\dfrac{d\psi}{dt}}{V_x - t\dfrac{d\psi}{dt}}$$

Aerodynamic drag force:

$$F_d = \frac{\rho}{2} C_d A_d V_x^{\,2}$$

Calculation of static vertical tyre loading:

Vertical displacement at spring centre:

$$d_x = \frac{M_b g}{2K_{sf} + 2K_{sc} + 2K_{sr}}$$

Horizontal distance from spring centre to rear axle:

$$Q = \frac{2LK_{sf} + K_{sc}L}{2K_{sf} + 2K_{sc} + 2K_{sr}}$$

Static pitch due to loading:

$$\theta_s = \sin^{-1}\left(\frac{aM_b g - LK_{sc}d_x - 2LK_{sr}d_x}{LK_{sc}(0.5L - Q) - 2K_{sr}QL}\right)$$

Static vertical deflection at each axle and centre of gravity:

$$d_f = -d_x - (L - Q)\sin\theta_s$$

$$d_c = -d_x - (0.5L - Q)\sin\theta_s$$

$$d_r = -d_x + Q\sin\theta_s$$

$$d_{cg} = -d_x - (L - Q - a)\sin\theta_s$$

Resultant static vertical tyre loads:

$$F_{zsf} = -d_f K_{sf} + M_{wf} g$$

$$F_{zsc} = -d_c K_{sc} + M_{wc} g$$

$$F_{zsr} = -d_r K_{sr} + M_{wr} g$$

A.1.4 Full Vehicle Model

Here are any additional / modified equations that are used in the full vehicle model.

Longitudinal motion:

$$M_b(\frac{dV_x}{dt} + V_z\frac{d\theta}{dt} - V_y\frac{d\psi}{dt}) = F_{wx1} + F_{wx2} + F_{wx3} + F_{wx4} + F_{wx5} + F_{wx6} - F_d$$

Lateral motion:

$$M_b(\frac{dV_y}{dt} + V_x\frac{d\psi}{dt} - V_z\frac{d\phi}{dt}) = F_{wy1} + F_{wy2} + F_{wy3} + F_{wy4} + F_{wy5} + F_{wy6}$$

Vertical motion:

$$M_b(\frac{dV_z}{dt} + V_y\frac{d\phi}{dt} - V_x\frac{d\theta}{dt}) = F_{s1} + F_{s2} + F_{s3} + F_{s4} + F_{s5} + F_{s6}$$

Rolling motion:

$$I_x\frac{d^2\phi}{dt^2} + (I_z - I_y)\frac{d\theta}{dt}\frac{d\psi}{dt} = t_s(-F_{s1} + F_{s2} - F_{s3} + F_{s4} - F_{s5} + F_{s6}) + M_\phi$$

Pitching motion:

$$I_y\frac{d^2\theta}{dt^2} + (I_x - I_z)\frac{d\phi}{dt}\frac{d\psi}{dt} = -aF_{s1} - aF_{s2} - bF_{s3} - bF_{s4} + cF_{s5} + cF_{s6} + M_\theta$$

Yawing motion:

$$I_z\frac{d^2\psi}{dt^2}+(I_y-I_x)\frac{d\phi}{dt}\frac{d\theta}{dt}=t(F_{wx1}-F_{wx2}+F_{wx3}-F_{wx4}+F_{wx5}-F_{wx6})$$
$$+aF_{wy1}+aF_{wy2}+bF_{wy3}+bF_{wy4}-cF_{wy5}-cF_{wy6}+M_z$$

Moments due to lateral and longitudinal acceleration:

$$M_\varphi=M_b g(H_{cgB}-H_{rc})\sin\phi+M_b A_y(H_{cgB}-H_{rc})\cos\phi$$

$$M_\theta=M_b g(H_{cgB}-H_{pc})\sin\theta-M_b A_x(H_{cgB}-H_{pc})\cos\theta$$

Suspension forces at strut:

$$F_{ss1}=K_{sf}(Z_1-Z_{b1})+C_{sf}(\frac{dZ_1}{dt}-\frac{dZ_{b1}}{dt})\quad F_{ss2}=K_{sf}(Z_2-Z_{b2})+C_{sf}(\frac{dZ_2}{dt}-\frac{dZ_{b2}}{dt})$$

$$F_{ss3}=K_{sc}(Z_3-Z_{b3})+C_{sc}(\frac{dZ_3}{dt}-\frac{dZ_{b3}}{dt})\quad F_{ss4}=K_{sc}(Z_4-Z_{b4})+C_{sc}(\frac{dZ_4}{dt}-\frac{dZ_{b4}}{dt})$$

$$F_{ss5}=K_{sr}(Z_5-Z_{b5})+C_{sr}(\frac{dZ_5}{dt}-\frac{dZ_{b5}}{dt})\quad F_{ss6}=K_{sr}(Z_6-Z_{b6})+C_{sr}(\frac{dZ_6}{dt}-\frac{dZ_{b6}}{dt})$$

Suspension forces as seen by body:

$$F_{s1}=F_{ss1}+F_{b1}BSF\qquad F_{s2}=F_{ss2}+F_{b2}BSF\qquad F_{s3}=F_{ss3}+F_{b3}BSF$$

$$F_{s4}=F_{ss4}+F_{b4}BSF\qquad F_{s5}=F_{ss5}+F_{b5}BSF\qquad F_{s6}=F_{ss6}+F_{b6}BSF$$

Vertical tyre forces:

$$F_{t1}=K_{tf}(x_{o1}-Z_1)+C_{tf}(\frac{dx_1}{dt}-\frac{dZ_1}{dt})\qquad F_{t2}=K_{tf}(x_2-Z_2)+C_{tf}(\frac{dx_2}{dt}-\frac{dZ_2}{dt})$$

$$F_{t3}=K_{tc}(x_3-Z_1)+C_{tc}(\frac{dx_3}{dt}-\frac{dZ_3}{dt})\qquad F_{t4}=K_{tc}(x_4-Z_4)+C_{tc}(\frac{dx_4}{dt}-\frac{dZ_4}{dt})$$

$$F_{t5}=K_{tr}(x_5-Z_5)+C_{tr}(\frac{dx_5}{dt}-\frac{dZ_5}{dt})\qquad F_{t6}=K_{tr}(x_6-Z_6)+C_{tr}(\frac{dx_6}{dt}-\frac{dZ_6}{dt})$$

Load transfer effects due to lateral accelerations:

$$F_{latacc1}=\frac{M_{wf}H_{cgA}A_y}{t}+\frac{F_{zs1}H_{rc}A_y}{g.t}\quad F_{latacc2}=\frac{M_{wf}H_{cgA}A_y}{t}+\frac{F_{zs2}H_{rc}A_y}{g.t}$$

$$F_{latacc3}=\frac{M_{wc}H_{cgA}A_y}{t}+\frac{F_{zs3}H_{rc}A_y}{g.t}\quad F_{latacc4}=\frac{M_{wc}H_{cgA}A_y}{t}+\frac{F_{zs4}H_{rc}A_y}{g.t}$$

$$F_{latacc5} = \frac{M_{wr} H_{cgA} A_y}{t} + \frac{F_{zs5} H_{rc} A_y}{g.t} \quad F_{latacc6} = \frac{M_{wr} H_{cgA} A_y}{t} + \frac{F_{zs6} H_{rc} A_y}{g.t}$$

Forces in suspension due to longitudinal accelerations:

$$F_{longacc1} = \frac{M_{wf} H_{cgA} A_x}{a} \qquad F_{longacc2} = \frac{M_{wf} H_{cgA} A_x}{a}$$

$$F_{longacc3} = \frac{M_{wc} H_{cgA} A_x}{b} \qquad F_{longacc4} = \frac{M_{wc} H_{cgA} A_x}{b}$$

$$F_{longacc5} = \frac{M_{wr} H_{cgA} A_x}{c} \qquad F_{longacc6} = \frac{M_{wr} H_{cgA} A_x}{c}$$

Vertical wheel motion:

$$M_{wf} \frac{dZ_1}{dt} = F_{t1} - F_{s1} SWF - F_{latacc1} + F_{longacc1}$$

$$M_{wf} \frac{dZ_2}{dt} = F_{t2} - F_{s2} SWF + F_{latacc2} + F_{longacc2}$$

$$M_{wc} \frac{dZ_3}{dt} = F_{t3} - F_{s3} SWF - F_{latacc3} + F_{longacc3}$$

$$M_{wc} \frac{dZ_4}{dt} = F_{t4} - F_{s4} SWF + F_{latacc4} + F_{longacc4}$$

$$M_{wr} \frac{dZ_5}{dt} = F_{t5} - F_{s5} SWF - F_{latacc5} - F_{longacc5}$$

$$M_{wr} \frac{dZ_6}{dt} = F_{t6} - F_{s6} SWF + F_{latacc6} - F_{longacc6}$$

Body motion:

$$\frac{d^2 Z_{b1}}{dt^2} = \frac{dV_z}{dt} - t_s \frac{d^2\phi}{dt^2} - a \frac{d^2\theta}{dt^2} \qquad \frac{d^2 Z_{b2}}{dt^2} = \frac{dV_z}{dt} + t_s \frac{d^2\phi}{dt^2} - a \frac{d^2\theta}{dt^2}$$

$$\frac{d^2 Z_{b3}}{dt^2} = \frac{dV_z}{dt} - t_s \frac{d^2\phi}{dt^2} - b \frac{d^2\theta}{dt^2} \qquad \frac{d^2 Z_{b4}}{dt^2} = \frac{dV_z}{dt} + t_s \frac{d^2\phi}{dt^2} - b \frac{d^2\theta}{dt^2}$$

$$\frac{d^2 Z_{b5}}{dt^2} = \frac{dV_z}{dt} - t_s \frac{d^2\phi}{dt^2} + c \frac{d^2\theta}{dt^2} \qquad \frac{d^2 Z_{b6}}{dt^2} = \frac{dV_z}{dt} + t_s \frac{d^2\phi}{dt^2} + c \frac{d^2\theta}{dt^2}$$

Vertical tyre forces:

$$F_{z1} = F_{zs1} + F_{s1} SWF + F_{latacc1} - F_{longacc1}$$

$$F_{z2} = F_{zs2} + F_{s2}SWF - F_{latacc2} - F_{longacc2}$$

$$F_{z3} = F_{zs3} + F_{s3}SWF + F_{latacc3} - F_{longacc3}$$

$$F_{z4} = F_{zs4} + F_{s4}SWF - F_{latacc4} - F_{longacc4}$$

$$F_{z5} = F_{zs5} + F_{s5}SWF + F_{latacc5} + F_{longacc5}$$

$$F_{z6} = F_{zs6} + F_{s6}SWF - F_{latacc6} + F_{longacc6}$$

Compliant steering system:

$$\ddot{\delta}_f = \frac{1}{(I_{wzf} + S_r I_{wzc})} * (S_g K_s \delta_{hw} + E - C_{ss}\dot{\delta}_f - S_g^2 K_{ss}\delta_f) - \ddot{\psi}$$

$$E = M_{zf} + M_{zc} - r_w \tan\lambda_c (F_{wyf} + F_{wyc})$$

Pneumatic trail:

$$X_{traili} = b_9 (e^{(F_{zi} b_8)} - 1)\left[\frac{\sin((b_4 {\alpha_i}^2 + b_5\alpha_i)b_6)^{b_1}}{\cosh((b_4 {\alpha_i}^2 + b_5\alpha_i)b_6)^{b_2} + 1}\right]$$

Transient tyre force lag:

$$F_{wx\_out} = \frac{1}{1 + \frac{Rl_x}{V_x}s} F_{wx\_in}$$

$$F_{wy\_out} = \frac{1}{1 + \frac{Rl_y}{V_x}s} F_{wy\_in}$$

A.2 Vehicle Parameters

Here are the parameters used in the full vehicle model.

Note: When values for the actual vehicle were not available, values from similar off-road vehicles were used.

A.2.1 Unladen Parameters

Dimensions:

$t = 1.14$	Half wheel track in m
$t_s = 1.00$	Suspension half track in m
$r_w = 0.59$	Wheel Radius in m

a = 1.185	Distance for front axle to CofG in m
b = -0.565	Distance for central axle to CofG in m
c = 2.315	Distance for rear axle to CofG in m
$X_{trail} = 0.25$	Static pneumatic trail in m
$H_{cgA} = 0.59$	Height of Unsprung CoG in m
$H_{cgB} = 1.23$	Height of Sprung CoG in m
$H_{rc} = 0.25$	Height of roll centre in m
$L = 3.50$	Wheel base in m
$A_d = 4.5$	Front vehicle area in m^2
$Longrl = 0.18$	Longitudinal tyre relaxation length in m
$latrl = 0.59$	Lateral tyre relaxation length in m

Masses Inertia's and Forces

$M_b = 7580$	Body mass in kg
$M_{wf} = 365$	Front tyre mass in kg
$M_{wc} = 365$	Central tyre mass in kg
$M_{wr} = 365$	Rear tyre mass in kg
$I_{wf} = 100$	Front wheel spin inertia in kgm^2
$I_{wc} = 100$	Central wheel spin inertia in kgm^2
$I_{wr} = 100$	Rear wheel spin inertia in kgm^2
$I_z = 9650$	Vehicle body yaw inertia in kgm^2
$I_y = 11500$	Vehicle body pitch inertia in kgm^2
$I_x = 9060$	Vehicle body roll inertia in kgm^2
$I_{wz} = 260$	Wheel steer inertia in kgm^2

Stiffness and damping

$K_{tf} = 750000$	Front tyre vertical stiffness in N/m
$K_{tc} = 800000$	Central tyre vertical stiffness in N/m
$K_{tr} = 800000$	Rear tyre vertical stiffness in N/m
$C_{tf} = 500$	Front tyre damping coefficient in Ns/m
$C_{tc} = 500$	Central tyre damping coefficient in Ns/m
$C_{tr} = 500$	Rear tyre damping coefficient in Ns/m
$K_{ss} = 80025$	Steering system stiffness in Nm/rad
$C_{ss} = 10000$	Steering system damping in Nms/r
$K_{sf} = 328000$	Front suspension stiffness in N/m
$K_{sc} = 136000$	Central suspension stiffness in N/m
$K_{sr} = 136000$	Rear suspension stiffness in N/m
$C_{sf} = 40000$	Front suspension damping coefficient in Ns/m
$C_{sc} = 40000$	Central suspension damping coefficient in Ns/m
$C_{sr} = 40000$	Rear suspension damping coefficient in Ns/m
$C_{\lambda f} = 203000$	Front tyre longitudinal stiffness in N/m
$C_{\lambda c} = 102600$	Central tyre longitudinal stiffness in N/m
$C_{\lambda r} = 102600$	Rear tyre longitudinal stiffness in N/m

$C_{\alpha f} = 147500$	Front tyre cornering stiffness in N/rad
$C_{\alpha c} = 91240$	Central tyre cornering stiffness in N/rad
$C_{\alpha r} = 91240$	Rear tyre cornering stiffness in N/rad

Other parameters

$g = 9.81$	Acceleration due to gravity in m/s^2
$\lambda_c = 0.0872$	Castor angle in rad
$\varepsilon_r = 0.015$	Road Adhesion reduction factor in s/m
$C_t = 1.2433$	Scalar factor for Dugoff tyre model
$S_r = 0.5$	Ratio of central steer angle to front
$S_g = 22.5$	Ratio of hand wheel angle to road wheel angle
$S_d = 0.2$	Desired wheel slip for traction control
$C_d = 0.5$	Aerodynamic drag coefficient
$BWF = 1/1.34$	Bumpstop force to wheel force
$SWF = 0.5$	Strut force to wheel force
$BSF = 1.49$	Bumpstop force to strut force

The following are variables used for determining desired yaw rate promoting slight understeer:

$dM_b = 12215$	Body mass in kg
$da = 1.6$	Distance for front axle to CofG in m
$db = -0.15$	Distance for central axle to CofG in m
$dc = 1.9$	Distance for rear axle to CofG in m
$dC_{\alpha f} = 146480*2$	Front axle cornering stiffness in N/rad
$dC_{\alpha c} = 146480*2$	Central axle cornering stiffness in N/rad
$dC_{\alpha r} = 146480*2$	Rear axle cornering stiffness in N/rad

A.2.2 Laden Parameters

Dimensions:

$t = 1.14$	Half wheel track in m
$t_s = 1.00$	Suspension half track in m
$r_w = 0.59$	Wheel Radius in m
a = 1.890	Distance for front axle to CofG in m
b = 0.14	Distance for central axle to CofG in m
c = 1.61	Distance for rear axle to CofG in m
$X_{trail} = 0.25$	Static pneumatic trail in m
$H_{cgA} = 0.59$	Height of Unsprung CoG in m
$H_{cgB} = 1.83$	Height of Sprung CoG in m
$H_{rc} = 0.20$	Height of roll centre in m
$L = 3.50$	Wheel base in m
$A_d = 4.5$	Front vehicle area in m^2

$Longrl = 0.18$	Longitudinal tyre relaxation length in m
$latrl = 0.59$	Lateral tyre relaxation length in m
Masses Inertia's and Forces	
$M_b = 16580$	Body mass in kg
$M_{wf} = 365$	Front tyre mass in kg
$M_{wc} = 365$	Central tyre mass in kg
$M_{wr} = 365$	Rear tyre mass in kg
$I_{wf} = 100$	Front wheel spin inertia in kgm^2
$I_{wc} = 100$	Central wheel spin inertia in kgm^2
$I_{wr} = 100$	Rear wheel spin inertia in kgm^2
$I_{wz} = 260$	Wheel steer inertia in kgm^2
$I_z = 20730$	Vehicle body yaw inertia in kgm^2
$I_y = 40720$	Vehicle body pitch inertia in kgm^2
$I_x = 16400$	Vehicle body roll inertia in kgm^2
Stiffness and damping	
$K_{tf} = 750000$	Front tyre vertical stiffness in N/m
$K_{tc} = 800000$	Central tyre vertical stiffness in N/m
$K_{tr} = 800000$	Rear tyre vertical stiffness in N/m
$C_{tf} = 500$	Front tyre damping coefficient in Ns/m
$C_{tc} = 500$	Central tyre damping coefficient in Ns/m
$C_{tr} = 500$	Rear tyre damping coefficient in Ns/m
$K_{ss} = 80025$	Steering system stiffness in Nm/rad
$C_{ss} = 10000$	Steering system damping in Nms/r
$K_{sf} = 336000$	Front suspension stiffness in N/m
$K_{sc} = 448000$	Central suspension stiffness in N/m
$K_{sr} = 448000$	Rear suspension stiffness in N/m
$C_{sf} = 40000$	Front suspension damping coefficient in Ns/m
$C_{sc} = 40000$	Central suspension damping coefficient in Ns/m
$C_{sr} = 40000$	Rear suspension damping coefficient in Ns/m
$C_{\lambda f} = 263300$	Front tyre longitudinal stiffness in N/m
$C_{\lambda c} = 240500$	Central tyre longitudinal stiffness in N/m
$C_{\lambda r} = 240500$	Rear tyre longitudinal stiffness in N/m
$C_{\alpha f} = 147500$	Front tyre cornering stiffness in N/rad
$C_{\alpha c} = 178700$	Central tyre cornering stiffness in N/rad
$C_{\alpha r} = 178700$	Rear tyre cornering stiffness in N/rad
Other parameters	
$g = 9.81$	Acceleration due to gravity in m/s^2
$\lambda_c = 0.0872$	Castor angle in rad
$\varepsilon_r = 0.015$	Road Adhesion reduction factor in s/m

$C_t = 1.2433$	Scalar factor for Dugoff tyre model
$S_r = 0.5$	Ratio of central steer angle to front
$S_g = 22.5$	Ratio of hand wheel angle to road wheel angle
$S_d = 0.2$	Desired wheel slip for traction control
$C_d = 0.5$	Aerodynamic drag coefficient
$BWF = 1/1.34$	Bumpstop force to wheel force
$SWF = 0.5$	Strut force to wheel force
$BSF = 1.49$	Bumpstop force to strut force

The following are variables used for determining desired yaw rate promoting slight understeer:

$dM_b = 12215$	Body mass in kg
$da = 1.6$	Distance for front axle to CofG in m
$db = -0.15$	Distance for central axle to CofG in m
$dc = 1.9$	Distance for rear axle to CofG in m
$dC_{\alpha f} = 146480*2$	Front axle cornering stiffness in N/rad
$dC_{\alpha c} = 146480*2$	Central axle cornering stiffness in N/rad
$dC_{\alpha r} = 146480*2$	Rear axle cornering stiffness in N/rad